REGENERATIVE REACTOR FOR NOx ABATEMENT

Donald K. Fleming, et al

Institute of Gas Technology

Prepared for:

Picatinny Arsenal

May 1974

Unclassified
Security Classification

AD 779 455

DOCUMENT CONTROL DATA - R & D

(Security classification of title, body of abstract and indexing annotation must be entered when the overall report is classified)

1. ORIGINATING ACTIVITY (Corporate author)
Institute of Gas Technology
3424 South State Street
Chicago, Illinois 60616

2a. REPORT SECURITY CLASSIFICATION
Unclassified

2b. GROUP

3. REPORT TITLE
Regenerative Reactor for NO_x Abatement

4. DESCRIPTIVE NOTES (Type of report and inclusive dates)
Final Report, Mar. 1972 – Dec. 1972

5. AUTHOR(S) (First name, middle initial, last name)
Donald K. Fleming
John C. Sharer

6. REPORT DATE	7a. TOTAL NO. OF PAGES	7b. NO. OF REFS
May 1973	246	36

8a. CONTRACT OR GRANT NO.	9a. ORIGINATOR'S REPORT NUMBER(S)
DAAA 21-72-C-0455	
b. PROJECT NO. AMCMS 4932.05.4114	
c.	9b. OTHER REPORT NO(S) (Any other numbers that may be assigned this report)
d.	8935

10. DISTRIBUTION STATEMENT
Distribution of this document is unlimited.

11. SUPPLEMENTARY NOTES	12. SPONSORING MILITARY ACTIVITY
	Picatinny Arsenal Facilities and Protective Technology Division-MTD, Dover, New Jersey

13. ABSTRACT

A novel reactor, capable of regenerating heat of reaction into the inlet stream, was analyzed for application to NO_x reduction in nitric acid tail gas. The process was evaluated thermodynamically and kinetically over conventional catalysts. The device was simulated mathematically, and isothermal bed characteristics were obtainable. The simulated unit was also demonstrated with bench-scale hardware. Satisfactory performance was achieved on feed streams that could not otherwise be processed in single reactors.

DD FORM 1 NOV 68 1473 REPLACES DD FORM 1473, 1 JAN 64, WHICH IS OBSOLETE FOR ARMY USE.

Unclassified
Security Classification

14. KEY WORDS	LINK A		LINK B		LINK C	
	ROLE	WT	ROLE	WT	ROLE	WT
Catalytic Reaction						
Cobalt Oxide						
Heat Transfer						
Kinetics						
Mass Transfer						
Mathematical Modeling						
Methane						
Nitric Oxides						
Noble Metal						
Pollution Abatement						
Regeneration						
Thermodynamics						

ia

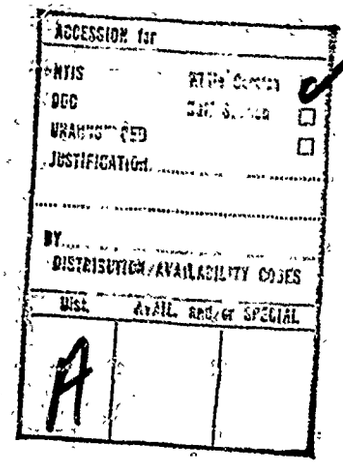

The findings in this report are not to be construed as an official Department of the Army position, unless so designated by other authorized documents.

DISPOSITION

Destroy this report when no longer needed. Do not return it to the originator.

DAAA 21-72-C-0455
Project No. 8935
AMCMS 4932.05.4114

REGENERATIVE REACTOR FOR NO_x ABATEMENT

Final Report
(Including Supplemental Data)

to

Facilities and Protective Technology Division
Manufacturing Technology Directorate
Picatinny Arsenal
Dover, New Jersey 07801

Principal Investigators

Bender, S. K.
Fleming, D. K.
Sharer, J. C.
Toczycki, W.
Weil, S. A.

Institute of Gas Technology
3424 South State Street
Chicago, Illinois 60616

May 1974

TABLE OF CONTENTS

TABLE OF CONTENTS, Cont.

TABLE OF CONTENTS, Cont.

TABLE OF CONTENTS, Cont.

TABLE OF CONTENTS, Cont.

TABLE OF CONTENTS, Cont.

LIST OF FIGURES

LIST OF FIGURES, Cont.

LIST OF FIGURES, Cont.

LIST OF FIGURES, Cont.

LIST OF FIGURES, Cont.

LIST OF FIGURES, Cont.

LIST OF TABLES

1. SUMMARY

This report presents the results of a pollution abatement program sponsored by the U.S. Army, Picatinny Arsenal, under Contract DAAA 21-72-C-0455. The program objective was the initial development of a novel, rotary regenerative reactor for the abatement of NO_x pollution from nitric acid tail gas. The reactor is based upon the catalytic reaction of NO_x (and oxygen) with methane, but incorporates internal heat recovery to circumvent the problems of lightoff, excessive temperature, and necessarily low oxygen concentration which plague the currently available systems.

This initial development program was successful, starting with a concept and culminating in the operation of a simulated regenerative reactor and the design of a prototype, pilot-unit reactor to process 1000 SCF/hr of tail gas.

1.1. The Pollution Abatement Problem

In the manufacture of nitric acid, ammonia is catalytically burned to nitric oxide and nitrogen dioxide which are then absorbed in water, producing the product acid. The absorption of these nitrogen oxides by water is imperfect; therefore, a waste gas containing about 3000 ppm NO_x is discharged from the absorber tower. This NO_x is a serious pollutant and an important intermediate in photochemical smog formation; the tail gas must be chemically treated to minimize the NO_x discharged to the atmosphere. Currently available NO_x abatement processes have generally not operated well. The relatively low operating temperature limitation of the catalysts, in conjunction with the high temperature required for reaction initiation, is the underlying cause of abatement problems using inexpensive methane fuel. The rotary regenerative reactor, developed in this program, overcomes these problems. In addition, it permits operation with relatively high oxygen concentrations in the tail gas with maximum control of the process.

1.2. The Novel Reactor Concept

The heart of the novel reactor is the incorporation of regenerative heat recovery into the system. The exothermic heat of the necessary methane-oxygen combustion is used to preheat the inlet gases, absorbing the heat of the reaction from the reacting gases. Regenerative heat exchange is capable of high efficiency and is particularly amenable to the honeycomb catalysts conventionally used in this reacting system. In essence, the reactor operates like a catalyzed wheel. The reacting

gases pass over this wheel and react on the catalyzed surface, leaving the exothermic heat of reaction in the solids of the wheel. The wheel is rotated to place the hot solids in the path of the incoming gases, and the heat is transferred from the wheel into the untreated tail gas.

1.3. Program Achievements

1.3.1. Thermodynamic Analysis

A thermodynamic analysis proved that the NO_x in the tail gas should theoretically decompose to acceptable limits without treatment. However, in practice, the rate of decomposition is slow. When fuel is added to the tail gas, the theoretical concentration of the NO_x pollutants is decreased by several orders of magnitude. Practice has proved that the abatement reactions can occur over noble metal catalysts. However, the extremely low theoretical NO_x concentrations have not been realized. Even the achievement of the new Federal pollution standards, equivalent to 209 ppm NO_x, has been difficult. The thermodynamic analysis also predicted that the formation of other possible pollutants — NH_3, HCN, and CO — could be held within acceptable limits.

1.3.2. Mathematical Model

A simplified model was derived to predict the temperatures and reactant concentrations in the novel reactor as functions of the chemical and physical parameters of the system. Several modes of operation were modeled: simple heat exchange, simple reaction, cocurrent regenerative reaction, countercurrent operation, and mixed cocurrent and countercurrent flow of reacting gases with the incoming tail gas. The cocurrent mode of operation proved to be ideal. In this mode, the configuration of the reactor is defined by the chemical characteristics of the system, forcing the temperature in the reactor to be essentially constant. The resulting system would provide maximum reaction rate with inherent control capabilities.

1.3.3. Experimental Kinetic Study

Kinetic data necessary for the design of the regenerative reactor were not available from the open literature or the catalyst vendors. We therefore tested samples of commercial NO_x abatement catalysts to determine these chemical parameters. We found that the chemical reaction rate (for the reduction of oxygen by methane) was high and, at 90 psig operating pressure, controlled primarily by the rate of diffusion within the honeycomb carrier. The NO_x reduction could be directly

related to the reaction of oxygen with methane. Satisfactory NO_x reduction, using a factor of safety to achieve the EPA standards, could be achieved at a standard space velocity of 27,500 hr^{-1}. Employing proposed bed modifications, the design space velocity might be increased to 66,000 hr^{-1}. Also, work with reformed natural gas for fuel predicts reduced operating temperatures with lessened probability of catalyst degradation. Data on non-noble catalysts indicate promise for cost reduction.

1.3.4. Regenerative Reactor Operation

The outputs of the reactor modeling task and the kinetic evaluation were integrated to specify the operation of a cyclic reactor which simulated the performance of the rotary regenerative reactor. The cyclic reactor operated with 5.2% oxygen in the simulated tail gas, yet it reduced the NO concentration from 3000 ppm to 16 ppm. Oxygen consumption was 99.5% without exceeding the temperature limitations specified by the catalyst manufacturer, and the temperature variation through the length of the bed was predictable. Federal standards were met in another test even with a degraded catalyst.

1.3.5. Design of Prototype Rotary Regenerative Reactor

A small-scale rotary regenerative reactor was designed to treat 1000 SCF/hr tail gas. This reactor is 7 in. in diameter x 3 in. deep and incorporates a variable partition between the preheating and reaction sections of the rotary reactor. This feature permits modification of the reactor operating characteristics to compensate for changes in the chemical parameters of the reaction system. Reactor designs for both cocurrent and countercurrent operation were prepared.

1.4. Proposed Reactor Development

For a continuation of this successful development program, the small-scale rotary regenerative reactor should be built and operated in the NO_x abatement process.

2. OBJECTIVE

The purpose of the work in this program was the initial development of a novel reactor for abatement of NO_x pollution from the tail gas produced in nitric acid manufacture. Conceptually, this reactor offers significant operational advantages over currently available abatement systems.

Additional efforts, under a project continuation grant, were directed at improved performance of existing simple reactors, studying four areas:

- System modeling, using experimental reaction rates
- Kinetic studies on non-noble catalysts
- Kinetic studies with reformed natural gas fuel
- Catalyst degradation studies

3. INTRODUCTION

3.1. Introduction to the Problem

The production of nitric acid has been a basic industry for at least 40 years, and the manufacturing procedures have become well established.[25,28] Recently, however, interest in improving the process has been reawakened because of the NO_x emissions in the stack gas and their effect on environmental quality.[4,10] Although only 2.1% of the total NO_x emitted from stationary installations in the United States is attributable to noncombustion sources, the NO_x pollution from nitric acid manufacturing facilities is severe because of the locally high pollutant concentrations.[11]

Of the nitric acid plants in North America, less than half incorporate stack decolorization facilities and few have reliable total NO_x abatement processes. Esso's[11] report to NAPCA discusses the operating problems and relative performances of the proposed solutions for total NO_x abatement from nitric acid plants. More recently (1971 and 1972), Adlhart et al.[2] and Newman[23,24] presented data on the merits of their abatement systems. No process has been proved to be entirely satisfactory in the field, according to Reference 11.

The Institute of Gas Technology has conceived an improved reactor for combining the heat transfer and chemical reactions that are necessary for minimizing the NO_x emissions from nitric acid plants. The purpose of this program was to evaluate the feasibility of that reactor.

3.2. Nitric Acid Manufacturing Process

3.2.1. The Process

Although nitric acid manufacturing is an established process, many variations exist, with at least 10 process licensors.[25] All of these processes employ the same chemical reactions, but equipment, pressures, and temperatures vary in the different plants. A typical plant might have the flow sheet illustrated in Figure 3-1, taken from Reference 13, which lists the process conditions. Filtered air is compressed to 100 psi and heated (by exchange with hot reaction products) before being mixed with ammonia. The ammonia burns with the air over a catalyst to make nitric oxide and water:

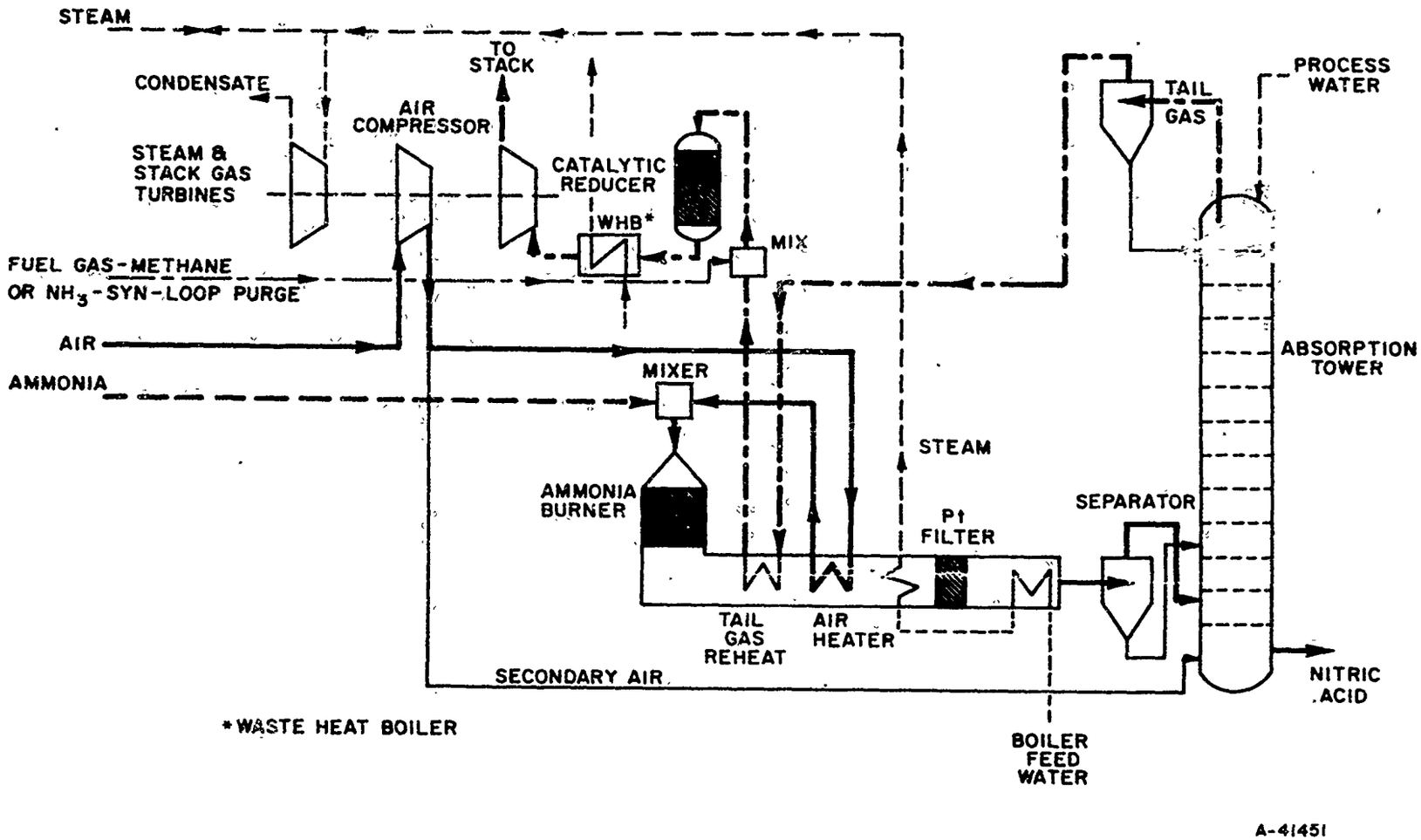

Figure 3-1. TYPICAL NITRIC ACID PLANT – PRESSURE PROCESS

$$4NH_3 + 5O_2 \rightarrow 4NO + 6H_2O \qquad (3\text{-}1)$$

The catalyst is usually platinum or platinum-rhodium gauze, although at least one licensor has developed a non-noble metal catalyst for Reaction 3-1.[22] The reaction products are cooled, and nitric oxide reacts with excess air, forming nitrogen dioxide:

$$2NO + O_2 \rightarrow 2NO_2 \qquad (3\text{-}2)$$

This gas is dissolved in water in the absorption tower to produce 50-60% nitric acid:

$$3NO_2 + H_2O \rightarrow 2HNO_3 + NO \qquad (3\text{-}3)$$

Secondary air feeds the bottom of the tower to reoxidize the nitric oxide. Theoretically, however, the water cannot absorb all of the NO_x unless the tower is infinitely large. Absorption units are currently sized on the economic recovery of NO; the resulting NO_x loss is the pollutant in the exhaust gas.

3.2.2. Tail Gas

The tail gas from the tower has the following "typical" properties:

Temperature: 85°F

Pressure: 92 psig

Composition:

Compound	vol %
NO	0.15
NO_2	0.15
O_2	3.5
H_2O	0.6
N_2	Balance

The oxides of nitrogen, NO and NO_2, are serious pollutants that are noxious in themselves and important intermediates in photochemical smog formation.

$$4NH_3 + 5O_2 \rightarrow 4NO + 6H_2O \qquad (3\text{-}1)$$

The catalyst is usually platinum or platinum-rhodium gauze, although at least one licensor has developed a non-noble metal catalyst for Reaction 3-1.[22] The reaction products are cooled, and nitric oxide reacts with excess air, forming nitrogen dioxide:

$$2NO + O_2 \rightarrow 2NO_2 \qquad (3\text{-}2)$$

This gas is dissolved in water in the absorption tower to produce 50-60% nitric acid:

$$3NO_2 + H_2O \rightarrow 2HNO_3 + NO \qquad (3\text{-}3)$$

Secondary air feeds the bottom of the tower to reoxidize the nitric oxide. Theoretically, however, the water cannot absorb all of the NO_x unless the tower is infinitely large. Absorption units are currently sized on the economic recovery of NO; the resulting NO_x loss is the pollutant in the exhaust gas.

3.2.2. Tail Gas

The tail gas from the tower has the following "typical" properties:

Temperature: 85°F

Pressure: 92 psig

Composition:

Compound	vol %
NO	0.15
NO_2	0.15
O_2	3.5
H_2O	0.6
N_2	Balance

The oxides of nitrogen, NO and NO_2, are serious pollutants that are noxious in themselves and important intermediates in photochemical smog formation.

3.3. The Conventional Catalytic Abatement Process

Three basic chemical reactions occur during the catalytic treatment of this tail gas over noble metal catalysts using methane as a reductant:

$$CH_4 + 4NO_2 \rightarrow 4NO + CO_2 + 2H_2O \quad \text{(decolorization)} \quad (3\text{-}4)$$

$$CH_4 + 2O_2 \rightarrow CO_2 + 2H_2O \quad \text{(combustion)} \quad (3\text{-}5)$$

$$CH_4 + 4NO \rightarrow CO_2 + 2H_2O + 2N_2 \quad \text{(abatement)} \quad (3\text{-}6)$$

An offensive red color in the tail gas is caused by NO_2. The NO_2 can be catalytically decolorized to NO (Reaction 3-4) over noble metal catalysts with minimum fuel addition. This reaction is kinetically more rapid than Reactions 3-5 or 3-6 and has been practiced in some plants for years.[24]

The catalytic reduction of oxygen (Reaction 3-5) is highly exothermic.[1,21] The temperature rise with methane is about 240°F for each percentage point of oxygen burned from the tail gas. Therefore, the tail gas can be decolorized and provide energy for gas turbines by catalytic combustion with controlled fuel addition.

The abatement reaction (3-6) will kinetically occur only after near completion of Reactions 3-4 and 3-5.[2,16] The catalytic removal of nitric oxide is an order of magnitude more difficult than decolorization because of thermal problems discussed in the next subsection.

3.3.1. Temperature Limitations

To ensure ignition of the tail gas with natural gas, its temperature must be raised to about 900°F. Lower temperatures are used with H_2 fuel, but the less expensive CH_4 is more refractory.[1,4] The conventional noble metal catalysts are temperature-limited to a maximum of 1400°F for satisfactory lifetime.[16] Because the combustion reaction is exothermic, the oxygen concentrations in the tail gas are limited to about 2.5% to avoid exceeding that maximum operating temperature in a single-pass reactor.[2,16] However, the absorption towers should be operated with high excess oxygen concentrations to ensure a bleached acid product. Various compromises are required in abatement process operation.

3.4. Existing Treatment Processes

3.4.1. Single-Stage, Fixed-Bed Catalytic Abatement

Figure 3-2 is a schematic diagram of a single-stage catalytic abatement process.[2]

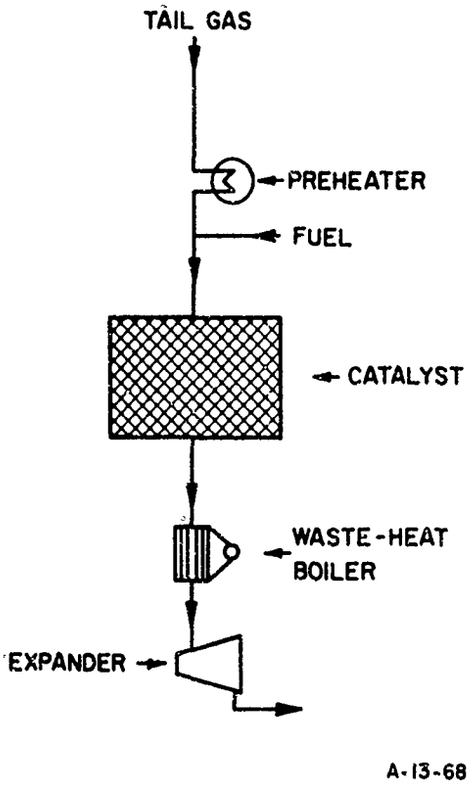

Figure 3-2. SINGLE-STAGE ABATOR SYSTEM DESIGN

The tail gas is preheated to 900°F, mixed with fuel, and passed over the noble metal catalyst. The hot, 90-psig treated tail gas is then exhausted through a gas turbine which recovers energy for compressing the inlet air to the process. Because the maximum inlet temperature of most commercial expanders is 1200°F, a waste-heat boiler is included before the turbine. Abatement is possible in a single-stage reactor but, as discussed earlier, only if the tail gas oxygen concentration is limited to about 2.5%; higher O_2 concentrations cause excessive temperature rise and catalyst degradation.

3.4.2. Two-Stage Catalytic Abatement Systems

A possible solution to the limitation on oxygen concentration is the use of a two-stage abatement system (Figures 3-3 and 3-4).

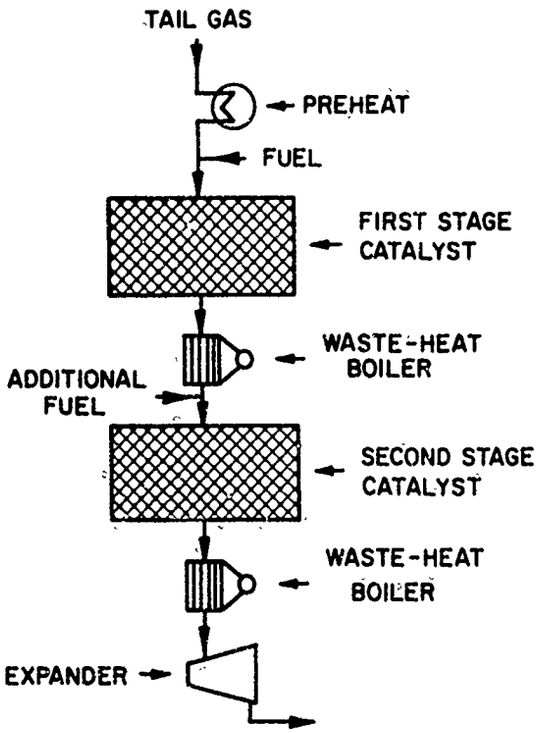

Figure 3-3. TWO-STAGE ABATOR SYSTEM DESIGN

After a first-stage catalyst bed (Figure 3-3), the temperature is reduced to 900°F in a waste-heat boiler, more fuel is added, and the gas is similarly passed over a second bed. Another operating technique is to inject water into the hot gas between the two stages. Figure 3-4 illustrates still another reactor configuration. Some of the tail gas bypasses the preheater and first reactor bed and is mixed into the first-stage reaction product for cooling before the second-stage reactor. The two-stage processes require more equipment and catalyst than the single-stage systems.

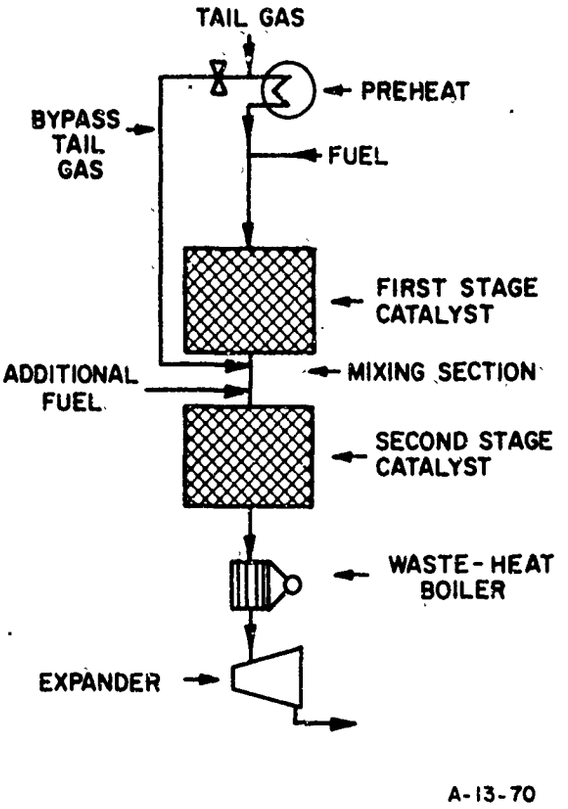

Figure 3-4. TWO-STAGE ABATOR SYSTEM WITH BYPASS PIPE

3.4.3. Hydrogen-Fueled Abatement System

The reaction initiation temperature (lightoff) is reduced to about 300°F using hydrogen fuel. With 300°F ignition, tail gas with nearly 4% O_2 content can be processed without exceeding the temperature limitations of the catalyst. Hydrogen, however, is relatively expensive. In one process version,[26] the methane fuel is steam-reformed in the waste heat of the ammonia burner, producing H_2. This system, however, has not yet been commercially exploited. If, however, the nitric acid facility plant is located near an ammonia plant, a purge gas is available with approximately 60% hydrogen content. This gas is a suitable fuel.

3.4.4. Selective NO_x Reduction

The oxides of nitrogen can be selectively reduced in an oxygen-containing stream using ammonia for fuel.[3,26] The ammonia, however, is expensive, causing high operating costs. Catalyst specialists do not recommend this system.

3.4.5. Molecular Sieves

Special molecular sieves are applicable for the selective sorption of NO_x from moisture-free tail gas.[15,35] This process has long-range potential; the technical and economic viability is now being proved in a DOD-EPA demonstration facility.

3.4.6. Increased Sorption Tower Size

Present absorption towers in nitric acid plants are sized for economic recovery of the NO_2 and NO. Greater recovery (and less pollution) is possible by increasing the operating pressure and/or the sorber size.[23] Assuming that both the NO oxidation and sorption obey conventional rate expressions, the tower size must be increased by 75% to meet EPA standards with no factor of safety. This alternative may be applicable for a new facility, but is expensive in acid-proof, high-pressure construction.

3.5. Rotary Regenerative Reactor

Although the rotary regenerator is relatively common in power generation and large industrial furnace applications, it is not well known to many engineers. This discussion is presented to describe the device and indicate its potential in fields other than simple thermal regeneration.

3.5.1. Regenerative Heat Recovery – Packed Bed

The subject of regeneration is best introduced by considering heat recovery in a packed bed. Assuming that the bed is initially cold and a hot gas is passed through it, heat will be transferred from the hot gas to the cold bed. The quantity of heat absorbed is a function of the mass, heat capacity, and temperature increase of the bed. After a given time interval, when the bed temperature approaches the gas temperature and little more heat can be recovered, the hot gas flow to the bed is stopped and cold gas is passed over it. The process is reversed, and heat is transferred from the bed into the cold gas, increasing its temperature. Thus, heat has been indirectly transferred from a hot gas to a cold gas.

Although this process appears cumbersome, high efficiencies of heat transfer can be achieved and the resulting equipment is often more economical than other types of heat exchangers. Usually, at least two similar beds are operated with automatic valving so that continuous flows can be employed.

3.5.2. Other Regenerative Processes — Packed Bed

Regeneration is used not only in heat transfer, but also in mass transfer (molecular sieves, etc.) and chemical reactions (regeneration of spent catalyst, etc.). All of these processes are cyclical, with interrupted flows, unless multiple beds are used. The packed bed is often preferred for regenerative processes, particularly if long cycle times are involved. Long cycle times, however, promote temperature and concentration extremes, with resulting loss of efficiency.

3.5.3. Rotary Regenerator

The deficiencies of the packed bed can be largely overcome by using the rotary regenerator. This device, continuously regenerating, constantly blends the products in each stream and operates at shorter effective cycle times. The rotary reactor is generally a porous wheel. Its porosity is generated by constructing a disk of corrugated metal or ceramic (Figure 3-5) so there is free passage for gas flow along the axis of the wheel, but gas transfer cannot occur radially. This wheel is rotated through the gas paths of two adjacent ducts, as illustrated schematically in Figure 3-6. Two ducts of semicircular cross section are intersected by the rotary wheel. The ducts in front of the wheel are not shown for clarity. Gases flowing in one duct will therefore pass through the wheel and continue in an extension of that duct.

Figure 3-6 illustrates an example in which exactly half the wheel is used for each function of the heat transfer; however, many different configurations are possible on this wheel. The proportions of the wheel used for each of the gas streams may vary, and more than two sectors of the wheel may be used if, for example, a steam purge is desirable.

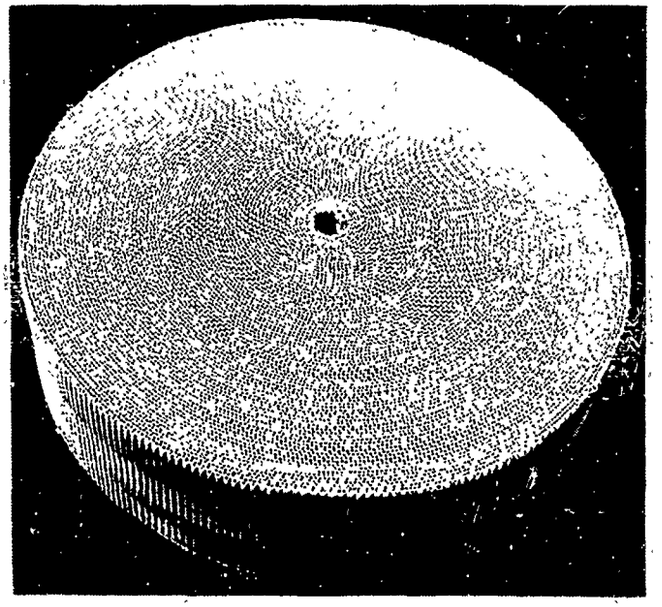

Figure 3-5. TYPICAL REACTOR WHEEL CONSTRUCTION

3.5.4. Present Applications

The rotary wheel has been used for many years as a heat transfer device. High heat transfer efficiencies can be attained in a regenerative exchanger of this type. Regenerators are common in large furnace installations, and regenerative air preheaters, called Ljungstrom Wheels, are used for economizers in electrical power plants. Chrysler Corporation used this type of device for cooling the exhaust from its prototype turbine-powered automobiles. The rotary regenerator is also used in commercially available ovens, industrial space heaters, and dehumidifiers.

In these applications, the wheel generally has a significant advantage over multiple-valved fixed-bed reactors because of its continuous operation and the relatively short cycle time. It has similar advantages over the fluidized-bed reactors because of the relatively high concentration of solid material in contact with the gas stream and the shorter cycle times.

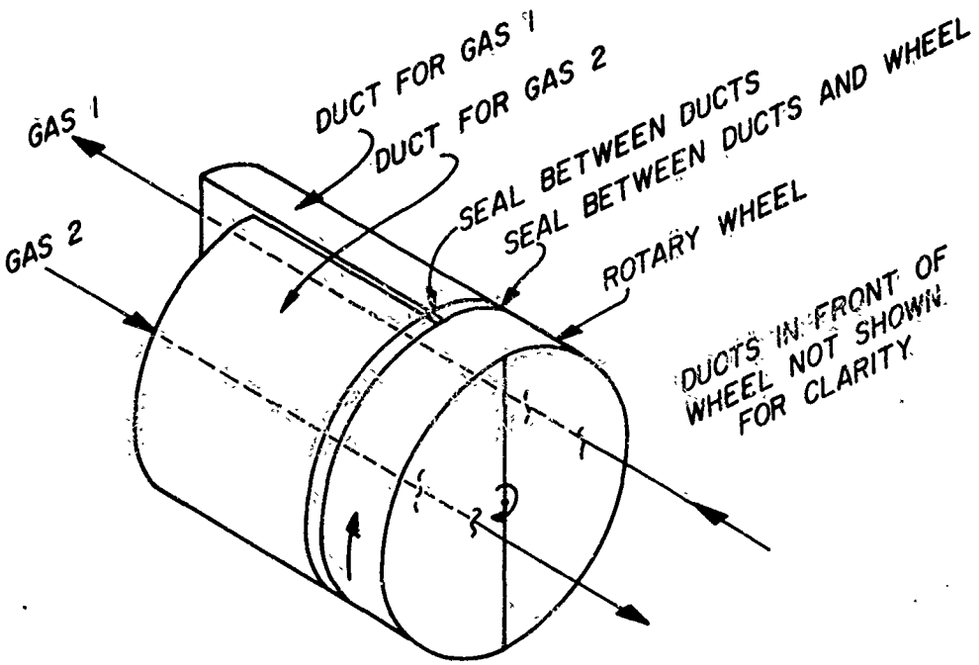

Figure 3-6. SCHEMATIC REPRESENTATION OF ROTARY REGENERATOR

3.5.5. Chemical Reaction on Rotary Regenerator

The NO_x abatement process is exothermic, largely caused by the oxygen burnout. Yet the temperature limitations of the process require sufficient preheat for reaction initiation. Conceivably, this catalytic process could operate in a catalyzed rotary regenerative heat exchanger, withdrawing the exothermic heat from the reacting gases and supplying that heat to the incoming gases for preheat. This concept is presented in detail in Section 6 of this report. In essence, the incoming tail gas is passed over the hot bed of solids, preheating the gas and cooling the solids. Fuel is then introduced, and the hot gas mix is passed back over the cooled solids. These solids are catalyzed, so the chemical abatement reaction occurs, releasing the exothermic heat to the solids, raising their temperature. The heat is regenerated in a manner similar to the rotary heat exchanger, but the source of that heat is the chemical

reaction occurring in the second pass of the rotary device. As the mathematics in Section 6 prove, the treated gas exit temperature is a function primarily of the oxygen content of the tail gas. It is sufficiently low so that the gas can be fed directly to the expansion turbines without cooling.

This process offers several advantages:

a. Maximum control of abatement process for minimum pollution.
b. Minimum equipment, with no interstage coolers.
c. Amenable to high oxygen content in tail gas.
d. Maximum energy recovery.
e. Separation of abatement reaction section of the nitric acid plant from ammonia burner.

The purpose of this project was to determine the feasibility of the novel concept.

3.6. Program Plan

The program was subdivided into three main tasks: mathematical, experimental, and design. This program was based upon the use of methane fuel over conventional noble metal catalysts.[12] The bulk of the developmental program, including the design of the pilot unit rotary regenerative reactor used this basis. However, a minor effort was directed at using alternative fuels or non-noble catalysts.

3.6.1. Mathematical Program

3.6.1.1. Thermodynamic Study

The thermodynamics of the N-O and C-H-N-O chemical systems were evaluated to determine if any theoretical barrier existed that would limit the chemical reduction of the NO_x pollutants.

3.6.1.2. Reactor Modeling

A simplified mathematical model of the novel, rotary, regenerative reactor was developed. The output of this machine computation, together with the experimental data, was used for the design of the first prototype reactor.

3.6.2. Experimental Program

3.6.2.1. Kinetic Study

The catalyst vendors or the open literature did not provide enough information for the design of the prototype reactor. Therefore, we were required to determine the chemical rate parameters experimentally.

3.6.2.2. Cyclical Reactor Study

A pair of fixed-bed reactors was operated cyclically to simulate the performance of the rotary regenerative reactor. Fixed-bed reactors are more readily instrumented than the rotary device, and they were used to check the validity of the concept.

3.6.3. Design Program

The culmination of the project was a conceptual design of a prototype rotary regenerative reactor capable of treating 1000 SCF/hr of nitric acid tail gas.

4. THERMODYNAMIC STUDY

4.1. Summary

Evaluation of the thermodynamic potential of the oxides of nitrogen proves that these compounds should, theoretically, decompose into oxygen and nitrogen in ambient atmospheres. The expected concentration of NO_x is less than 1 ppm. This decomposition does not spontaneously occur, however, indicating that the reaction kinetics are slow.

When fuel is added to a NO_x-containing system, in greater than stoichiometric quantities, the theoretical NO_x equilibrium concentration decreases by 10 orders of magnitude at 1000°F. Theoretically, the formation of other possible pollutants – HCN, NH_3, and CO – is small.

4.2. Objective

The purpose of this phase of the program was to determine the theoretical minimum concentration of NO_x pollutants in nitric acid tail gas. These calculations would define any potential theoretical barrier to NO_x pollution abatement.

4.3. Introduction

A chemical system can be analyzed thermodynamically to determine the theoretical equilibrium concentrations of the components. A thermodynamic evaluation of the NO_x abatement system would indicate the maximum degree of possible NO_x removal.

The thermodynamic studies were broken down into three sections: a) correlations of published data, b) determination of equilibrium composition of the N-O system, and c) determination of equilibrium composition of the C-H-N-O system.

The free energy of a given reaction is a measure of the potential (or driving force) for that reaction to occur. In this thermodynamic subprogram, we determined the concentrations of the products and reactants at which the overall free energy of the system is minimized. Under these conditions, further reaction will not occur, and the system is in equilibrium.

However, a thermodynamic study only determines the driving force for a reaction; it does not consider the resistance to the reaction.

Therefore, the thermodynamic study cannot determine the rates of reactions. (This is a function of the kinetic study presented in Section 7.)

4.4. Correlations of Published Free-Energy Data

The published data on the free energies of formation were correlated with temperature for use in the following two subsections of this study. The primary free energy-temperature data were taken from Rossini[27] and JANAF.[34] These basic sources list the free energies of formation of the necessary compounds as functions of temperature. They also present the logarithm of the equilibrium constant of formation, log K_f (a quantity directly related to the free energy of formation), which was used in this work. A correlation of the following form was used to relate K_f with the absolute temperatures (T).

$$\log K_f = A + B/T + C \log T + DT + ET^2 \qquad (4\text{-}1)$$

This equation should be valid if the heat capacities of the gaseous compounds have the form —

$$c_p = a + bT + cT^2 \qquad (4\text{-}2)$$

The constants A, B, C, D, and E were determined for each of the compounds of interest using a nonlinear least-means-squares regression technique to fit the data to the correlation. In general, the back-calculated values for log K_f agree closely with the published values, indicating the validity of the curve-fitting process.

4.5. Determination of Equilibrium Composition of N-O System

The second phase of the thermodynamic study was a determination of the equilibrium composition that should exist if the oxides of nitrogen in the tail gas could decompose to the theoretical limits. The five-component system of N_2, O_2, N_2O, NO, and NO_2 requires a simultaneous solution of six equations as derived in Appendix A. These equations contain the equilibrium constants of formation which were correlated as described in Subsection 4.4. The simultaneous solution was generated by a machine computation, and the results are presented graphically in Figure 4-1 for a typical tail gas containing 1500 ppm NO_2, 1500 ppm NO, 3.5% oxygen, with the balance nitrogen. This graph indicates that the concentration of the primary pollutant, NO, theoretically increases with

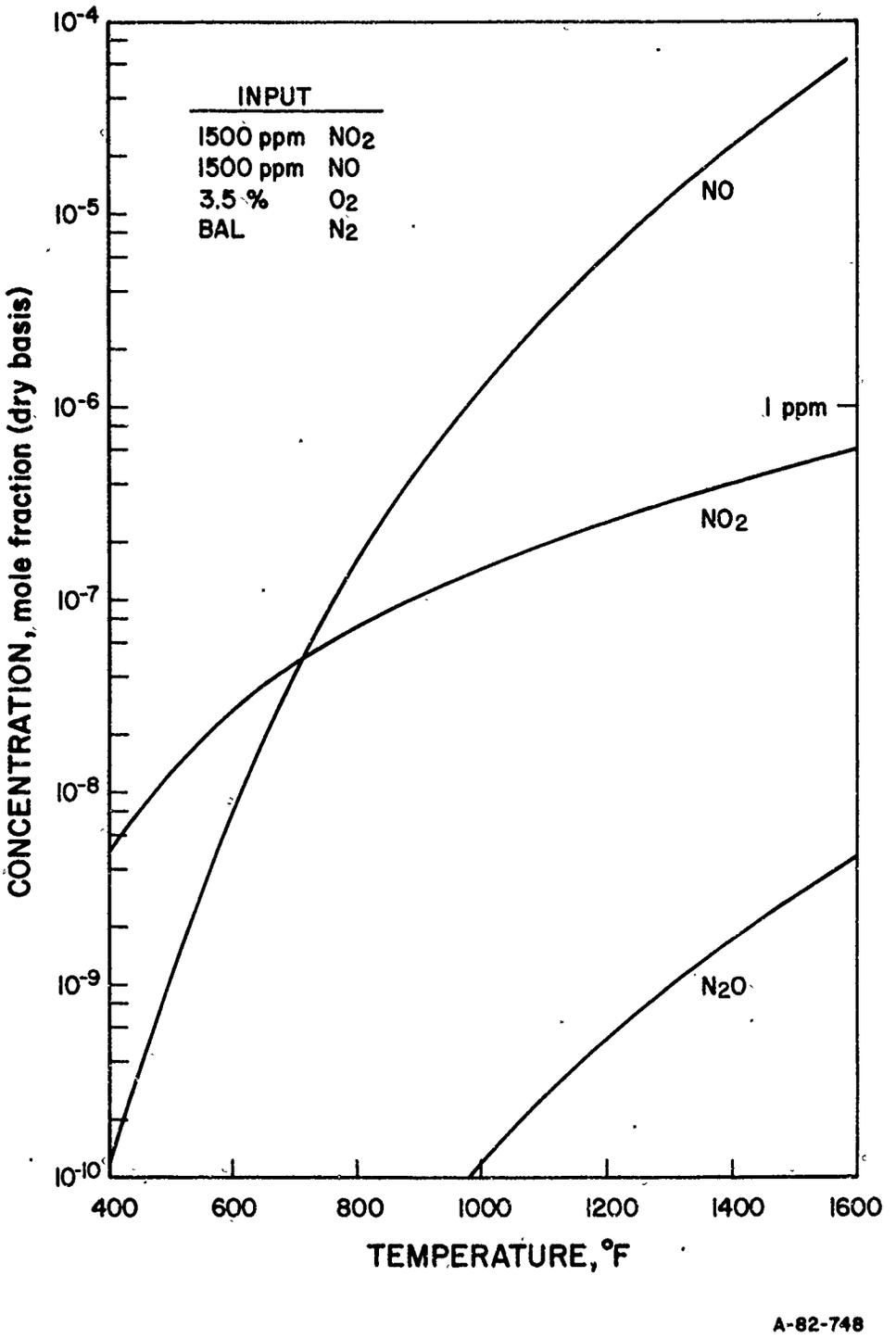

Figure 4-1. EQUILIBRIUM COMPOSITIONS – NO_x DECOMPOSITION

temperature, reaching 62 ppm at 1600°F (the highest temperature calculated because of catalyst limitations). These calculations show that the NO_x pollutants should theoretically decompose to concentration levels which are acceptable by today's Federal standards. Of course, the NO_x does not decompose to this extent in practice because of kinetic limitations.

4.6. Determination of Equilibrium Composition of C-H-N-O System

The third phase of the thermodynamic study was to determine the equilibrium concentrations of the various reactants and products expected in the combustion of nitric acid tail gas with methane, an alternative route to the simple decomposition described above. Appendix A presents the equations derived for machine computation of this equilibrium. Twelve compounds were considered as possible reactants or products of the reaction – N_2, O_2, N_2O, NO, NO_2, CH_4, CO, CO_2, H_2O, H_2, HCN, and NH_3. Higher hydrocarbons were not considered, although they would possibly exist in the concentration range we have calculated (down to 10^{-20} mole fraction). The feed composition was similar to that presented in the previous section, but humidified to 100°F. Methane was added in these calculations over a concentration range from 80 to 120% of the stoichiometric requirement.

Four graphs (Figures 4-2 through 4-5) illustrate the equilibrium concentration of major pollutants (NO, NH_3, HCN, and CO) as functions of the excess methane reductant at temperatures of 1000° and 1500°F. Five other graphs (Figures 4-6 through 4-10) present the concentrations of all the components as a function of temperature at various fuel utilizations.

The equilibrium concentration of the NO pollutant (Figure 4-2) is not significantly affected by the presence of methane in the feed stream until the methane concentration is above the stoichiometric requirement for combustion of the O_2 and NO_x. This suggests that the oxygen is burned out of the system before the majority of the NO reacts. The difference of the NO concentration at equilibrium between no reductant added and 95% of stoichiometric is only a reduction from 40 ppm to 10 ppm at 1500°F. However, at stoichiometric fuel addition, this concentration drops to 0.1 ppm, and at 5% fuel rich, the equilibrium NO concentration

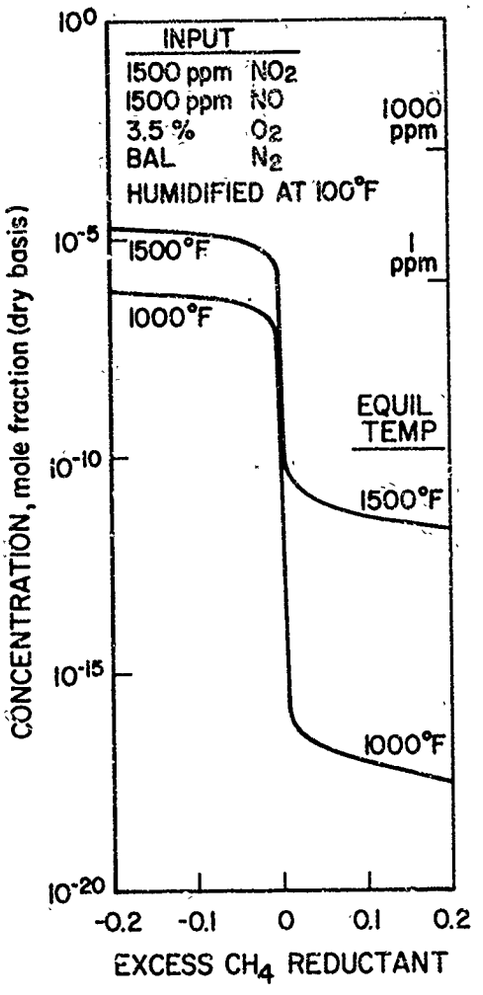

Figure 4-2. EQUILIBRIUM CONCENTRATIONS OF NO AS A FUNCTION OF EXCESS REDUCTANT

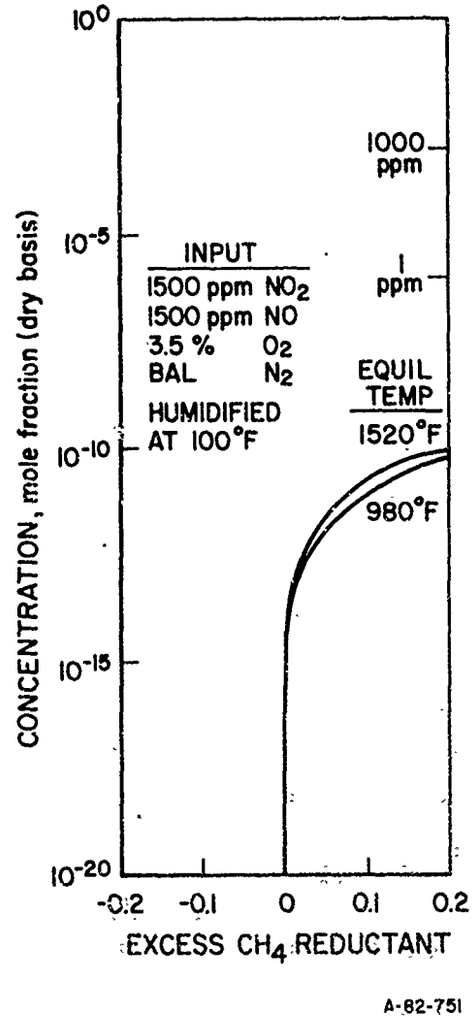

Figure 4-3. EQUILIBRIUM CONCENTRATIONS OF HCN AS A FUNCTION OF EXCESS REDUCTANT

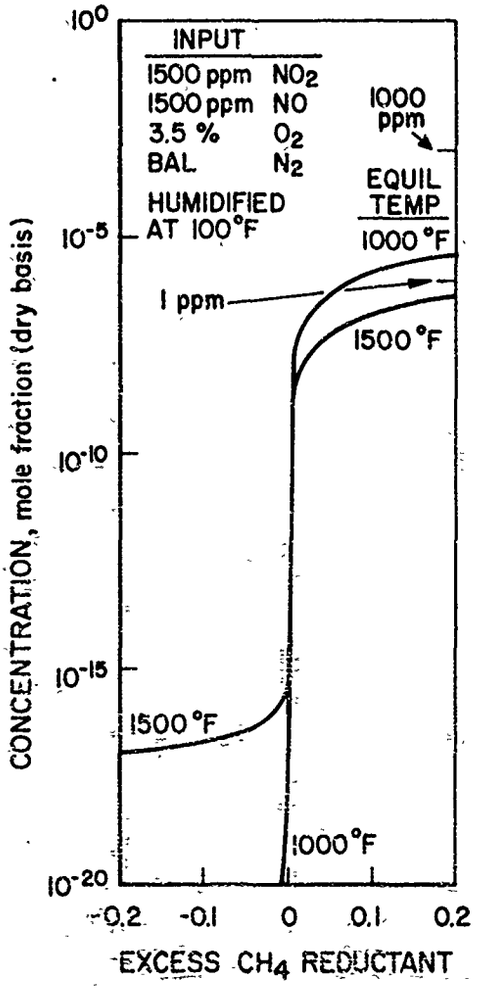

Figure 4-4. EQUILIBRIUM CONCENTRATIONS OF NH_3 AS A FUNCTION OF EXCESS REDUCTANT

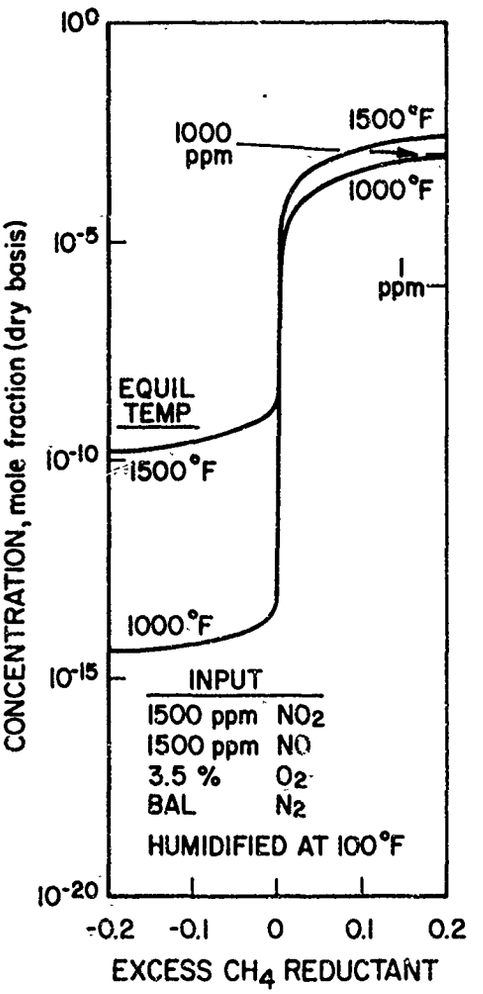

Figure 4-5. EQUILIBRIUM CONCENTRATIONS OF CO AS A FUNCTION OF EXCESS REDUCTANT

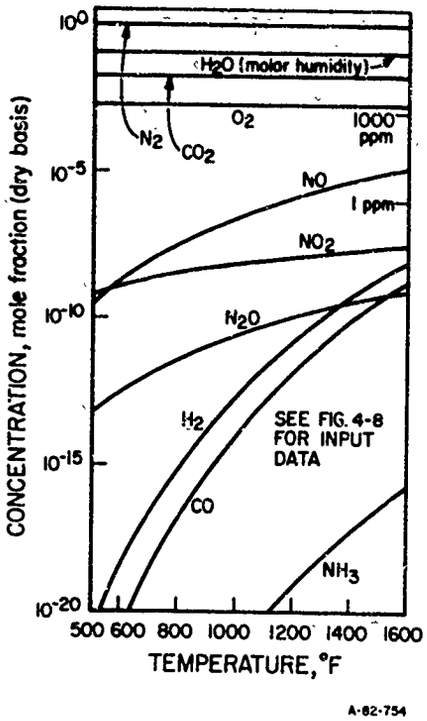

Figure 4-6. EQUILIBRIUM CONCENTRATIONS OF C-H-N-O SYSTEM, 5% LEAN FUEL

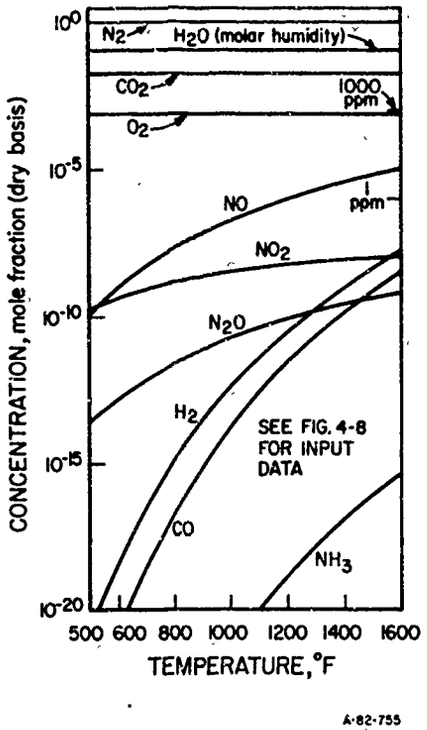

Figure 4-7. EQUILIBRIUM CONCENTRATIONS OF C-H-N-O SYSTEM, 2% LEAN FUEL

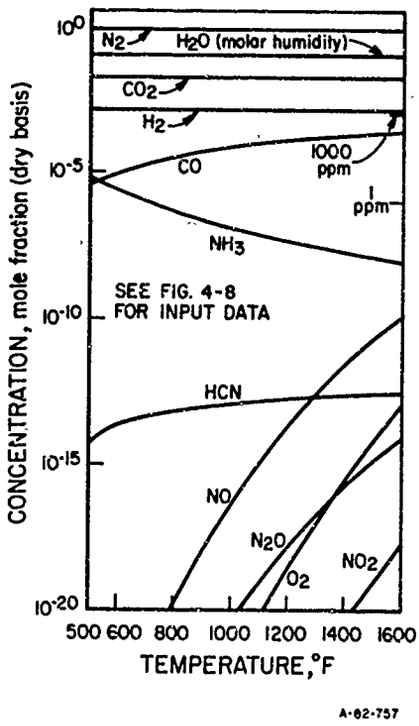

Figure 4-9. EQUILIBRIUM CONCENTRATIONS OF C-H-N-O SYSTEM, 2% RICH FUEL

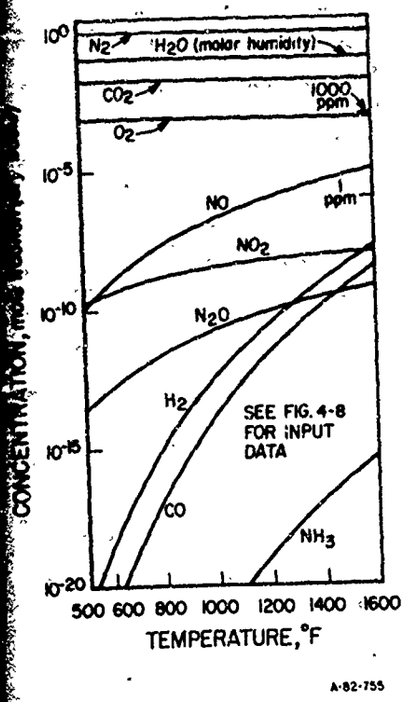

Figure 4-7. EQUILIBRIUM CONCENTRATIONS OF C-H-N-O SYSTEM, 2% LEAN FUEL

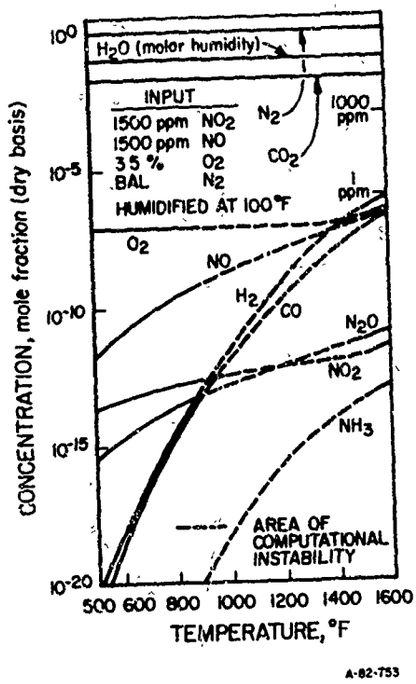

Figure 4-8. EQUILIBRIUM CONCENTRATIONS OF C-H-N-O SYSTEM, STOICHIOMETRIC FUEL

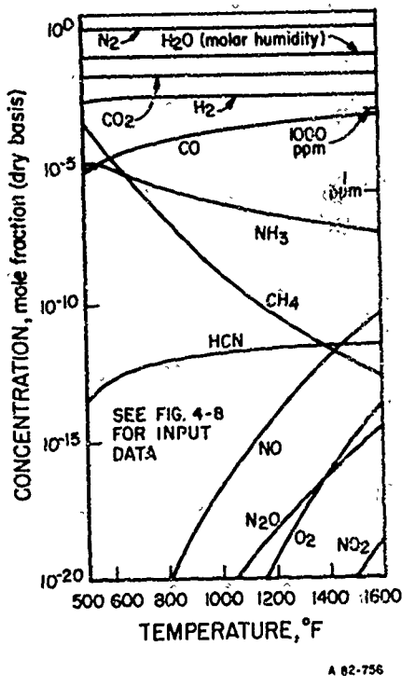

Figure 4-10. EQUILIBRIUM CONCENTRATIONS OF C-H-N-O SYSTEM, 5% RICH FUEL

is about 10^{-5} ppm. Excess reductant favors the decomposition of NO on a theoretical basis. This point is illustrated practically in the comparison of decolorization and abatement processes. In the decolorization process some methane is used for reducing the NO_2, but the NO is not significantly reduced until the reductant concentration exceeds the stoichiometric requirement.

The concentration of the other three pollutants, however, increases with excess reductant. The concentration of HCN (Figure 4-3) approaches 10^{-10} mole fraction at higher reductant usages. This concentration is significantly less than the generally accepted TLV (threshold limiting value) of 10 ppm concentration in air after dilution. Therefore, we do not expect HCN to be a problem in this work unless, by some kinetic mechanism, HCN is formed in concentrations 1 million times greater than expected.

Ammonia is also generated with excess reductant present (Figure 4-4). The NH_3 concentration increases as temperature decreases, but even at low temperatures the concentration is over an order of magnitude less than the TLV of 100 ppm. However, other investigators[5,6,7,8,9] have found that significant quantities of the NO are converted to NH_3 when using hydrogen reductant. Possibly the nitrogen atoms do not readily combine into an N_2 molecule at the catalyst site; the reduction can perhaps proceed to a greater extent than would be expected thermodynamically. This point has been checked in the experimental program. In a practical sense, however, the formation of NH_3 in the tail gas will generally not be noticed at a nitric acid manufacturing facility because of the strong general ammonia concentration in the area.

Carbon monoxide (CO) is the fourth major pollutant; it is generated in greater quantities at higher temperatures and higher excess methane concentrations (Figure 4-5). Theoretically, the CO concentration can exceed 1000 ppm in the tail gas if 20% excess methane is used. This concentration is 10 times greater than the TLV of 100 ppm but, of course, would be significantly reduced by dispersion in the air at the top of the stack. This expected concentration is only half of the 2000 ppm now permitted in large burner installations. Nevertheless, efforts should be made to run the reaction at lower temperatures and with lower excess reductant to minimize the manufacture of CO.

5. REACTOR MODELING – SIMPLE HEAT TRANSFER

5.1. Summary

A simplified heat transfer model has been developed to describe potential operating conditions if the regenerative device were used for heat transfer only. In other words, the chemical reaction is assumed to take place outside of the adiabatic regenerative heat exchanger, either as a heterogeneous catalytic reaction or a homogeneous, gas-phase reaction.

Operational regenerative heat exchangers can have efficiencies approaching 90%; high efficiencies are not acceptable in this system because extremely high temperatures result. Rather, operating conditions were determined in which efficiencies of approximately 50% were attained.

If conventional, noble metal catalysts are used in fixed-bed reactors, approximately 40-53% efficiency is required to achieve sufficient preheat temperature for ignition. The higher efficiencies are required with lower oxygen content than the tail gas stream. On this basis, the maximum temperature in the reactor will be about 1600°-2100°F, beyond the usable range of the noble metal catalysts. Therefore, simple regenerative heat exchange is not desirable with conventional noble metal catalysts unless other design features such as split beds, low oxygen concentration, interstage cooling, or other techniques are used to minimize the reaction temperature.

If non-noble catalysts are used in fixed-bed reactors, higher preheat temperatures are required for ignition with methane fuel. On this basis, approximately 48-60% efficiency is required in the adiabatic heat exchange device. In this case, the maximum temperature on the catalyst surface ranges from 1900° to 2400°F, perhaps above the usable temperature limit for these catalysts.

For a homogeneous reaction, an efficiency of about 54-67% would be required to achieve 1500°F preheat temperature. This should be sufficient temperature for initiation of the chemical reaction; adding the expected temperature rise of the exothermic reaction, temperatures of 2200°-2700°F might be expected. Our thermodynamic calculations were not extended to this temperature range; therefore, we cannot estimate if the equilibrium NO_x concentrations at these temperatures would be satisfactory.

The paragraphs above are based upon countercurrent regenerative heat exchangers. In general, cocurrent heat exchangers are not applicable to the system of external chemical reactions. In this system, the final exiting gas temperature is equal to the inlet temperature plus the adiabatic temperature rise. In a well-engineered heat cocurrent exchanger, the preheated gas temperature will approach the outlet gas temperature. Therefore, the system can have sufficient preheat gas temperature for the catalyst lightoff only if the feed gas contains sufficient oxygen so that the final gas leaving the cocurrent heat exchanger is above the lightoff temperature. With this quantity of oxygen in the tail gas, the maximum temperature in the external reactor will necessarily exceed the temperature limitations of the noble metal catalyst.

5.2. Objective

The purpose of this phase of the investigation was to develop a simplified model for regenerative, adiabatic, countercurrent heat exchange under conditions where an exothermic chemical reaction occurs in the process stream after the gas has been preheated, but before it is cooled in the exchanger. A secondary purpose is to introduce the heat transfer concepts which are used in the remainder of the reactor model.

5.3. Introduction

In this section of the report, we will consider the performance of a countercurrent, regenerative heat exchanger that operates with the same gas stream flowing in both passes of the exchanger; however, an exothermic chemical reaction occurs in the gas between the passes. As will be shown, this constraint results in a high-temperature reaction, even at moderate heat exchange efficiencies.

5.4. Discussion

5.4.1. General Adiabatic Heat Transfer

By definition of an adiabatic system, no heat is exchanged between the system and the surroundings. Generally, with higher temperature systems, this implies perfect insulation so that no heat is lost from the system (gases, reactors, or heat exchangers). Of course, this is an ideal situation but one that can be approached in practice when large quantities of heat are processed in relatively small equipment.

The concept of adiabatic heat exchange is shown schematically in Figure 5-1.

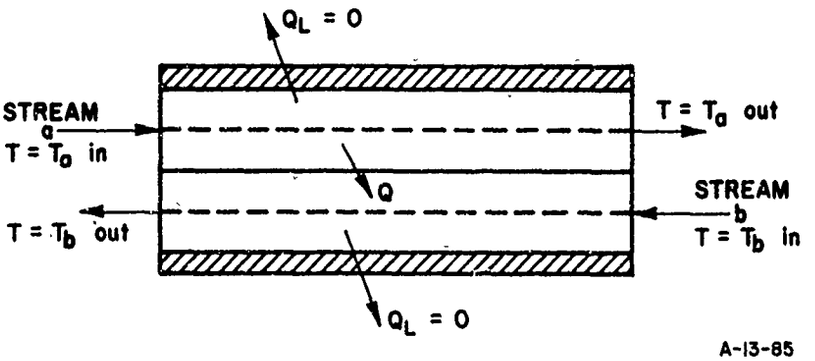

	STREAM a	STREAM b
MASS	m_a	m_b
HEAT CAPACITY	C_{pa}	C_{pb}
TEMPERATURE CHANGE	ΔT_a	ΔT_b
HEAT TRANSFER	$m_a C_{pa} \Delta T_a$	$m_b C_{pb} \Delta T_b$

Figure 5-1. SIMPLE ADIABATIC HEAT TRANSFER

In this drawing, stream a enters the system at an elevated temperature and stream b enters the system at a reduced temperature. They are heat-exchanged countercurrently (flowing in reverse directions) so that stream a is cooled and stream b is heated. Because the system is adiabatic, the total quantity of heat removed from stream a must appear in stream b or —

$$m_a c_{pa} \Delta T_a = m_b c_{pb} \Delta T_b \qquad (5\text{-}1)$$

One of the constraints in our process is that the gases in a and b are identical. Under this condition, $m_a = m_b$ and c_{pa} is similar to c_{pb}. Equation 5-1 reduces to —

$$mc_p \Delta T_a = mc_p \Delta T_b \qquad (5\text{-}2)$$

or the temperature rise of the colder stream must be equal to the temperature change of the hotter stream.

If the adiabatic heat exchange were perfect, the hotter gas stream would be cooled to the inlet temperature of the cooler gas stream. We can therefore define an efficiency of heat transfer for the system which is countercurrent, adiabatic, equal flow, and has an identical heat capacity:

$$\text{Efficiency} = \eta = \frac{T_{a\ in} - T_{a\ out}}{T_{a\ in} - T_{b\ in}} \qquad (5\text{-}3)$$

This definition of efficiency will be used throughout the rest of this report.

5.4.2. Adiabatic Heat Exchange With External Chemical Reaction

An interesting constraint is placed upon the system of heat transfer if the flowing gases undergo an external exothermic chemical reaction, as illustrated in Figure 5-2. Figure 5-2a illustrates this operation with the rotary regenerative heat exchanger. In this case, the feed gases enter the system at some inlet temperature, pass through the heat exchanger, and then undergo an adiabatic chemical reaction. The hot products of the chemical reaction pass back through the heat exchanger countercurrently, preheat the inlet gas, and leave the system. The entire system is assumed to be adiabatic: No heat is lost from the heat

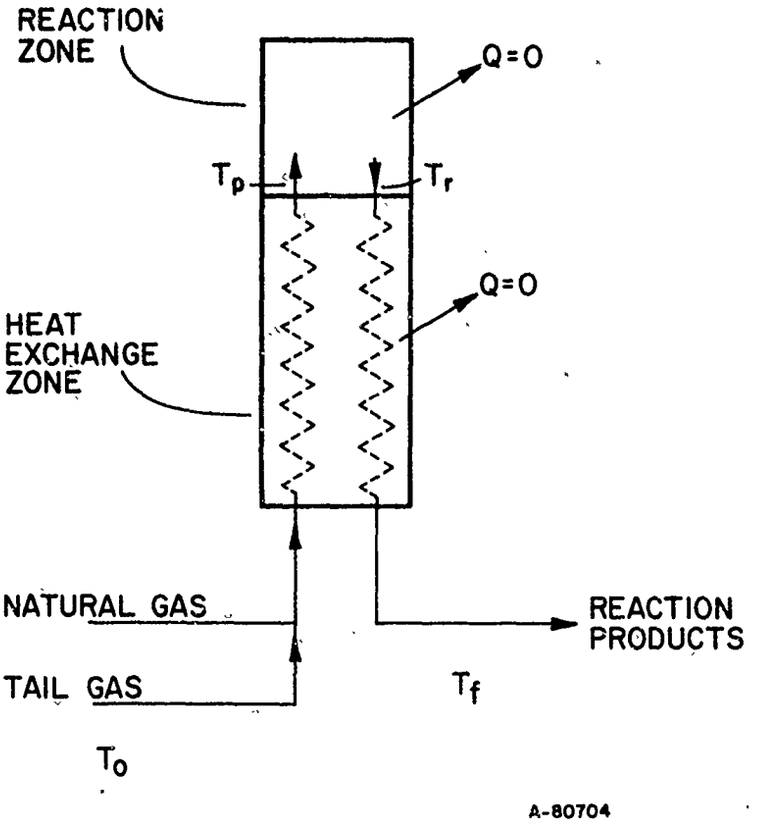

Figure 5-2. SCHEMATIC DIAGRAM OF COUNTERCURRENT HEAT TRANSFER WITH EXTERNAL CHEMICAL REACTION

exchanger or the reaction zone of the system. Under these conditions, the outlet gas temperature must always equal the inlet gas temperature plus the adiabatic temperature rise of the reaction.

In the system above, the mass of the two gas streams is identical and the heat capacities of these streams are usually similar. Therefore, the efficiency can be defined in terms of the temperatures in the system:

$$\text{efficiency} = \eta = \frac{T_r - T_f}{T_r - T_o} = \frac{T_p - T_o}{T_r - T_o} \qquad (5\text{-}3a)$$

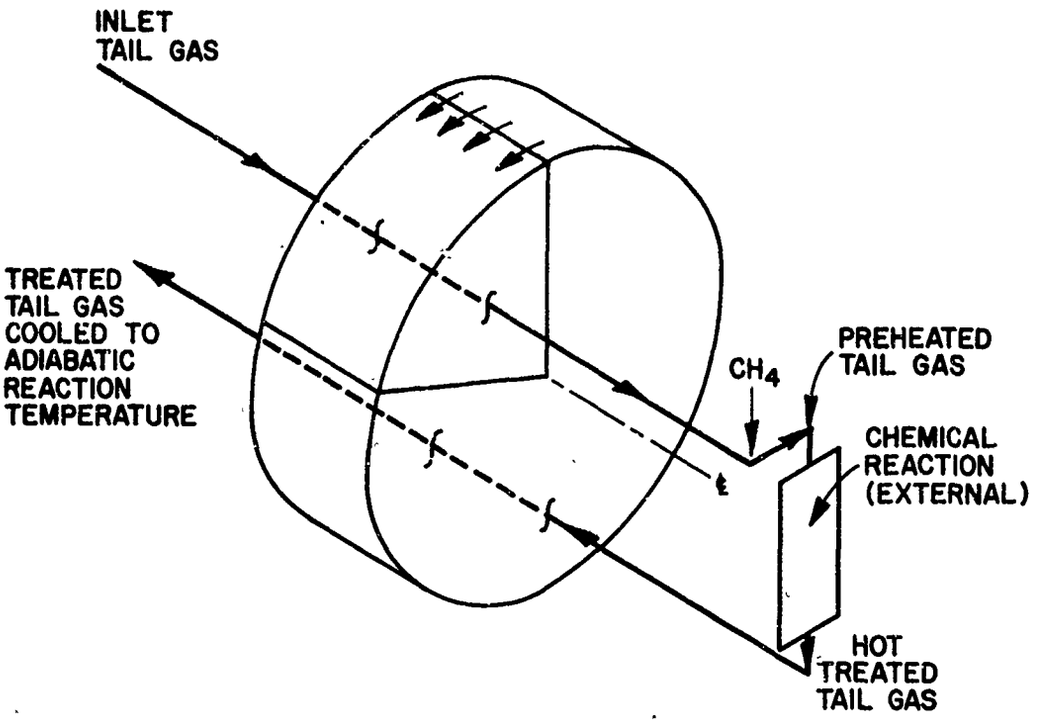

Figure 5-2a. OPERATION OF CYCLICAL BED AS COUNTERCURRENT HEAT EXCHANGER

This system is interesting because it feeds upon itself; higher reaction temperatures increase the preheat temperature, which in turn increases the reaction temperature.

In the simplest case of Figure 5-2, with no heat exchange, the heated gas temperature, T_p, is equal to the original inlet gas temperature, T_o, and the reaction temperature, T_r, is equal to the final outlet gas temperature, T_f. However, if heat exchange is permitted, T_p is greater than T_o. Because T_r is equal to T_p plus the adiabatic reaction temperature rise, T_r will also increase. Even with low efficiencies, therefore, T_r can become quite large, as will be shown later.

The definition of the efficiency, η (Equation 5-3a), may be manipulated to define the preheat gas temperature (T_p) and the maximum reaction temperature (T_r) in terms of the inlet gas temperature (T_o), the adiabatic temperature rise (ΔT_{ad}), and the efficiency (η):

$$\Delta T_{ad} = T_f - T_o = T_r - T_p \qquad (5\text{-}4)$$

$$T_p = T_o + \Delta T_{ad}\,(\eta/1 - \eta) \qquad (5\text{-}5)$$

$$T_r = T_o + \Delta T_{ad}/(1 - \eta) \qquad (5\text{-}6)$$

The equations above are used to determine the reaction temperatures for an adiabatic system in which the heat content of the exhaust products is recovered to preheat the reactants.

5.4.3. Adiabatic Heat Exchange With External NO_x Abatement Reaction

We shall now present the heat exchange efficiency required for the nitric oxide abatement process, assuming that the NO_x abatement chemical reaction occurs between the passes of a countercurrent heat exchanger. Three types of processes will be considered:

- In the first example, we will assume the use of conventional, noble metal catalysts in fixed-bed reactors. General practice, as confirmed by our data reported later (Section 7), indicates a preheated gas temperature requirement of 900°F for proper operation on these catalysts with methane fuel.

- In the second case, we will consider non-noble catalysts such as Co_3O_4. Our preliminary data indicate that these less-active catalysts require a preheated gas temperature of about 1200°F for operation with methane. These preliminary data, however, have not yet exhibited satisfactory NO reduction; the example is presented to indicate the potential and limitations of this catalyst system.

- For the third case, we shall assume sufficient temperature for a homogeneous, gas-phase reaction with methane. Past experience at IGT predicts that a preheated gas temperature of 1500°F would be required. Again, we do not know that satisfactory NO_x reduction can be achieved with this scheme.

Satisfactory reduction of NO_x from nitric acid tail gas requires that nearly all of the oxygen in the tail gas be reduced. This is the primary source of heat in the process. The temperature will rise approximately 237°F for each percentage point (by weight) of oxygen in the tail gas.

For proper bleaching of the nitric acid in the sorption tower, the tail gas should contain about 4% oxygen. Calculations below are made for 3% oxygen (713°F rise), 4% oxygen (950°F), and 5% oxygen (1187°F).

Table 5-1 presents the reaction temperature for each of the three preheat temperatures at the different oxygen concentrations. The preheat temperature of 900°F is used with noble metal catalysts. Even at the lowest oxygen concentration, the reaction temperature is above the operational limitation of these catalysts. Therefore, in this example, conventional beds are not satisfactory without severely limiting the oxygen concentration or operating two-stage systems. With the non-noble catalysts and 1200°F preheat, reaction temperatures of 1900°-2400°F are calculated. At this time, we do not know the upper temperature limitations of these catalysts. In the case of the homogeneous chemical reaction with 1500°F preheat, temperatures of 2200°-2700°F result. We have not extended our thermodynamic calculations to these temperatures, but we estimate that equilibrium would not permit satisfactory NO reduction.

Table 5-1. MAXIMUM REACTION TEMPERATURES*

Oxygen Concn, wt %	ΔT_{ad}, °F	Preheat Temperature, °F		
		900	1200	1500
3	713	1613	1913	2213
4	950	1850	2150	2450
5	1187	2087	2387	2687

* Inlet temperature = 100°F.

The proper preheat temperature with each system will be achieved if the heat exchange has the correct efficiency. Figure 5-3 indicates the preheat and reaction temperatures as a function of heat exchange efficiency when the tail gas contains 3 weight percent oxygen. Extremely high temperatures are possible if the efficiency approaches 80-90%, common for regenerative exchangers. In Table 5-2, the required efficiency, as calculated from Equation 5-5, is presented for the preheat temperatures and the three oxygen concentrations. These efficiencies of 40-66% are well within the range of available heat exchange equipment.

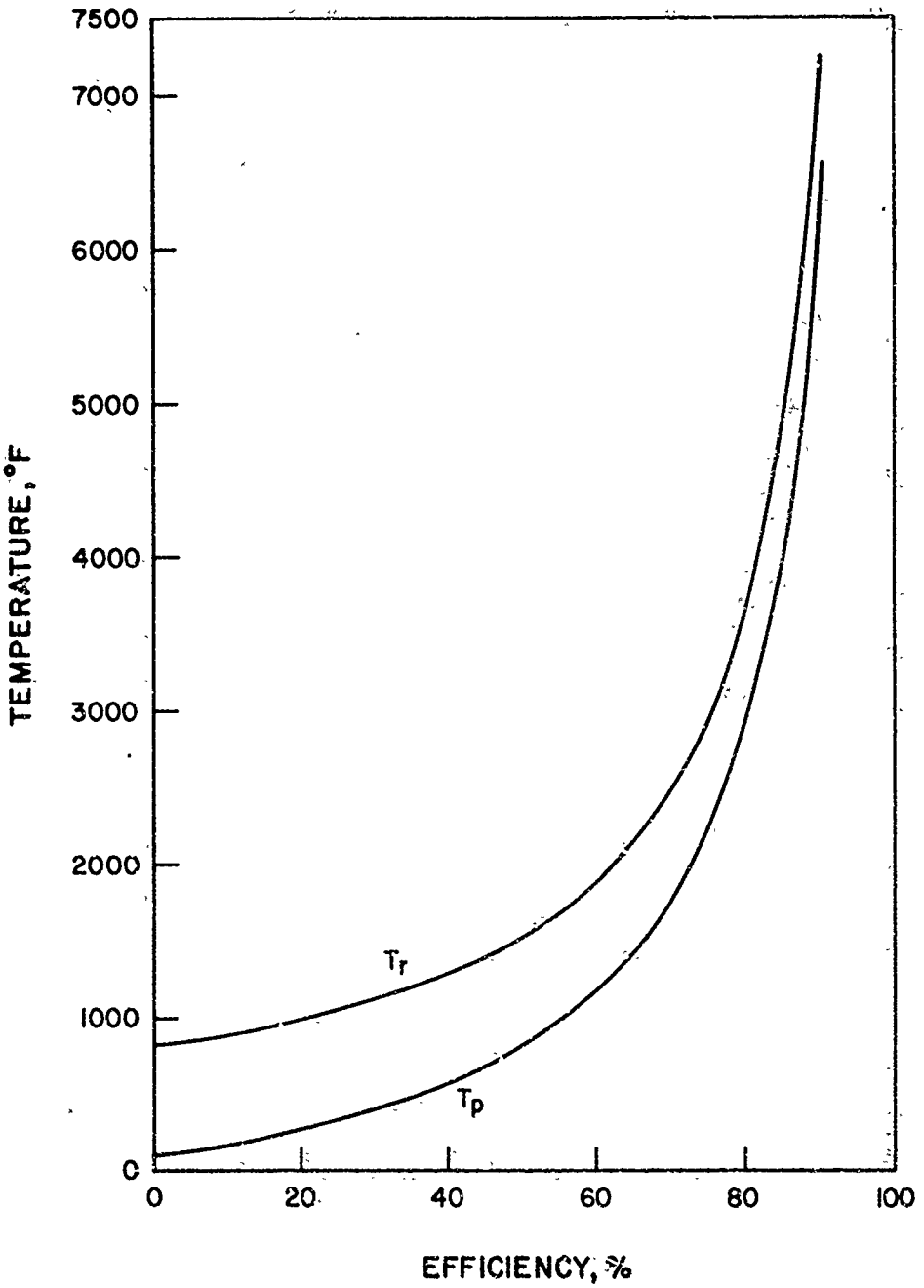

Figure 5-3. PREHEAT AND REACTION TEMPERATURES FOR SYSTEM OF FIGURE 5-2 WITH 3 WEIGHT PERCENT O_2 IN TAIL GAS

Table 5-2. REQUIRED HEAT EXCHANGE EFFICIENCY

Oxygen Concn, wt %	Preheat Temperature, °F		
	900	1200	1500
	%		
3	52.9	60.6	66.3
4	45.8	53.7	59.5
5	40.2	48.0	54.0

5.4.4. Design of Heat Recovery Equipment for Proper Efficiency

To this point, we have been discussing heat recovery in general. This heat recovery is usually accomplished in one of two modes – recuperation or regeneration.

In recuperation, the heat is transferred continuously through a solid wall which separates the two gaseous streams. Shell-and-tube or extended-area, compact heat exchangers are examples of the recuperative equipment are often used for heat recovery. However, with gaseous systems, large areas of recuperative equipment are generally required because low heat transfer coefficients are common.

In the alternative system, regeneration, the heat is transferred from one gas stream into a bed of solids, in which it is stored. Then, after a given time interval, valves are changed and the colder gases are passed over the same bed, withdrawing the stored heat from the solids. This regeneration of heat is similar to the regeneration of molecular sieve beds or spent fixed-bed catalysts.

In another type of regenerative heat exchange device, a fixed bed of solids is alternately located in the path of the hot gas and the cold gas streams. Consider a fixed disk of perforated ceramic, similar to the photograph of Figure 5-4, which rotates on its axis so that intersects two adjacent gas ducts, similar to Figure 5-5. With this device, the heat is transferred from the hot gas to the moving bed of ceramic, increasing the temperatures of the ceramic. When the ceramic moves out of the path of the hot gas stream and into the cold gas stream, it releases its heat to the colder gas. This system is quite commonly used for heat recovery from gas turbines and has been used for self-cleaning ovens, indirect-fired space heaters, etc., because very high heat transfer efficiencies can be achieved with small equipment.

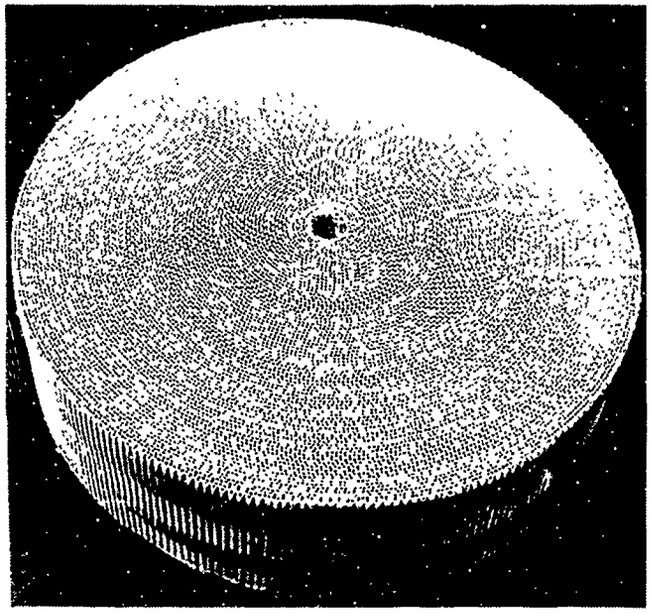

Figure 5-4. TYPICAL HEAT EXCHANGER WHEEL CONSTRUCTION

The heat exchange efficiency in the rotary regenerative heat exchanger can be directly related to the physical properties of the system. Appendix B derives this relationship.* In this derivation, we have assumed that the wheel rotates infinitely fast so that there is no temperature variation at any point in the solids as that point rotates through the cycle of the wheel. Therefore, this derivation indicates the average temperature of the solids in the wheel. The derivation also assumes that fully developed laminar flow conditions exist within the individual channels of the wheel. With the small channel sizes used, this assumption is reasonable unless discontinuities are present within the channels. This assumption permits

* More complete derivations, with fewer simplifying assumptions, are presented in Jakob[18] and Kays and London.[19]

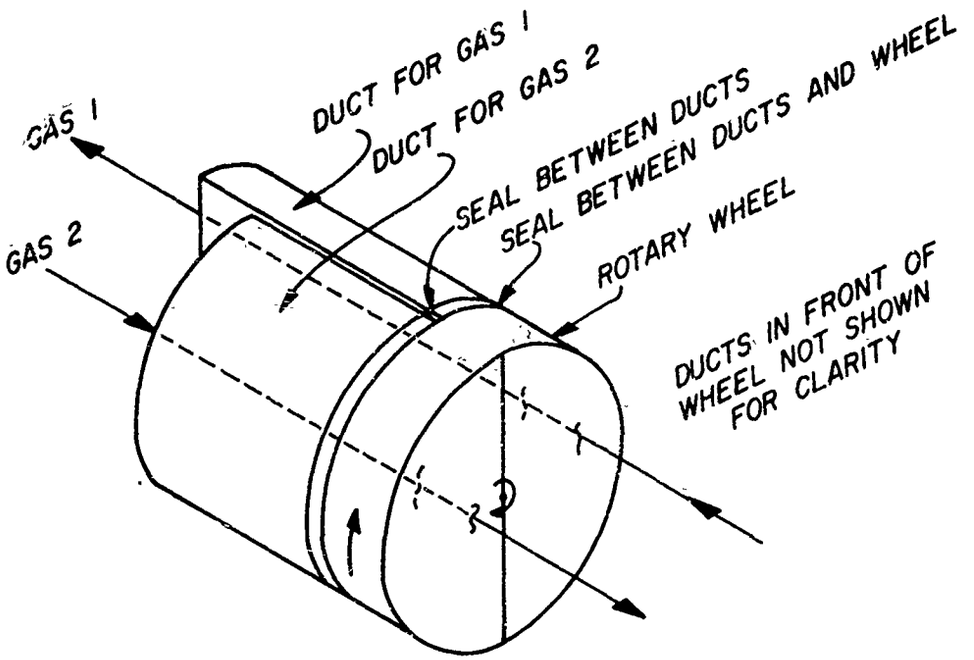

Figure 5-5. SCHEMATIC REPRESENTATION OF ROTARY REGENERATOR

the heat transfer coefficient to be directly related to the thermal conductivity of the gas, the hydraulic diameter of the channel, and the Nusselt number for the system – a dimensionless quantity which is essentially constant in laminar flow.

Figure 5-6 presents the regenerative heat exchange efficiency at a constant gas flow rate as a function of the wheel fraction which is operating in the preheat (or cooling) service, with parameters of channel diameter. The efficiency increases as the channel diameter decreases and is always a maximum when the preheat and cooling sections of the wheel are equal. Figure 5-7 presents the efficiency as a function of the division of the wheel heat exchanger at a constant channel diameter with parameters of gas flow rates. The efficiency increases as the gas flow decreases, again reaching a maximum at each flow rate at a 50:50 split between the two functions of the heat exchanger. Figure 5-8 presents

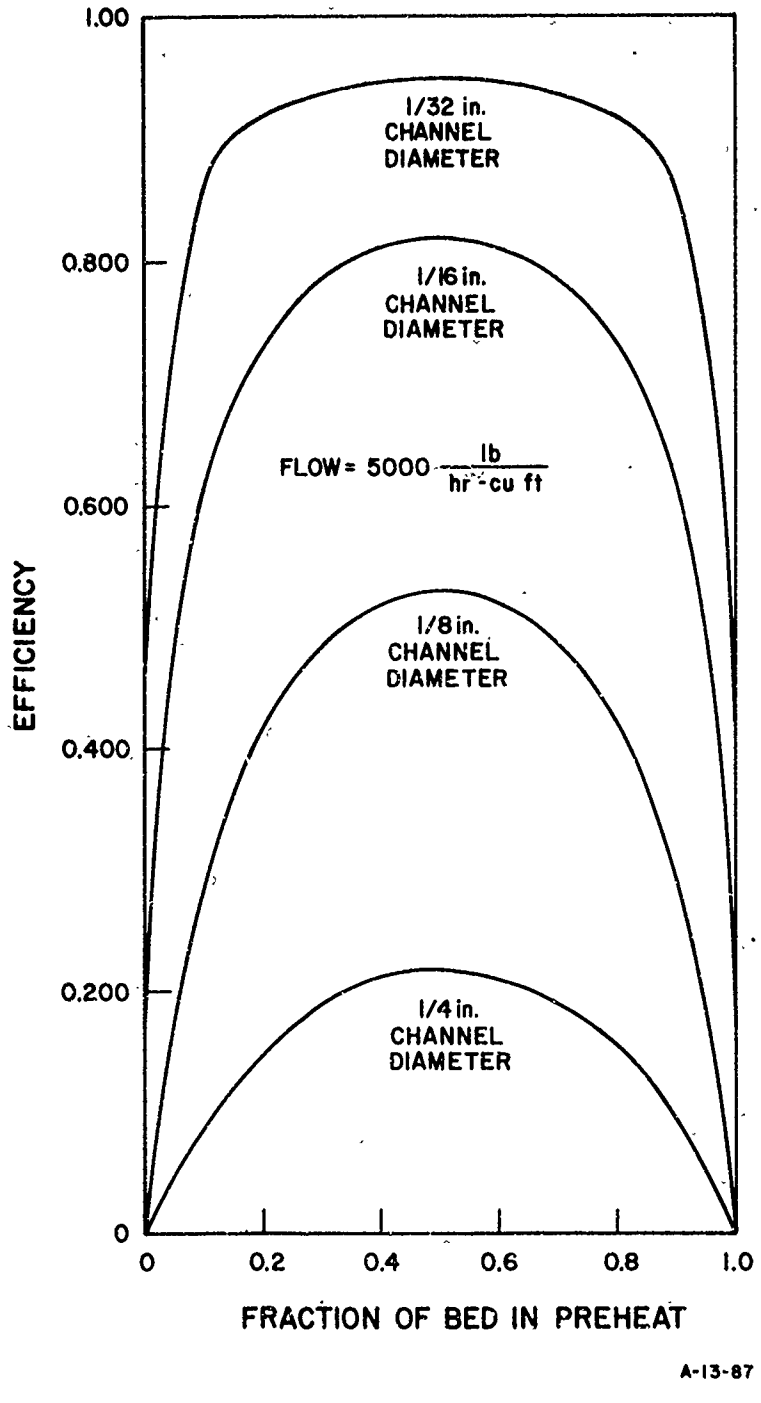

Figure 5-6. EFFICIENCY OF ROTARY REGENERATIVE HEAT EXCHANGER; FLOW = 5000 lb/hr-cu ft

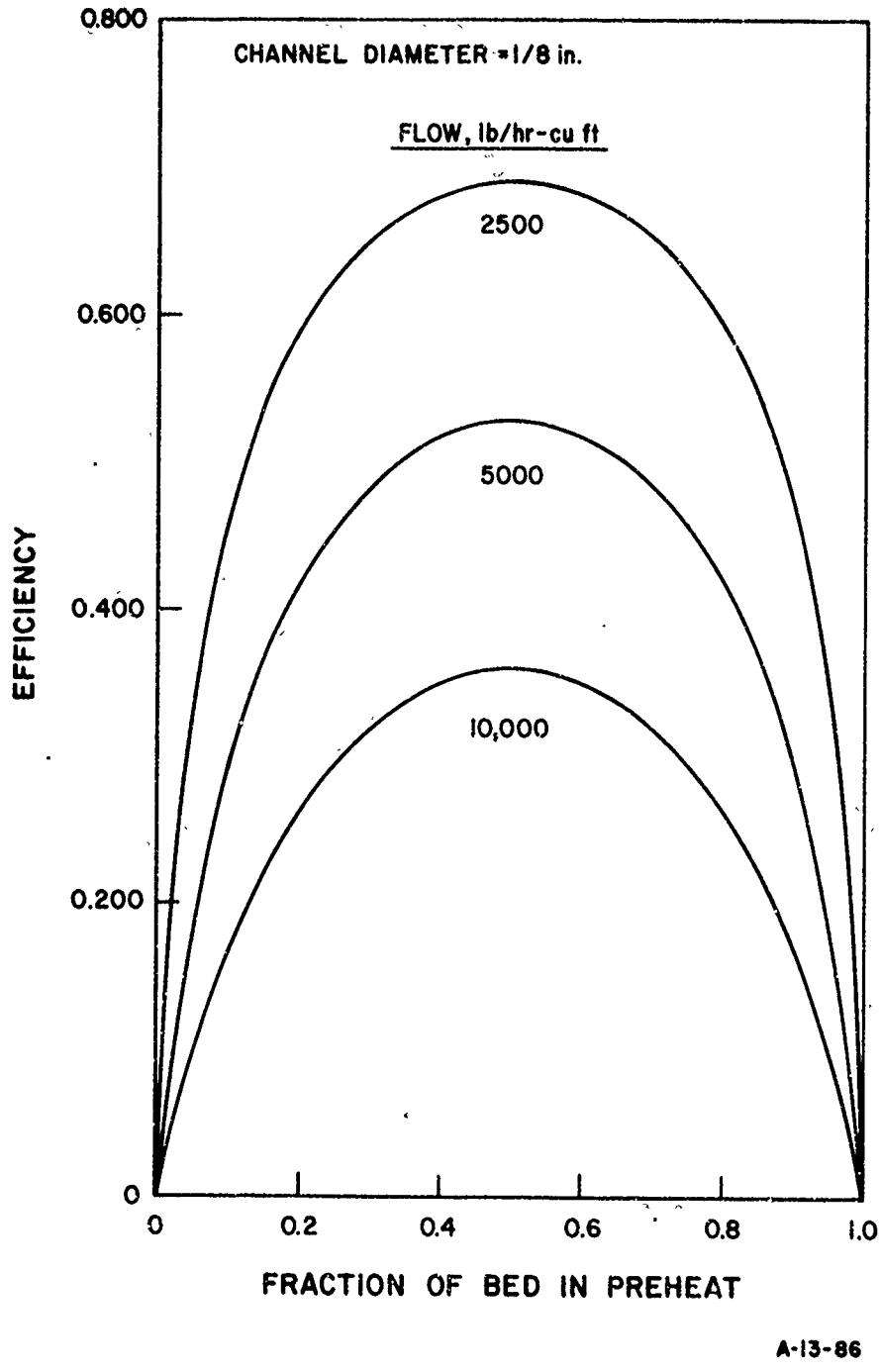

Figure 5-7. EFFICIENCY OF ROTARY REGENERATIVE HEAT EXCHANGER; CHANNEL DIAMETER = 1/8 in.

the maximum efficiency (at 50% preheat) as a function of the channel diameter with parameters of gas flow rate.

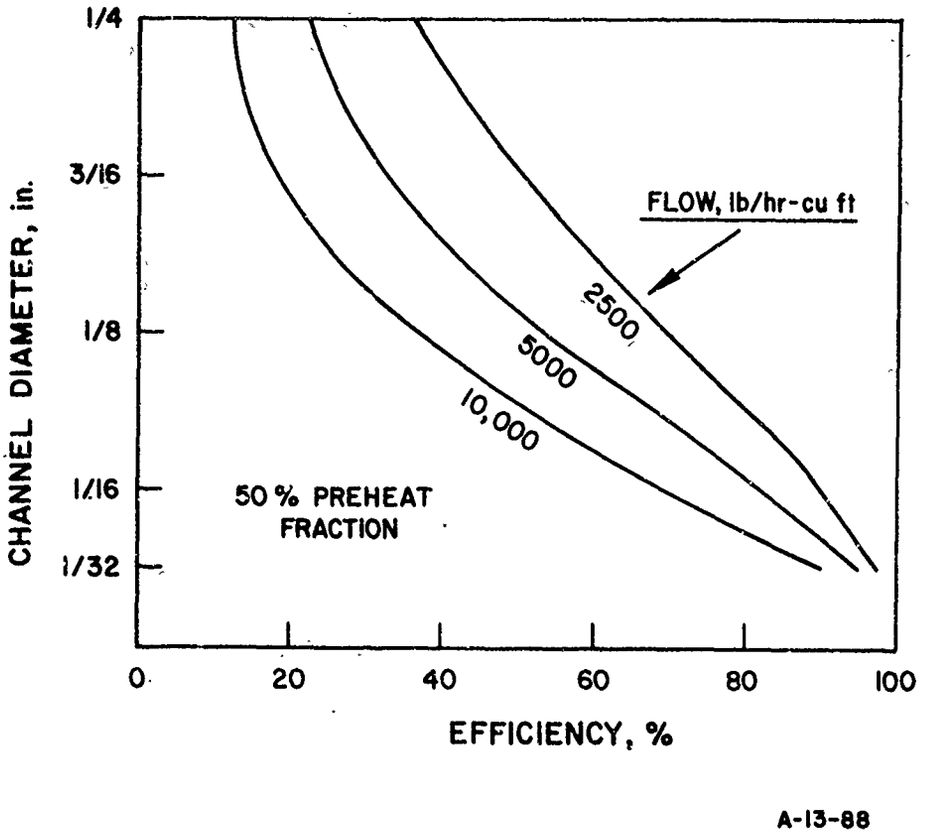

Figure 5-8. MAXIMUM EFFICIENCY

These three graphs indicate that relatively high heat transfer efficiencies can be attained with small channel diameters at lower gas flow rates. They also indicate that efficiencies required for Table 5-2 can be achieved by proper design of the rotary wheel heat exchanger.

Figure 5-9 presents the temperatures that would exist in a rotary heat exchanger under flow conditions that are similar to those used in the next section of this report. For this graph, we have assumed that the tail gas contains 3 weight percent O_2 for an adiabatic temperature rise of 713°F. The gas velocities are dictated by chemical reaction conditions,*

* Required for the simultaneous chemical reaction and heat exchange within the countercurrent regenerator, as calculated in Section 6.

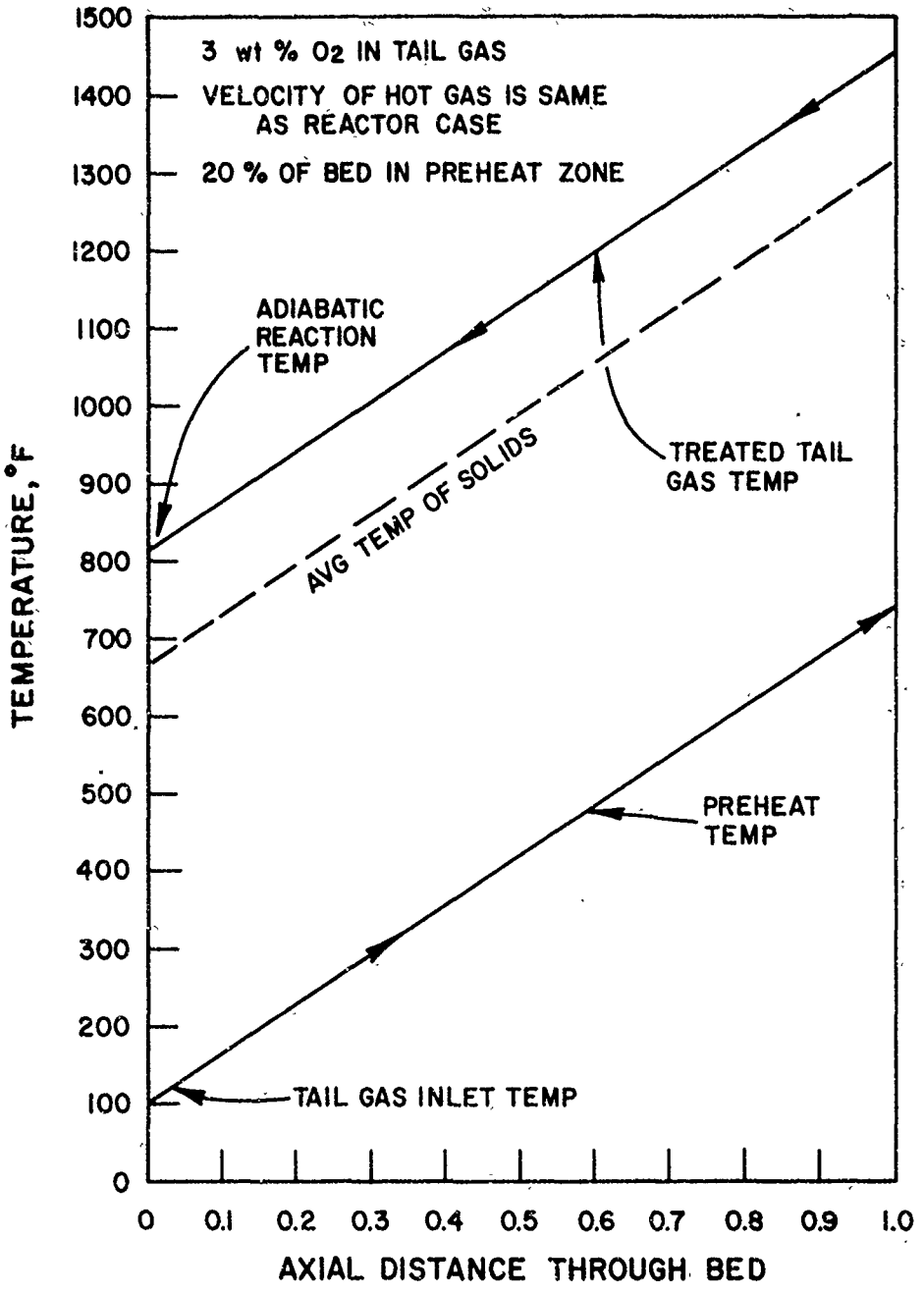

Figure 5-9. TEMPERATURES IN SIMPLE COUNTERCURRENT CYCLICAL HEAT EXCHANGE

and 20% of the heat exchange wheel is allotted to the preheat section. Figure 5-9 indicates that the tail gas enters the system at 100°F and rises linearly through the bed to a temperature of 740°F. After the reaction, the gas temperature is 1453°F, and this temperature drops to 813°F by the time it leaves the regenerative heat exchanger. The average temperature of the solids in the bed varies from 670°F at the cold face to 1315°F at the warm face of the heat exchanger. This is not necessarily an operable system, but serves to indicate the relationship of the temperatures in the system.

6. REACTOR MODELING – COMBINED REACTION AND HEAT TRANSFER

6.1. Summary

We have developed a simplified model to describe the operating conditions (temperature and reactant concentration) in an adiabatic reactor with internal heat recovery. The model is based upon a 3-pass reactor. Heat transfer is mandatory within each stage and among all stages. Chemical reaction is optional in any pass, and the size of any stage can be made vanishingly small. This model may therefore be simplified to cocurrent or countercurrent flow of reacting gases with the preheating gases; a simple, single-pass reactor with no preheating section; or a simple heat exchanger of the type that was discussed in Section 5.

Under cocurrent operation, the model predicts a nearly constant temperature profile in the solids if higher reaction conversions (greater than 90%) are achieved and the Lewis Number (or pseudo-Lewis Number) is in the range of 0.5 to 2. These conditions are expected with noble metal catalysts in the NO_x abatement reaction system. The temperature of the solids controls the chemical rate of the catalytic reaction; therefore, this system of operation permits the maximum controlled reaction rate and heat release. The system is operable with up to 5% oxygen in the tail gas without exceeding the maximum temperature limitations of the noble metal catalysts. External preheat of the tail gas for reaction initiation (lightoff) is not required. The cocurrent mode of operation appears ideally suited for use with conventional, noble metal, NO_x abatement catalysts.

In countercurrent operation, relatively high solids temperatures can be achieved for the start of the chemical reaction. This mode of operation may be desirable with non-noble, metal oxide catalysts with lower relative reaction rates and higher temperature limitations.

A complete 3-pass system, with reacting gases passing both countercurrently and cocurrently to the preheating gas, might prove more desirable for the non-noble catalyst under some conditions. Additional work is required, however, to determine these conditions.

When the model is reduced to indicate the conditions in a simple, single-pass reactor, it predicts the operations in the currently available reactor system.

In the program continuation, the model was expanded to incorporate variation of the reaction rate and the physical properties of the system as functions of temperature. The reaction rate of methane with oxygen was taken from Figure 7-10 and includes both kinetic and mass transfer effects. The revised model, when applied to the simple reactor concept, predicted bed temperatures at the gas exit end of the reactor which were high. Based upon the data in Section 7.11, severe catalyst degradation would be anticipated in this area. Also, the model predicted satisfactory operation at preheat temperatures which are lower than those practiced commercially; perhaps our experimental reaction rates are high compared to those realized with aged catalysts. When the modified model was applied to the cocurrent regenerative reactor concept, the essentially isothermal bed characteristic could still be achieved. Therefore, catalyst deactivation should be avoided in this mode. The deviation from a constant bed temperature, however, is more severe in this model when the operating conditions are incorrect. This deviation is caused by the compound effect of changing bed temperature and, consequently, changing reaction rate. The improved model predicts significantly better reactor operation with decreasing channel size; the effect of bed discontinuities, however, was not clear-cut.

6.2. Objective

The purpose of this phase of the program was to develop a simplified model for a regenerative reactor incorporating both exothermic chemical reaction and heat exchange. This model would predict the reactor operating conditions as functions of the mechanical and chemical parameters in the abatement system. With inputs of primary experimental data, this model could be used to design the prototype rotary regenerative reactor.

6.3. Introduction

The concept of the rotary regenerative reactor was introduced in Section 3 of this report. In essence, this device is similar to the simple heat exchanger discussed in Section 5, but the exothermic chemical reaction occurs within the device rather than externally. This may be accomplished for a catalytic reaction in a recuperative exchanger by catalyzing the walls of the exchanger in only the reaction pass, similar to Figure 6-1. For the regenerative wheel, one of the components of the reaction is introduced into the system after the preheat section, similar to the schematic diagram of Figure 6-2.

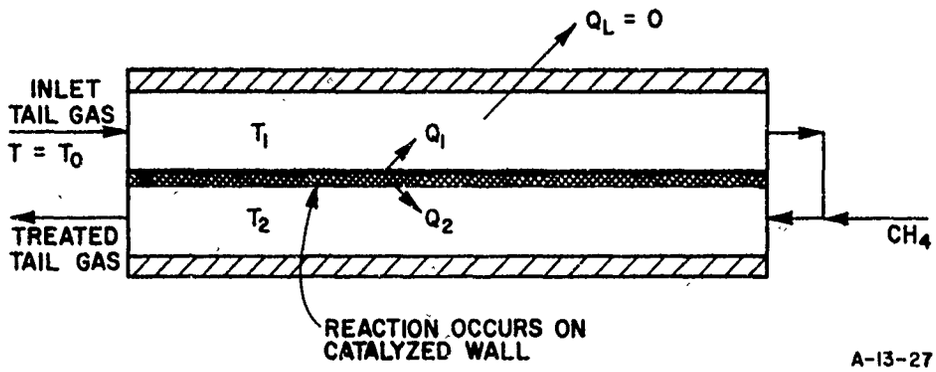

Figure 6-1. TWO-PASS COUNTERCURRENT REACTOR WITH INTEGRAL HEAT EXCHANGE

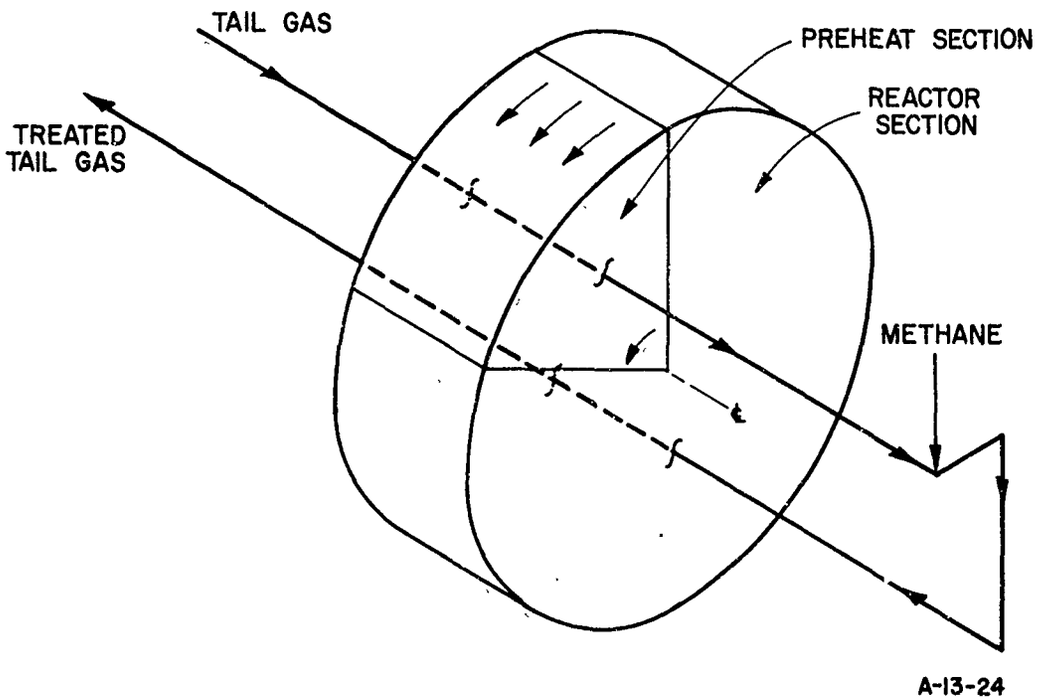

Figure 6-2. SCHEMATIC REPRESENTATION OF REGENERATIVE WHEEL REACTOR IN COUNTERCURRENT FLOW

In the combined reactor and heat exchanger, the reacting gases diffuse to the catalytic wall, react on the catalyst surface releasing the exothermic heat of reaction to the solids, and the reaction products counterdiffuse back into the bulk gas stream. The heat of the reaction is exchanged from the solids into both the reacting gas stream and the preheating gas stream according to the laws of convective heat transfer.

Figure 6-2 illustrates the reactor as it was originally conceived, with countercurrent flow of preheating and reacting gases. Consequently, this was the first reactor configuration to be modeled for machine computation. Subsequently, we generated a model with a 3-stream design, illustrated schematically in Figure 6-3.

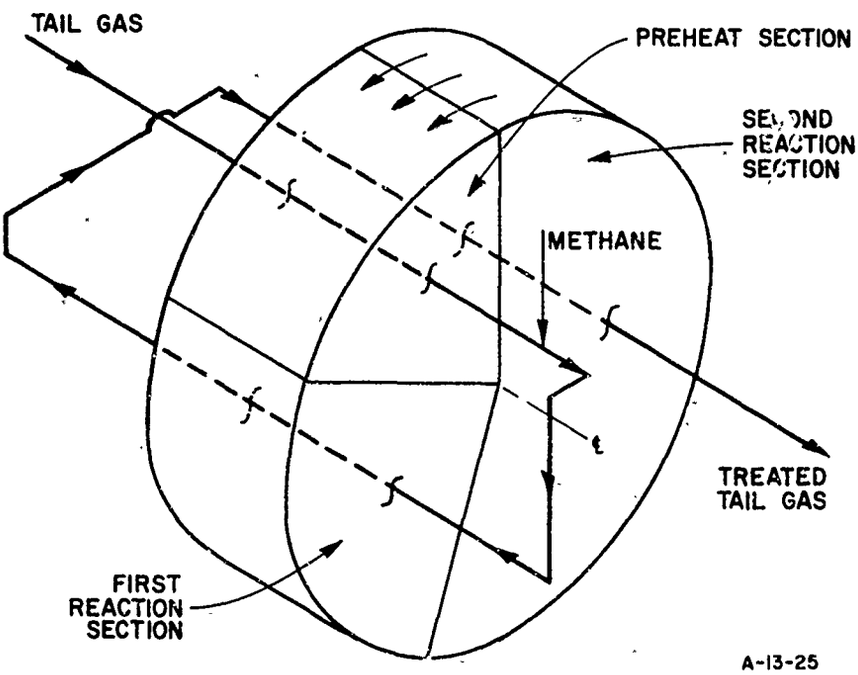

Figure 6-3. SCHEMATIC REPRESENTATION OF THREE-PASS REACTION SYSTEM AS APPLIED TO THE ROTARY REGENERATIVE REACTOR

By manipulation of the computational inputs, this model could be reduced to the original countercurrent configuration or to a cocurrent configuration in which the reacting and preheating gases pass through the reactor in the same direction. The model could be further simplified to predict

the performance of a simple, one-pass reactor or a heat exchanger without chemical reaction. In the more complex form, this model will permit reaction in the second two passes of the reactor, and the proportion of the reaction completion between these passes can be varied. Additionally, additional simple heat exchange area can be included on either face of the reactor.

The three-pass reactor had been conceived primarily for the more complex application; examination of the results of the countercurrent reactor had indicated that a third pass might be desirable to minimize the temperature range in the catalyst bed. The unexpectedly ideal behavior of the cocurrent reactor was discovered while manipulating the relative percentage of reaction permitted in the second two passes of the 3-stream reactor.

Although the reactor configurations were studied in the order presented above, we will present them in this discussion in the order of increasing complexity:

a. Simple reactor
b. Countercurrent reactor
c. Cocurrent reactor
d. 3-stream reactor

This order of presentation will permit increased understanding of the systems.

The derivations of the equations were prepared for machine computation, with several successive transformations of terms. The output of the machine computation was used for the various graphs presented in this section. The direct computer input, however, is too complex for explaining the system. We therefore rederived equations for each of these flow schemes (except the three-pass reactor) and reduced these expressions to the simplified forms presented in the following subsections.

The equations as derived are applicable for recuperative or regenerative operation. However, the small channels, required for reasonable heat and mass transfer coefficients, are representative of the physical parameters which could be obtained in the rotary regenerative wheel reactor. The recuperative reactor, however, should not be eliminated

from long-range consideration because these devices can be made with high areas of channel flow between parallel plates. Because the recuperative reactor is continuous, rather than cyclical, it offers a positive advantage of no temperature variation at a given point. Secondary advantages include the possibility to tailor the heat transfer and reaction areas separately, catalyzing only the reaction areas, and the absence of moving parts and seals. The primary disadvantage is the inability to compensate for catalyst age or process fluctuations by changing the relative fractions of the device in the preheat and reaction zones. This concept possibly also suffers from manifolding difficulties and cost penalties.

6.4. Assumptions

Several assumptions are implicit in the simplified mathematical model presented later. We first assumed an overall mechanism for the reaction, with the rate of diffusion controlling the chemical reaction rate. The chemical reaction occurs instantaneously when the diffusing reactants reach the catalyzed surface. The heat of the reaction is released in that surface and is then transferred to the gas streams by convection. This model implicity assumed a honeycomb-type catalyst with fully developed laminar gas flow. This assumption permitted calculation of the heat transfer coefficient from the Nusselt Number, which is known to be constant under these conditions. The assumption of the diffusion control was not restrictive; the equations which govern a first-order chemical reaction (of the type expected for this system) are identical to those for diffusion-controlled mass transfer, as will be shown in a later section on the experimental reaction kinetics. The model is therefore applicable to diffusion or chemical kinetic rate control. The restriction of channel flow is also not restrictive because the primary catalysts for the service are supplied in this form.

The equations are based on an adiabatic reactor, with no heat loss from the system. This assumption is valid because the expected high reaction rate, per unit of reactor volume, would result in minimal heat loss from the system.

The equations assume that the cyclical reactor operates at infinitely fast rotational speeds. Therefore, the temperatures derived in this section are those which are the average throughout the cycle. A more rigorous derivation of regenerative heat transfer, using real cycle times, indicates that the heat transfer efficiency will be decreased. Using the parameters of our system and a rotational speed of 1/2 rpm, the heat transfer efficiency falls by 5% when compared with the operation at infinitely fast speed.

Because the same wheel structure rotates through both the reaction and preheat zones, the physical configuration of the channels is identical. Also, the entire surface of the preheat, as well as the reaction section of wheel, is catalyzed. Therefore, the methane fuel is not added to the system until the rest of the tail gas stream has been preheated in the first section of the wheel. For our calculations, we assumed that this mass of methane was negligible and that this fuel injection did not affect the temperature of the flowing stream. We also assumed that the heat capacity of the reaction products was identical to the incoming tail gas. All of these assumptions are reasonable, considering the low concentration of the reactants. This system also required that the natural gas does not immediately react with the preheated tail gas. Rather, the only reaction takes place heterogeneously on the catalyzed surface and that reaction is complete to CO_2 and H_2O.

The primary limitation in the model is the assumption of constant chemical and physical properties within the reactor, irrespective of temperature variations. This assumption was warranted at this stage of the program: The simplified model would be adequate for evaluating the feasibility of the reactor concept. The model becomes significantly more complex by including temperature effects, and we elected to postpone this additional effort in the preliminary phase of the development.

For each computation, we assigned values for the temperature-sensitive variables — heat of reaction, thermal conductivity of the gas, heat capacity, and density. We also specified the reaction rate as a function of the heat transfer rate. As will be shown, a nearly constant bed temperature can be achieved under readily obtainable conditions of cocurrent operation. In this instance, variation of the parameters with temperature is unnecessary. Similarly, if the chemical reaction is strictly diffusion-controlled, the rate of reaction will not vary severely with temperature and the approximation is reasonable. However, these

parameters must be included as functions of temperature in an improved system model if we are to deviate significantly from the limitations above.

6.5. One-Pass, Simple Reactor

The case of the simple, one-pass reactor is presented here to introduce the concept of simultaneous reaction (and heat generation) on the catalyzed solids and heat transfer from the solids to the gas. This is the simplest reaction case, and it provides a basic understanding of the more complicated concepts which will be presented later.

Consider the following system: A nitric acid plant tail gas with a known weight fraction of oxygen (ξ_o) and excess methane enter a fixed-bed honeycomb catalyst at an inlet temperature of T_0. The methane and oxygen diffuse to the walls of the honeycomb where they react on the catalyst, leaving the heat of reaction in the honeycomb solids. The CO_2 and H_2O products counterdiffuse back to the bulk gas stream. Simultaneously, the heat of reaction is transferred from the solids to the main gas stream by the laws of convective heat transfer.

In this system, the rate of reaction is controlled by the overall rate of reactant and product diffusion, k_g,* and the heat transfer is governed by the heat transfer coefficient, h. Equations for the temperature of the solid, T_s, and the temperature of the gas, T, are presented in detail in Appendix C-1. The results are —

$$T - T_0 = \frac{H_r}{C_p} \xi_o \left(1 - e^{-\alpha x/L}\right) \tag{6-1}$$

$$T_s - T_0 = \frac{H_r}{C_p} \xi_o \left[1 - (1 - \lambda)e^{-\alpha x/L}\right] \tag{6-2}$$

---

* As shown in Section 7, the reaction rate may be governed by first-order kinetic laws with the same equations and results.

where —

C_p = gas heat capacity, Btu/lb gas-^{0}F

h = heat transfer coefficient, Btu/hr-sq ft-^{0}F

H_r = heat of reaction, Btu/lb reactant

k_g = mass transfer coefficient, cu ft/hr-sq ft

L = reactor length, ft

T = gas temperature, ^{0}F

T_0 = initial gas temperature, ^{0}F

T_s = solids temperature, ^{0}F

x = distance into reactor, ft

α = ln ξ_o/ξ_f, dimensionless

λ = Lewis Number = $k_g C_p \rho/h$, dimensionless

ρ = gas density, lb/CF

ξ_o = initial reactant concentration, wt fraction

ξ_f = final reactant concentration, wt fraction

These equations present the temperatures of the gas and the solid honeycomb as functions of the axial length down the bed and the parameters of the system.

The above expressions were derived for this report; the figures presented later were calculated by simplification of the 3-pass system (Subsection 6.8) and machine computation.

Figure 6-4 presents the temperature of the solids in the simple, single-pass reactor as a function of the relative bed length with parameters of the Lewis Number, the ratio of the mass diffusivity to the thermal diffusivity in the system. For this graph, we assumed an inlet gas temperature of 100^{0}F and 5.0 weight percent oxygen in the tail gas. At a Lewis Number of 1.0, the bed temperature is independent of bed length, as would be expected from Equation 6-2. The bed temperature is equal to the adiabatic reaction temperature that would exist at 100% conversion of the reactants. This may be only slightly above the

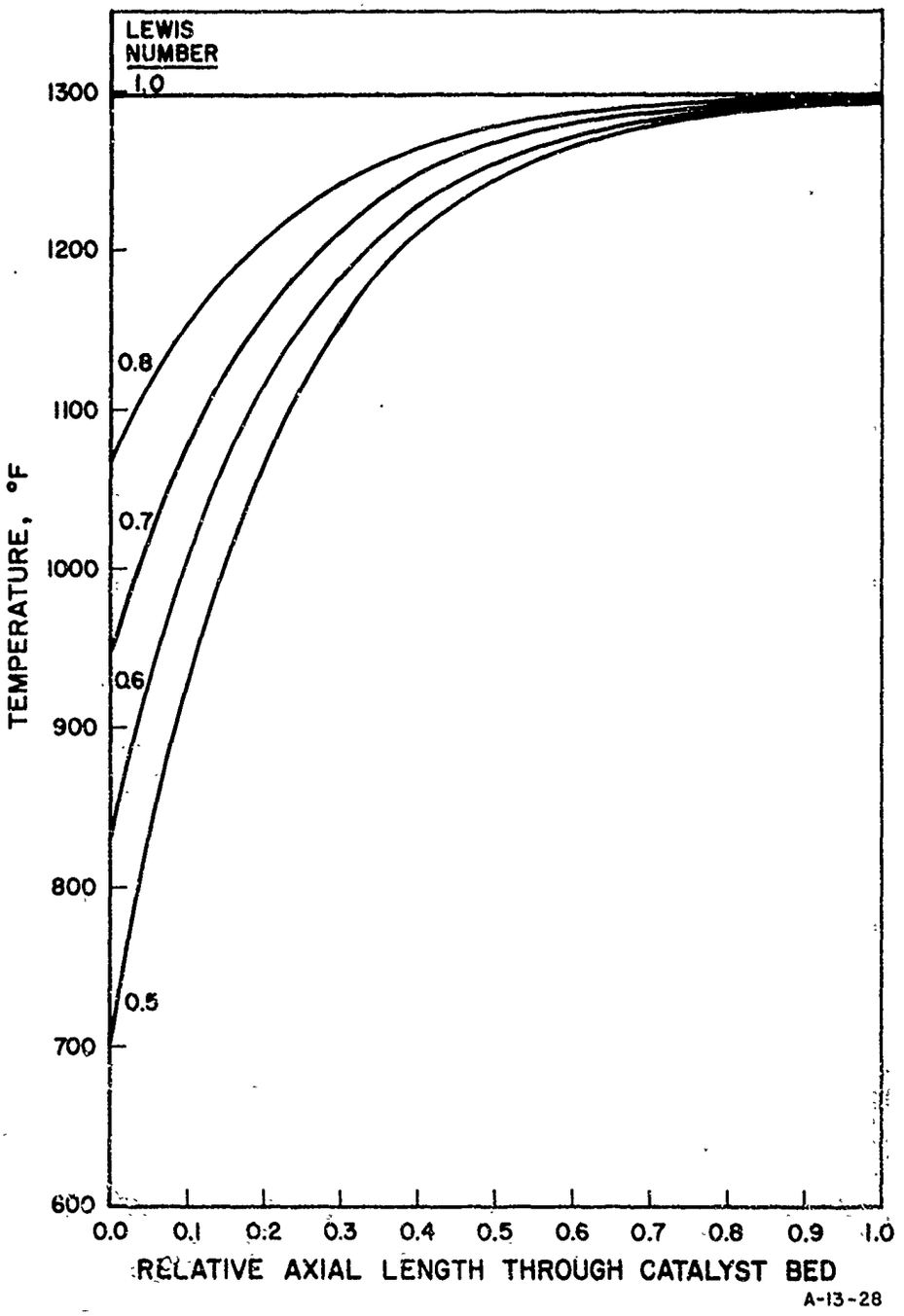

Figure 6-4. BED TEMPERATURE IN SIMPLE REACTOR

adiabatic reaction temperature (Equation 6-1 at x = L) at high conversion, but could be 120°F above the adiabatic reaction temperature at only 90% converted.

At lower Lewis Numbers, the temperature of the catalyst at the beginning of the bed can be significantly less than the outlet temperature. The Lewis Number is a measure of the relative mass to thermal diffusivity of this system. At a lower Lewis Number, the reactants cannot diffuse to the catalyst as fast as the heat of reaction can be carried away. However, at steady state, the heat released on the solids must be exactly compensated by the heat removed from the solid. Therefore, with a higher relative heat transfer coefficient, the temperature difference between the solids and the gas must decrease (T_s must be lower) because of the reduced heat generation rate.

While the gas passes through the bed, its temperature rises because of the heat transfer, and the solids temperature correspondingly rises. At the exit of the bed, the solids temperatures are greater than the adiabatic reaction temperature and this difference is accentuated by lower fractional conversions and higher Lewis Numbers. For lower Lewis Numbers, longer beds are required to achieve the same fractional conversion because the reaction rate is lower (lower k_g). However, Figure 6-4 was prepared on the basis of relative bed length for purposes of comparison.

The Lewis Number for the diffusion of methane in air at standard temperature and pressure is about 0.82. Using the scale-up factors (discussed in Section 7) for the effect of temperature upon diffusivity, the expected Lewis Number is 0.87* at 1200°F. When this Lewis Number is substituted into Equation 6-2, the initial solids temperature for Figure 6-4 should be 1150°F. Therefore, the simple reactor should operate in this system without any preheat if the reaction is strictly diffusion-controlled. However, as illustrated by the data in Section 7, the chemical kinetics significantly reduce the rate of reaction. Even operating at 7 atm pressure, the reaction rate constant is less than 80% of the mass transfer coefficient; therefore, the pseudo-Lewis Number, based

---

* This value of the Lewis Number, in conjunction with the channel diameter and the theoretical Nusselt Number of 4.0, yields a k_g which is identical to the experimental value reported in Section 7.

upon the average rate constant, is 0.68. With this pseudo-Lewis Number and 5% oxygen in the tail gas, the initial solids temperature is 916°F. Because the pseudo-Lewis Number falls to less than 0.4 at this temperature, the fixed-bed reactor is inoperable without excessive oxygen concentrations in the tail gas or preheating the inlet feed. This effect therefore checks operational practice of fixed-bed reactors.

Figure 6-5 was drawn to indicate the probable temperature profile in an operable fixed-bed reactor with 900°F tail gas preheat and an oxygen concentration of 2.2 weight percent (1.9 volume percent).

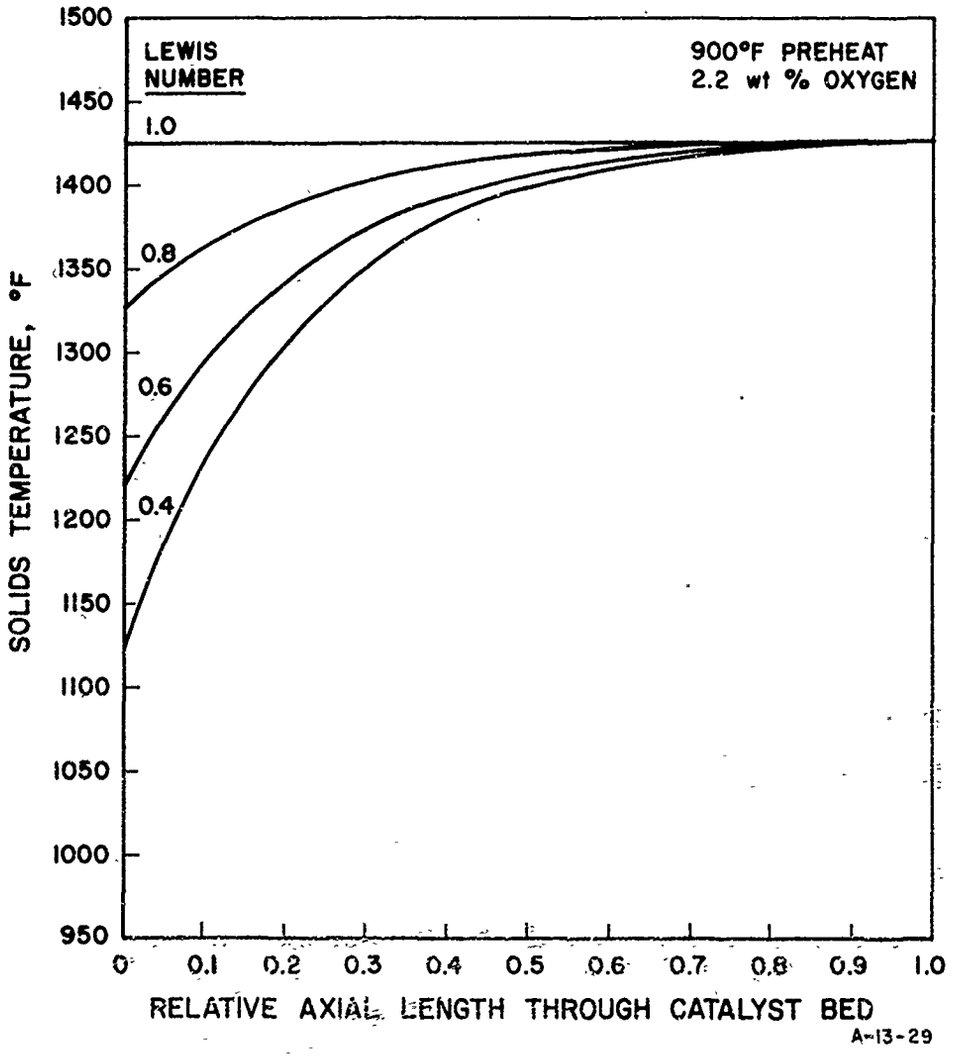

Figure 6-5. CONVENTIONAL FIXED-BED REACTOR SOLIDS TEMPERATURE PROFILE

Under these conditions, the adiabatic reaction temperature is 1422°F, near the upper limit of conventional noble metal catalysts. In this case, the bed temperature varies from about 1250° to 1425°F as the Lewis Number increases from 0.7 to 0.8. This analysis indicates that the tail gas preheat could be decreased and the oxygen content increased after start-up in a conventional fixed-bed reactor.

6.6. Two-Pass Reactor – Countercurrent Flow

This concept was the preliminary basis for the project. It promised adequate preheat of the inlet tail gas for system lightoff, satisfactory reactor exhaust temperatures for the expansion turbine, and separation of the abatement section of the plant from the ammonia burner. Subsequent work with the general model indicated that other reaction modes were preferable. However, this was the first system developed, and a large number of the basic graphs relate specifically to this mode of operation.

Consider a system which is identical to the simple, adiabatic, countercurrent heat exchange problem discussed in Section 5, except that the exothermic chemical reaction occurs within the second pass of the exchanger (now a reactor), instead of externally. Figure 6-6 illustrates this concept schematically, and Figure 6-7 is an isometric diagram of a countercurrent rotary regenerative reactor for this application.

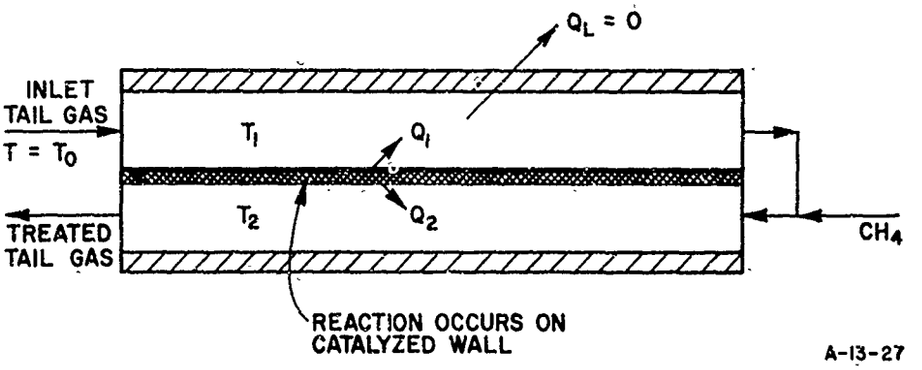

Figure 6-6. TWO-PASS COUNTERCURRENT REACTOR WITH INTEGRAL HEAT EXCHANGE

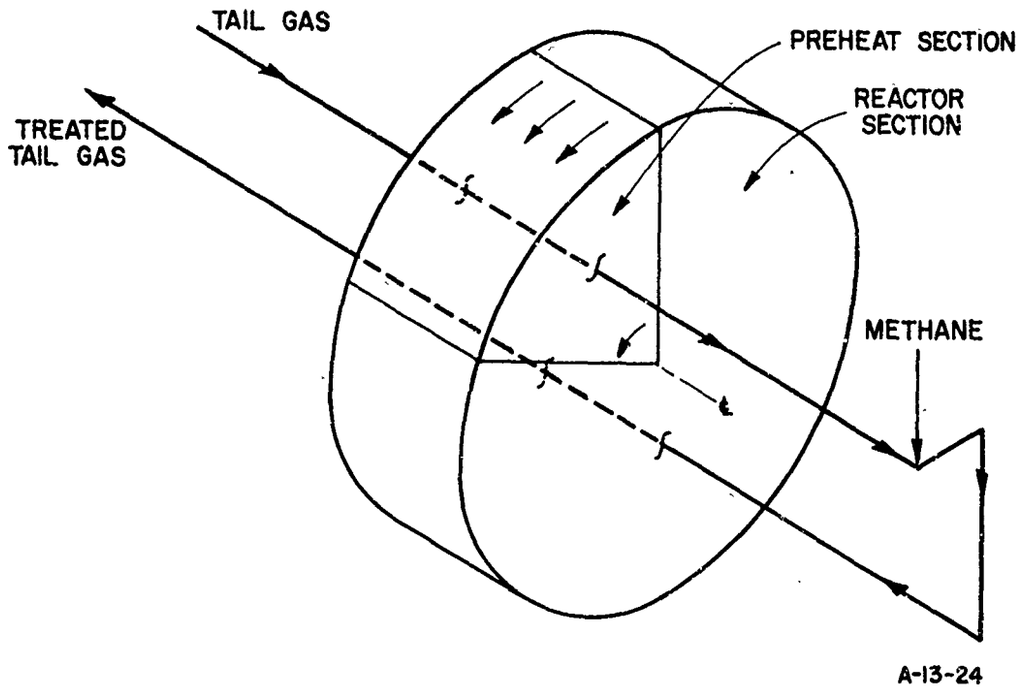

Figure 6-7. SCHEMATIC REPRESENTATION OF REGENERATIVE WHEEL REACTOR IN COUNTERCURRENT FLOW

The cold tail gas enters the preheat zone of the reactor and is heated by the hot walls of the channels. The hot tail gas exits the preheat zone, and the reductant is added. This gas reverses direction and passes back through the reaction section, countercurrent to the flow of the preheating gas. The reactor is catalyzed so the exothermic reaction occurs on the catalyst, releasing its heat of reaction to the walls of the channels. This reaction heat is then transferred to the preheat gas and to the reacting gases according to the laws of convective heat exchange. The rate of the chemical reaction (and heat release) is controlled by the rate of diffusion of the gaseous products or by first-order chemical reaction kinetics, as explained earlier.

A derivation of the equations used for the countercurrent operation is presented in Appendix C-2. These expressions must be used carefully because different bases were used in this derivation than in the rest of the computational work. These derivations were prepared for computer

application. They have been simplified below. The temperature of the preheating gas, T_1, is –

$$T_1 - T_1^0 = \frac{\eta_1 H_r}{C_p} \xi_f [(1 - 1/\lambda)(e^{\alpha x/L} - 1) + \frac{\alpha e^{\alpha}}{\lambda} x/L] \qquad (6\text{-}3)$$

The temperature difference between the preheating gas and the reacting gas, $T_2 - T_1$, is –

$$T_2 - T_1 = \frac{H_r}{C_p} \xi_f (e^{\alpha x/L} - e^{\alpha}) \qquad (6\text{-}4)$$

and the temperature of the solids, T_s, is given by –

$$T_s - T_1^0 = \frac{H_r}{C_p} \xi_f \{[\eta_1(1 - 1/\lambda) - \eta_2(1 - \lambda)] e^{\alpha x/L}$$

$$+ \frac{\eta_1 \alpha e^{\alpha}}{\lambda} x/L + \eta_1(1 - 1/\lambda) + \eta_2 e^{\alpha}\} \qquad (6\text{-}5)$$

where, in addition to the nomenclature on page 53 –

T_1 = gas temperature in preheat section, ^0F
T_2 = gas temperature in reaction section, ^0F
T_1^0 = initial temperature of gas to preheat, ^0F
η_1 = area fraction of reactor in preheat
η_2 = area fraction of reactor in reaction

Examination of Equation 6-5 proves that the solids temperature is linear with axial length when the Lewis Number is equal to 1.0. Under this condition, the temperature of the solids is nearly identical to the case for simple heat exchange if the reaction conversion is high.* Therefore, the graphs presented later at a Lewis Number of 1.0 are also applicable for the temperature of the solids in simple heat exchange with external reaction.

---

* When the reaction conversion is high, $e^{\alpha} \approx e^{\alpha} - 1$. The term e^{α} in Equations 6-3 to 6-5 yields a temperature equivalent to 100% conversion of the reactants, but $(e^{\alpha} - 1)$ is applicable for the true adiabatic temperature rise.

Figure 6-8 presents the temperatures of both gases and the solids in a countercurrent reactor with a Lewis Number of 1.0.

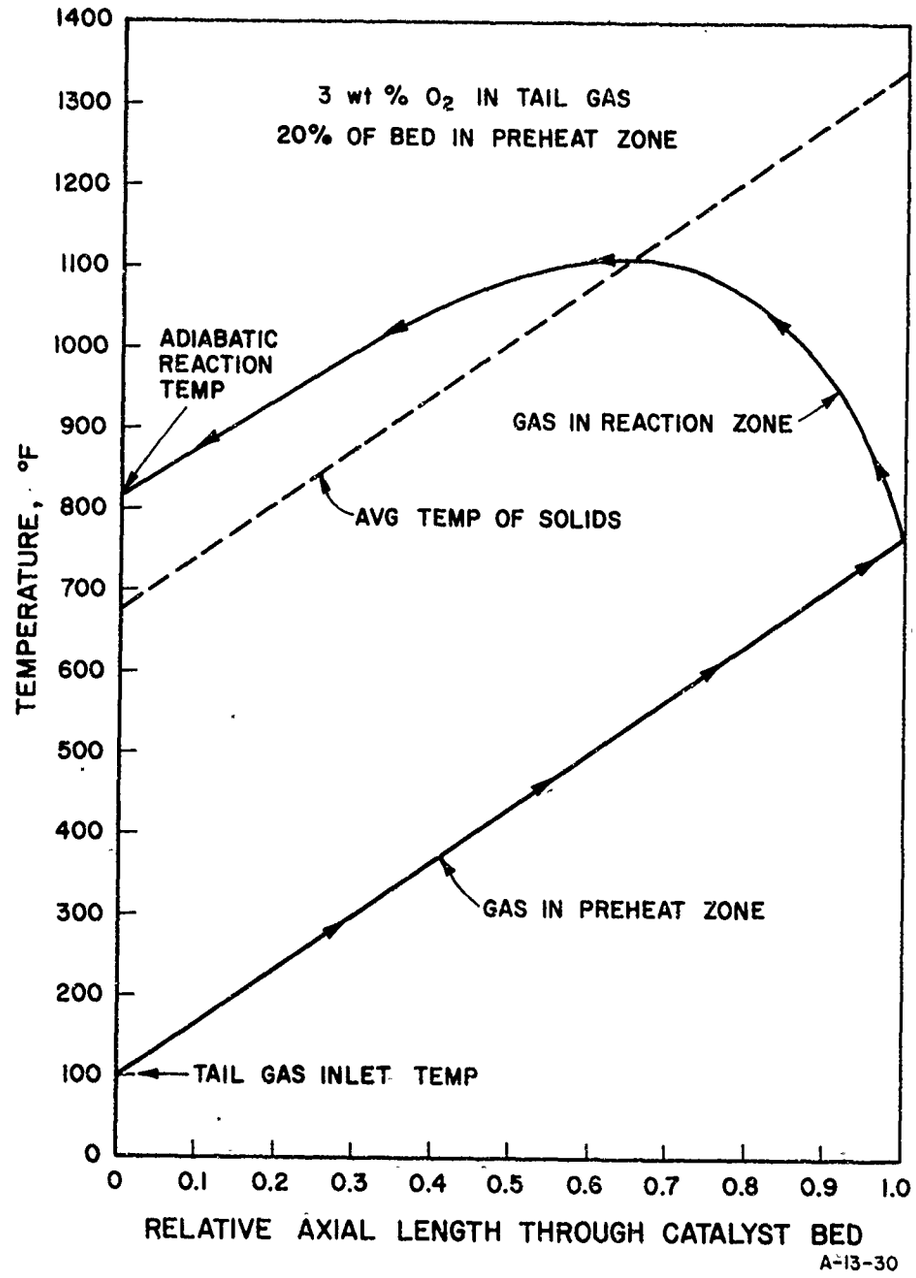

Figure 6-8. TEMPERATURES IN CYCLICAL REACTOR WITH 2-STREAM COUNTERCURRENT FLOW (Channel Flow, Diffusion-Controlled Reaction)

Both the temperature of the solids and the temperature of the preheating gas are linear with axial length. After the tail gas exits from the preheat zone, it is mixed with the methane and passed back through the reactor countercurrently. The gas contacts the hot solids and starts to react, leaving its heat of reaction on solids. This heat is transferred to both the reacting gases and the preheating gases. The temperature of the reacting gases rises rapidly as these gases pass back through the reactor. The solids temperature, however, falls because the reactant concentration (and reaction rate) decrease. At some point, the temperature of the gases in the reaction zone and the temperature of the solids are equal. At this point, the reacting gases pass through a maximum in temperature. The temperature of the gases then decreases with distance because heat is transferred from the gases to the solids.

In Figure 6-8, the solids temperature profiles are nearly identical to that presented earlier in Figure 5-9 for simple heat exchange, using the same gas flow rates and reactant concentration, indicating the similarity between the two cases at the Lewis Number equal to 1.0. In this system, the temperature of the solids at the original bed inlet is too low to maintain a reasonable reaction rate. Techniques to increase this temperature, such as additional uncatalyzed heat transfer area in the wheel and a three-pass reactor, will be discussed later. Similarly, the temperature at the hottest part of the wheel is too high for satisfactory catalyst lifetime, even with minimum heat transfer efficiency (large hydraulic diameter and small preheat area fraction) and low reactant concentration. This temperature will be decreased at the lower Lewis Numbers expected in the operating system.

Figure 6-9 presents the fraction conversion of the reactants as a function of the relative bed length. This graph is general and applies to all of the reaction systems in this report: The logarithmic relationship is characteristic of either a diffusion-controlled reaction or a first-order chemical reaction. This graph is drawn for 99% conversion at a relative bed length of 1.0, the basis for most of the figures presented in this report.

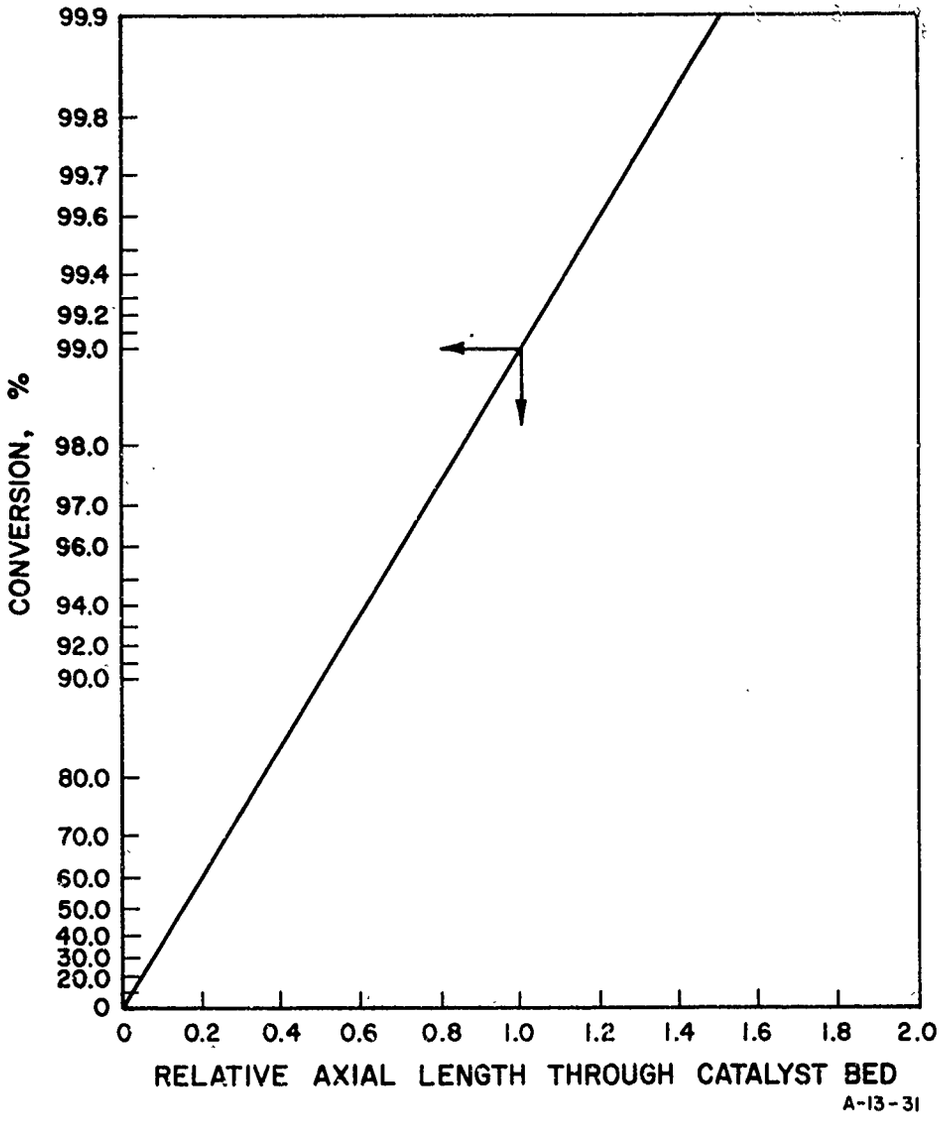

Figure 6-9. RELATIVE CONVERSION OF REACTANTS

Figure 6-10 presents the relative space velocity in this system for 99% conversion as a function of channel diameter, with diffusion control.

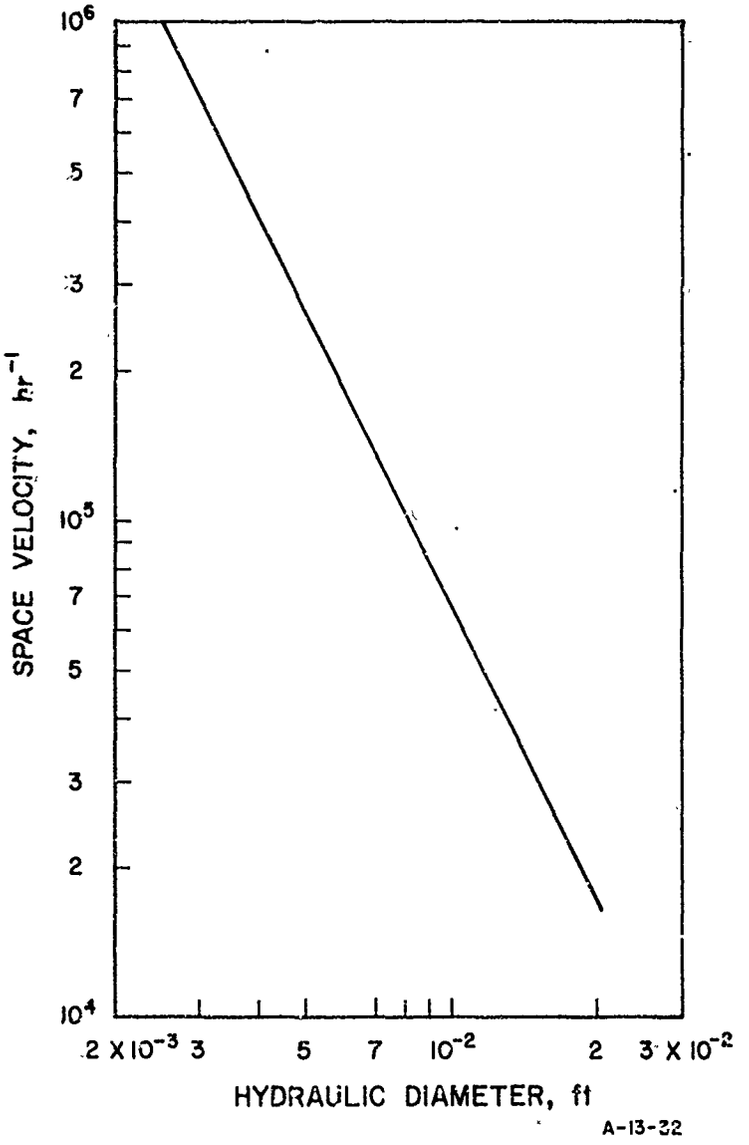

Figure 6-10. SPACE VELOCITY AS A FUNCTION OF CHANNEL DIAMETER, 99% CONVERSION. REACTION RATE CONTROLLED BY DIFFUSION.

This graph is based upon a constant Lewis Number. Therefore the mass transfer coefficient is directly related to the heat transfer coefficient, which, in turn, is a definite function of the channel diameter in laminar flow. Although the channel diameter does not appear explicitly in these equations, it is implicit in the size of the reactor for a given conversion.

Figure 6-11 presents the temperature gradients in the countercurrent bed as a function of the channel diameter (with a Lewis Number of 1.0). In this graph, small channel diameters promote greater heat transfer efficiency, similar to that expected from the simple heat transfer problem. A channel diameter of 1/8 in. was chosen for the remainder of the work because 1) it results in reasonably high surface area-to-volume ratios, 2) the temperature gradient is not excessively high, and 3) this size is one of the standard configurations for commercial honeycomb catalyst carriers.

Figure 6-12 presents the temperature gradients in the catalyzed bed as a function of the relative fraction of the wheel in the preheat and reaction zones. Again, the temperature gradient increases with increasing fraction in the preheat zone, as would be expected from Equation 6-5. However, based upon the heat transfer studies, a maximum thermal efficiency is expected when the two area fractions are equal at values of 0.5. In this problem, however, we are maintaining constant conversion, so the overall size of the regenerative reactor increases as the reaction zone fraction decreases. This explains the increasing temperature gradient at preheat area fractions greater than 0.5. In the limit, at the preheat area equal to 1.0, the reactor size is infinite. At the other limit, with the preheat fraction at zero, the equation is reduced to the simple, single-pass reactor case of Subsection 6.5 (allowing for the slight difference in nomenclature for these two cases). The lines at various preheat fractions all cross at a single point on this figure. Analysis of Equation 6-5 proves that this should occur at the adiabatic reaction temperature. However, the axial length at which they cross is a function of the chemical and mechanical parameters of the system.

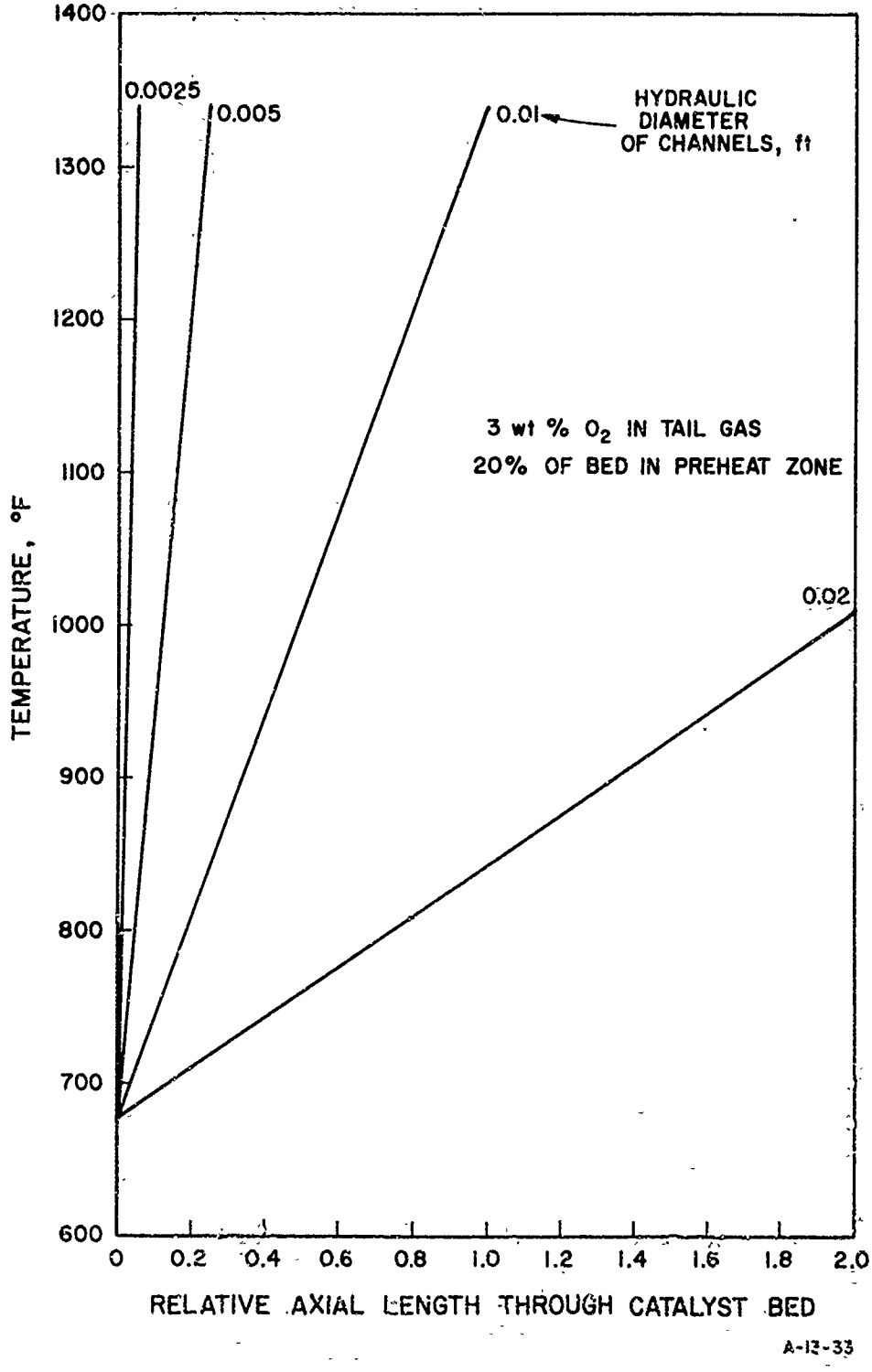

Figure 6-11. TEMPERATURE OF BED IN CYCLICAL REACTOR WITH 2-STREAM COUNTERCURRENT FLOW

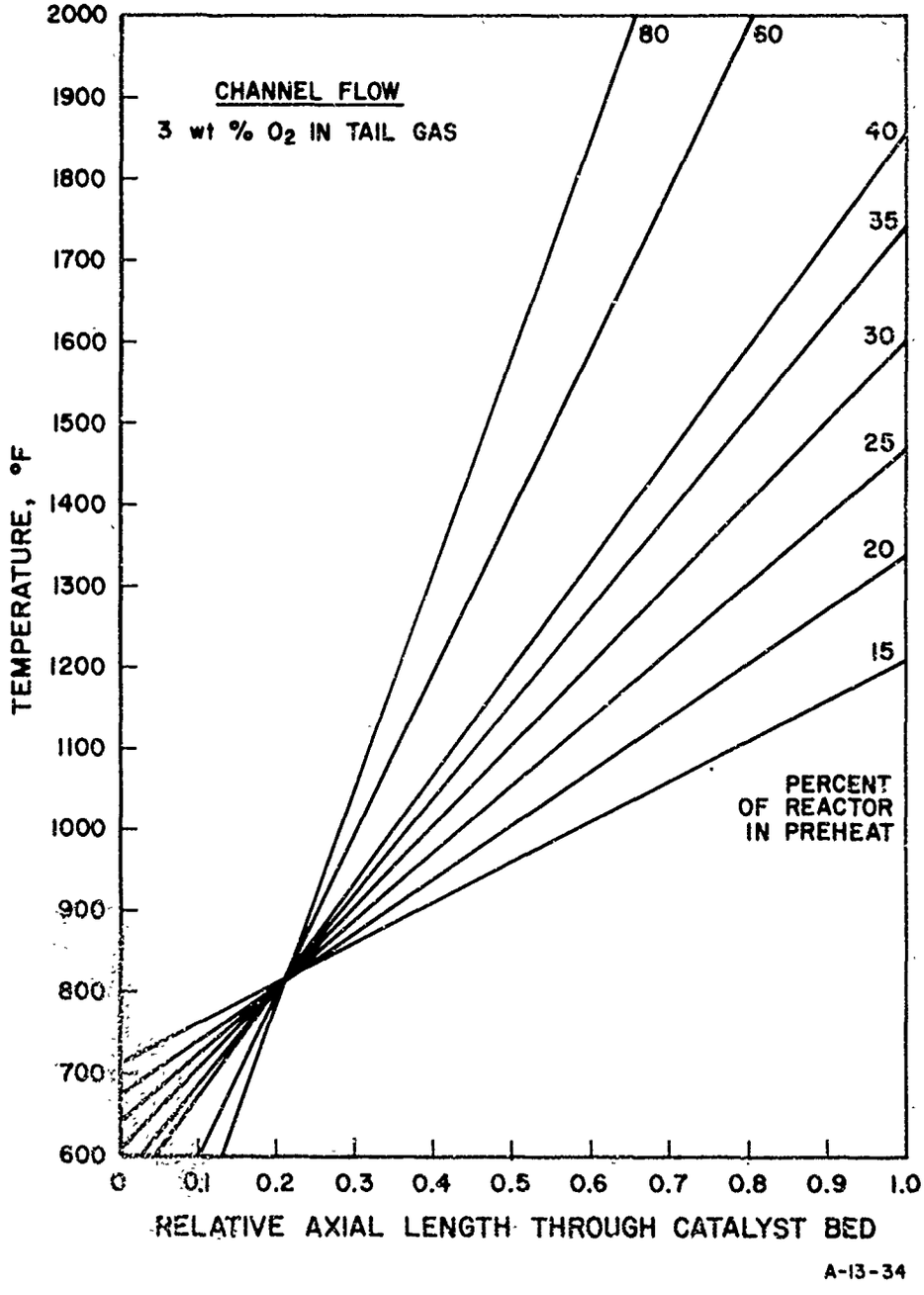

Figure 6-12. TEMPERATURE OF CATALYST IN CYCLICAL REACTOR WITH 2-STREAM, COUNTERCURRENT SYSTEM

An area fraction of 20% in the preheat zone was chosen for the remainder of the work with the countercurrent flow reactors because it results in the minimum temperature gradient that can be practically realized, considering the mechanical configuration of the rotary regenerative reactor.

Figure 6-13 presents the temperature gradients in the system as a function of the oxygen concentration in the tail gas. As expected from Equation 6-5, the temperature level and temperature gradients increase with increasing oxygen content.

The low temperature of the catalytic solids at the cooler face of the regenerative wheel reactor would be unsatisfactory. The reaction rate would be lowest in the zone where it is most necessary — where the final traces of oxygen are being removed and the majority of the NO_x is reduced. Consequently, we considered the possibility of incorporating additional, uncatalyzed length in the wheel reactor to effect simple heat exchange between the exhaust gases and the incoming tail gas. Figure 6-14 illustrates the results with the Lewis Number in the reactor section equal to 1.0. The effect of the simple heat exchange volume is to increase the level of the temperature in the reaction zone by the amount of heat exchange accomplished. Although the temperature of the solids at the warm face of the reactor is excessive for conventional noble metal catalysts, an operable system can be envisioned. Sufficient additional simple heat transfer area would be included so that the minimum temperature of the catalyzed surface would be about 1050^0F. The catalyst in the temperature zone of 1050^0-1350^0F would be conventional, noble metal. The catalyst in the higher temperature zones would be non-noble metal oxide catalysts.

The temperature profile appears to be a continuous function in both the simple heat exchange and reaction sections of the combined reactor. As discussed above, the solids temperature profile in the regenerative countercurrent reactor is nearly identical to simple heat exchange when the Lewis Number is 1.0 and the reaction conversion is relatively high. For this graph we have assumed identical physical configurations in both the reaction section and heat exchange section, including the relative fractions of the wheel in the preheat and reaction (cooling) zones.

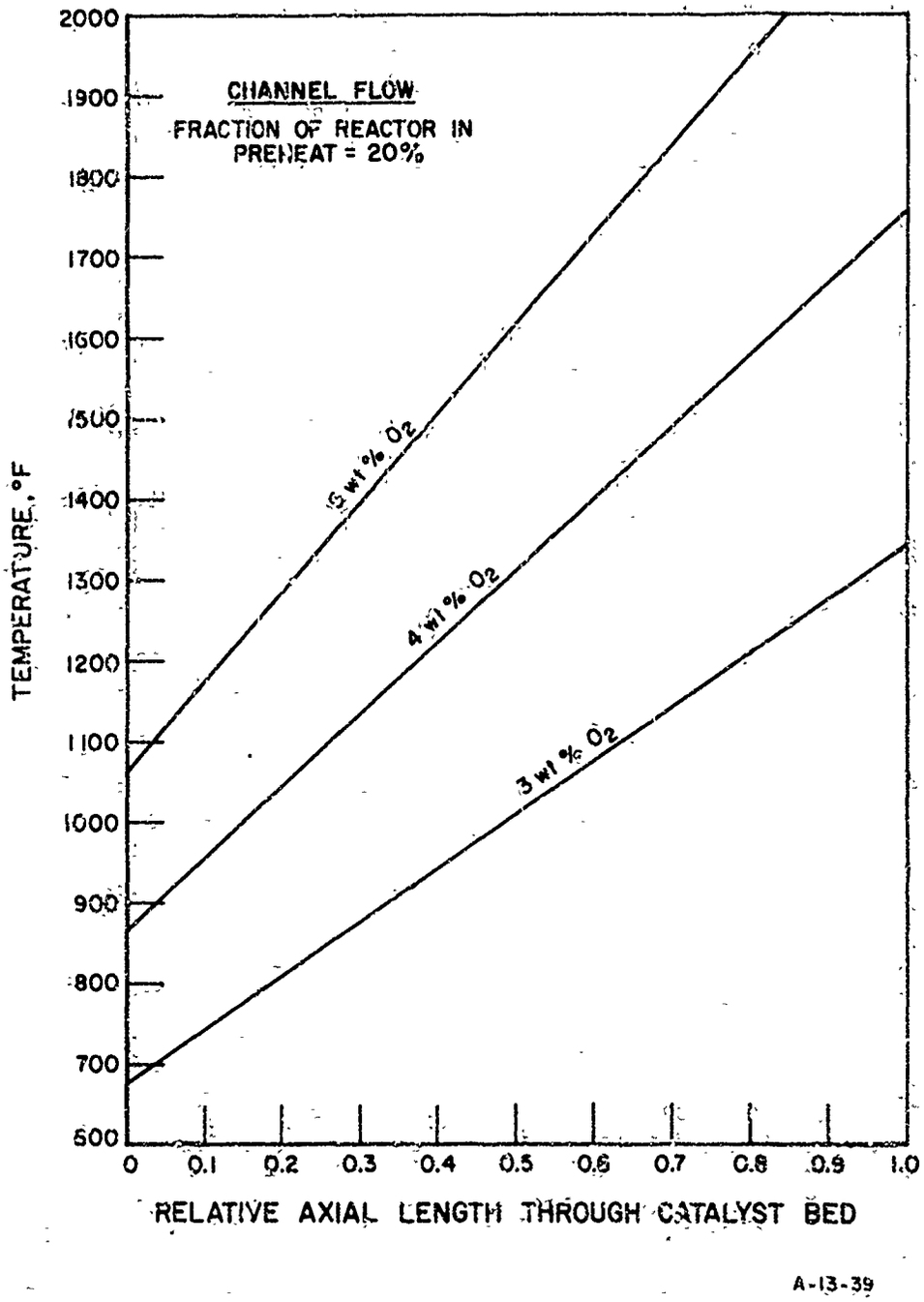

Figure 6-13. TEMPERATURE OF CATALYST IN CYCLICAL REACTOR WITH 2-STREAM, COUNTERCURRENT FLOW

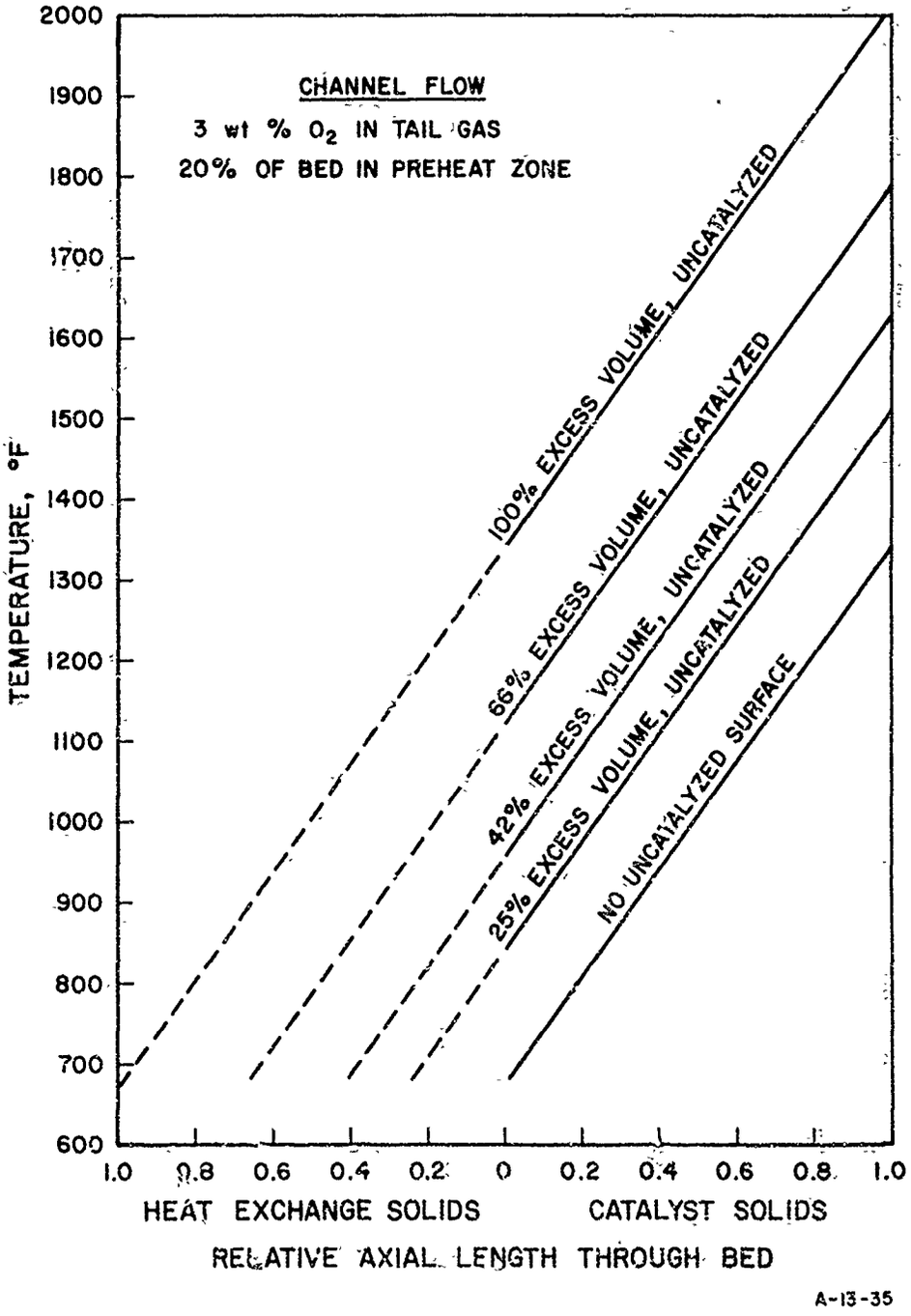

Figure 6-14. TEMPERATURE OF BED IN CYCLICAL REACTOR WITH 2-STREAM COUNTERCURRENT FLOW

Simple heat exchange at the higher temperature face of the wheel-reactor would be ineffectual. The gas temperatures of both streams at this face are identical. A third alternative, thermal exchange of the preheated tail gas with the incoming tail gas, was not calculated because an additional heat exchanger is required. However, a rederivation of Equation 6-5 incorporating this heat exchange indicates that the initial solids temperature would be raised and the solids temperature gradient would be moderated by this technique. Additional work with this approach would be justified in improving the countercurrent adiabatic regenerative reactor.

The results presented to this point have been based upon an assumed Lewis Number of 1.0. As explained in detail in the preceding subsection, the expected Lewis Number for strict diffusion control of this reaction is about 0.87 at 1200°F. The kinetic data on noble metal catalysts indicate that the pseudo-Lewis Number* will be in the range of 0.5 to 0.8. Insufficient data have been collected to permit estimation of Lewis Numbers on non-noble oxide catalysts, but they probably will be about the same at higher operating temperatures.

Figure 6-15 presents the temperature profiles in the reactor as a function of the Lewis Number. For this graph, we adjusted the fraction conversion for each Lewis Number so that the beds were the same actual length. Otherwise, the effect of changing the Lewis Number would be partially obscured by the improved relative heat transfer which would occur in the longer beds associated with the lower Lewis Number.

When the results of Figure 6-15 are considered with additional, uncatalyzed simple heat transfer area (similar to Figure 6-14), the operation of the mixed-metal rotary regenerative reactor becomes even more favorable. Perhaps, with sufficient simple heat transfer volume, the noble metal catalyst could be eliminated entirely.

---

* Based upon the average effective reaction rate constant as modified by the mass transfer coefficient.

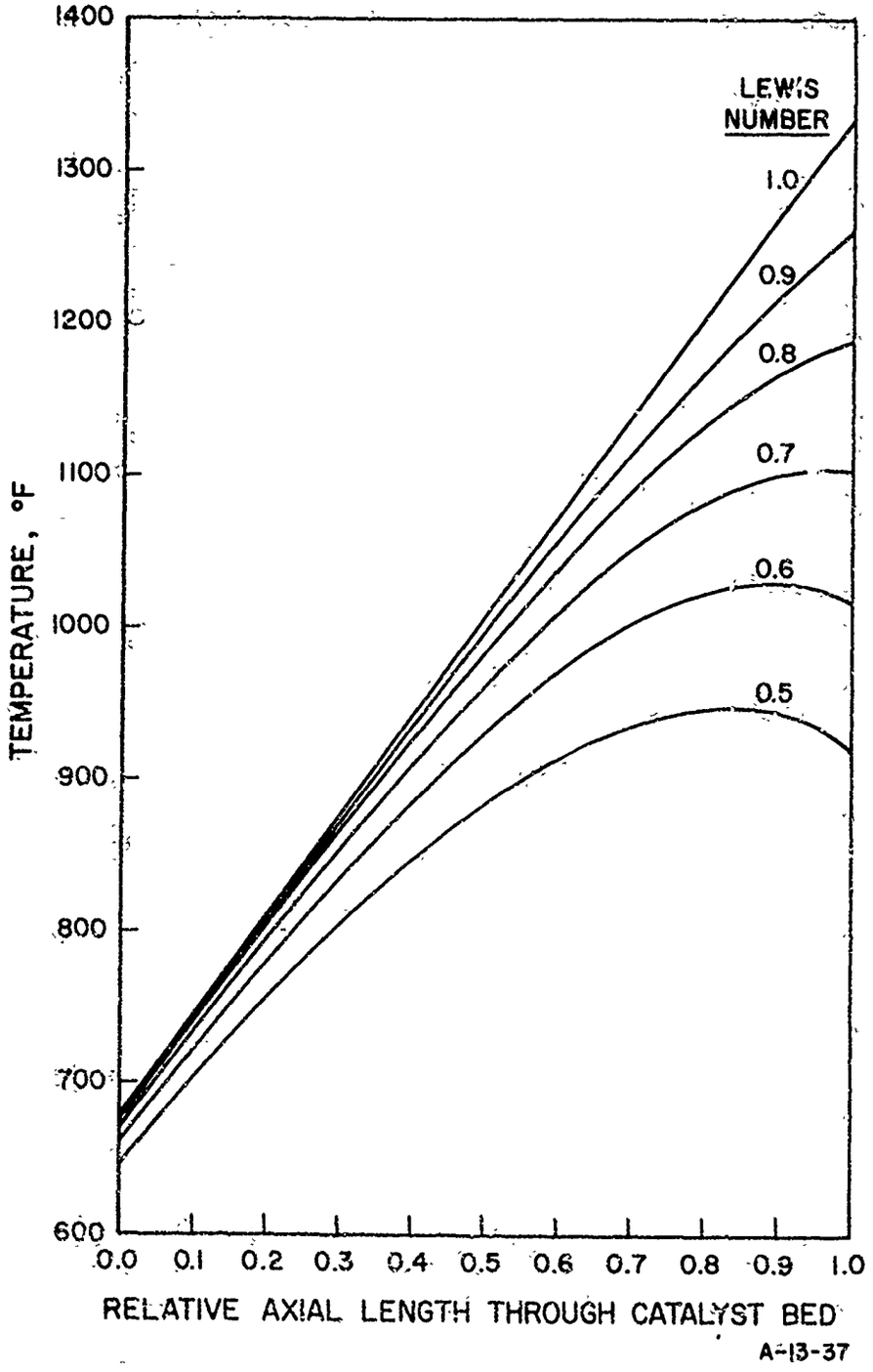

Figure 6-15. BED TEMPERATURE IN COUNTERCURRENT REACTOR

6.7. Two-Pass Cocurrent Reactor

The temperature profile of the solids in a cocurrent reactor can be quite uniform under certain, readily achievable modes of operation. These benefits of the cocurrent reactor were discovered while evaluating the three-pass reactor concept discussed in the next subsection.

In physical operation, the cocurrent reactor is similar to the countercurrent reactor discussed in the preceding subsection, except that the preheated gases return to the original face of the reactor and pass through the reactor in the same direction as the preheating gases. Figure 6-16 illustrates this concept for a rotary regenerative reactor.

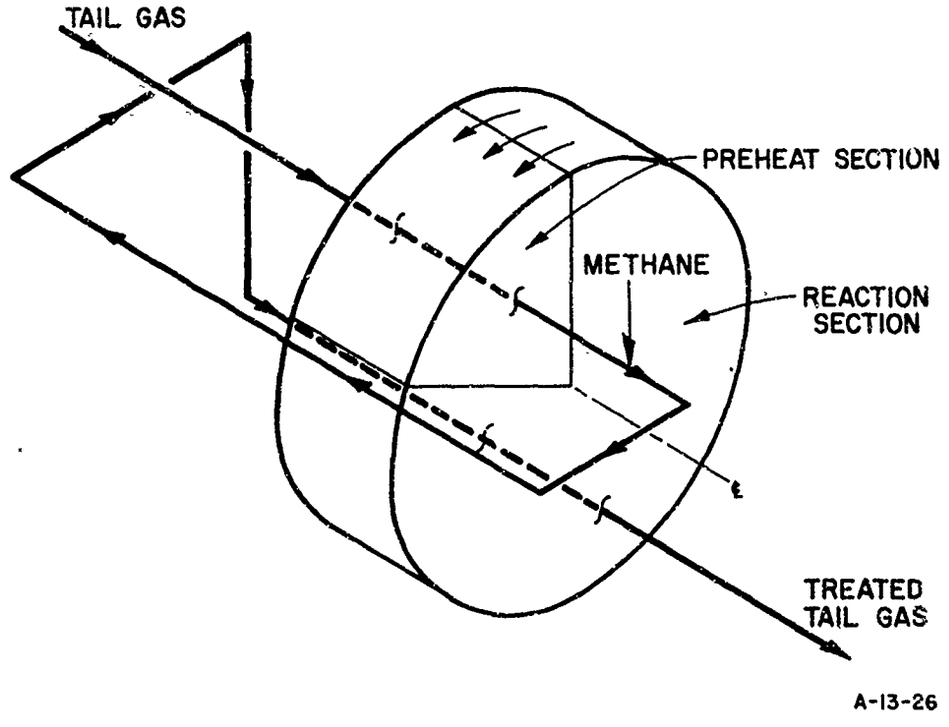

Figure 6-16. SCHEMATIC REPRESENTATION OF COCURRENT FLOW SYSTEM

A derivation of the equations governing the performance of this reactor concept is presented in Appendix C-3. A simplification of the equation for the temperature of the solids is given below:

$$T_s - T_1^0 = \frac{H_r}{C_p} \xi_o \{\eta_1 + \frac{\eta_1(\eta_2 - \eta_1)}{2\eta_1 - \lambda} + e^{-\alpha x/L}[\eta_2\lambda - \eta_1][1 + \frac{(\eta_2 - \eta_1)}{2\eta_1 - \lambda}] \quad (6\text{-}6)$$

$$+ [1 + (\eta_2 - \eta_1)e^{-2\eta_1\alpha x/\lambda L}][\frac{\eta_1(1 + \frac{\eta_2 - \eta_1}{2\eta_1 - \lambda})(1 - e^{-\alpha}) - \frac{\lambda(\eta_2 - \eta_1)}{2\eta_1 - \lambda}}{1 + e^{-2\eta_1 \alpha/\lambda}}]\}$$

This relationship is relatively complex in its complete form. However, under certain conditions, it is greatly simplified. For example, when the fractions of the wheel allotted to preheat and reaction are equal and the Lewis Number is 1.0, the solids temperature is constant with axial length and nearly equal to the adiabatic reaction temperature:

$$T_s - T_1^0 = \frac{H_r}{C_p} \xi_o[1 - e^{-\alpha}/(1 - e^{-\alpha})] \quad (6\text{-}7)$$

Similarly, when the ratio of the preheat cross-sectional area to the reaction area is equal to the Lewis Number (for Lewis Numbers $\neq 1$), the solids temperature profile is –

$$T_s - T_1^0 = \frac{H_r}{C_p} \xi_o\{1 - e^{-\alpha}[1 + (\eta_2 - \eta_1)\, e^{-2\eta_2\alpha x/L}]/(1 + e^{-2\eta_2\alpha})\} \quad (6\text{-}8)$$

As will be shown, this temperature does not vary greatly with axial length at Lewis Numbers between 0.5 and 2 or with conversions greater than 90%.

A third simplification is of interest in comparing the cocurrent reactor with a simple, single-pass reactor. Both of these reactors exhibit a constant solids temperature at a Lewis Number of 1.0 if the area fractions in the cocurrent reactor are equal. We can estimate the effect of the Lewis Number in the cocurrent reactor by equating the area fractions. If the fractional conversion is high, the solids temperature profile is –

$$T_s - T_1^0 = \frac{H_r}{C_p} \xi_o[1 - 1/2(1 - \lambda)\, e^{-\alpha x/L}] \quad (6\text{-}9)$$

Notice that the effect of the Lewis Number in Equation 6-9 is only half as great as we found for the simple reactor in Equation 6-2. In addition, the effect of the Lewis Number can be counterbalanced over a wide range by varying the area ratio in the cocurrent reactor according to Equation 6-8. These points will be presented graphically in the rest of this subsection.

Figure 6-17 illustrates the effect of varying the preheat zone in the cocurrent reactor with a Lewis Number of 1. Low preheat fractions tend to generate higher solids temperature at the front face of the reactor, while high preheat fractions decrease the temperature at this face. At both area fractions equal to 0.5, the solids temperature is constant.

Figure 6-18 illustrates the constant temperature profiles with parameters of oxygen concentration in the inlet tail gas. As expected, the higher oxygen concentration causes a higher adiabatic temperature rise and a hotter reactor.

Figure 6-19 presents the temperature profiles of both the solids and the gases in the cocurrent reactor with a Lewis Number of 1.0 and equal area fractions in the preheat and reaction zones. This graph illustrates that most of the heat released by the reaction is used to preheat the incoming gas and that the temperature of the reacting gases is nearly equal to the temperature of the solids.

Figure 6-20 illustrates the temperature profiles in the cocurrent reactor at equal area ratios, but varying Lewis Numbers. A lower Lewis Number tends to decrease the temperature at the front face of the reactor. Also included on this graph are similar functions for the simple, single-pass reactor taken from Figure 6-4. Comparing the curves at equal Lewis Numbers indicates the immediate benefit of using the cocurrent reactor.

Decreasing the Lewis Number tends to decrease the temperature on the front face of the reactor, and decreasing the preheat area fraction tends to increase the solids temperature at that point. These effects may be counterbalanced. If a reacting system has a Lewis Number less than 1.0, a reduced preheat area could be used to compensate. Figure 6-21 presents the temperature profile for a Lewis Number of 0.6 with varying preheat fraction. This graph indicates that a nearly constant temperature profile might be obtained at a preheat fraction between 0.35 and 0.4.

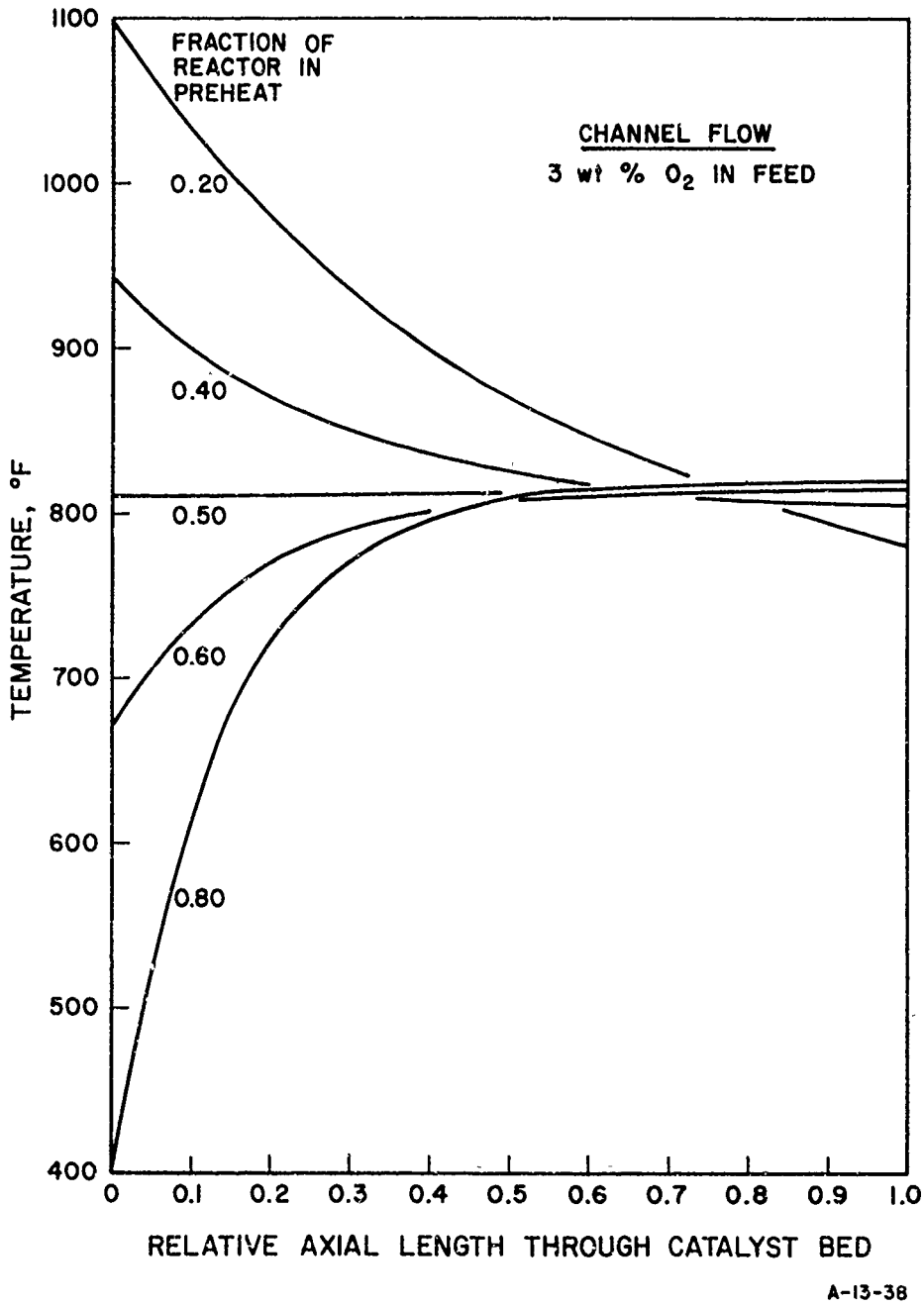

Figure 6-17. TEMPERATURE OF CATALYSTS IN CYCLICAL REACTOR WITH 2-STREAM, COCURRENT SYSTEM

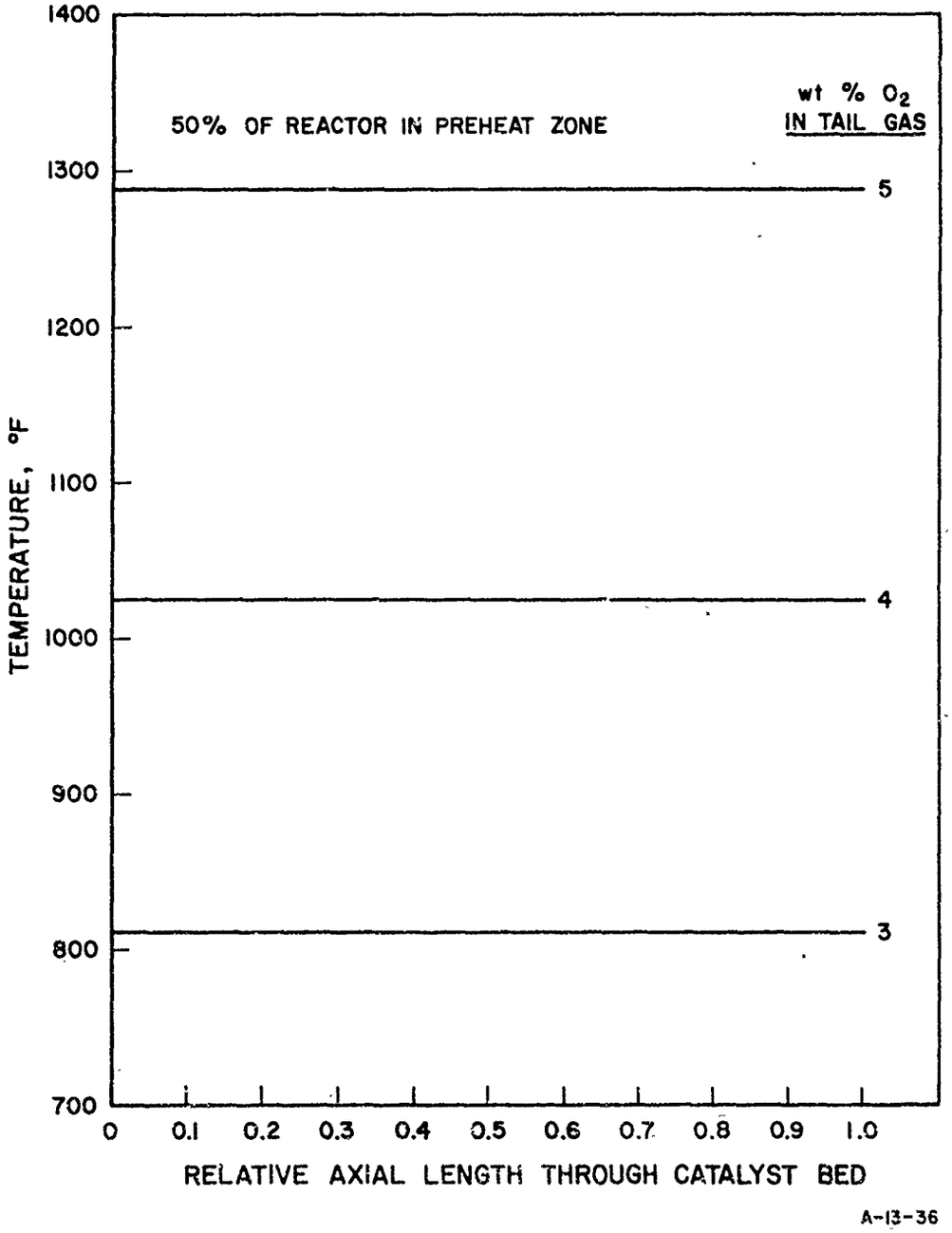

Figure 6-18. TEMPERATURE OF SOLIDS IN CYCLICAL REACTOR WITH 2-STREAM, COCURRENT SYSTEM

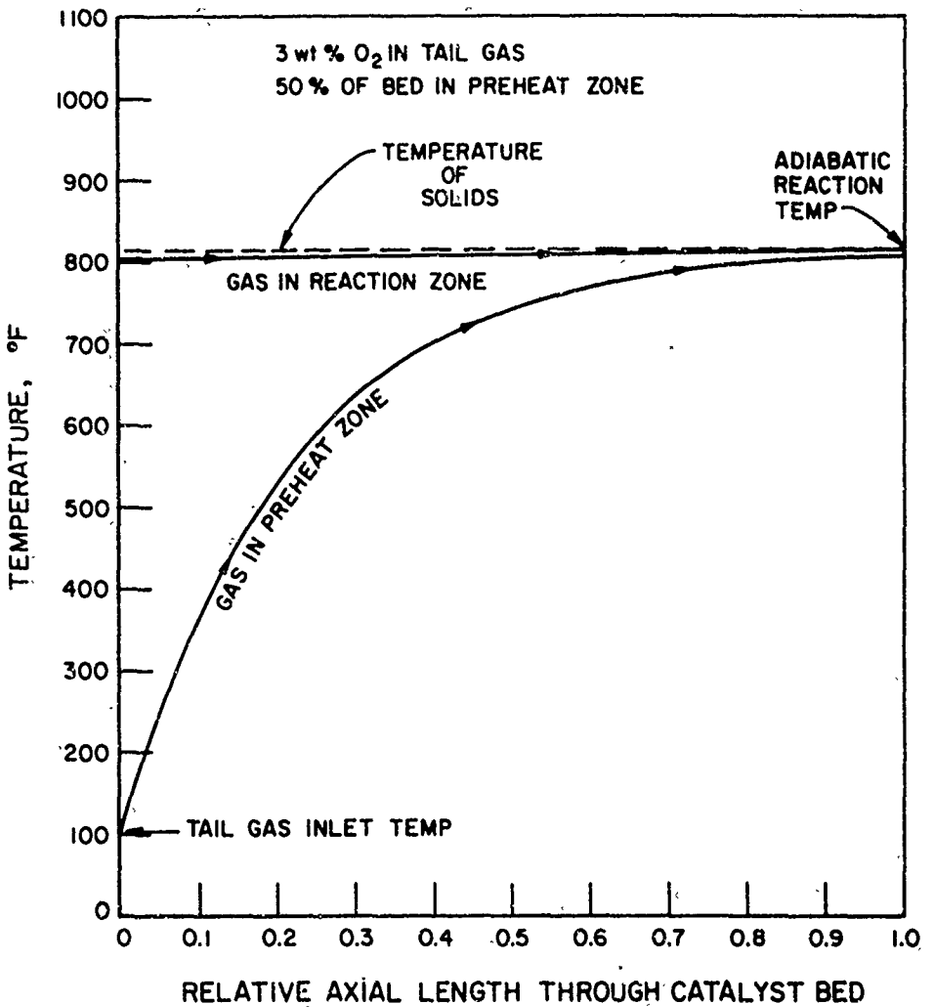

Figure 6-19. TEMPERATURES IN CYCLICAL REACTOR WITH 2-STREAM, COCURRENT FLOW

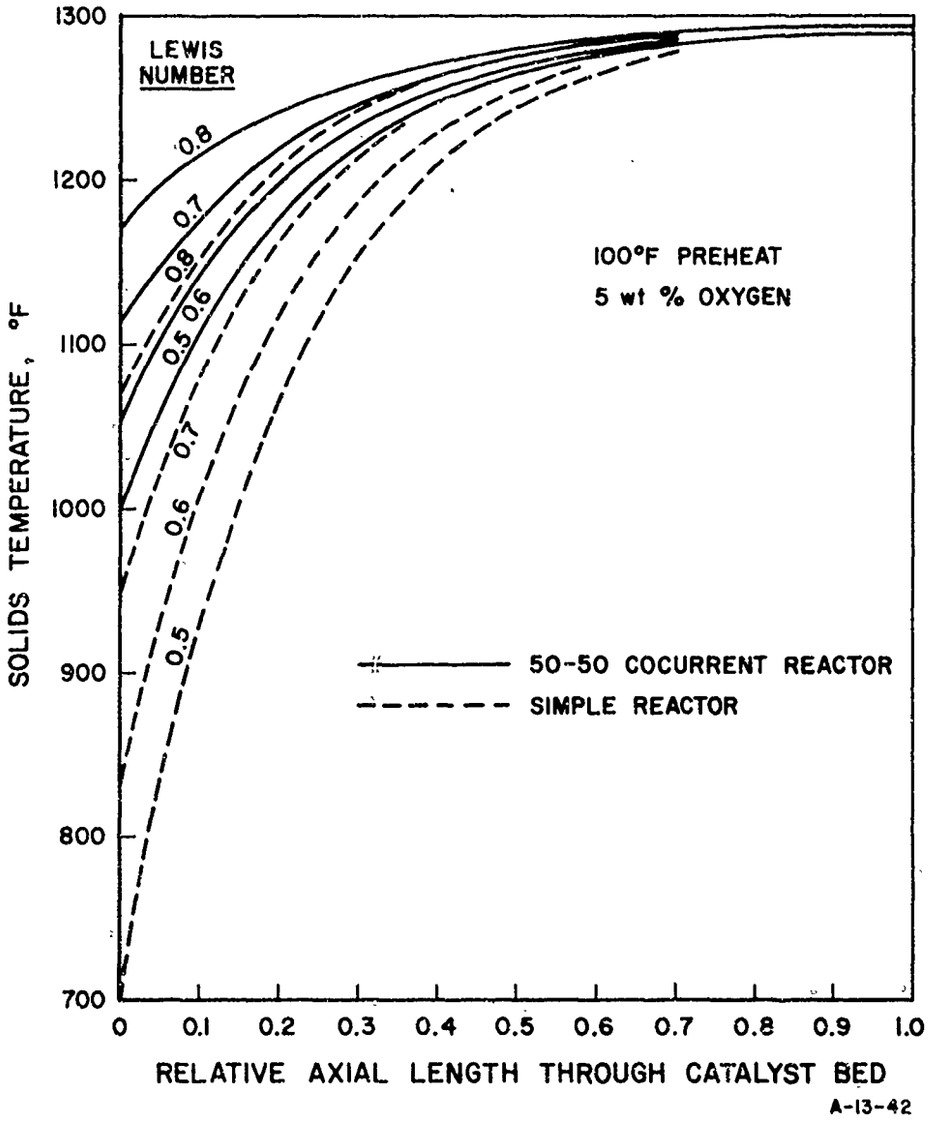

Figure 6-20. SOLIDS TEMPERATURE VERSUS AXIAL LENGTH FOR VARIOUS LEWIS NUMBERS

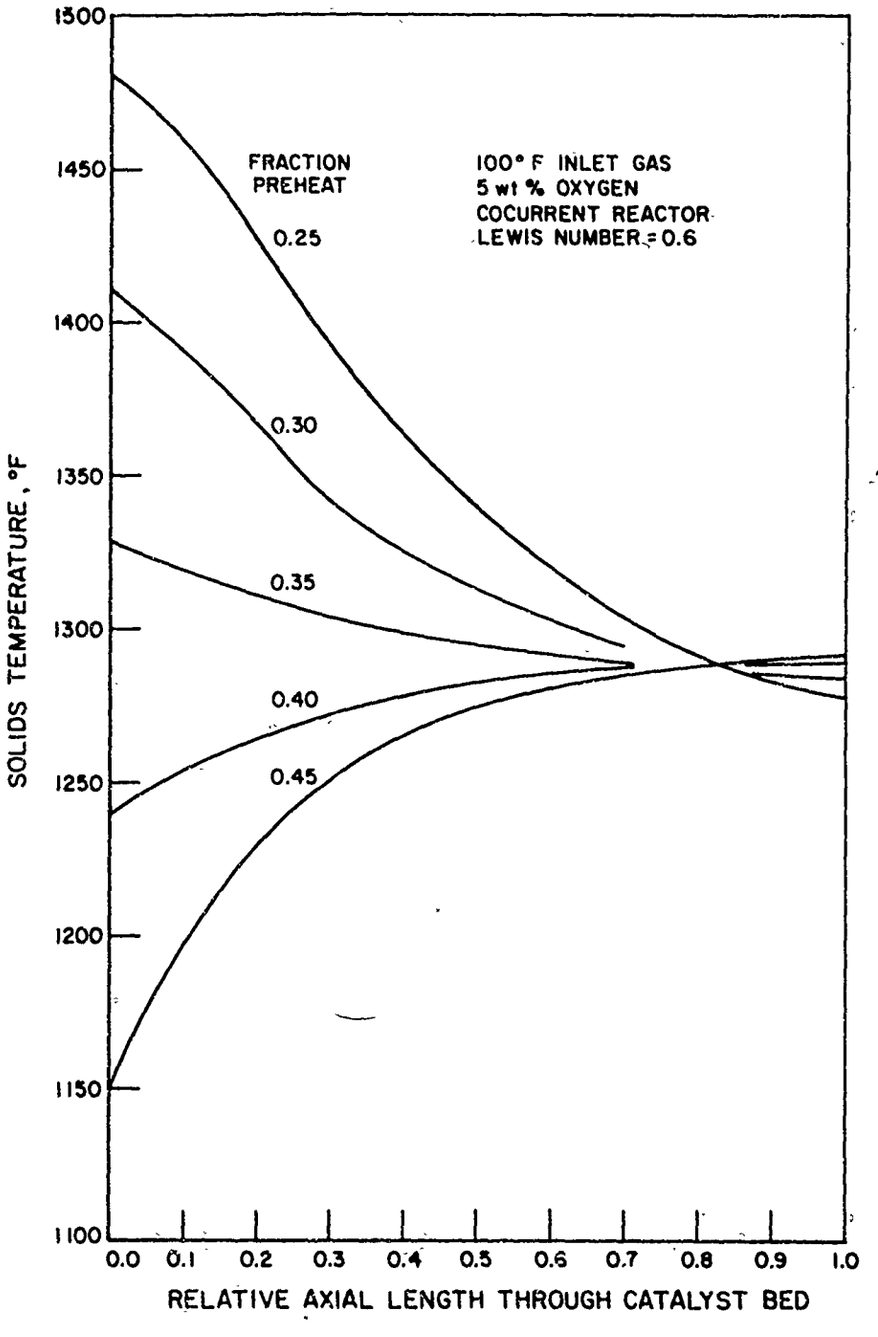

Figure 6-21. SOLIDS TEMPERATURE AS A FUNCTION OF AXIAL LENGTH FOR VARIABLE PREHEAT AREA

The maximum temperature variation is plotted against preheat fraction in Figure 6-22 for a series of Lewis Numbers. This graph can be used to select the preheat area fraction which would force the two faces of the reactor to equal temperature. The tabulation on Figure 6-22 indicates that the solids temperature will be constant when the ratio of the preheat zone to the reaction zone is equal to the Lewis Number. However, this ratio is not precise. For example, at a Lewis Number of 0.6, the calculated preheat area fraction using this relationship as 0.375 rather than the 0.372 observed. The data input for Figure 6-22 is so sufficiently accurate that a slight discrepancy is noted. This difference is caused by the small effect of the x/L term in Equation 6-8.

Figures 6-23, 6-24, and 6-25 indicate the temperature profiles when the area ratio of the reactor wheel is equal to the Lewis Number. These graphs have been prepared for varying Lewis Numbers and degrees of reaction completion. In general, the deviations from the ideal relationship become more pronounced as the Lewis Number is decreased or the fraction conversion of the reactant is decreased. In most cases, further compensation for these deviations could be achieved by slight adjustment in the relative area fractions in the regenerative reactor. However, these modifications are not warranted with our simplified model; we should include the effects of temperature upon reaction rate and physical properties of the system before we refine these design relationships. In addition, the data of Section 7 indicate that at least 98% conversion will be necessary for satisfactory abatement; therefore, the bed temperatures can be essentially constant in this process.

The constancy of the solids temperature in the cocurrent regenerative wheel reactor is ideal for reaction control. No problems would be experienced in overheating the catalyst, causing degradation, and there would be no problems with reaction lightoff with higher oxygen concentrations in the tail gas.

However, the temperature in the reactor is controlled only by the oxygen concentration. This temperature may be too low for satisfactory reaction rate at lower oxygen contents. Simple heat exchange on either side of the wheel is ineffectual. At the rear face of the wheel, where the product gases exit, both the preheated gases and the product gases have similar temperatures so no heat exchange is possible. At the front face of the wheel, the inlet tail gas can be preheated by the gases which are going to reaction, but the exchange of heat does not affect the total quantity of heat which is carried to this face of the wheel by the two

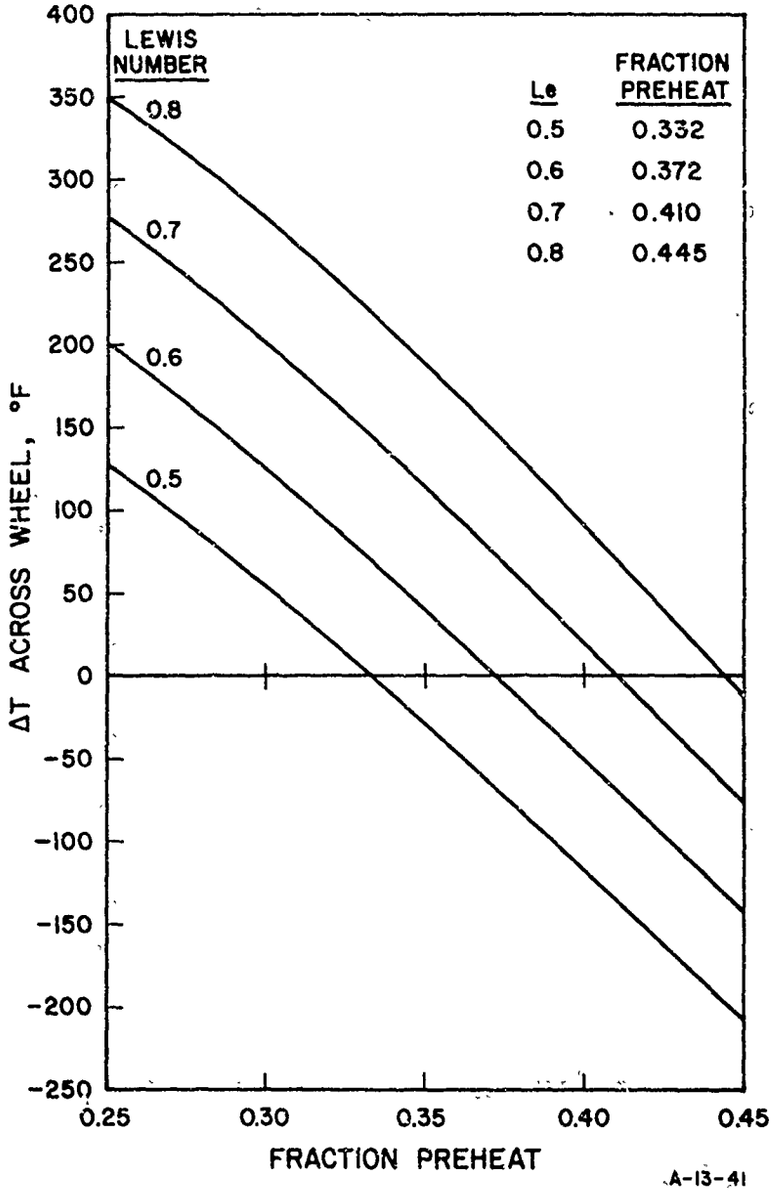

Figure 6-22. TEMPERATURE DIFFERENCE ACROSS WHEEL VERSUS FRACTION PREHEAT AT CONSTANT LEWIS NUMBERS

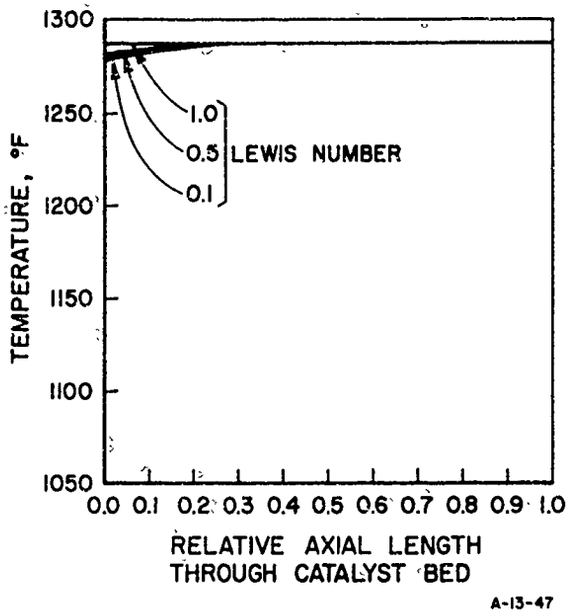

Figure 6-23. TEMPERATURE IN 2-PASS COCURRENT REACTOR. AREA RATIO = LEWIS NUMBER; 99% CONVERSION

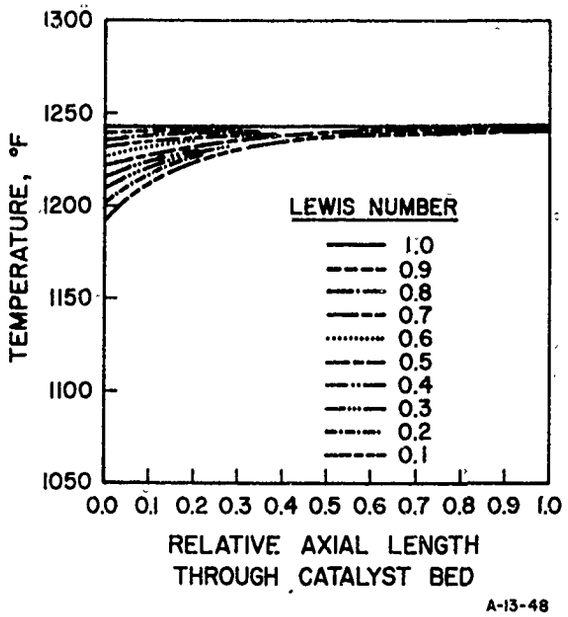

Figure 6-24. TEMPERATURE IN 2-PASS COCURRENT REACTOR. AREA RATIO = LEWIS NUMBER; 95% CONVERSION

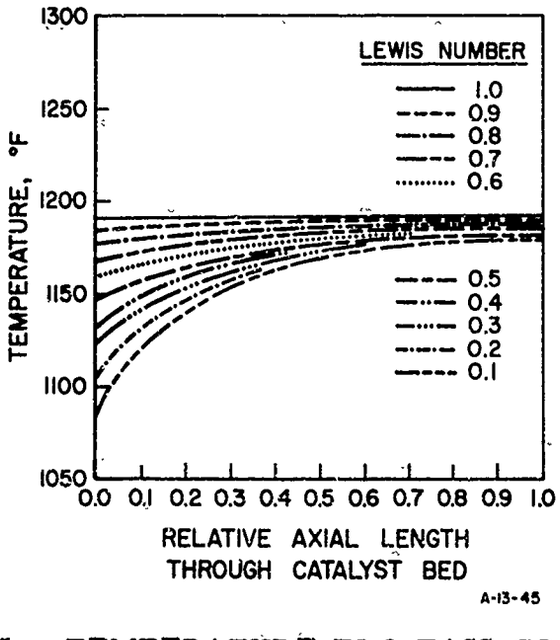

Figure 6-25. TEMPERATURE IN 2-PASS COCURRENT REACTOR. AREA RATIO = LEWIS NUMBER; 90% CONVERSION

gas streams. The only way to increase this temperature is to preheat the inlet tail gas with some other source of energy, perhaps the reaction products discharging from the reactor. Incorporating heat exchange of this type, the cocurrent reactor is operable with even low oxygen concentrations in the tail gas at temperatures up to 1350°F for conventional, noble metal catalysts. Higher temperatures may be achieved for use with non-noble oxide catalysts.

6.8. Three-Pass Combined Cocurrent and Countercurrent Reactor

The three-pass reactor was conceived as an improvement on the countercurrent reactor. In this scheme, the reaction does not go to completion in the first reacting pass, as controlled by the quantity of reductant added or the size of this reacting area. The reacting gases are turned around again and passed back through the reactor cocurrent to the original flow of the preheating gas. This flow stream is illustrated schematically in Figure 6-26. The derivation of the equations for this reactor concept are presented in Appendix C-4. These equations become quite complex, so only the important points are detailed. Similarly, these equations have little obvious meaning, so they are not presented here.

Figure 6-27 presents the temperature profiles of the solids in the three-pass reactor with a Lewis Number of 1.0, a preheat zone of 20%, and varying fractions of reaction completion in the first pass. Figure 6-28 illustrates the same reactor with uncatalyzed simple heat exchange volume on the incoming face of the reactor. Examination of these two graphs indicates that a variety of temperature profiles may be obtained by varying the operating parameters in the system. For the NO_x abatement system, we would suggest a reactor configuration in which the final outlet face was relatively hot. This would ensure maximum cleanup of the final product gas, after the majority of the oxygen had been reacted. Such a reactor might be achieved with 20% preheat, 80% of the reaction in the first countercurrent path of the reactor with the remainder in the cocurrent path, and 4.5 to 5 weight percent oxygen in the tail gas. This set of conditions is not presented in Figure 6-27, but would result in a slowly rising temperature in the reacting bed, varying from about 1150° to 1350°F.

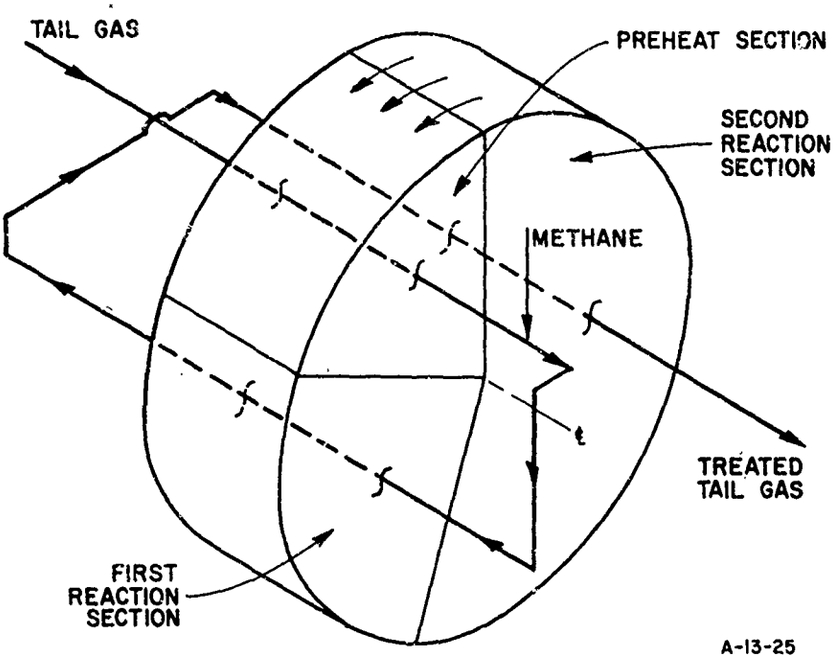

Figure 6-26. SCHEMATIC REPRESENTATION OF THREE-PASS REACTION SYSTEM

Work on the three-pass reactor was suspended when the advantages of the cocurrent reactor became known. The cocurrent reactor probably gives better reaction control and higher reaction rates than the three-pass reactor, without the added complexity of double recycle of the gases.

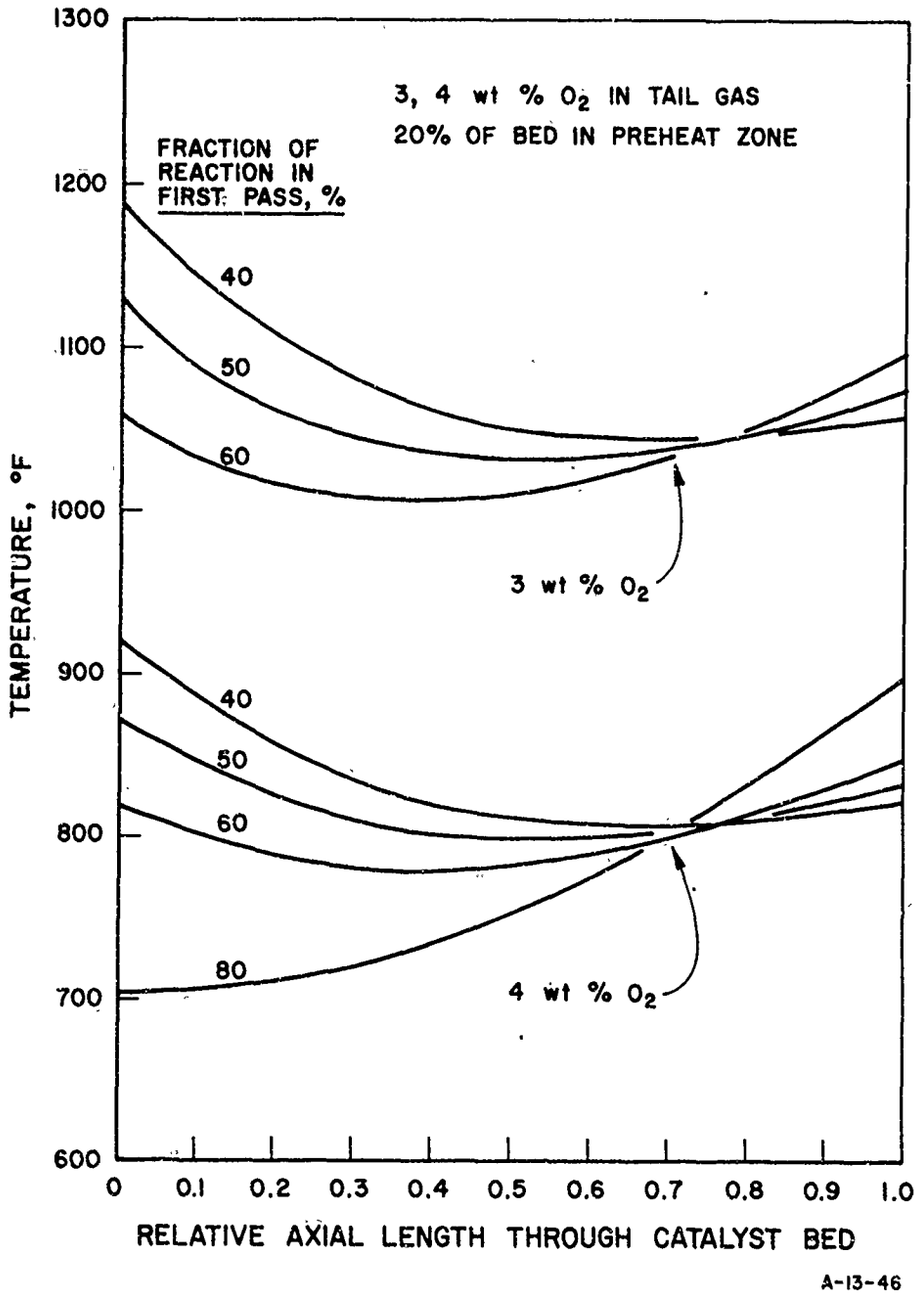

Figure 6-27. TEMPERATURE OF BED IN CYCLICAL REACTOR WITH 3-STREAM FLOW SYSTEM

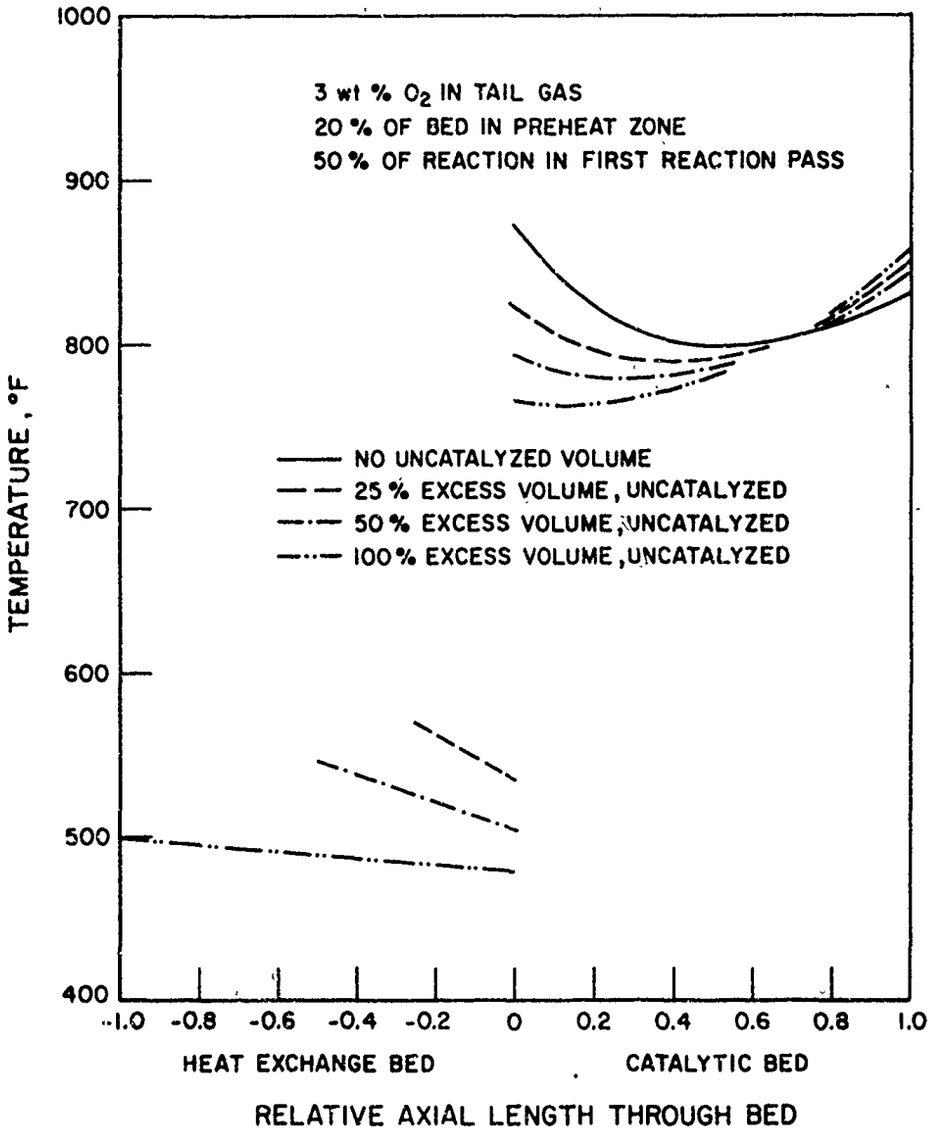

Figure 6-28. TEMPERATURE OF BED IN CYCLICAL REACTOR WITH 3-STREAM FLOW SYSTEM

6.9. Reactor Modeling – Incorporation of Experimental Reaction Rate

6.9.1. Reactor Modeling

The computer program, discussed in Section 6.7, was modified to incorporate the variation of experimental reaction rate with temperature. This modified model, which is more rigorous than the simplified model used earlier, permits a more realistic evaluation of the isothermal reactor-bed concept.

Numerical evaluation of the equations for $k_g\pi$ at 1 and 7 atm was determined based on our experimental data; these data are graphed in Figure 7-10. Knowing that –

$$\frac{1}{K} = \frac{1}{k_r\pi} + \frac{1}{k_g\pi} \qquad (6\text{-}10)$$

and

$$K = \ln \frac{C_o}{C_f} \frac{SV_o}{RT_o} \left(\frac{\pi_o}{\pi}\right) \qquad (6\text{-}11)$$

we can determine the dependence of oxygen conversion on temperature, pressure, and space velocity.

6.9.2. Simple Reactor

A simple fixed-bed reactor was mathematically simulated. The expected reactor performance, based on our experimental kinetic studies, was evaluated as simple changes were made in the assumed operating conditions. A feed composition of 2.5 volume percent oxygen, preheat temperatures of 600°-1000°F, and space velocities of 30,000-60,000 hr^{-1} were chosen. We also tested the effects of changing the physical characteristics of the honeycomb catalyst carrier.

Figures 6-29 and 6-30 show the solids temperature profile in the bed for different preheat temperatures. For these graphs, the system was set up with a feed composition of 2.5 volume percent oxygen, a space velocity of 40,000 hr^{-1}, a Nusselt Number of 4.0, a channel diameter of 1/8 inch, and operating pressures of 7 and 1 atm. Note the inflection of the curves at 7 atm pressure (Figure 6-29) between 700° and 600°F. A similar inflection is noted at 1 atm pressure (Figure 6-30) between 900° and 800°F. At the lower preheat temperatures, the reaction rate

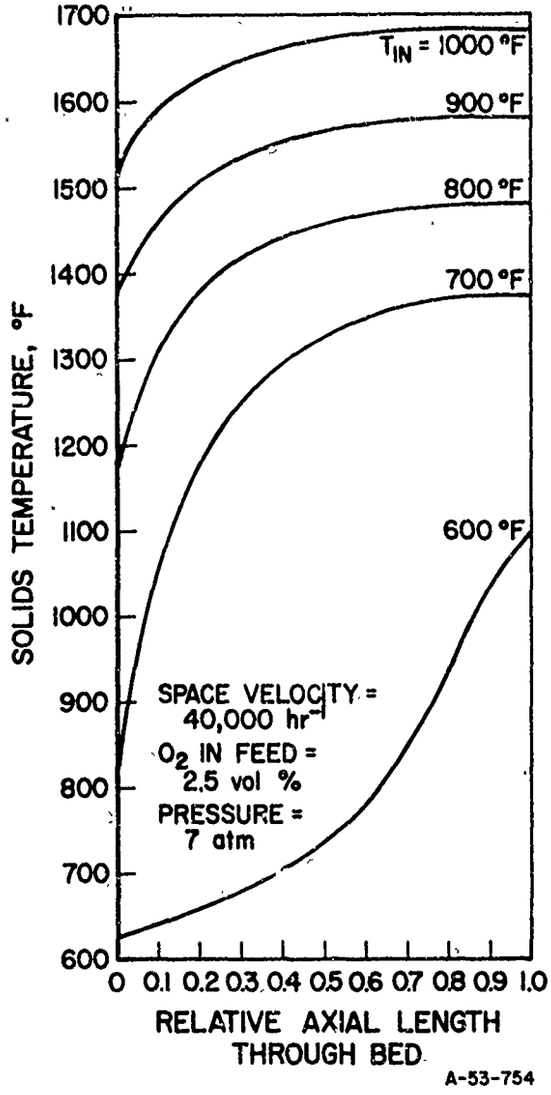

Figure 6-29. SOLIDS TEMPERATURE IN SIMPLE REACTOR AT 7 atm AND VARIOUS PREHEAT TEMPERATURES

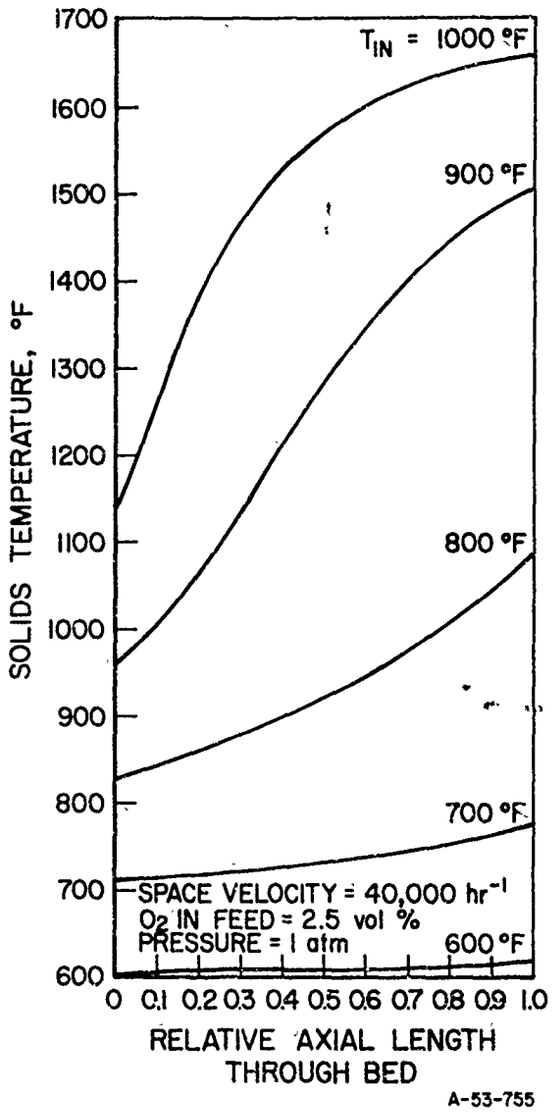

Figure 6-30. SOLIDS TEMPERATURE IN SIMPLE REACTOR AT 1 atm AND VARIOUS PREHEAT TEMPERATURES

is insufficient to raise the solids temperature to a more favorable, higher level. These inflections therefore may be indicative of the reaction initiation temperatures at the respective pressures.

Figure 6-31 shows the variation of oxygen conversion with space velocity for different preheat temperatures at 1 and 7 atm. Our earlier kinetic studies showed that to attain the desired nitric oxide removal, 98-99% of the oxygen must be converted. Such results can be attained on the model at high pressure and low space velocity. However, at 600°F and 7 atm (not presented in Figure 6-31), conversion is low. The poor performance at these conditions confirms the temperature profile data in Figure 6-29.

One qualification should be made; that is, low preheat temperatures (lower than those utilized by industry) produce good conversion at higher pressure. Perhaps the estimated heat transfer coefficient is too low, or our experimental reaction rate is high compared with that for aged catalysts. Changing these relative rates would decrease the conversion in our model.

The channel diameter was reduced to 3/32 and then to 1/16 inch to evaluate this effect on the model. Significantly improved conversions were attained. Decreasing the channel diameter improves the mass transfer rate, in addition to increasing the surface area per unit volume of catalyst. Therefore, changing the channel size has an exponential effect on the conversion. At 7 atm and a 700°F preheat, the conversion increased from 95.3 to 99.4% when the channel diameter was reduced from 1/8 to 3/32 inch. By further reducing the channel diameter to 1/16 inch under the same conditions, a 99.9% conversion was attained at 70% of the catalyst depth. Under such conditions a higher space velocity could be incorporated and a lower catalyst volume could be used.

Another set of runs was made to simulate interrupted channel lengths. The Nusselt Number and the k_g factor were doubled to simulate the effect of turbulence. The results were interesting. Simulated turbulence caused improved performance at preheat temperatures of 700°F and above. At lower preheat temperatures, poorer results were obtained, caused by

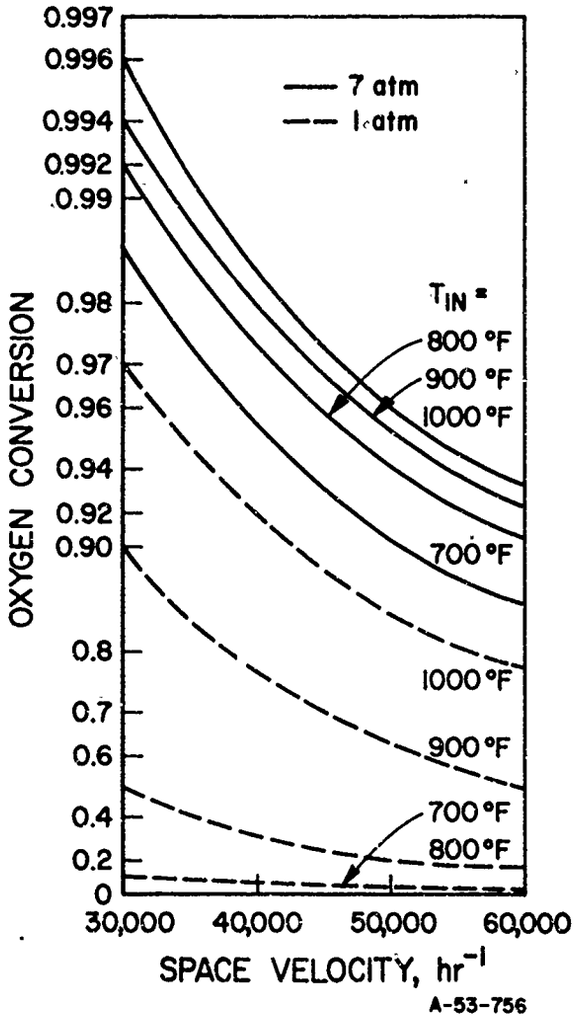

Figure 6-31. OXYGEN CONVERSION VERSUS SPACE VELOCITY IN SIMPLE REACTOR AT 1 AND 7 atm AND VARIOUS PREHEAT TEMPERATURES

lower solids temperatures. The heat generated by the reaction was transferred away from the solids too fast to sustain good conversion on the catalyst surface.

These two carrier design modifications, as simulated in the complex model, suggest possible modifications in existing reactors. Reducing the channel size in the commercial reactor and using the same catalyst loading (on an area basis) should significantly improve abatement. A similar effect should be noted in an operable reactor when many thin, nonoriented layers of the original channel size are used. However, if the present reactor performance is marginal, the staggered layer concept can force reduced reactor performance.

6.9.3. Regenerative Wheel Reactor

The primary function of the modified computer program was to simulate more rigorously a cocurrent regenerative reactor (described in Section 6.7). Inlet gas temperatures of 100^0 and 200^0F were tested at a pressure of 7 atm and a Nusselt number of 4.0. The model indicated that the system has two stable operating conditions. In the primary stable condition, the oxygen combusted in the reaction zone delivers enough heat in the preheat zone to preheat the gas sufficiently; that is, the system can sustain combustion. In the secondary stable condition, insufficient combustion occurs and the gas cannot be preheated. The outlet gas temperature equals the inlet temperature, and the resultant conversion is negligible.

The major objective in this improved model study was to determine whether an isothermal solids temperature could be achieved in the wheel reactor. By mathematically varying the space velocity and the fraction of the wheel in the preheat zone (similar to Figures 6-21 and 6-22), this condition was readily attained. We observed, however, that if the space velocity and/or preheat zone were too large, the system would degenerate to its secondary stable condition. Therefore, if this reactor configuration is pushed too far beyond its design operating range, it reverts to inoperability. *

---

* Although preliminary analysis indicates that the operating condition is stable, more detailed study may be desirable to indicate the degree of operating excursion that can be tolerated.

In this model, similar to the effect noted in the simplified model, the isothermal bed is achieved when the ratio of the preheat zone to reaction zone is approximately, but not precisely, equal to the pseudo-Lewis Number of the system. The deviation from a constant bed temperature, however, is more severe in this model when the operating conditions are incorrect. This deviation is caused by the compound effect of changed bed temperature and, consequently, changed reaction rate.

A bed of layered honeycomb with many discontinuities was simulated in the model by doubling the Nusselt Number and k_g and by not changing the reaction rate constant. Under proper conditions, this modification has a significant effect on reactor performance; in some cases, it more than halves the amount of unconverted oxygen.

The reaction channel diameter also was reduced by a factor of 2 in this example. This reduction doubles the heat transfer coefficient, the mass transfer coefficient, and the surface-to-volume ratio of the catalyst. This modification greatly improves conversion, as noted in the simple reactor studies.

7. REACTION KINETICS STUDIES

7.1. Summary

The purpose of this phase of the investigation was to determine the chemical operating parameters of the process experimentally. The catalyst vendors could only supply design specifications for conventional abatement reactors, but would not provide the kinetic data required for the design of this novel rotary regenerative reactor. The literature provided some insight into the problem, but experimental data were required for incorporation into our reactor model.

The literature and catalyst vendors indicated that the NO would not be removed until the oxygen was almost completely consumed. The program was therefore directed toward determining the characteristics of the reduction of oxygen by methane over conventional NO_x abatement catalysts.

Matthey Bishop, Inc., supplied a mixed noble metal catalyst of proprietary composition, supported on 1/8-in. cell honeycomb, for use in this work. The data were satisfactorily correlated assuming that the reaction was first-order in the limiting reactant, in agreement with the literature. The Arrhenius correlation with temperature yielded an activation energy of about 15 kcal/g-mol., midway between literature values of 10 and 20 kcal/g-mol. for platinum. At higher temperatures, the rate of reaction was moderated by the rate of gaseous diffusion within the channels in the honeycomb. The correlation with pressure proved that diffusion became a dominant control at higher operating pressures. At 90 psig operating pressure, the required space velocity for 99% oxygen removal is 27,500 hr^{-1} and for 98% removal is 32,000 hr^{-1}; the rate is relatively insensitive to temperature because of the effect of diffusion control. The pseudo-Lewis Number at this condition is in the range of 0.5 to 0.8. At 1 atm operating pressure, the required space velocity for 99% oxygen conversion is 11,700 hr^{-1}. These design criteria are based upon relatively new catalysts operating at 1200°F and compare to a space velocity of 40,000 hr^{-1} recommended by the manufacturer for satisfactory operation over a 1-year period.

The mechanism of NO chemical reduction from nitric acid tail gas has not been completely determined. Certainly, our data prove that much of the NO is reduced simultaneously as the oxygen is consumed by methane. However, at high oxygen removal, the methane is incompletely oxidized. The resulting CO is a more powerful reductant and should

increase the rate of NO removal. A conservative interpretation of our data indicates that satisfactory NO effluent concentrations of 150 ppm should be achieved with 99% removal of the oxygen in the tail gas. With 98% removal of the oxygen, the expected NO concentration in the effluent is 200 ppm, the EPA standard for NO_x emissions. A more optimistic interpretation of our results would predict NO concentrations about half of those reported above. Therefore, space velocities of 27,500-32,000 hr^{-1} should be satisfactory for meeting Federal standards for NO_x emissions.

We have proposed bed modifications which could increase the design space velocity by a factor of 2.4, to 66,000 hr^{-1}. Under these conditions, the pseudo-Lewis Number decreases to the range of 0.3 to 0.5.

A palladium catalyst from Engelhard Industries exhibited activity similar to the Matthey Bishop catalyst. However, the Engelhard catalyst was subject to severe degradation, apparently by fuel cracking and refractory carbon deposition. Some samples of the Matthey Bishop catalyst also degraded, but the mechanism has not been determined.

In the program continuation, the Matthey Bishop catalyst was tested with a hydrogen-rich fuel simulating the gas product from a natural gas reformer. These data proved that the noble metal catalyst is active for the hydrogen-oxygen reaction at temperatures about 500°F lower than required for the more refractory methane fuel. When using the honeycomb catalyst, however, the system is still apparently faced with the same diffusion barrier. The overall reaction rate expected with the hydrogen fuel is not significantly greater than can be achieved with an active catalyst and methane fuel. The primary advantage of the hydrogen fuel appears to be that it can operate at a lower temperature to achieve the same result, thus minimizing potential catalyst degradation caused by temperature excursions. These results suggest that steam-reforming the natural gas fuel might be a satisfactory correction mechanism for those facilities which have NO_x abatement reactors that are continually plagued by catalyst deactivation.

A non-noble catalyst of cobalt oxide (Co_3O_4) was tested in this system. The catalyst showed activity for the reduction of oxygen with methane or hydrogen, but at temperature levels of approximately 400°F higher than required by the noble metal catalyst. The use of cobalt catalyst at 1500°F compares favorably with the use of noble metal catalyst at 1200°F. Space velocities of 19,000-23,000 hr^{-1} are required for 99 and 98% conversion of the oxygen in the tail gas. The nitric oxide reduction on this catalyst, however, is not high. Therefore, the cobalt oxide cannot be directly sub-

stituted for the noble metal catalyst in NO_x abatement. These results suggest an attractive alternative: The majority of the oxygen can be reduced with hydrogen or methane over this cobalt catalyst, yielding partially depleted tail gas. This partially treated gas would be low in oxygen concentration; it therefore could be treated more readily than the original tail gas on conventional, noble metal catalysts.

This experimental work was performed to specify the engineering design of a novel reactor. The data are reproducible and agree well with predicted behavior. Additional work is suggested with smaller catalyst channel size, and other, non-noble metal catalysts.

7.2. Objective

The purpose of this phase of the investigation was to determine the rates of the chemical reactions experimentally as functions of the operating parameters of the system. These rates would be used in conjunction with the mathematical model to design the novel rotary regenerative reactor system.

7.3. Introduction

At the inception of this program, we had planned to obtain catalyst operating characteristics from the catalyst vendors. However, the vendors were unable to give us the type of data that we required — controlling mechanisms, activation energies, reaction order, and values of the rate constant. This type of data is required for the design of the novel reactor.

Engelhard Industries had earlier specified its palladium honeycomb catalyst for nitric acid tail gas abatement at a space velocity of 100,000 hr^{-1}. This sizing basis was used for single-stage abatement reactors with 900°F inlet tail gas temperature and an oxygen concentration of 2.6% or less. However, at the inception of the program, the EPA had just published standards equivalent to 209 ppm total NO_x in the product gas.[14] These standards were not being met in existing plants using methane fuel, so Engelhard was no longer recommending the honeycomb catalyst; rather, it was suggesting pelletized catalyst at space velocities of 30,000 hr^{-1}. The pelletized catalyst could be usable in the novel reactor, but the low pressure drop characteristics of the honeycomb catalyst are a definite advantage.

Matthey Bishop, Inc., markets noble metal honeycomb catalysts for nitric acid tail gas abatement. These catalysts are primarily platinum

based, although other noble metals are admixed in some proprietary formulations. Matthey Bishop had originally quoted space velocities of 100,000 hr^{-1} for its catalyst, but moderated this rating to 80,000 hr^{-1} after the publication of the NO_x standards. Matthey Bishop prefers the 2-stage abatement process, with interstage cooling or bypassing a portion of the feed gas. The quoted space velocity is for each stage of the dual reactor, so the effective overall space velocity is about 40,000 hr^{-1} (depending upon the proportion of the gas bypassing the first reactor). In one version of the 2-stage process, all of the fuel is fed to the first-stage reactor. The oxygen in that gas is essentially consumed, but the excess methane appears in the exhaust as CO and H_2 because of incomplete combustion and shifting of the gases on the catalyst. These reductants are more active in the combustion of the oxygen and nitric oxide in the second-stage reactor.

The open literature has provided some information on the problem. A group of articles[2,16,23,24] in the February 1971 and April 1972 issues of Chemical Engineering Progress described the operation of existing nitric acid tail gas abatement units. This problem is similar to NO_x abatement from automotive exhausts, a subject that has been responsible for a series of articles[30,31] from Ford Motor Company. In particular, Shelef and Kummer[29] presented an excellent literature review. Also, Ayen and his co-workers[5,6,7,8,9] have studied the reaction of NO with a variety of reductants over copper chromite catalysts. This catalyst was apparently subject to severe degradation, but this work illustrates the relative performance characteristics of various fuels.

Primary literature on the oxidation of methane was published by the Bureau of Mines [32,33] and Malinsky.[20] The Bureau of Mines reports activation energies of about 20 kcal/g-mol. for both palladium and platinum catalysts and indicates that the reaction is approximately first order in methane, the limiting reactant, and very low order in oxygen, the excess reactant. Malinsky concurs in the reaction order, but reports activation energies of about 10 kcal/g-mol. for platinum and 20 kcal/g-mol. for palladium. Both of these sources tested a wide range of non-noble catalysts. Activity was shown by Cr_2O_3, CuO, Co_3O_4, Fe_2O_3, and MnO_2. These articles show that the catalytic activity varies significantly with the method of catalyst separation. Also, commercial catalysts, prepared by those skilled in the art, are superior to nonstandard research catalysts.

Researchers at Bell Laboratories[16] have recently announced that certain rare-earth-doped, mixed-metal oxides are catalysts for this reaction, with an activity approximately equivalent to that of platinum. This research may potentially be rewarding in finding a less expensive substitute for this noble metal.

A paper by R. D. Hawthorn[17] discusses the physical characteristics of honeycomb-type catalyst carriers and offers correlations for heat transfer, mass transfer, and pressure-drop characteristics. This paper verified the mixed diffusion and chemical control which we have found.

Our primary problem is to eliminate NO_x. The literature had indicated that satisfactory NO concentrations would be achieved only if the oxygen concentrations were reduced. It contained contradictory hints as to whether the reduction reactions with NO and oxygen were simultaneous or consecutive. Our first problem, therefore, was to evaluate the oxygen removal with methane and then examine the NO removal to determine if the reaction occurred simultaneously.

7.4. Theory

The rate of chemical reaction for the reduction of oxygen with methane is assumed to follow first-order laws, based upon the literature. The rate of chemical reaction for a first-order system is directly proportional to the activity, or partial pressure, of the reacting species according to Equation 7-1.

$$r_a = \frac{1}{S}\frac{dn_a}{dt} = -k_r\, p_a \qquad (7\text{-}1)$$

where —

k_r = reaction rate constant, lb-mol./hr-sq ft-atm

n_a = quantity of species a, lb-mol.

p_a = partial pressure of species a, atm

r_a = rate of reaction of species a, lb-mol./hr-sq ft of catalyst area

S = nominal area of catalyst, sq ft

t = time, hr

For a continuous flow system, at constant temperature, pressure, and flow rate —

$$r_a = \frac{G}{\pi} \frac{dC_a}{dS} = - k_r C_a \qquad (7\text{-}2)$$

where —

C_a = concentration of species a, mol /vol

G = molar flow rate, mol /hr

π = pressure, atm

which may be integrated to determine the reaction rate constant over the reactor length —

$$\ln \frac{C_o}{C_f} = \frac{k_r \pi}{G/S} \qquad (7\text{-}3)$$

or

$$k_r = (\ln \frac{C_o}{C_f}) \frac{Sv_o}{\phi RT} (\frac{T}{T_o} \cdot \frac{\pi_o}{\pi}) \qquad (7\text{-}4)$$

where —

C_f = final reactant concentration, mol /vol

C_o = initial reactant concentration, mol /vol

R = gas constant, 0.73 atm-cu ft/mol -^{0}R

Sv_o = space velocity, std vol/hr-vol of catalyst

T = temperature, ^{0}R

T_o = standard absolute temperature, ^{0}R

π_o = standard pressure, atm

ϕ = specific area of catalyst, sq ft/cu ft

The reaction rate constant in Equations 7-1 to 7-4 is a function only of the temperature according to Equation 7-5.

$$k_r = Ae^{-E/RT} \qquad (7\text{-}5)$$

where —

A = pre-exponential factor, mol /hr-sq ft-atm

E = activation energy, kcal/g-mol.

R = gas constant, 1.987 kcal/g-mol. - ^{0}K

T = absolute temperature, ^{0}K

The activation energy, E, is specific for a given reaction over a particular catalyst, but care must be exercised in using values from the literature because different definitions (or units) of k_r can affect the value of the activation energy. The value of E in Equation 7-5 varies from approximately 10 to 30 kcal/g-mol. for most catalytic oxidation-reduction reactions.

The reaction rate over a honeycomb type of catalyst can also be controlled by the rate of diffusion of the reactants to the catalyst wall because the flow regime in the small channels is usually laminar, even at relatively high space velocities. The rate of diffusion is governed by Equation 7-6.

$$r_{ad} = \frac{1}{S}\frac{dn_a}{dt} = -k_g(p_a - p_{aw}) \qquad (7\text{-}6)$$

where —

k_g = mass transfer coefficient, mol /hr-sq ft-atm

p_a = partial pressure of a in bulk, atm

p_{aw} = partial pressure of a at wall, atm

r_{ad} = rate of diffusion of species a, mol /hr-sq ft

If the partial pressure of the reacting species of the wall, p_{aw}, is zero,* then Equation 7-6 is identical in form to Equation 7-1 and can be integrated similarly into Equations 7-7 and 7-8:

---

* Assuming that the chemical reaction rate is much higher than the diffusion rate and that the diffusing species reacts instantaneously when it reaches the catalyst.

$$\ln \frac{C_o}{C_f} = \frac{k_g \pi}{G/S} \tag{7-7}$$

or

$$k_g = (\ln \frac{C_o}{C_f}) \frac{Sv_o}{\phi RT} (\frac{T}{T_o} \cdot \frac{\pi_o}{\pi}) \tag{7-8}$$

The mass transfer coefficient, k_g, is related to the diffusivity of the system according to the Sherwood Number, a dimensionless group, which is essentially constant in fully developed laminar flow:

$$N_{SH} = k_g' \, d_H/D \tag{7-9}$$

where —

N_{SH} = Sherwood Number, dimensionless

k_g' = $k_g RT$, ft/hr

d_H = hydraulic diameter of channel, ft

D = mass diffusivity of species a, sq ft/hr

According to molecular theory, the diffusivity of the system is inversely proportional to temperature raised to the 1.75 power:

$$D = D_o (\frac{T}{T_o})^{1.75} \frac{\pi_o}{\pi} \tag{7-10}$$

where D_o = diffusivity at standard conditions.

Therefore, although the mass transfer coefficient is a function of both the temperature and the pressure, the rate of mass transfer is independent of pressure:

$$k_g \pi \approx D_o \frac{\pi_o}{RT_o} (\frac{T}{T_o})^{0.75} \tag{7-11}$$

The exponential temperature relationship for the rate of mass transfer cannot be readily distinguished from an Arrhenius relationship with an apparent activation energy of about 1.1 kcal/g-mol. In other words, a system with low apparent activation energy might be channel-diffusion controlled, and uniform pressure data will not be sufficiently precise to prove diffusion or kinetic control. High apparent activation energies, however, are indicative of kinetic control.

The overall rate of reaction in this system will probably change from kinetic to diffusion control as the temperature or pressure is increased. In the region where both controlling parameters exert influence, the partial pressure of the reacting species at the wall, p_{aw}, is not zero, but rather is the controlling pressure for the chemical reaction rate:

$$r_{ad} = - k_g(p_a - p_{aw}) = - k_g\left(p_a - \frac{r_a}{-k_r}\right) \qquad (7\text{-}12)$$

At equilibrium, the chemical reaction rate and the diffusion rate must be equal and —

$$r_a = - \frac{k_g\, p_a}{1 + k_g/k_r} = - K\, p_a \qquad (7\text{-}13)$$

where —

$$\frac{1}{K} = \frac{1}{k_r} + \frac{1}{k_g}$$

More conveniently, we divide by pressure and define the new term K_m —

$$\frac{1}{K_m} = \frac{1}{k_r \pi} + \frac{1}{k_g \pi} \qquad (7\text{-}14)$$

where

$$\ln \frac{C_o}{C_f} = \frac{K_m}{G/S}$$

In this relationship, k_r is independent of pressure and the overall chemical reaction rate increases with increasing pressure. However, for the diffusion portion of the control, the quantity $k_g \pi$ is independent of pressure and the rate of diffusion is therefore not a function of pressure. The average reaction rate constant, K_m, increases with pressure until the diffusion control becomes predominant.

7.5. Bench-Scale Equipment and Test Procedure

The experimental hardware for the bench-scale tests is shown on the process flow and P&I drawings (Figures 7-1 and 7-2). A nitrogen stream was humidified (D1) and sent to an electric heater (E1) where the gas was heated to the range of 900°-1600°F. Oxygen and nitric oxide were blended in specially designed mixers (M1 and M2) consisting of

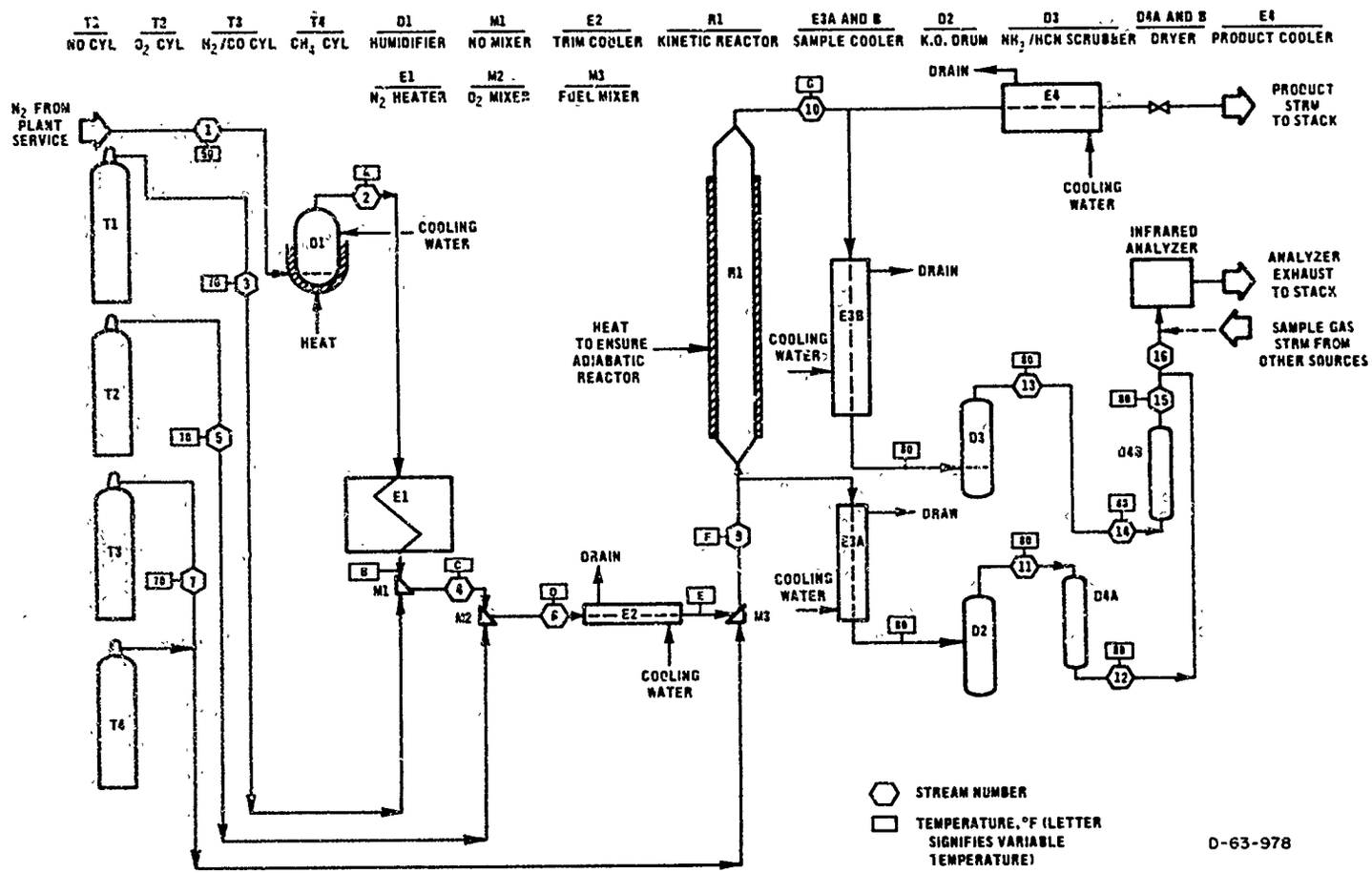

Figure 7-1. PROCESS FLOW – KINETIC STUDY

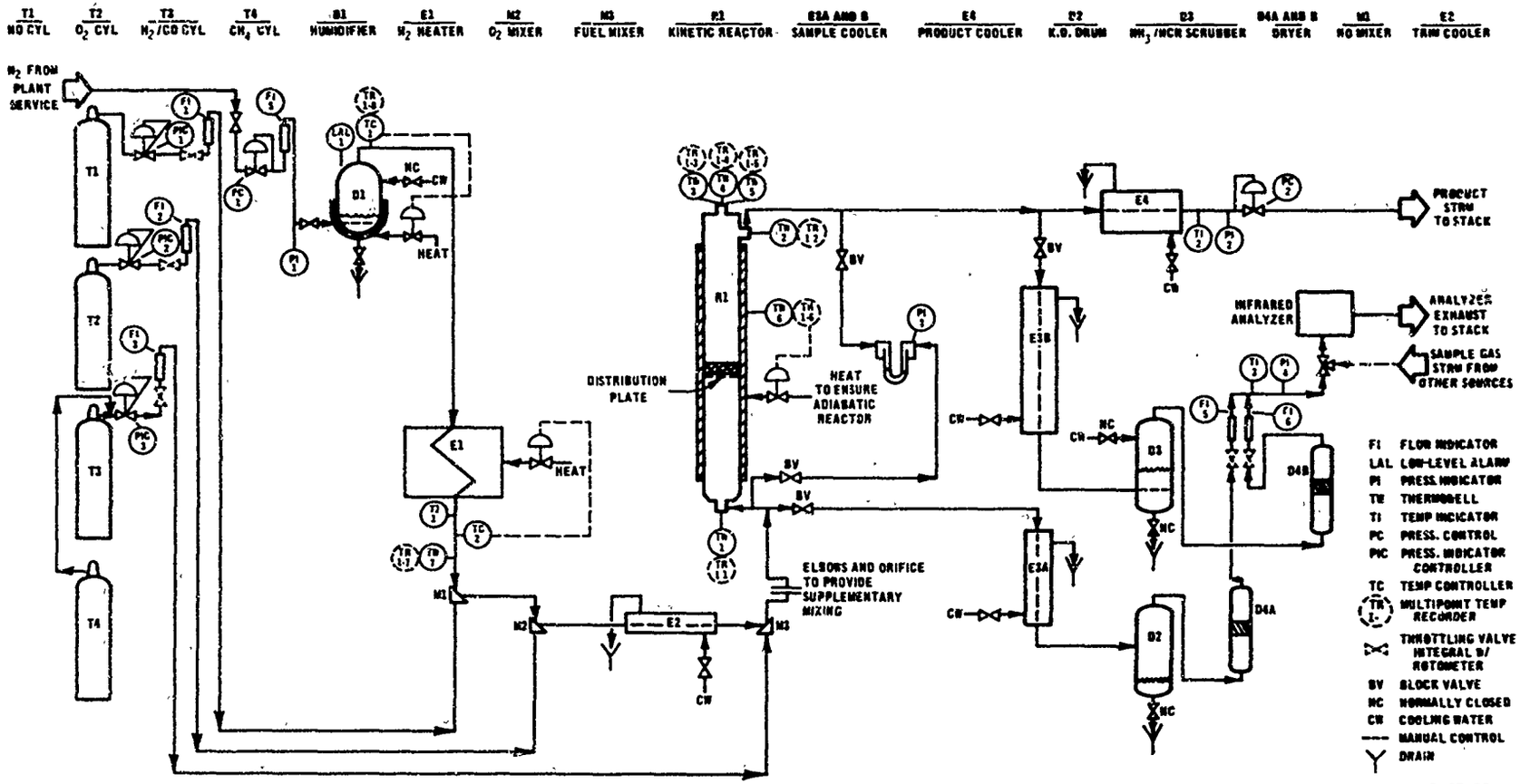

Figure 7-2. PIPING AND INSTRUMENTATION – KINETIC STUDY

blocked stainless steel tubes with perpendicular orifices, inserted into a tee in the flowing nitrogen line. The fuel was injected in a similar nozzle (M3) constructed of alumina to avoid methane cracking. The resulting stream was forced through eight close-coupled tube elbows for mixing, and the preheated gas was sent to the reactor (R1). After reaction, the tail gas was cooled and vented into a forced-air exhaust.

There were two sample points. One sample was taken at the inlet to the reactor with a cooler (E3a), a knockout pot (D2) to determine water balance, and a desiccant pot (D4a) to ensure a dry sample to the analyzer train. The outlet of the reactor was similarly sampled with the addition of a scrubber (D3) instead of a knockout pot. The water in the scrubber was analyzed for traces of NH_3 and HCN in the treated tail gas.

Either of the sampling points could be analyzed continuously for oxygen, methane, carbon monoxide, carbon dioxide, and nitric oxide. The oxygen analyzer was a Beckman Model 742 electrolytic cell with full scale ranges of 1%, 5%, 10%, and 25% O_2. We measured CO, CO_2, CH_4, and NO on Beckman Model 315D NDIR analyzers, each with three measuring ranges. Midway through the program, additional MSA NDIR analyzers were obtained for CH_4, CO_2, and CO.

The experimental reactor was a 1-in.-diameter tube which was externally resistance-heated to maintain an adiabatic condition. The heat rate to the reactor was controlled so that there was no temperature change from the inlet to the exit of the bed when preheated nitrogen was flowing. We measured the bed temperature with three shielded thermocouples located at the inlet, center, and exit of the catalyst honeycomb. Calculations of radiant and convective heat transfer coefficients indicate that these thermocouples should measure the bed temperature.

The honeycomb itself was supported on a 1/2 in. bed of 1/8 in. alumina pellets to improve the uniformity of gas flow to the honeycomb. The pellets were supported by a perforated plate of stainless steel. Midway through the program, an additional perforated plate was used between the pellets and the honeycomb to eliminate channel blockage problems.

Nitrogen from the plant LN_2 supply was gasified, pressure-controlled, and metered into the system. It was humidified at controlled temperature for water addition.

The O_2, NO, and CH_4 flow rates were established by measuring the gas concentrations in the feed sample. The fuel was plant-supply natural gas which had been desulfurized and compressed for storage. Sulfur content of this gas, if any, was too low for measurement (less than 200 parts per billion). The oxygen was compressed, breathing grade from the Linde Division of Union Carbide Corp., and the nitric oxide was obtained from Matheson Gas Products Co. Photographs of the test station and the gas analyzer train are presented in Figures 7-3 and 7-4.

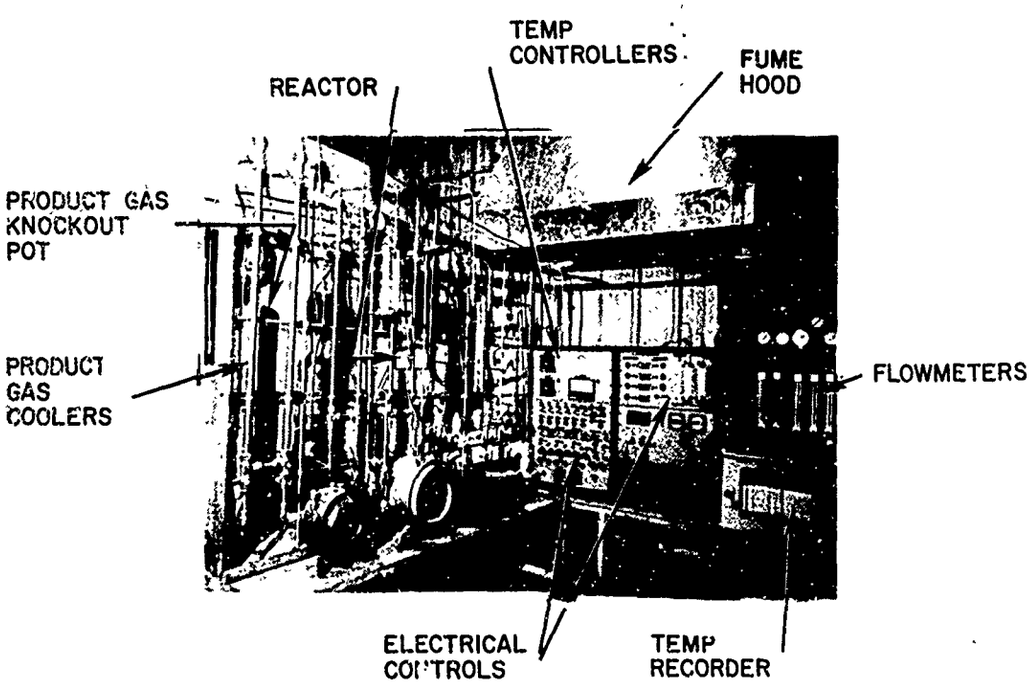

Figure 7-3. REACTOR TEST STATION

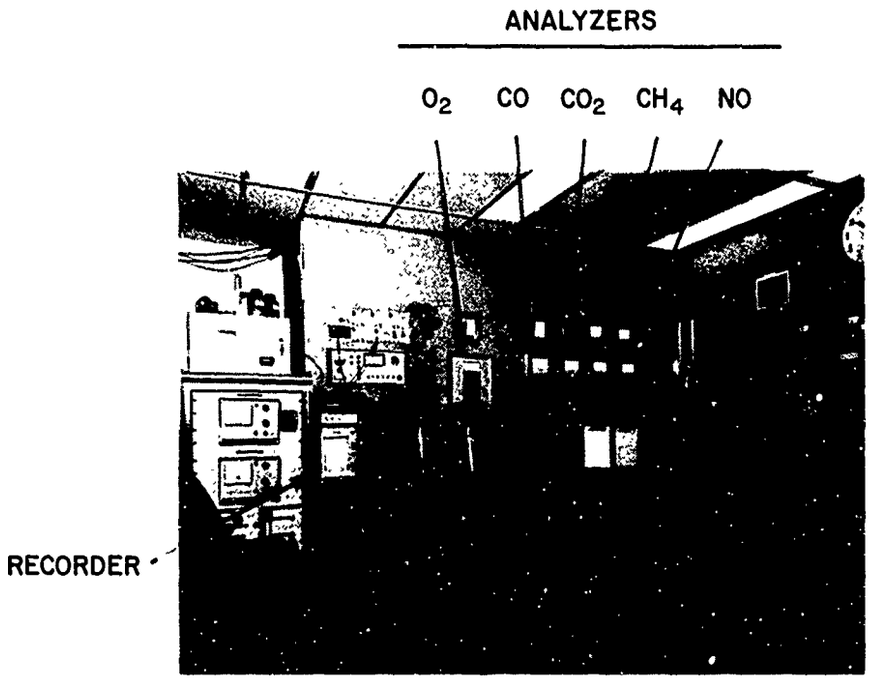

Figure 7-4. GAS ANALYSIS STATION

In operation, the reactor was charged with a catalyst sample which was 1/2 in., 1 in., or 2 in. long, depending upon the operating conditions. The operating temperatures of the reactor and the gas preheater were preset between 600^0 and 1400^0F. The flow rate of the simulated tail gas to the reactor was set at 71.7, 143, 286, or 572 std cu cm/s. When these flow rates are combined with the catalyst volumes, the effective space velocity varies from 10,000 to 320,000 cu ft/hr-cu ft of catalyst.

Most of the tests were conducted at atmospheric pressure. The pressure-dependence relationship was determined by also operating at pressures of 10, 20, and 30 psig.

The feed gas used for these tests was low in oxidant concentration to minimize the rate of exothermic heat release in the reactor. Our standard gas mixture contained 1% O_2, 1000 ppm NO, and 0.58% CH_4 (10% excess CH_4 over stoichiometric requirements). Some of the earlier tests were operated without the NO component (with reduced CH_4 addition) because we were shaking down the equipment and operating procedure.

Blank tests were run by passing the standard feed gas mixture through uncatalyzed honeycomb. The reaction rate constant at 1400°F was 3 orders of magnitude lower than the value for catalyzed solids, and the reactant conversion at 900°F was immeasurable (<5 ppm).

7.6. Experimental Results — Engelhard Catalyst

Engelhard Industries supplied a commercial NO_x abatement catalyst in which the active ingredient was palladium. The palladium was supported on a corrugated honeycomb made of cordierite manufactured by American Lava Division of 3M Co. The honeycomb has approximately 1/16-in. triangular openings, and the catalyzed mass is tan compared with the white carrier.

Four samples of catalysts were tested: One sample yielded the preliminary data presented in Figure 7-5; the other three samples poisoned rapidly, apparently by deposition of refractory carbon.

7.6.1. Sample 1 — System Checkout

The initial 3-in.-long section of Engelhard catalyst was used for the system checkout. The original methane analyzer was inoperative at that time and the backup analyzer had not yet been obtained, so the first data were preliminary. This system was started in an oxidizing atmosphere (1% O_2), and a low flow rate of methane was introduced to the system. The methane reacted and was converted to CO_2 and H_2O; no significant amounts of CO were generated. At higher methane flow rate, when nearly all of the oxygen had been consumed, some carbon monoxide was generated. In each test, the oxygen consumed was balanced with the measured production of CO and CO_2, and the hydrogen in the CH_4 was oxidized to H_2O.

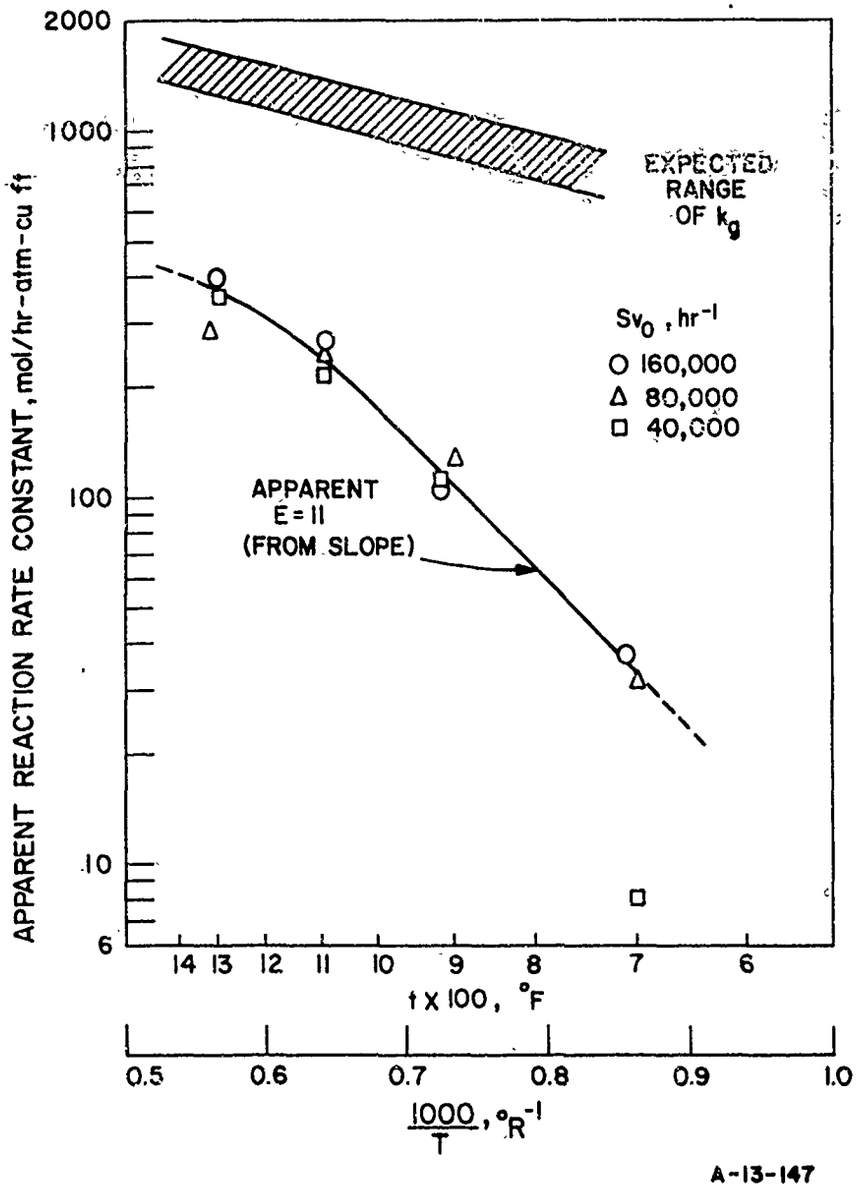

Figure 7-5. EXPERIMENTAL REACTION RATE CONSTANT FOR ENGELHARD CATALYST

This sample of catalyst was started up several times as the system was checked out. Toward the end of this period, we noticed that the catalyst did not have the same high degree of oxygen removal. When removed from the system, the catalyst was generally black as contrasted to its initial light-tan color. We suspected carbon deposition, perhaps from improper initial operating conditions, and proceeded to test another sample of the catalyst.

7.6.2. Sample 2 – Rate Data

The second test with the Engelhard Catalyst was made with a 1-in.-long section of the honeycomb. A series of 12 data points was collected. They are presented in Table 7-1 and are correlated in Figure 7-5 as an Arrhenius function. In this test, the feed contained 1% O_2 (for reduced temperature rise), no NO, and 10% excess CH_4 over the stoichiometric quantity required for oxidation to carbon dioxide. The data were correlated as a first-order reaction in oxygen. Although Figure 7-5 is based upon oxygen removal, the data on the amount of CO and CO_2 generated can be analyzed to give a nearly identical graph. The graph indicates an apparent activation energy of about 11 kcal/g-mol. in the lower temperature range with some tail off at higher temperatures, perhaps caused by diffusion control.

A band for the expected range of the mass transfer coefficient, k_g, is presented in Figure 7-5. This estimate is based upon the channel diameter; the Sherwood Number, a constant in fully developed laminar flow; and temperature extrapolation of the diffusivity of the methane in the air. This is a tenuous extrapolation on only a theoretical basis, but should indicate the order of magnitude of the diffusion coefficient. The coefficient can also be estimated from the experimental data at 1300°F and the reaction rate constant, k_r (extrapolated to 1300°F). This value is 1160 mol/hr-atm-cu ft, just below the calculated band.

7.6.3. Samples 3 and 4 – Catalyst Poisoning

Additional data were required to establish the position on the Arrhenius graph (Figure 7-5) more definitely. Also, data at elevated pressure were necessary to evaluate this effect. Tests 3 and 4 were run on additional samples of Engelhard catalysts to provide these data.

Table 7-1. DATA ON ENGELHARD CATALYST

Run No.	Time	Temp, °F	Sv_o, hr^{-1}	Outlet Concentration				k (O_2), lb-mol./ hr-atm-cu ft
				O_2, %	CO_2, %	CH_4, %	CO, ppm	
Feed	0630	--	--	1.0	1.0	0.55	5	--
1A	0700	710	160K	0.92	0.03	0.52	40	37
1B	0830	920	160K	0.79	0.08	0.46	10	105
1C	0945	1100	160K	0.55	0.20	0.375	30	266
1D	1100	1310	160K	0.41	0.28	0.27	80	397
2D	1130	1320	80K	0.28	0.38	0.17	20	283
2C	1155	1100	80K	0.34	0.345	0.21	30	240
2B	1220	900	80K	0.56	0.22	0.345	20	129
2A	1315	700	80K	0.87	0.065	0.505	10	31
3A	1330	700	40K	0.93	0.05	0.52	10	8
3B	1425	920	40K	0.38	0.325	0.255	10	108
3C	1500	1100	40K	0.14	0.43	0.16	10	219
3D	1530	1300	40K	0.04	0.47	0.07	280	358

The third test with the Engelhard catalyst was run on a fresh, 1-in.-long section of honeycomb. This sample was cut from the block of catalyst adjacent to the sample which was used in the preceding test. The performance of this catalyst sample was unsatisfactory. At lower temperatures, the conversion constant was 1/2 to 2/3 of the value presented in Figure 7-5. When the temperature was increased in succeeding tests, the rate constant did not correspondingly increase. At lower space velocities, the reaction rate was almost constant with temperature, but at the maximum space velocity, the rate constant at 1300°F was only 1/3 of that indicated in Figure 7-5. If the highest space velocity data are adjusted to a constant temperature (by an apparent activation energy of 11 kcal/g-mol.), the apparent rate constant decreased by a factor of 2 during the 5 hours of testing. The apparent degradation at lower space velocity was more severe. In contrast, the data of Table 7-1 (catalyst sample 2) can be adjusted to constant temperature by the activation energy, and decrease in rate constant is not uniform nor nearly so severe.

When catalyst sample 3 was removed from the reactor, it was black with apparent deposited carbon, similar to catalyst sample 1. In contrast, sample 2, when removed from the reactor, was not coated with the black deposit and, perhaps, was slightly lighter in color than the virgin catalyst.

A fourth test was run specifically to check for age. A catalyst sample, taken from the main block adjacent to sample 3, was placed in the reactor and operated at a space velocity of 80,000 hr^{-1} at 1100°F. The feed was 1% O_2 with 0.55% CH_4 (10% in excess of stoichiometric requirement). The initial rate constant of this test was about 75% of that achieved with sample 2. The oxygen conversion fell over a 5-hour period by 50%. At this time, we stopped the methane feed and watched the bed temperature for an indication of a carbon burn-off over the palladium at 1100°F in 1% oxygen. No temperature rise was observed during a 30-min period. When the fuel was reintroduced, the degree of conversion was even poorer than before, indicating that the carbon had not been removed but rather that the catalyst sample further degraded. When the catalyst was removed from the reactor, it too was black with apparent carbon deposition.

These findings disagree with the experience reported from the Engelhard Industries laboratories. It generally found that any carbon deposited by catalytic cracking of the methane feed can be readily oxidized over the palladium catalyst at temperatures as low as 700°F. The reason for excessive carbon deposition could not be explained either because we had adequate mixing of the feed gas and a measured quantity of fuel so that the methane was not greatly in excess.

Three of the four catalyst samples of Engelhard catalyst exhibit excessive poisoning by methane cracking and carbon deposition. One sample, however, operated "normally," indicating promise for the catalyst. However, we did not attempt to solve this problem because catalysts from other manufacturers had not exhibited this severe poisoning. We suspended testing on the Engelhard palladium catalyst because of the carbon deposition problem.

7.7. Experimental Results — Matthey Bishop Catalyst With Methane Fuel

Matthey Bishop, Inc., of Malvern, Pa., supplied a Type THT-2 catalyst on 1/8-in. Du Pont hexagonal honeycomb. This catalyst composition is a proprietary mixture of noble metals and has not been analyzed. In appearance, the material is a dark-gray coating deposited on the white mullite honeycomb.

7.7.1. Catalytic Oxygen Reduction

7.7.1.1. Correlation With Space Velocity

The first tests with this catalyst were made in a 1-in.-diameter reactor with catalyst depths of 1/2 and 1 in. Space velocity was varied from 20,000 to 320,000 hr^{-1}, and the temperature was varied from 700° to 1300°F in 200°F increments. The feed gas contained 1% O_2 and 0.55% CH_4 (10% over stoichiometric) in nitrogen, as measured by the same instruments that indicate the output gas composition. The feed in this test did not contain nitric oxide. The results of these tests are listed in Tables 7-2 and 7-2a and are presented graphically in Figure 7-6 as the output oxygen concentration against the standard space velocity.

Table 7-2, Part 1. DATA ON MATTHEY BISHOP CATALYST

Time, hr	Temp, °F	Sv_o, hr^{-1}	O_2 %	NO, ppm	k (O_2) lb-mol./ hr-atm-cu ft
0			1.0 (Feed)	0	--
0	700	320K	0.99	--	9.5 (1/2-in. catalyst)
0.5	700	240K	0.985	--	10.8
1.25	700	160K	0.97	--	14.5
1.75	700	80K	0.93	--	17.2
2	700	40K	0.87	--	16.6
2.5	900	40K	0.72	--	39.1
3	900	80K	0.855	--	37.3
3.25	900	160K	0.92	--	39.7
3.5	880	240K	0.985	--	10.8
3.65	900	320K	0.99	--	9.6
4	1100	320K	0.88	--	121
4.33	1120	240K	0.81	--	150
0	1100	160K	0.70	--	170 (Shutdown, new 1/2-in. catalyst)
0.5	1100	80K	0.48	--	175
0.75	1100	40K	0.19	--	198
1.25	1310	320K	0.73	--	300
1.5	1300	240K	0.61	--	350
1.75	1310	160K	0.53	--	302
3.25	1310	80K	0.24	--	340
3.5	1310	40K	NR	--	--
0	Feed	--	1.0	--	--
0	700	160K	NR	--	-- (1-in. catalyst)
0.5	700	120K	0.96	--	14.6
1.0	700	80K	0.98	--	4.8
1.5	700	40K	0.92	--	9.9
2	700	20K	0.80	--	13.3
3	900	160K	0.95	--	24.4
3.75	900	120K	0.92	--	29.8

Table 7-2, Part 2. DATA ON MATTHEY BISHOP CATALYST

Time, hr	Temp, °F	Sv_o, hr^{-1}	O_2, %	NO, ppm	k (O_2) lb-mol./ hr-atm-cu ft
4	900	80K	0.89	--	27.8
4.25	900	40K	0.76	--	32.7
4.5	900	20K	0.54	--	36.7
5.5	1100	160K	0.92	--	39.7
6.25	1100	120K	0.74	--	107
7.5	1100	80K	0.52	--	156
8	1100	40K	0.21	--	186
9	1100	20K	0.08	--	150
9.5	1300	160K	0.62	--	228
10	1300	120K	0.44	--	293
10.5	1300	80K	0.25	--	330
11	1300	40K	0.07	--	316
11.5	1300	20K	NR	--	--
		--	1.0 (Feed)	750	-- (1-in. catalyst)
	1300	40K	0.06	40	313
	1300	80K	0.24	160	318
	1300	120K	0.52	310	218
	1100	40K	0.20	300	179
	1100	80K	0.48	370	163
	1100	120K	0.71	540	114
	1200	160K	0.91	570	42 (2-in. catalyst)
	1200	80K	0.86	570	33
	1200	40K	0.14	190	219
	1200	20K	0.05-0.02	100-50	167-217
	1400	80K	0.67	600	89 (580 extrap.)
	1200	80K	0.86	650	33 (extrap. basis = 215)
	1000	80K	0.95	685	11.4 (74)
	800	80K	0.99	710	2.2 (14.3)
	600	20K	0.90	650	5.8
	700	20K	0.86	685	8.4

Table 7-2, Part 3. DATA ON MATTHEY BISHOP CATALYST

Date	Temp, °F	Sv_o, hr^{-1}	O_2, %	NO, ppm	k (O_2) lb-mol. / hr-atm-cu ft
					2-in. catalyst
9/12/72			1.0 (Feed)	1000	--
	600	20K	0.995	900	0.279
	700	20K	0.97	910	1.67
	800	20K	0.97	920	1.67
	900	20K	0.98	960	1.25
	1000	20K	0.87	1000	7.76
	1100	20K	0.65	1000	24.0
	1200	20K	0.46	1000	43.3
	1300	20K	0.44	1000	45.7
	1400	20K	0.24	890	79.5
9/16/72					1-in. catalyst
	1100	40K	0.36	625	113.8
	1200	40K	0.19	520	185.0
	1300	40K	0.13	480	227.3
	1400	40K	0.07	430	296.0
9/19/72	700	40K	0.95	830	20.8
	800	40K	0.98	850	18.1
	950	40K	0.71	750	32.1
	1140	40K	0.35	400	102.1
	1200	40K	0.25	325	125.2
	1400	40K	0.13	150	211.4

Table 7-2a. DATA ON MATTHEY BISHOP CATALYST – PRESSURE DATA

Date	Temp, °F	Sv_o, hr^{-1}	Press., psig	O_2, %	NO, ppm	k (O_2) lb-mol./ hr-atm-cu ft
9/26/72	1000	40K	10	0.32	350	75.6
	1400	40K	10	0.09	205	160
	1400	40K	20	0.05	160	141.4
	1000	40K	20	0.20	225	76.0
	1000	40K	30	0.13	200	74.8
	1400	40K	30	0.04	140	118
	1000	40K	0	0.85	990	18
	1200	40K	0	0.31	400	130
	1200	40K	10	0.20	300	107
	1000	40K	10	0.42	510	57.5
	1000	40K	20	0.31	480	55.3
	1200	40K	20	0.26	380	63.6
	1200	40K	30	0.20	370	60.0
	1000	40K	30	0.26	410	49.4

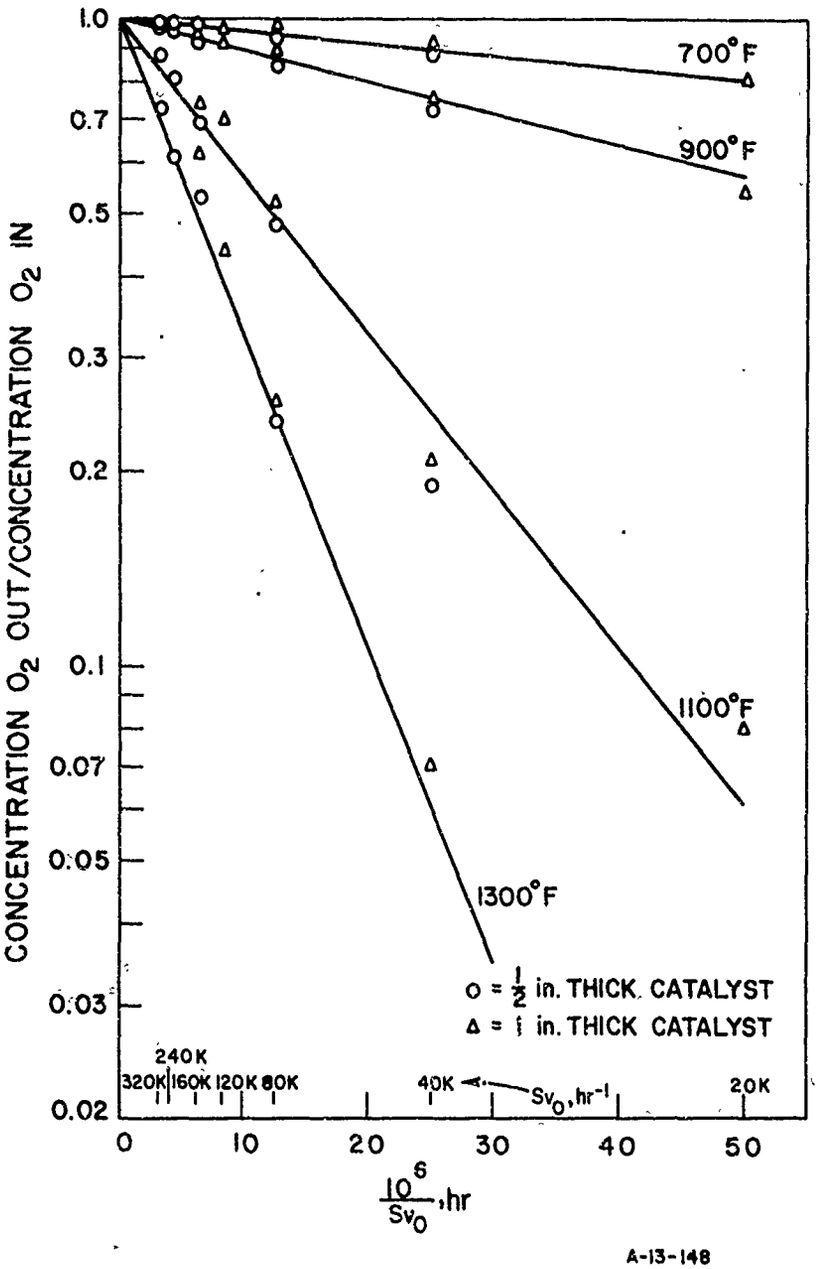

Figure 7-6. OXYGEN REMOVAL AS A FUNCTION OF SPACE VELOCITY FOR MATTHEY BISHOP CATALYST

For a constant temperature, the data form a straight line on the semilog graph. This exponential relationship is correct if the reaction follows first-order rate laws. Therefore, our assumption of a first-order reaction is satisfactory. The apparent rate constant at high gas velocity was low and a function of true velocity rather than space velocity. This was probably a mechanical problem caused by blockage of the honeycomb channels by the 1/8-in. alumina gas distribution pellets. This problem was eliminated in later tests by covering the distribution pellets with a sheet of perforated plate.

7.7.1.2. Correlation With Temperature

In later tests conversion data were collected as functions of space velocity, temperature, and pressure. Figure 7-7 presents the data collected with the Matthey Bishop catalyst as an Arrhenius graph. These data form a band on Figure 7-7 varying by ±50%. In general, the earlier data tend to fall near the top of this band while the later data operate at lower rate constants. This discrepancy may be caused by two separate batches of catalyst from the supplier, or it may reflect our greater experience with the experimental system. In either case, we shall disregard the earlier data; the use of the lower data provides a more conservative design basis.

The data near the higher edge of the band on Figure 7-7 can be reasonably compared with the Engelhard data because they were generated about the same time. Comparing Figure 7-7 with Figure 7-5, the apparent rate constants are similar for these two catalysts.

7.7.1.3. Estimated Mass Transfer Coefficient

Also included in Figure 7-7 is a band indicating the estimated mass transfer coefficient, k_g, for the 1/8-in. honeycomb, based on the diffusivity of methane in air. The coefficient was calculated from Equations 7-9 and 7-10, using the Sherwood Number. The lower edge of this band assumes a Sherwood Number of 4.0 for fully developed laminar flow. The upper edge of this k_g band is based upon a Sherwood Number of 6.6, predicted from the correlation of R. D. Hawthorn[17] which includes entrance and exit effects in the honeycomb structure. This band is based on methane diffusivity; the oxygen diffusivity is similar. For the reaction products, the counter-diffusivity of the water is higher, but the

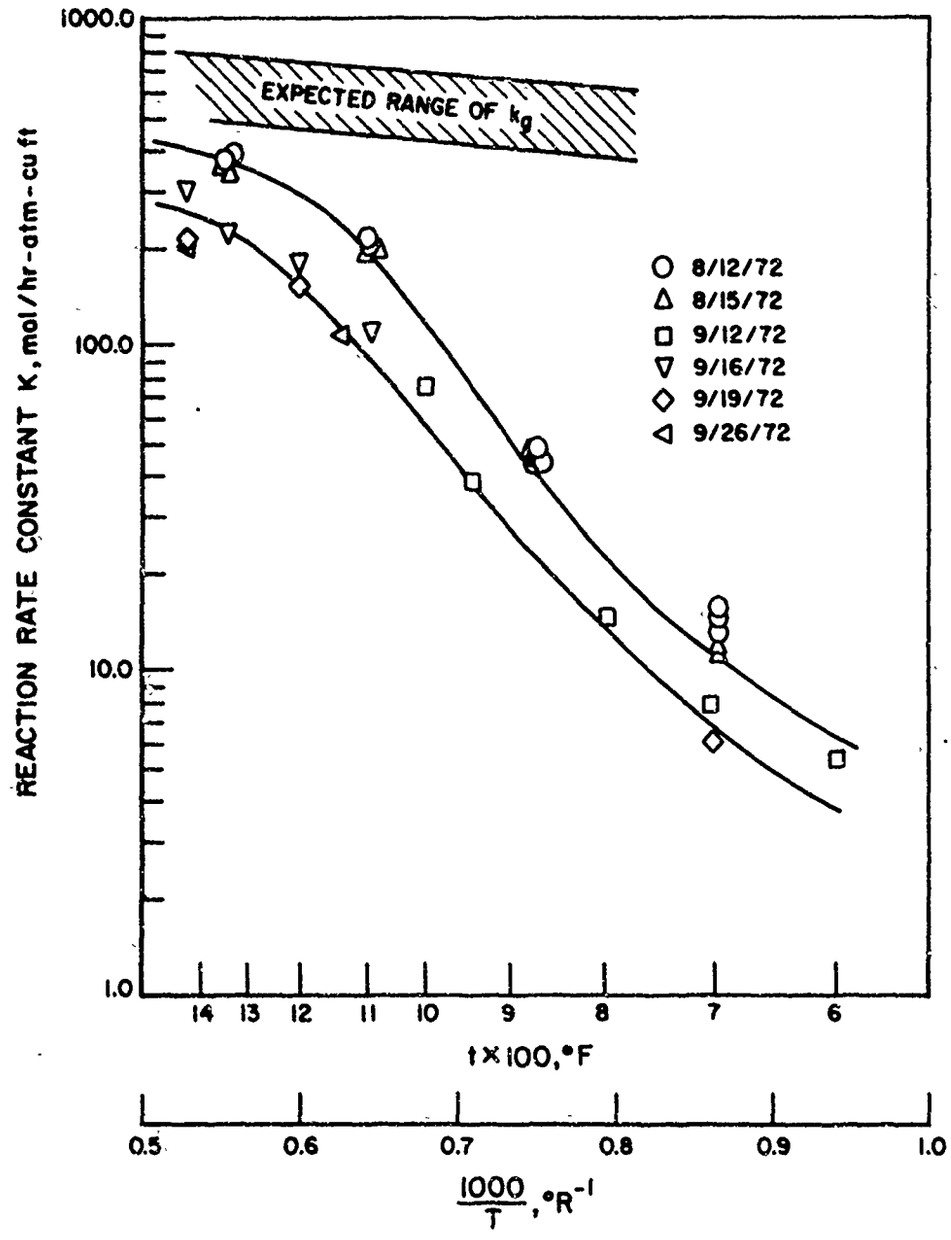

Figure 7-7. REACTION RATE CONSTANT FOR CH_4-O_2 REACTION OVER MATTHEY BISHOP CATALYST

diffusivity of the carbon dioxide is lower. Conceivably, a blanket of carbon dioxide could cause a decrease in k_g below the values indicated in Figure 7-7.

7.7.1.4. Correlation With Pressure

The reaction constants are correlated with pressure on Figure 7-8 according to Equation 7-14.

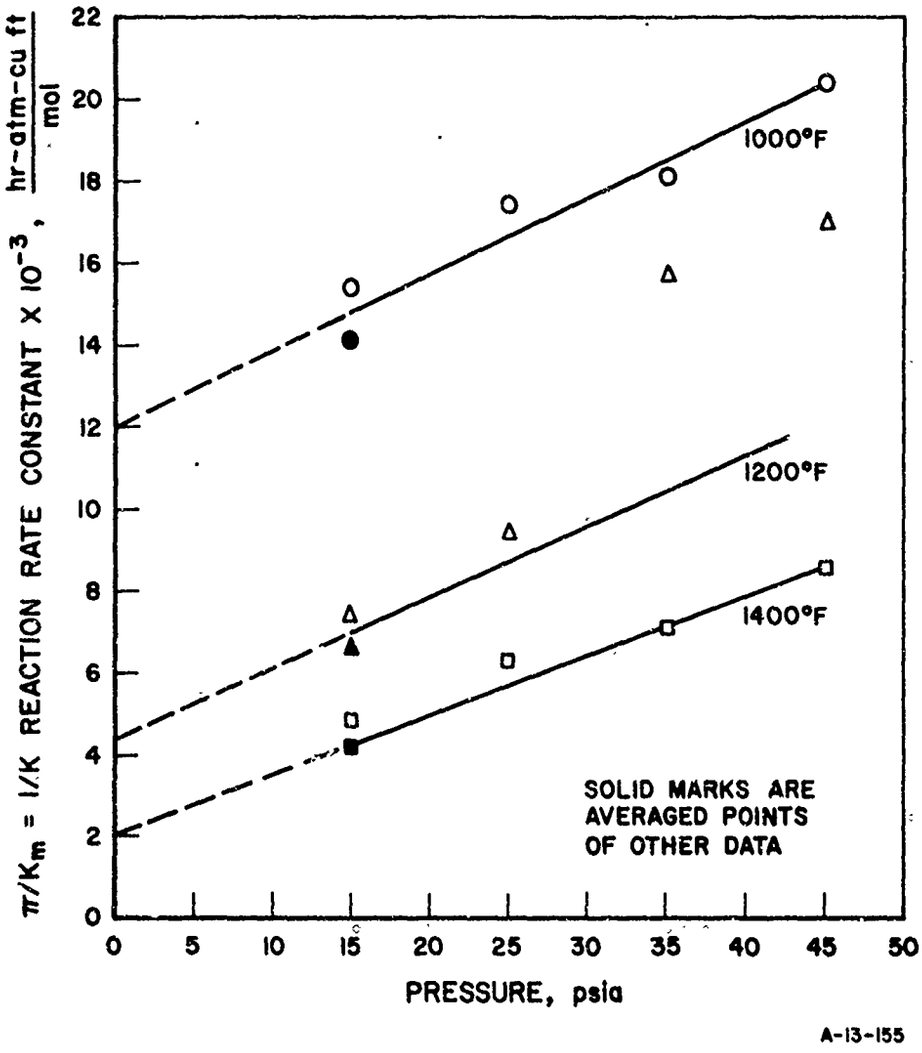

Figure 7-8. INVERSE REACTION RATE CONSTANT VERSUS ABSOLUTE PRESSURE (Matthey Bishop Catalyst)

Data at 1000° and 1400°F show good correlations; data at 1200°F exhibit scatter. The intercepts of these lines give the chemical rate constants at zero pressure. Because the chemical rate constant is independent of pressure, the intercept is the true chemical kinetic reaction rate constant, independent of diffusion effects. The mass transfer coefficient, k_g, for the diffusion effects can be calculated from the slopes of the lines of Figure 7-8.

Figure 7-9 is an Arrhenius plot for the reduction of oxygen with methane over the Matthey Bishop catalyst. It contains the conservative data from Figure 7-7, along with the extrapolated values of k_r and k_g, as determined from Figure 7-8. The activation energy for the chemical reaction rate is 14.5 kcal/g-mol., a reasonable value for the methane-oxygen reaction over an unknown noble metal catalyst.

The calculated mass transfer coefficient is 450 mol /hr-atm-cu ft at 1200°F, which agrees with the value extrapolated from the methane-air diffusivity at a Sherwood Number of 4.0. This agreement has not, however, proved this value of the Sherwood Number. The temperature extrapolation is tenuous, and the effects of slower diffusing species such as CO_2 have not been considered.

7.7.1.5. Design Rate Constants

Figure 7-10 presents the design rate constant as a function of temperature with parameters of absolute pressure. This rate constant includes a pressure term according to Equation 7-14, so the diffusion line in Figure 7-10 presents a constant barrier to increased rate. Based on the design rate constant from Figure 7-10, the required space velocity for 99% conversion of the oxygen at 1200°F and 7 atm absolute pressure (about 90 psig) is 27,500 hr^{-1}. At 1 atm pressure, the maximum space velocity is 11,800 hr^{-1}. The rate is increased with temperature at the lower pressure. It is relatively insensitive to temperature at the higher pressure because of the effects of diffusion control. If 98% oxygen removal is satisfactory, the indicated space velocities are 32,000 and 15,000 hr^{-1}, respectively, at 1200°F.

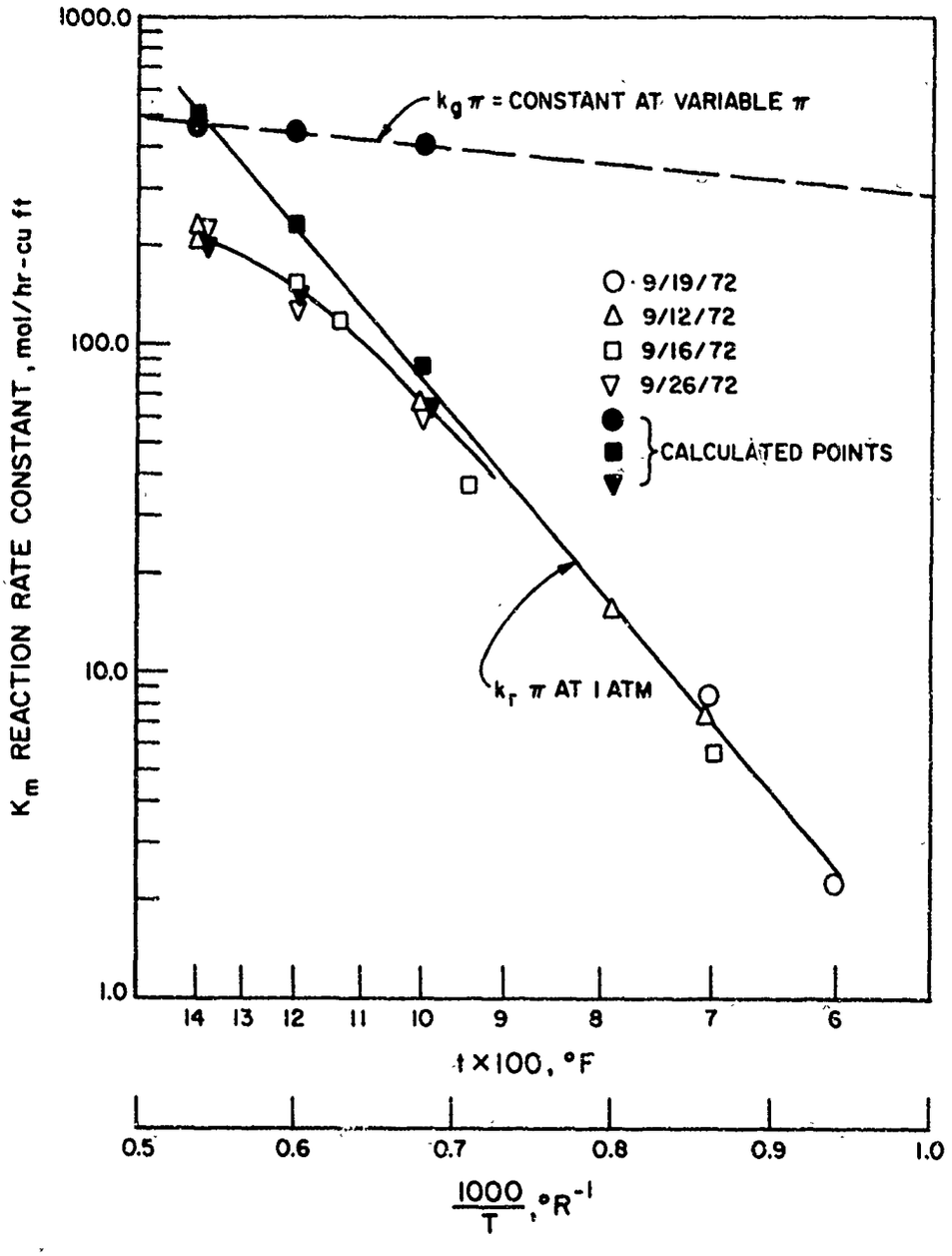

Figure 7-9. REACTION RATE CONSTANT FOR CH_4-O_2 REACTION VERSUS INVERSE TEMPERATURE (Matthey Bishop Catalyst)

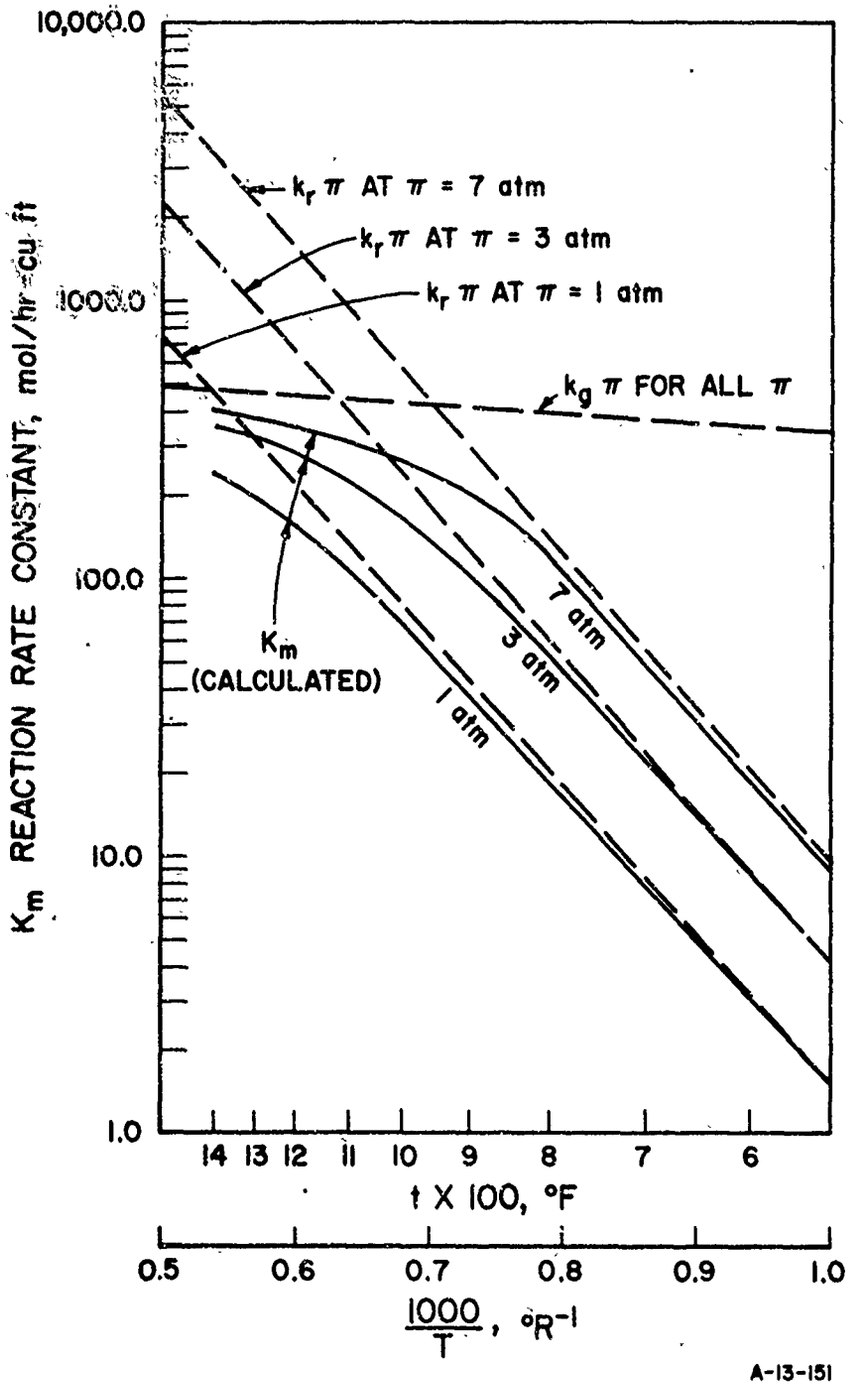

Figure 7-10. CALCULATED REACTION RATE CONSTANT AT 1 atm, 3 atm, AND 7 atm PRESSURE (Matthey Bishop Catalyst)

The value of the Lewis Number can only be estimated from Figure 7-10. Although the reaction rate constant for combined diffusion and chemical control is now known, we still have no proof for the value of the Sherwood Number. If the Sherwood Number were known, the Nusselt Number, and, hence the heat transfer coefficient (for use in the Lewis Number), could be accurately estimated. In fully developed laminar flow, the Sherwood Number should be equal to 4.0; however, entrance effects in this catalyst may raise the value of the Sherwood Numbers to nearly 7. We therefore calculate only that the Lewis Number will be in the range of 0.5-0.8 in this system at 1200°F and 90 psig. These values are supplied as an input to the mathematical modeling and pilot-unit design programs.

7.7.2. Catalytic Nitric Oxide Reduction

Tables 7-2 and 7-2a list the nitric oxide concentrations in the treated tail gas, and Figure 7-11 presents the nitric oxide removal as a function of the oxygen removal using the methane fuel over the Matthey Bishop catalyst. The data scatter significantly, but a line has been drawn through the lower data, giving a conservative design basis. Using this line, 95% nitric oxide removal will be accomplished at 99% oxygen removal. On this basis, a feed gas containing 3000 ppm NO_x would be reduced to 150 ppm, a reasonable factor of safety under the Federal requirement of 209 ppm. These requirements would just be met at an oxygen removal of 98%.

Figure 7-11 is not founded in theory. Rather, the Arrhenius relationship and pressure dependency should be plotted. However, the nitric oxide combustion data scattered too widely; relationships of the type derived for the oxygen could not be used for the nitric oxide. In general, we would expect Figure 7-11 to have theoretical validity only if the methane-nitric oxide reaction had the same activation energy as the methane-oxygen reaction, and if they were both affected similarly by the diffusion barrier. The majority of the data in Figure 7-11 are in the operating temperature range of 1000°-1400°F so the temperature effect is minimized. However, the nitric oxide reaction should not be as limited, theoretically, as the oxygen reaction by diffusion because the reaction rate constant is much less. Therefore, we would expect that a higher relative nitric oxide removal could be achieved at higher operating pressures. However, the nitric oxide removal data scatter and do not support this

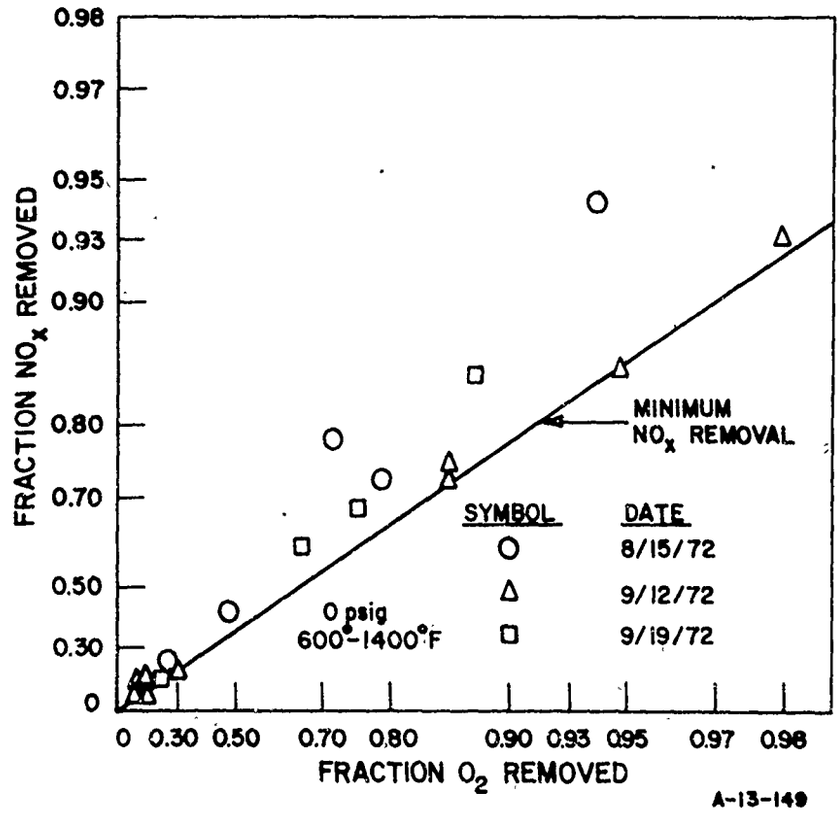

Figure 7-11. FRACTION NITRIC OXIDE REMOVED VERSUS FRACTION OXYGEN REMOVED (Matthey Bishop Catalyst)

reasoning. Similarly, at high oxygen conversions, the product gas contains carbon monoxide (and presumably hydrogen caused by the water-gas shift reaction). These are stronger reductants and should improve the rate of nitric oxide reduction. This reasoning suggests that high excess fuel rates are desirable but, again, the data do not necessarily support this hypothesis.

7.7.3. Effect of Modified Honeycomb

This analysis indicates that the reaction rate at 7 atm absolute pressure is definitely limited by the diffusion process. The overall rate of mass transfer can be increased by decreasing the channel size of the honeycomb. If the channel size were halved, the mass transfer coefficient (per unit area) should be theoretically doubled. Also, the area for mass transfer is increased per volume of bed. Even allowing for the decreased effects of entrance and exit turbulence upon the Sherwood Number, halving the channel diameter should increase the overall rate of mass transfer by a factor greater than 2.0. On this basis, a significant increase in the hourly space velocity should be possible for the same reactant conversion.

An alternative bed modification employs the concept proposed by Hawthorn[17] – deliberately introducing discontinuities into the honeycomb structure to promote turbulence. If the bed were constructed of many thin layers of honeycomb with misaligned channels, the value of the Nusselt and Sherwood Numbers could be doubled. This effect would be more pronounced at high bed L/D ratios, causing higher linear velocities.

Either of the two modifications above could double the heat and mass transfer rates. If the value, k_g, from Figure 7-9, were doubled, the space velocity required for 99% conversion of O_2 at 1200°F and 90 psig increases to 45,000 hr^{-1}. Incorporation of both modifications might increase this design basis to 66,000 hr^{-1}.

The incorporation of these modifications into the rotary regenerative reactor would affect the engineering design because the pseudo-Lewis Number would be reduced. Although k_g and h have been increased proportionally, the chemistry of the catalyst is unchanged and the pseudo-Lewis Number decreases. A 40% reduction, at the 66,000 hr^{-1} design basis yields pseudo-Lewis Numbers in the range of 0.3-0.5.

7.7.4. Catalyst Degradation

Although the Matthey Bishop catalyst maintained nearly constant activity in any series of tests, certain samples of catalyst did not give good performance. When removed from the reactor, these samples were a light-tan color. The walls of the hexagonal cells were notably thicker than in the virgin catalyst, apparently from the formation of a scale. The original dark-gray catalyst was still present under this scale.

Figure 7-12 is a photograph showing a used catalyst that behaved normally, a sample of catalyst that developed the scale, and a virgin catalyst.

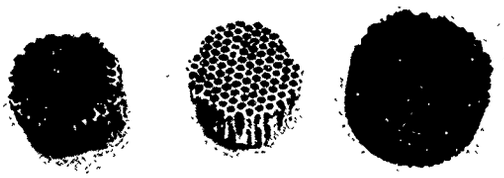

Figure 7-12. CATALYST SAMPLES. FROM LEFT: USED, ACTIVE CATALYST; USED, DEGRADED CATALYST; AND VIRGIN CATALYST. NOTE THE LIGHTER COLOR AND THICKER CELL WALLS ON THE DEACTIVATED CATALYST.

The samples were not analyzed to determine the nature of this scale because of our agreement with the manufacturer of this proprietary catalyst mixture.

7.7.5. Catalytic Manufacture of HCN, NH_3, and CO

The possible manufacture of other pollutants was checked. The water from the product gas scrubber, downstream from the reactor, was tested for HCN and NH_3. Hydrogen cyanide was not found with a sensitive spot test, and ammonia was not detected by odor. However, when the sample was causticized, the vapors activated moist litmus paper. The odor suggested that an amine, rather than ammonia, was present. The concentration, however, was low.

Carbon monoxide could be generated in the reactor. The CO concentration was a function of the oxygen conversion and the quantity of excess methane used. Based upon these data and the operation of the cyclic reactor (Section 8), we expect CO concentrations in the treated gas of about 800 ppm when operating at design conditions with 10% excess fuel.

7.7.6. Summary – Matthey Bishop Catalyst and Methane Fuel

In summary, nitric acid tail gas containing 3000 ppm NO_x will be reduced to 150 ppm, 25% below the Federal standards, when the oxygen removal is 99%. This oxygen removal can be achieved at 90 psig and 1200°F at a space velocity of 27,500 hr^{-1}. Under these conditions, the conversion is relatively insensitive to temperature or pressure. At 1 atm (absolute) operating pressure, the required space velocity for 99% conversion is 11,800 hr^{-1} at 1200°F, and the conversion increases with temperature and pressure. The Federal standards could be precisely met at 98% oxygen conversion, which requires space velocities of 32,000 and 15,000 hr^{-1} at 7 atm (absolute) and 1 atm (absolute) pressures, respectively. These design conditions are conservative because of the inherent factors of safety in Figures 7-9 and 7-11, as discussed in the preceding paragraphs. Incorporation of proposed bed modifications might increase the design space velocity to 66,000 hr^{-1} for 99% reduction of the oxygen at 90 psig and 1200°F.

7.8. Experimental Results – Matthey Bishop Catalyst and Hydrogen Fuel

A few exploratory tests were made with hydrogen-containing fuel, simulating a reformer effluent. The operation of the carbon monoxide and oxygen analyzers was erratic in these tests, so absolute data cannot be presented. However, the nitric oxide concentration was reduced by

a factor of 2, compared with tests with the methane fuel, at the same 10% excess fuel rate. Nitric oxide concentrations as low as 30 ppm were observed at 1000°F and a space velocity of 40,000 hr^{-1}. Additional work was done in this system in the contract extension; those results are presented in Section 7.11.

These results, although tentative, indicate a potential solution for those nitric acid plants which have abatement systems that operate unsatisfactorily. Steam-reforming of the methane fuel converts this refractory reductant into more reactive species. Considering the heat required for the reforming reaction, the total methane load for the plant would be approximately equivalent to a present facility using 70% excess CH_4 fuel.

The use of hydrogen-containing fuels suggests two additional alternatives for the new plant. The exhaust gas from the catalytic abatement unit contains enough heat above 1000°F that it can supply the endothermic heat of a low-temperature reforming reaction. Commercial, non-noble catalysts exist which will probably function satisfactorily in this service, although they have not been developed for this use. The expected gas composition from a low-temperature steam-reforming reactor using these catalysts is about 65% H_2, 12% CO_2, 10% CO, and 13% CH_4, a highly active fuel for this application. A second alternative is to incorporate the steam-reforming reaction into the wheel reactor. The catalysts which are active for the methane-oxygen reaction are also active for the reaction of methane and steam into carbon dioxide and hydrogen. The total quantity of methane to be treated is relatively small compared with the volume of tail gas, so the required fraction of the wheel area will be low, even at low effective space velocity. There is adequate heat available in the wheel for this duty because the overall thermodynamics of the "black box" remain unchanged.

7.9. Experimental Results -- Cobalt Oxide Catalyst

Du Pont provided a catalyst of cobalt oxide (Co_3O_4) deposited on 1/8-in. hexagonal honeycomb. Cobalt oxide was chosen for this catalyst because of its activity for the reaction as reported by Malinsky[20] and the Bureau of Mines,[32] in addition to our earlier work at IGT. A relatively heavy deposit of Co_3O_4 was used to minimize the cobalt-support phenomenon noted by the Bureau of Mines. Consequently, the catalyst had a dark-black appearance as contrasted to the white ceramic honeycomb.

The results of our preliminary investigations are presented in Table 7-3 and Figures 7-13 and 7-14. The Arrhenius relationship of Figure 7-13 for the cobalt oxide catalyst also includes the band from Figure 7-7 for the range of data with the noble metal catalyst. The cobalt oxide is active for the reaction, although at temperatures approximately 400°F higher than was found with the noble metal catalyst. In other words, at any temperature, the reaction rate constant for the cobalt oxide is about 10% of the rate obtained with the noble metal. This is not a severe depreciation, considering that the non-noble catalyst is not yet limited by the rate of diffusion in the channel pores. Assuming that the same diffusion characteristics are present with both catalysts, the cobalt oxide catalyst would operate at 7 atm (absolute) pressure with about 40% of the rate of the noble metal catalyst at temperatures of 1200°-1400°F. In addition, the non-noble metal oxide catalyst is probably not so severely temperature-limited as the platinum catalyst; therefore, it can operate at higher temperatures to further reduce the difference in the reaction rates.

Figure 7-14 illustrates that the ratio of nitric oxide conversion to oxygen conversion is less for the Co_3O_4 catalyst than for the noble metal catalyst. This factor requires further investigation, particularly at higher oxygen removals.

Based upon these preliminary data, the cobalt oxide catalyst is promising. The cobalt catalyst should enjoy a sizable price advantage over the noble metal catalyst. This differential should increase in the future because of an expected upward pressure on noble metal prices caused by demand for automotive emission catalysts.

The required reactor for non-noble oxide catalysts is about 250% of the size for noble metal catalysts with the same operating conditions. The cobalt catalyst can probably operate at higher temperatures, further reducing this size difference. Another approach to this catalyst is the use of reformed natural gas fuel, as discussed in the previous subsection, for improved reaction rate and nitric oxide removal.

Further work with this catalyst was done under the contract extension; those results are presented in Section 7.10.

Table 7-3. DATA ON Co_3O_4 CATALYST

Temp, °F	Sv_o, hr^{-1}	O_2, %	NO, ppm	k (O_2) lb-mol/ hr-atm-cu ft
		1.0 (Feed)	1000	2-in. bed
1200	20K	0.78	890	13.8
1200	10K	0.42	750	24.1
1200	40K	0.90	930	11.7
1000	10K	0.85	915	4.5
1100	10K	0.81	1000	5.7
1200	10K	0.78	860	6.9
1300	10K	0.40	775	25.5
1400	10K	0.24	710	40.0
1500	10K	0.20	670	44.8
1600	10K	0.18	660	47.8
200	10K	0.41	850	29.2

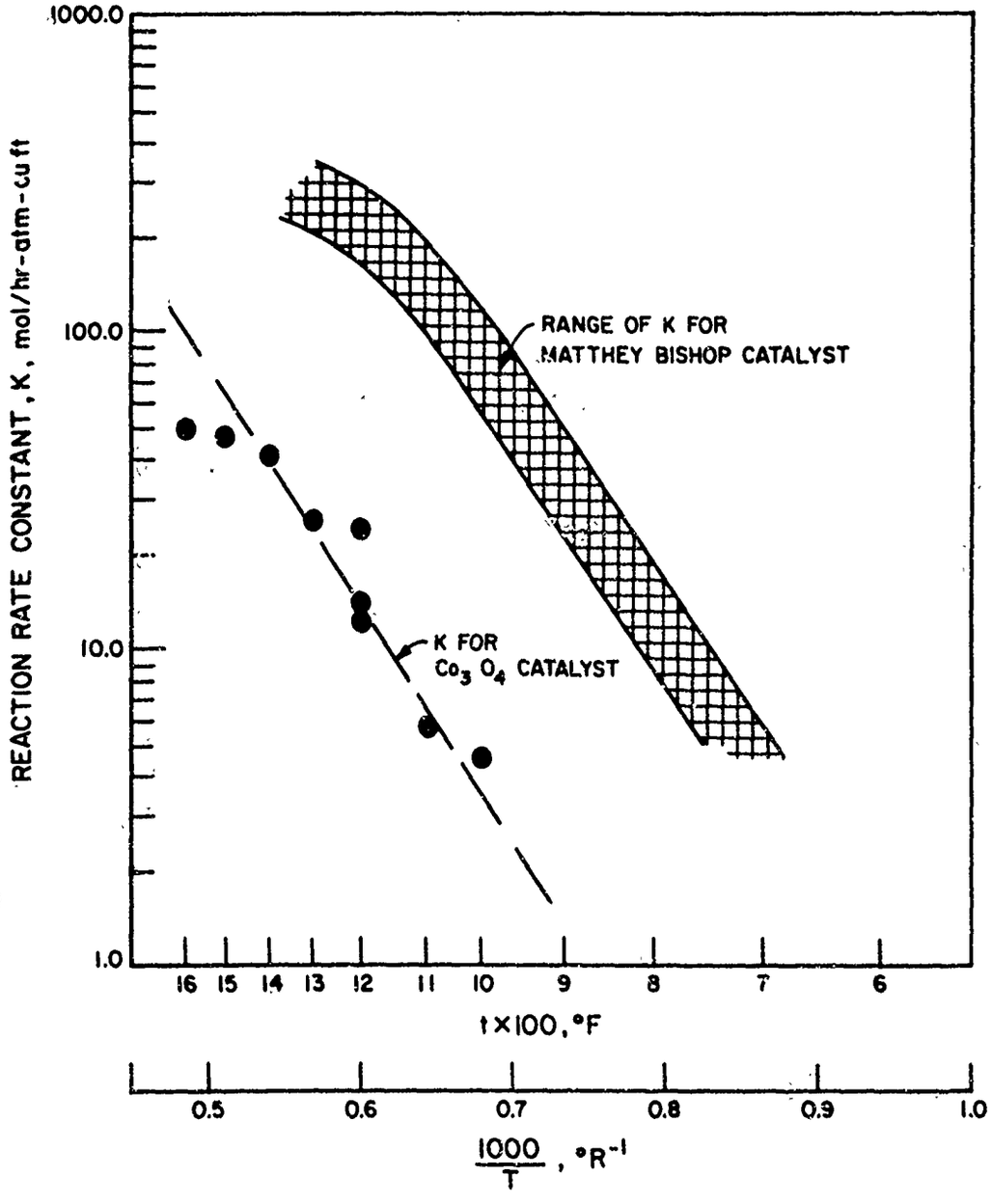

Figure 7-13. REACTION RATE CONSTANT FOR CH_4-O_2 REACTION OVER Co_3O_4 CATALYST

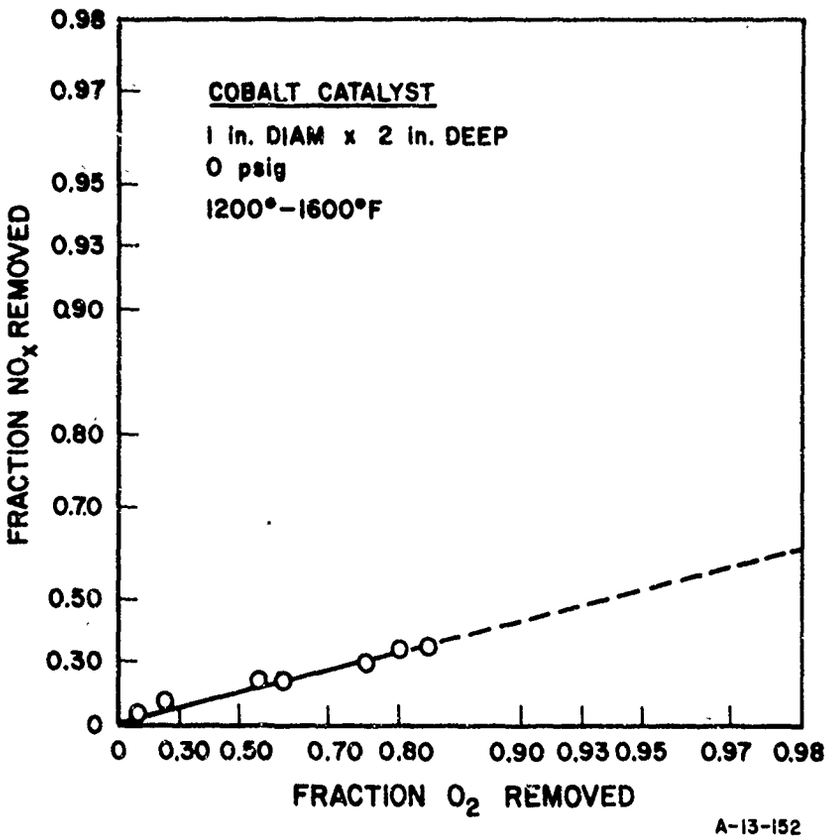

Figure 7-14. FRACTION NITRIC OXIDE REMOVED VERSUS FRACTION OXYGEN REMOVED (Co_3O_4 Catalyst)

7.10. Additional Experimental Results — Cobalt Oxide Catalyst

An extension of the contract provided for additional work on the cobalt oxide catalyst. The purpose of this work was to determine if this non-noble catalyst could be applied in nitric acid plants for reduction of NO_x emissions. If applicable, substitution of this catalyst could result in decreased operating costs compared with the currently used noble metal catalysts.

The results of this work indicate that the cobalt oxide is active for the reduction of oxygen with methane or hydrogen. However, nitric oxide reduction on this catalyst is not high. Therefore, the cobalt oxide cannot be directly substituted for the noble metal NO_x abatement catalysts. However, these results do suggest an attractive alternative: The majority of the oxygen could be reduced with methane over this cobalt catalyst, yielding a partially treated tail gas. This partially treated gas would be low in oxygen concentration, so it could be more readily treated on conventional, noble metal catalysts than the original tail gas. The catalyst would have particular applicability to the first bed of the two-stage catalytic reduction process where it could be less expensive.

Exploratory tests, using a hydrogen-rich fuel simulating a reformer product, proved that the cobalt oxide catalyst (with H_2 fuel) could be more active for O_2-reduction than the noble metal catalyst with methane fuel. This alternative for oxygen reduction, in conjunction with the NO_x reduction over noble metal catalysts using reformed gas (Section 7.11), suggest that this approach may be practical for those facilities which now have unsatisfactory abatement equipment.

In other tests, we found that the cobalt oxide catalyst had essentially no activity for the reforming, water-gas shift, and methanation reactions but that the catalyst appears to be active for the selective reduction of nitric oxide with ammonia. However, when we operated that system at higher temperatures, we found that the ammonia was oxidized to additional nitric oxide. Perhaps this catalyst has application for the replacement of the platinum-rhodium gauze in the original ammonia burner in the nitric acid plant.

7.10.1. Catalytic Oxygen Reduction — Methane Fuel

The cobalt oxide (Co_3O_4) catalyst, as described in Section 7.9, was supplied by Du Pont as a heavy, black deposit on 1/8-inch hexagonal honeycomb carrier. This is the same carrier used with the Matthey Bishop noble metal catalyst described in detail in Section 7.7.

The experimental apparatus and techniques used in the test work under the contract extension were the same as described in Section 7.5. A catalyst depth of 1 inch was used in the 1-inch reactor for these tests. The primary data on oxygen reduction were obtained with a feed gas containing 1.0% oxygen and 0.55% methane (10% over stoichiometric requirements), as determined by the same instruments that measure the product gas composition. In later tests, while evaluating NO_x abatement characteristics, 0.1% nitric oxide was added to the feed and the methane concentration was increased to account for this oxidant.

7.10.1.1. Correlation With Space Velocity

The feed gas space velocity, measured at standard conditions, was varied from 10,000 to 40,000 hr^{-1} at 1200°F. The data are listed in Table 7-4 and presented graphically in Figure 7-15.

Table 7-4. ADDITIONAL OXYGEN-REDUCTION DATA ON COBALT OXIDE CATALYST-CH_4 FUEL

Temp, °F	Sv_o, hr^{-1}	O_2, %	NO, ppm	$k(O_2)$, lb-mol./hr-atm-cu ft
--	--	1.0 (feed)	1000	--
1000	40,000	1.0	--	0
1200	40,000	0.88	--	14.0
1500	40,000	0.46	--	85.9
1200	40,000	0.85	--	18.1
1200	20,000	0.76	--	15.3
1200	10,000	0.55	--	16.6
1200	20,000	0.78	--	13.8
1200	10,000	0.63	--	12.9
1200	40,000	0.86	--	14.2
1200	20,000	0.76	--	13.9
1200	10,000	0.77	--	9.9
1200	5,000	0.63	--	6.4
1200	40,000	0.90	--	11.7
1040	20,000	0.96	--	2.4
1180	20,000	0.875	--	12.0
1350	20,000	0.70	--	20.0
1080	20,000	0.92	--	4.8

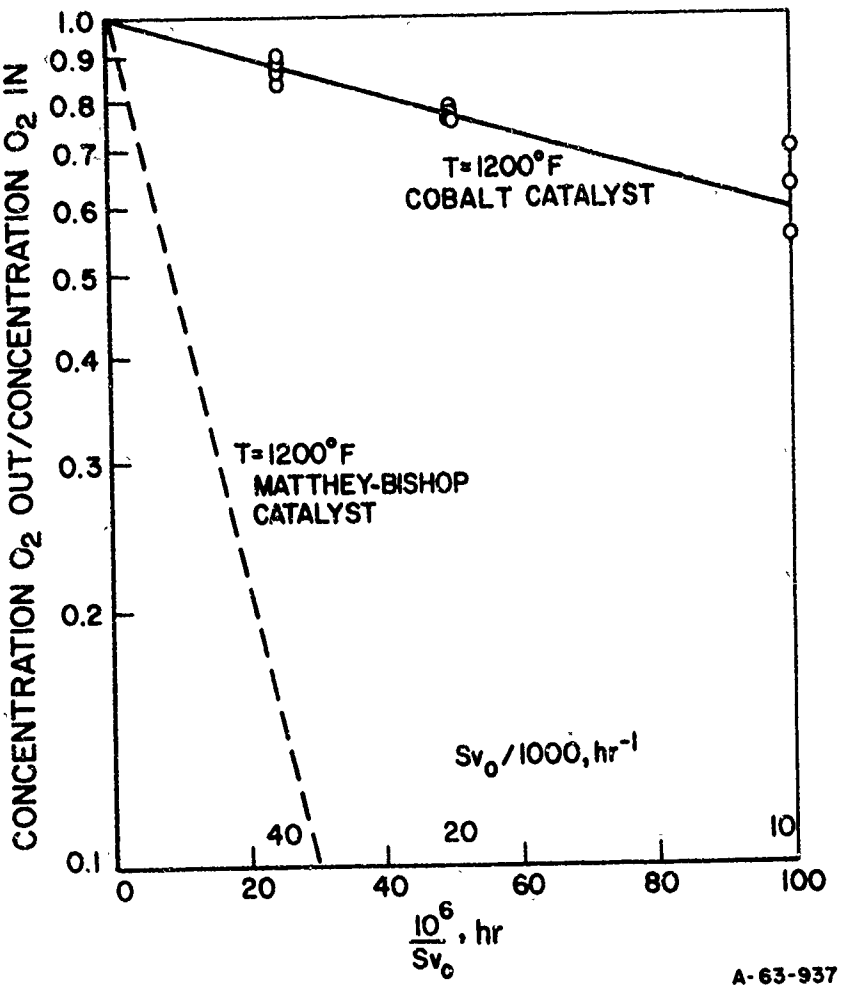

Figure 7-15. OXYGEN REMOVAL AS A FUNCTION OF SPACE VELOCITY FOR COBALT OXIDE CATALYST

This figure also contains the data for the noble metal catalyst (from Figure 7-6) at the same temperature. Data from the cobalt oxide catalyst form a straight line on this semilog graph, confirming our assumption of a first-order reaction. As expected from earlier work, the oxygen conversion with the cobalt oxide catalyst is lower than we had obtained with the noble metal.

7.10.1.2. Correlation With Temperature

The data from Table 7-4, together with the earlier data from Table 7-3, are plotted in Figure 7-16 as an Arrhenius graph. The data form a reasonably straight line with an apparent activation energy of about 18 kcal/g-mol., slightly greater than the experimental value (14.5) for the noble metal catalyst reported in Section 7.7.1.4. The Arrhenius graphs for both the cobalt catalyst and the noble metal catalyst are compared in Figure 7-17. The lines for the two catalysts are similar, with a 400°-500°F advantage for the noble metal catalyst. However, at this time we believe that the cobalt catalyst will not degrade as rapidly as the noble metal catalyst at higher temperatures, and may, therefore, be operated in a higher temperature range to obtain maximum activity.

The line for the noble metal catalyst in Figure 7-17 exhibits a tail-off from linearity at higher temperatures (lower inverse temperatures). As was explained in Section 7.7.1, this deviation is caused by the effects of mass transfer limitations. These effects are not evident with the cobalt oxide catalyst because of the lower relative activity of the Co_3O_4 for this reaction. We would expect, however, that the diffusion effects would become noticeable at temperatures of 1600°-1800°F where the relative reaction rate would be higher.

7.10.1.3. Correlation With Pressure

Table 7-5 presents the data on oxygen reduction with methane fuel over the cobalt catalyst at various pressures. We attempted to correlate these data according to the relationships presented in Section 7.7.1.4. However, as discussed above, the pressure effect is small. The effect of pressure could be readily masked by small variations in temperature and other data scatter. Therefore, these results are not graphed.

We expect, because the same physical geometry is used in both the cobalt and the noble metal catalysts, that the mass transfer coefficients will be similar. Therefore, the expected decrease in reaction rate at 1500°F caused by mass transfer effects, compared with simple kinetic control, is 50% at 7 atmospheres operating pressure and 10% at 1 atmosphere. At 1200°F, the decreases are 20% and 3% at 7-atmosphere and 1-atmosphere operating pressures.

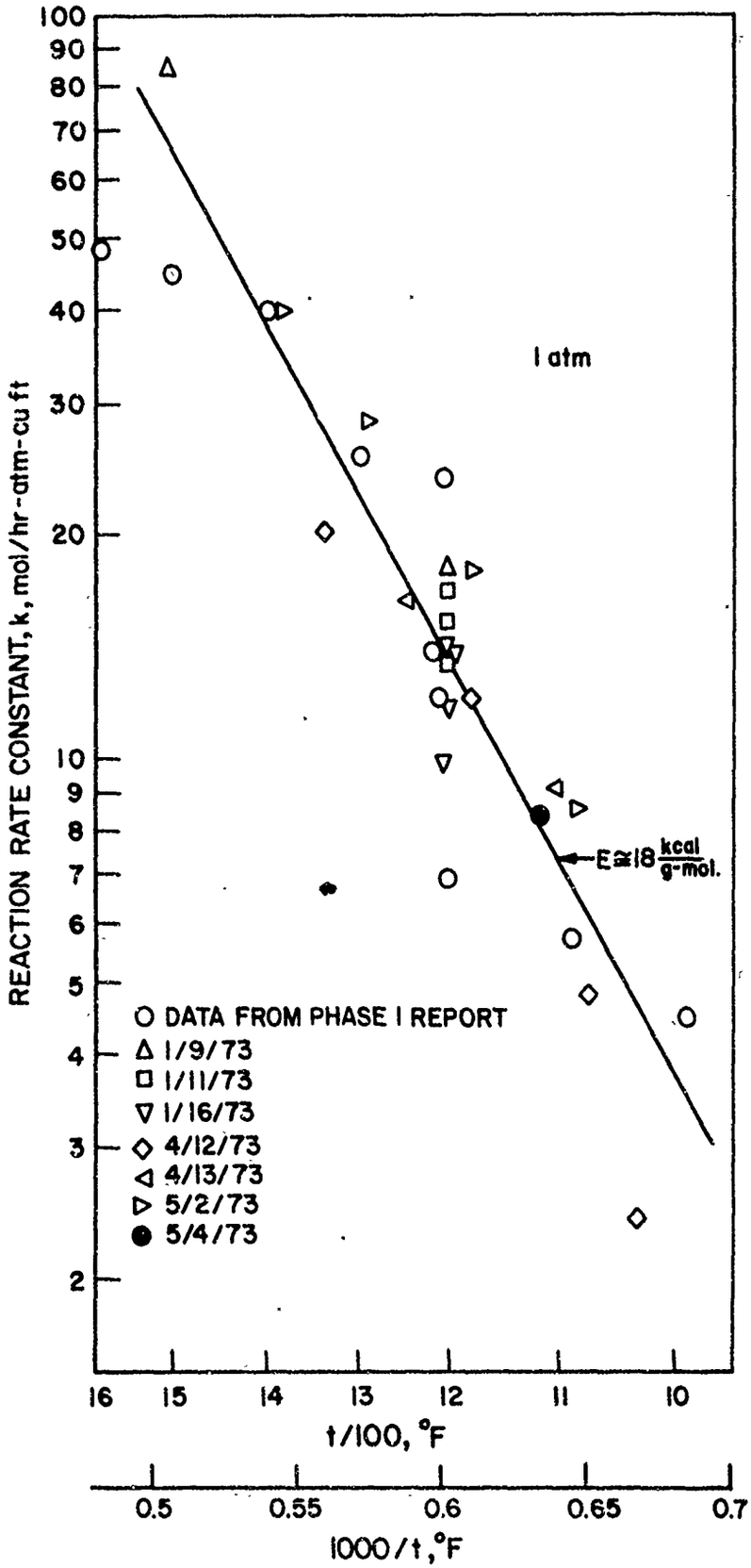

Figure 7-16. REACTION RATE CONSTANT FOR CH_4-O_2 REACTION OVER COBALT OXIDE CATALYST

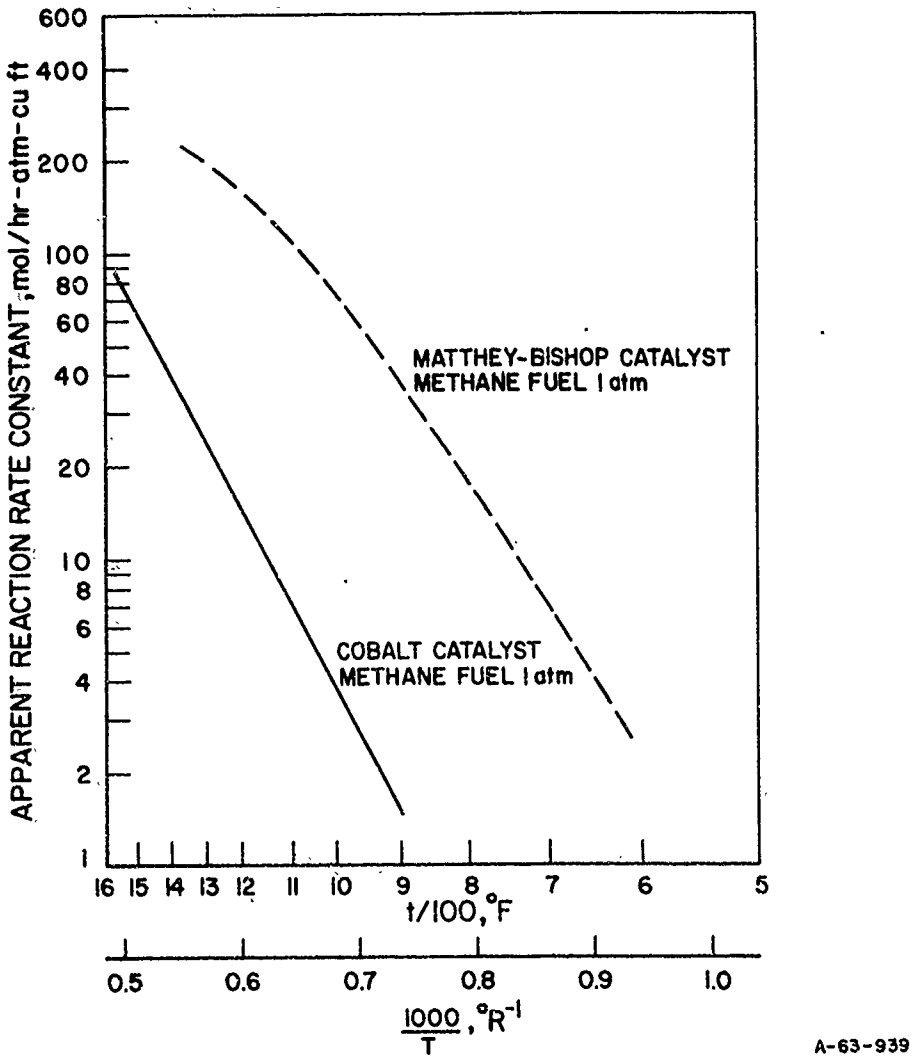

Figure 7-17. COMPARISON OF COBALT OXIDE AND NOBLE METAL CATALYSTS ON METHANE FUEL

Table 7-5. COBALT OXIDE CATALYST DATA WITH PRESSURE

Temp, °F	S_{v_o}, hr^{-1}	Press., psig	O_2, %	$k(O_2)$, lb-mol./hr-atm-cu ft
1100	20,000	0	0.85	9.1
1250	20,000	0	0.75	16.2
1250	20,000	20	0.74	7.1
1320	20,000	20	0.63	11.0
1080	20,000	20	0.89	3.1
1080	20,000	7	0.95	2.0
1250	20,000	7	0.85	6.2
1100	20,000	30	0.87	2.6
1280	20,000	30	0.70	6.4

7.10.1.4. Design Rate Constants

The experimental reaction rates for the cobalt oxide catalyst, from Figure 7-16, have been combined with the expected effects of mass transfer, according to the preceding subsection. Design space velocities were then calculated for 7 atmospheres (absolute) operating pressure using the first-order reaction equations presented in Section 7.4. These space velocities are presented in Table 7-6 for temperatures of 1200° and 1500°F for 98 and 99% conversion of the oxygen in the inlet tail gas. For operation at 1 atmosphere pressure, the space velocities should be decreased by a factor of 6 at 1200°F and a factor of 3.5 at 1500°F.

Table 7-6. DESIGN SPACE VELOCITY, COBALT OXIDE CATALYST AT 7-atm PRESSURE

	Oxygen Conversion, %	
	98	99
Temperature, °F	—Space Velocity, hr^{-1}—	
1200	7,800	6,600
1500	23,000	19,000

The use of cobalt catalysts at 1500°F compares favorably with the use of noble metal catalyst at 1200°F. At 7 atmospheres operating pressure, the reactor size required for the same conversion is only 40-50% greater for the less expensive, non-noble catalyst.

7.10.2. Catalytic Nitric Oxide Reduction

Tables 7-3 and 7-7 present the nitric oxide conversion over the cobalt oxide catalyst with methane fuel.

Table 7-7. NITRIC OXIDE CONVERSION COMPARED WITH O_2 CONVERSION

Temp, °F	Sv_o, hr^{-1}	O_2, %	NO, ppm	k(O_2), lb-mol. / hr-atm-cu ft
1080	20,000	0.86	985	8.6
1180	20,000	0.72	985	18.0
1290	20,000	0.60	985	28.3
1390	20,000	0.49	980	39.8

Figure 7-18 presents these data graphically by correlating the NO_x conversion to the oxygen conversion.

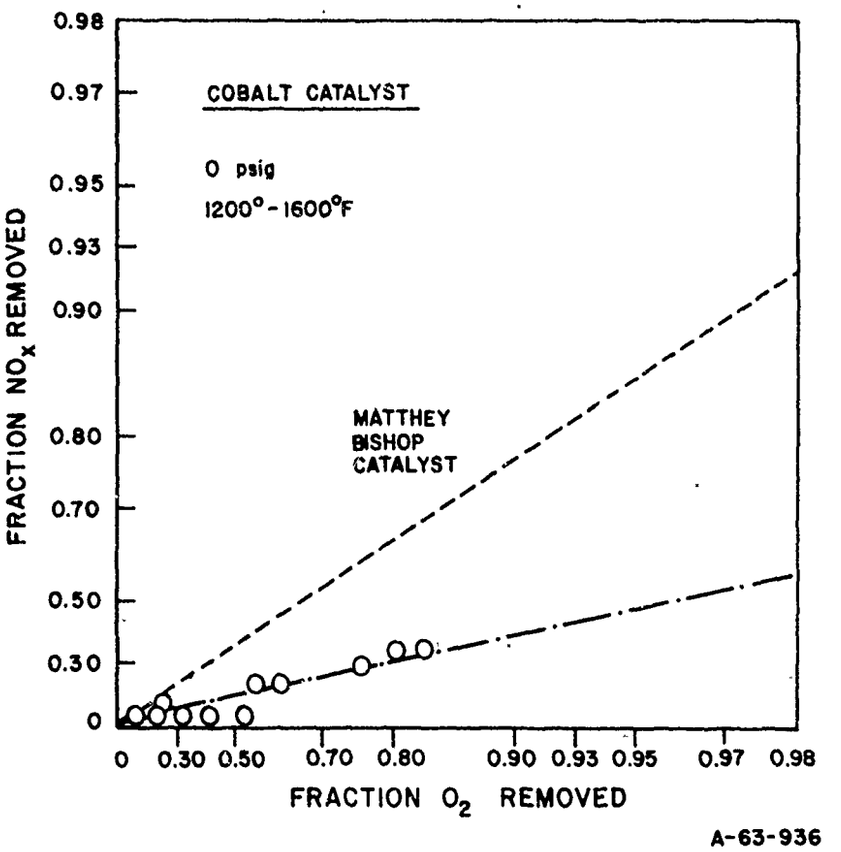

Figure 7-18. FRACTION NITRIC OXIDE REMOVED VERSUS FRACTION OXYGEN REMOVED (Cobalt Oxide Catalyst)

Also included in Figure 7-18 is the line representing the data for the Matthey Bishop noble catalyst. These data illustrate that the nitric oxide conversion over the cobalt oxide catalyst is not high. Approximately 3-5 times as much NO_x will remain after treatment with the cobalt oxide catalyst as compared with noble metal catalyst treatment.

Although the cobalt oxide catalyst is not as active as the noble metals for nitric oxide removal, it is definitely preferable for oxygen removal. We therefore suggest that both of these catalysts could be used in an NO_x abatement facility, each catalyst operating where it can be used to most advantage. The first catalyst in this system would be cobalt oxide,

operating at higher temperature and relatively high space velocities (30,000 hr^{-1}) to remove the majority of the oxygen from the system. A cocurrent regenerative reactor would probably be desirable in this application for maintaining the reaction temperature while preheating the inlet tail gas. The treated gas from this reactor, containing approximately 3000 ppm each of NO_x and O_2 at 1500°F, would be cooled in a waste-heat boiler to the operating temperature of the noble metal catalyst. Here, the nitric oxide would be removed along with the remainder of the oxygen. The oxidant concentration of this stream is now low, so temperature excursions in this catalyst would be minimized. This fixed-bed reactor should have improved operability and catalyst life time when compared with NO_x abatement reactors in use at present. The exit gas from this reactor would be 1200°-1300°F, a reasonable inlet temperature for existing turbo-expanders.

7.10.3. Catalytic Reduction – Hydrogen Fuel

A few exploratory tests were made for oxygen reduction over the cobalt oxide catalyst using fuels simulating the product of a natural gas reformer (79.7% hydrogen, 20% carbon dioxide, and 0.3% carbon monoxide). With 1% oxygen and 0.1% nitric oxide in the feed gas, the required hydrogen fuel addition is 2.3%. Because we did not have a hydrogen analyzer, this flow rate was set by measuring the CO_2 concentration in the feed gas and ratioing the hydrogen flow rate by the mass spectrometer analysis of the cylinder mixture.

Table 7-8 presents the oxygen reduction, and Figure 7-19 presents the reaction rate constants for the hydrogen-oxygen reaction as an Arrhenius graph. The cobalt oxide is an active catalyst for this reaction, achieving over 50% removal at 570°F and 90% removal at 920°F.

Table 7-8. COBALT OXIDE CATALYST DATA WITH REFORMED GAS FUEL

Temp, °F	Sv_o, hr^{-1}	O_2, %	$k(O_2)$, lb-mol. / hr-atm-cu ft
570	20,000	0.47	39.8
650	20,000	0.26	72.8
740	20,000	0.18	93.2
850	20,000	0.13	111.4
920	20,000	0.10	126.0

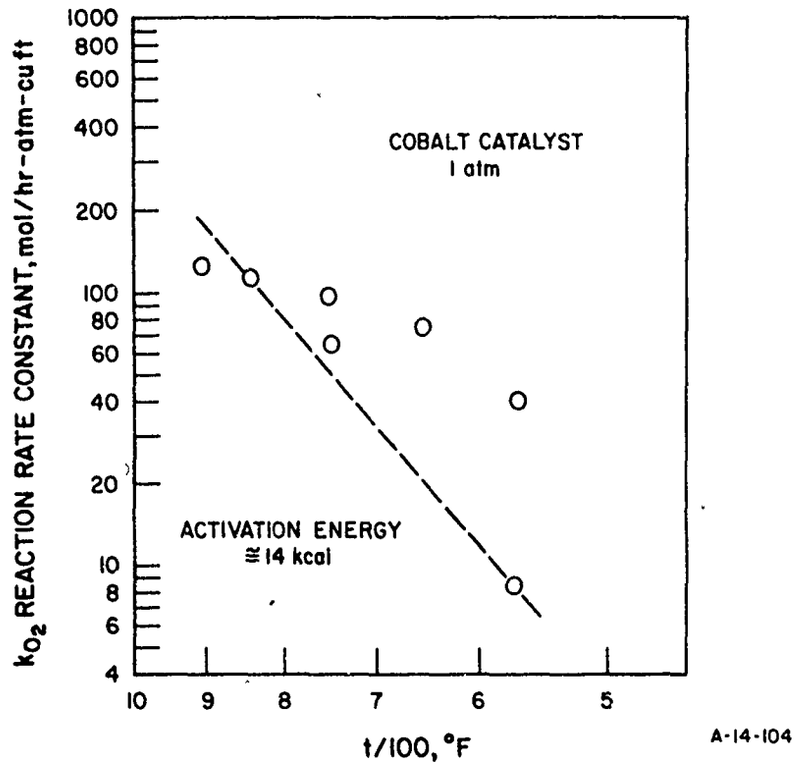

Figure 7-19. REACTION RATE CONSTANT FOR REFORMED GAS-O_2 SYSTEM OVER THE COBALT OXIDE CATALYST

The line representing the data in Figure 7-19 is tentative. When the data were first analyzed, the low point at 570°F was disregarded as spurious. However, after the hydrogen data of Section 7.11 were analyzed, this datum point had added meaning. Apparently, the catalyst can be activated with hydrogen fuel; performance greater than the minimum can be achieved after activation. This subject is discussed in greater detail in Section 7.11. The line drawn in Figure 7-19 indicates an activation energy of about 14 kcal/g-mol., in line with the methane-oxygen data. A line with a much lower slope could be drawn, but it would not indicate the minimum reaction rate, without activation of the system.

Figure 7-20 presents the relative reactivities of the noble metal catalyst with the methane fuel and the cobalt catalyst with the hydrogen fuel. This graph illustrates the high reaction rates that can be obtained with the hydrogen-oxygen system over the cobalt oxide catalyst.

The majority of the tests on hydrogen fuel did not contain nitric oxide in the feed. Some of the preliminary tests, not recorded in Table 7-8, did utilize nitric oxide. As was experienced with the methane fuel, the nitric oxide reduction over the cobalt oxide catalyst was not high, even at higher oxygen conversions.

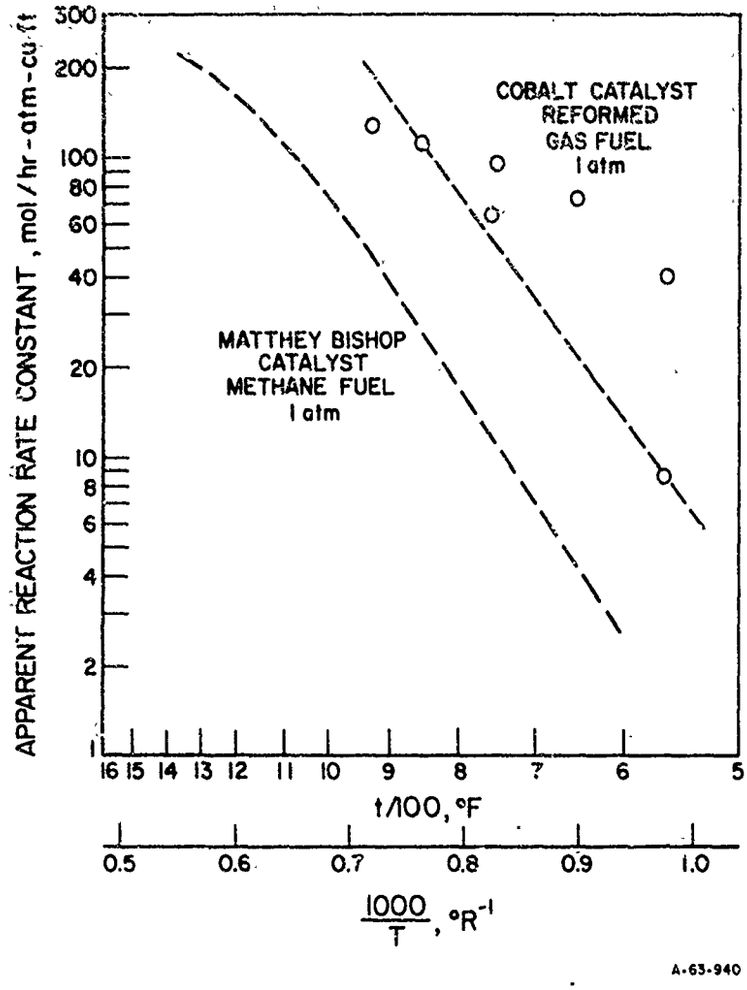

Figure 7-20. COMPARISON OF COBALT OXIDE (H_2 Fuel) WITH NOBLE METAL (CH_4 Fuel)

7.10.4. Catalytic Effects – Ammonia Fuel

A few tests were made with ammonia fuel in the oxygen-nitric oxide system. In these tests, we were looking for the selective reduction of nitric oxide with ammonia, without substantial oxygen reduction, as reported in the literature for the catalysts.[2,29] At a space velocity of 20,000 hr^{-1}, the nitric oxide content of the treated gas decreased 25% at 390°F and 42% at 430°F. At high temperatures, the nitric oxide concentration rose, indicating a temperature criticality for the selective reaction of nitric oxide with ammonia. Perhaps, at lower space velocities, this catalyst would be applicable for significant reduction of nitric oxide with ammonia at about 400°F.

At temperatures approaching 600°F, the nitric oxide concentration had reached its initial input value. At higher temperatures, nitric oxide is generated in the system, indicating that the ammonia was being oxidized to nitric oxide by the oxygen in the simulated tail gas. Perhaps this cobalt oxide catalyst could be active for the initial ammonia burner in the nitric acid plant, replacing the expensive platinum-rhodium gauze.

7.10.5. Catalytic Effects — Other Reactions

The various fuel streams were passed over the catalyst at temperatures of 500°-1300°F to examine their activity for other reactions.

A feed stream containing excess moisture and 0.6% methane was tested at a space velocity of 4000 hr^{-1} for the reforming reaction —

$$CH_4 + H_2O \rightleftharpoons CO + 3H_2 \qquad (7\text{-}15)$$

There was no apparent manufacture of carbon monoxide (less than 5 ppm) during these tests. These space velocities (the lowest we can practically use on our setup) may be too high, and the maximum temperature tested is relatively low for the reforming reaction, yet some carbon monoxide should have been observed if the catalyst has significant activity. Apparently, the cobalt oxide is relatively inert for the reforming reaction.

We tested for the reverse water-gas shift reaction:

$$CO_2 + H_2 \rightleftharpoons CO + H_2O \qquad (7\text{-}16)$$

with a feed gas containing 2% hydrogen, 0.5% carbon dioxide, and 75 ppm carbon monoxide in nitrogen. Again, the carbon monoxide concentration measured in the effluent did not change significantly from the inlet value over the entire temperature range at a space velocity of 4000 hr^{-1}. We assume, therefore, that the cobalt oxide is not active as a catalyst for this reaction.

The same conditions used in the preceding paragraphs were tested for the two methanation reactions —

$$CO + 3H_2 \rightleftharpoons CH_4 + H_2O \qquad (7\text{-}17)$$

$$CO_2 + 4H_2 \rightleftharpoons CH_4 + 2H_2O \qquad (7\text{-}18)$$

In these tests, the carbon monoxide concentration did not change from its initial value of 75 ppm and no methane could be detected, indicating that the catalyst is not active for either methanation reaction.

7.11. Additional Experimental Results – Matthey Bishop Catalyst

An extension of the contract specified additional work on the Matthey Bishop noble metal catalyst. The purpose of this work was to determine if reforming of the natural gas fuel into a hydrogen-rich mixture would be a suitable approach for correction of those facilities which have nitric oxide abatement reactors that are not performing satisfactorily. Also, additional work was directed toward catalyst degradation studies, and exploratory tests were made to determine the activity of this catalyst for other reactions that might take place in this system. The results of this work indicate that the noble metal catalyst is very active for promoting the reduction of oxygen with hydrogen. Measurable reactions occurred at temperatures as low as 175°F. This increased activity, however, does not prove that hydrogen fuel will result in improved NO_x reduction; the hydrogen-oxygen reaction is still apparently limited by the same mass transfer barriers that prohibited increased rates with the methane-oxygen reaction. A substitution of hydrogen for methane would, however, permit operation at lower temperatures where catalyst degradation, caused by temperature upsets, would not be severe. Alternatively, the system could be operated with higher oxygen concentrations, with hydrogen fuel, without exceeding the upper temperature limits for the catalyst.

The results of the catalyst degradation studies were not clear; apparently, the catalyst can be degraded by short exposure to elevated temperature, but gradual degradation was not noted, within the accuracy of the data, during 48-hour life tests.

In other exploratory work, the catalyst showed significant activity for the selective NH_3-NO_x reaction at temperatures of about 400°F. At higher temperatures, the ammonia reacted with the oxygen to generate additional NO_x. This catalyst had no measurable activity for promoting the reforming, methanation, or water-gas shift reactions.

7.11.1. Catalytic Oxygen Reduction – Hydrogen Fuel

The oxygen-reduction characteristics over the Matthey Bishop noble metal catalyst were evaluated using a fuel that simulated the effluent of a natural gas reformer. This fuel is rich in hydrogen, a more reactive species than the natural gas.

Natural gas, or methane, can be reacted with water over nickel catalysts at temperatures of about 1500°F in a process called reforming:

$$CH_4 + H_2O \rightleftharpoons CO + 3H_2 \qquad (7\text{-}15)$$

The carbon monoxide (CO) produced can be further reacted with water to form additional hydrogen in the water-gas shift reaction:

$$CO + H_2O \rightleftharpoons H_2 + CO_2 \qquad (7\text{-}19)$$

Equation 7-19 is equilibrium-limited; therefore, the carbon monoxide concentration in the product gas cannot be driven to ppm quantities. Rather, the product gas after reforming and shifting, with high water ratios, might have the following composition:

	%
Hydrogen	79.7
Carbon Dioxide	20.0
Carbon Monoxide	0.3

Packaged chemical plants to make hydrogen using these reactions are commercially available.

The reduction of oxygen with methane –

$$CH_4 + 2O_2 \rightleftharpoons CO_2 + 2H_2O \qquad (7\text{-}20)$$

requires one-half unit of methane for each unit of oxygen. When hydrogen is the reductant –

$$2H_2 + O_2 \rightleftharpoons 2H_2O \qquad (7\text{-}21)$$

two units of fuel are required for each unit of oxygen. Therefore, for oxygen reduction, one unit of methane is equivalent to four units of hydrogen. This is the same ratio of hydrogen to methane that is obtained in natural gas reforming. Therefore, the initial methane consumption should be the same for both reaction paths. The natural gas reformer, however, requires significant additional energy input because Reaction 7-15

is endothermic. This energy is usually supplied in the form of additional natural gas – an added expense which would reduce the thermal efficiency of the abatement process. P. L. Romeo[26] of Engelhard Industries has patented a novel reformer which is located in the initial ammonia burner of the nitric acid plant. This means of heat recovery may regain the efficiency which is normally lost in reforming.

The experimental reactor arrangement was similar to that used earlier in the methane fuel studies; this apparatus is described in detail in Section 7.5. The primary difference from the original setup was that the fuel was a gaseous mixture of hydrogen, carbon dioxide, and carbon monoxide simulating a reformer effluent. The stoichiometric hydrogen requirement for a gas containing 1% oxygen is 2% hydrogen. A nitric oxide concentration of 1000 ppm requires an additional 1000 ppm of hydrogen. Adding 10% excess fuel, the required total hydrogen concentration is about 2.3% in the gas stream. Our analytical instrumentation, however, did not provide means for measuring the hydrogen concentration directly. Therefore, we set the concentration of hydrogen in the feed gas by measuring the carbon dioxide content and ratioing the hydrogen content according to the composition as analyzed by the mass spectrometer. The overall resultant mixture fed to the catalyst sample had the following composition:

	%
Oxygen	1
Nitric Oxide	0.1
Hydrogen	2.3
Carbon Dioxide	0.67
Carbon Monoxide	0.009

The hydrogen, carbon dioxide, and carbon monoxide are not in the strict proportions expected from the natural gas reformer because of the inaccuracy of the purchased gaseous mixture.

The gas mixture listed above was reacted over Matthey Bishop Type THT-2 catalyst, 0.86 inch in diameter by 1 inch long, at space velocities of 13,000-30,000 hr^{-1} in the temperature range of 140°-640°F.

7.11.1.1. Correlation With Temperature

The data for the catalytic reduction of oxygen with reformed gas fuel are presented in Table 7.9 and are graphed as an Arrhenius function in Figure 7-21.

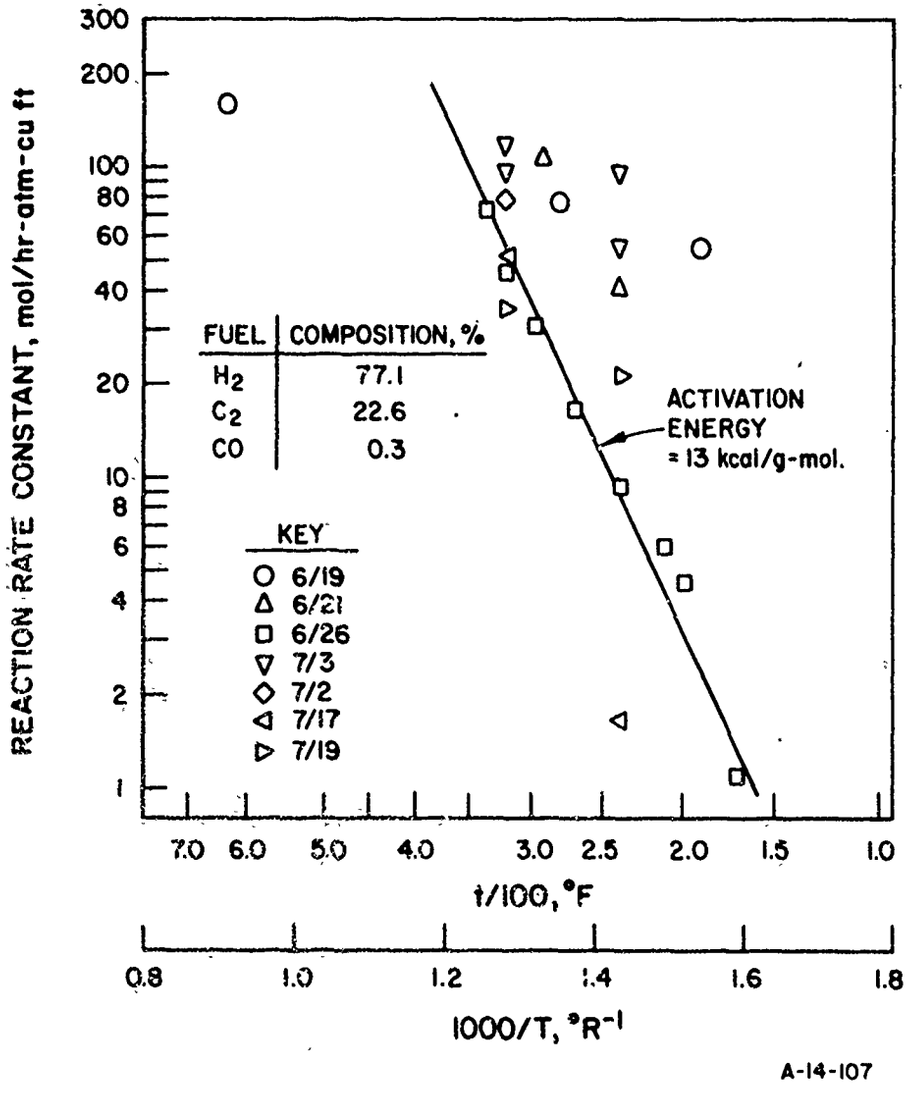

Figure 7-21. OXYGEN REDUCTION ON MATTHEY BISHOP CATALYST – REFORMATE FUEL

Table 7-9. OXYGEN REDUCTION WITH REFORMED NATURAL GAS FUEL (Fuel: 77.1% H_2, 22.6% CO_2, 0.3% CO; Catalyst: Matthey Bishop Type THT-2)

Date	Temp, °F	SV_o, hr^{-1}	O_2, %	NO, ppm	$k(O_2)$ lb-mol./hr-ctm-cu ft
6/19	640	20,000	1.0(Feed)	1000	156.7
	140	20,000	0.06	0.0	0.0
	280	20,000	0.26	260	75.0
	190	20,000	0.38	920	53.6
6/21	150	27,800	1.00	980	0.0
	290	27,800	0.26	260	104.3
	160	14,700	1.00	950	0.00
	240	14,700	0.37	700	40.7
6/26	140	20,000	1.00	1000	0.00
	170	20,000	0.98	970	1.1
	200	20,000	0.92	1000	4.6
	210	20,000	0.90	920	5.9
	240	20,000	0.85	890	9.1
	270	20,000	0.74	830	16.8
	300	20,000	0.58	690	30.3
	320	20,000	0.44	560	45.7
	340	20,000	0.27	360	72.9
7/3	240	30,000	0.52	--	54.6
	320	30,000	0.31	--	97.9
	320	15,000	0.06	100	117.6
	240	15,000	0.10	160	96.2
7/2	320	26,200	0.34	390	78.7
7/17	240	30,000	0.98	1000	1.7
	320	30,000	0.56	700	48.5
7/19	240	13,000	0.56	--	21.0
	320	13,000	0.39	--	34.1

B-24-329

The data exhibited a "shot gun" scatter with little correlation in the testing from day to day. Within a given day's testing, the data exhibited Arrhenius slopes varying from about 4 to 13 kcal/g-mol. Further study revealed that data taken with an ascending temperature-time profile exhibited the high apparent activation energy, while lower values were obtained when the data were taken on a descending temperature schedule. Apparently, therefore, the catalyst was subject to an activation phenomenon. When the catalyst was activated by operating at a higher temperature, the data taken immediately following at a lower temperature showed higher reaction rates than would be expected if the catalyst had previously been cooler. We, therefore, selected the data of June 26, with an ascending temperature schedule, as representative of the kinetic behavior which might be expected from this system. The activation energy for these data is approximately 13 kcal/g-mol., in agreement with the activation energies for the other oxidation-reduction reactions studied in this program.

The activation phenomenon apparently was also present with the hydrogen fuel and the cobalt catalyst, discussed in 7.10. In our first analyses of that preliminary data, we had drawn a line through the majority of the data with an activation energy of approximately 5 kcal/g-mol. However, when the activation phenomenon was discovered in the work of this subsection, the single datum point at low temperature took added significance: Apparently the hydrogen fuel was causing an activation phenomenon also on the cobalt catalyst. Figure 7-22 compares the Arrhenius graphs for the hydrogen-rich fuel over both the noble metal and cobalt oxide catalyst. The noble metal catalyst apparently has a temperature advantage of about 350°F over the cobalt oxide catalyst.

Figure 7-23 compares the methane and hydrogen-rich fuels on the noble metal catalyst. The activation energy for the two fuels on the same catalyst are similar, and the hydrogen-rich fuel enjoys a temperature advantage of about 500°F over the methane fuel.

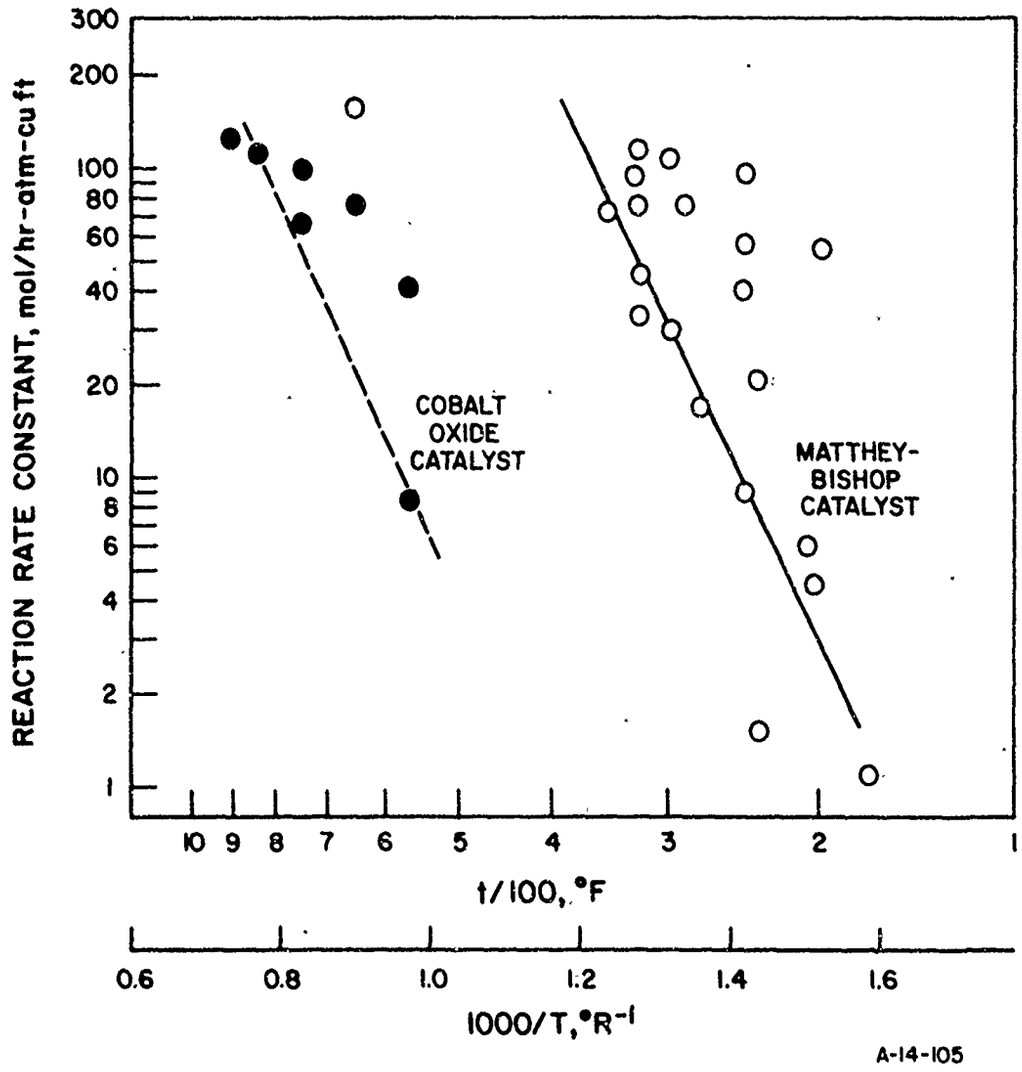

Figure 7-22. COMPARISON OF CATALYSTS FOR OXYGEN REDUCTION – REFORMATE FUEL

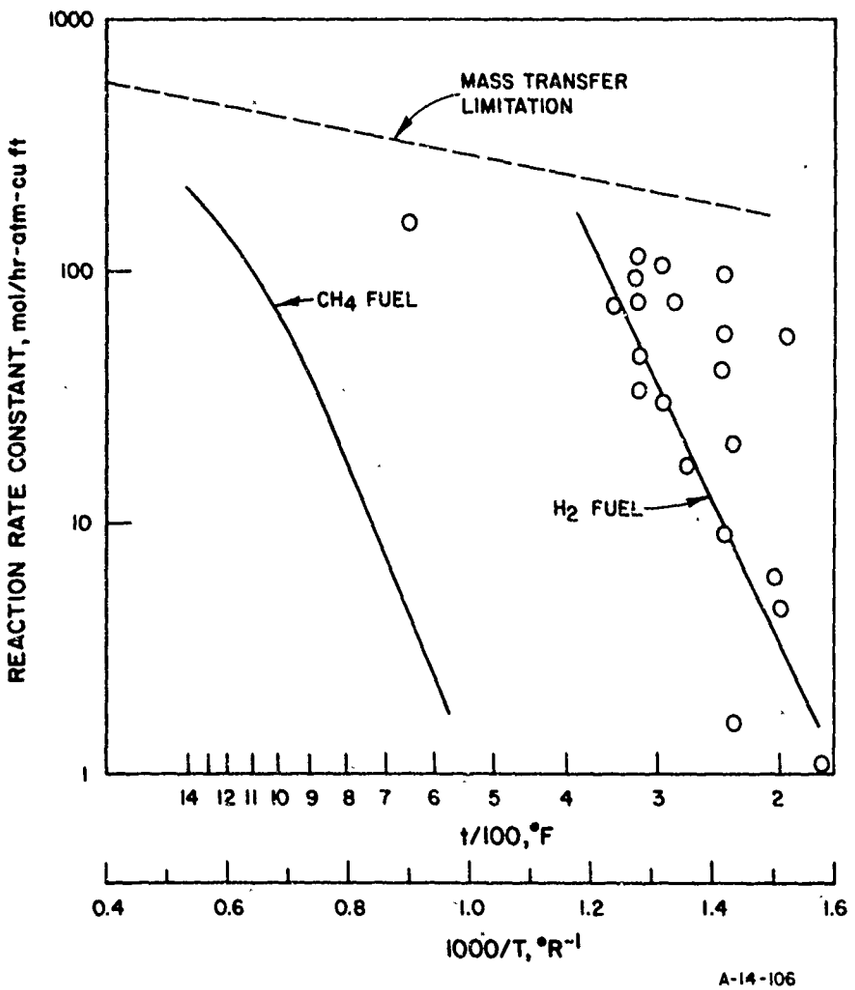

Figure 7-23. COMPARISON OF METHANE AND HYDROGEN FUELS ON MATTHEY BISHOP CATALYST

7.11.1.2. Correlation With Space Velocity and Pressure

The activation phenomenon discussed in the preceding subsection prevented the generation of meaningful data on the correlation of the reaction rate with space velocity or pressure. The activation was not readily reproducible, and the variation in activation masked the effects of these variables.

The purpose of the pressure correlation was to define the degree of diffusion control of the reaction, according to mass transfer limitations. The methane-oxygen reaction was largely controlled by diffusion at higher operating pressure (Figure 7-10). A similar diffusion barrier should exist for the hydrogen-oxygen reaction, as presented in the following discussion. Referring back to Figure 7-23, we note that none of the H_2-O_2 data violates the barrier which would have been imposed by mass transfer limitations, assuming the same diffusion barrier existed for the hydrogen fuel as was present for the methane fuel. This mass transfer barrier was initially calculated on the basis of the diffusivity of methane through nitrogen and verified experimentally. Hydrogen is a faster-diffusing molecule than methane; however, the diffusivity of oxygen is similar to that of methane and that species could be the controlling factor. Similarly, counter-diffusivity of water vapor is required for both reactions, and carbon dioxide could set up a diffusion barrier for both reactions. Therefore, the mass transfer limitation imposed upon the methane-oxygen reaction might be similar to the barrier imposed upon the hydrogen-oxygen reaction, assuming a reformate fuel.

The calculated mass transfer barrier was verified experimentally in Section 7.7.1.4. We therefore know that such a barrier exists. The cause of the barrier — methane, oxygen, carbon dioxide, or water vapor — is unknown. Such a barrier should logically also exist for the hydrogen-oxygen reaction. The location of this mass transfer limitation, however, could not be proved in this subsection. Certainly, the mass transfer limitation should not be lower than that for the methane fuel, because no slower-diffusing species are present in this reaction. Perhaps the mass transfer limitation for this reaction will permit a higher rate; however, for conservative design, we should assume that the mass transfer limitation is the same as was measured for the methane-oxygen reaction.

The methane-oxygen reaction was largely controlled by the mass transfer barrier at higher operating pressures. If the mass transfer barriers are similar, the overall rate of the hydrogen-oxygen reaction cannot be much greater than the methane-oxygen reaction at elevated pressures and temperatures of 900°F and greater. Our estimate, based on Figure 7-10, is that perhaps a 25-30% increase in the reaction rate constant (and the design space velocity) would be possible with the hydrogen fuel. The chemical reaction rate would be high under these conditions, and only the mass transfer barrier would be active.

Therefore, a system which was designed to operate with methane fuel at 1200°F, 7-atm absolute pressure, and a space velocity of 27,500 hr^{-1}, could possibly operate at the same temperature and pressure with the hydrogen fuel at a space velocity of 35,000 hr^{-1}. Alternatively, at the lower space velocity, the oxygen concentration in the effluent would be about 30% of that obtained with the methane fuel.

The observations in the preceding paragraph do not prove that hydrogen has marginal utility as fuel in this system. Rather, the reverse is indicated, when system operability is considered. The hydrogen-oxygen system can be operated at lower temperatures to achieve the same oxygen conversions. The use of lower temperatures eliminates the catalyst degradation from temperature excursions. For example, a 200°F temperature rise (which is quite possible if the tail gas oxygen content increases by one percentage point and high excess fuel is used) would cause severe degradation if the catalyst had been operating at 1400°F, but little effect would be noted if the nominal operating temperature were 900°F.

The use of hydrogen fuel permits higher oxygen concentrations in the tail gas because the reaction initiation temperature is lower. For example, with methane fuel, the maximum inlet oxygen concentration to a single-stage, simple reactor is about 2.5% because the inlet gas temperature must be 900°F to ensure reaction stability. With higher oxygen concentrations, the temperature of the catalyst would exceed the limits imposed by degradation. With a 300° or 400°F inlet gas temperature, however, much higher inlet oxygen concentrations may be tolerated without danger of degradation.

The hydrogen-rich fuel also offers significant advantages when used with honeycomb catalyst of smaller channel size. In this case, the mass transfer barrier is raised to much higher levels. With the methane fuel, the natural reactivity of the methane-oxygen reaction causes a significant limitation when the mass transfer barrier is increased to higher values. However, the higher reactivity of hydrogen fuel may be used advantageously in this situation. Design space velocities of 100,000 hr^{-1} might be used for 99% oxygen reduction at elevated temperatures and pressures.

7.11.1.3. Catalytic Nitric Oxide Reduction

The squares in Figure 7-24 present the data obtained on the catalytic reduction of nitric oxide using a hydrogen-rich fuel. This graph is a copy of Figure 7.11 and presents the nitric oxide removal as a function of the oxygen removal. Also presented in Figure 7-24 are additional data with methane fuel which were collected during the catalyst aging studies discussed later.

The hydrogen-rich fuel appears to have the same activity for reducing nitric oxide as the methane fuel. In general, the data points for the active catalysts fall in the same range as the other data. Therefore, the same design basis can be used for the hydrogen-rich fuel as was used for the methane fuel: 98% oxygen removal will just meet the Federal emission requirement of 209 ppm; 99% oxygen removal provides a reasonable factor of safety.

7.11.2. Catalytic Nitric Oxide Reduction — Ammonia Fuel

A few exploratory tests were made to examine the selective removal of nitric oxide in the presence of oxygen using ammonia fuel. According to the literature,[29] nitric oxide will react directly with ammonia fuel in the presence of oxygen according to the following reaction:

$$3NO + 2NH_3 \rightleftharpoons 5/2N_2 + 3H_2O \qquad (7\text{-}22)$$

This reaction is enhanced in the presence of oxygen because the following reaction can also take place:

$$NO + NH_3 + 1/4O_2 \rightleftharpoons N_2 + 3/2H_2O \qquad (7\text{-}23)$$

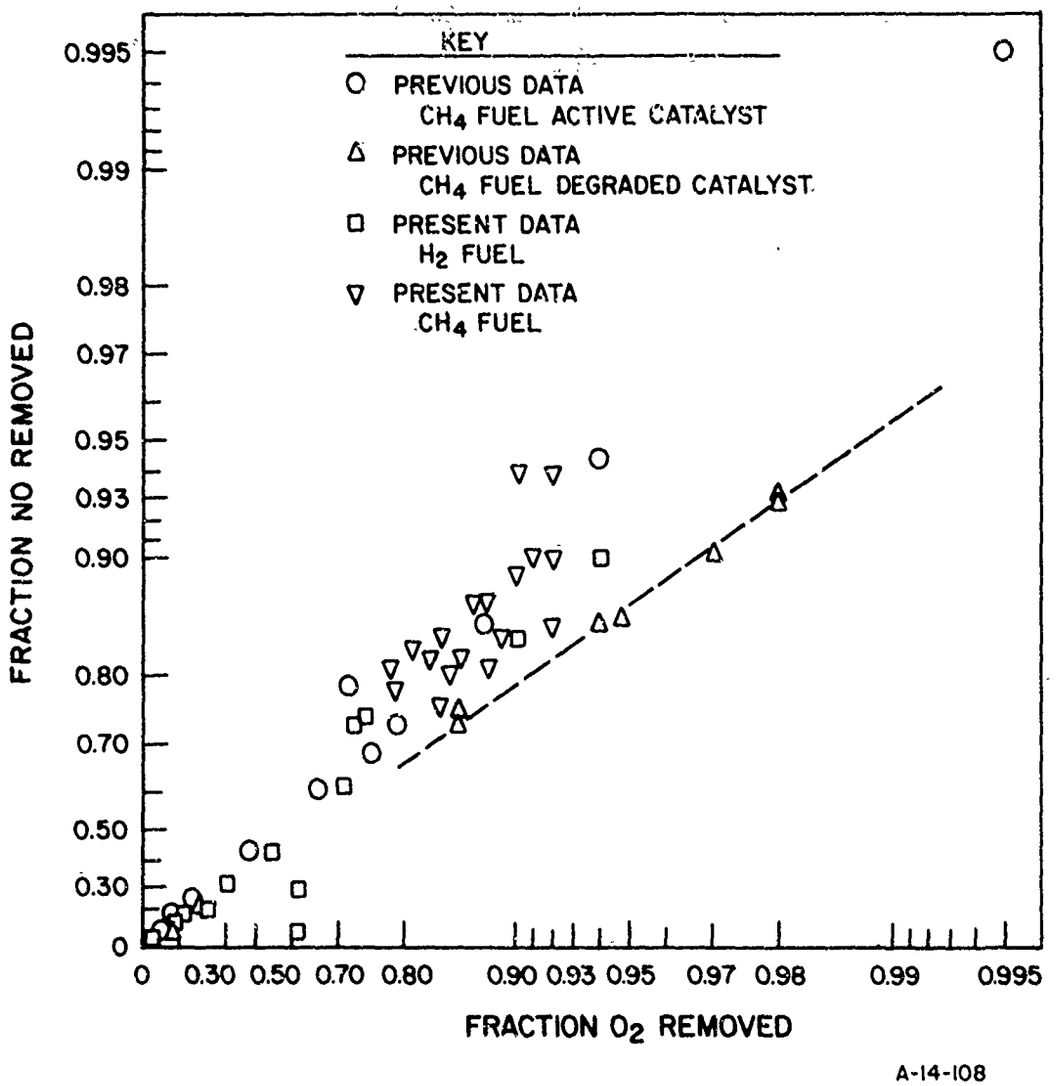

Figure 7-24. NITROGEN OXIDE REMOVAL OVER MATTHEY BISHOP CATALYST

Isotopic labeling studies have proved that the nitrogen formed in Reaction 7-23 is made by a union of nitrogen atoms from the nitric oxide and the ammonia. The selective reduction of nitric oxide by ammonia takes place because the catalytically bonded nitrogen from one species reacts with the nitrogen from the other species, rather than requiring the union of two chemisorbed nitrogen species as is required with the general reduction of NO by other fuels.

The competing reactions, consuming ammonia for oxygen reduction, are as follows:

$$4NH_3 + 3O_2 \rightarrow 2N_2 + 6H_2O \qquad (7\text{-}24)$$

$$4NH_3 + 5O_2 \rightarrow 4NO + 6H_2O \qquad (7\text{-}25)$$

Reaction 7-24 consumes oxygen with the formation of atmospheric nitrogen, but Reaction 7-25 is the initial reaction considered for the fixation of nitrogen from ammonia into nitric oxide. These reactions can compete with the catalytic reduction of NO for the consumption of the ammonia fuel.

Table 7-10 and Figure 7-25 present the exploratory data that were gathered on the system. The experimental setup was similar to the earlier tests, except ammonia was used as the fuel. Ammonia was supplied at triple the stoichiometric requirement of nitric oxide, according to Reaction 7-23, in these tests.

The data proved that the ammonia has significant activity for the selective removal of nitric oxide at temperatures of about 400°F over the noble metal catalysts. Greater than 50% nitric oxide removal was observed at 390°F at a space velocity of 20,000 hr^{-1}. Greater removals might have been expected at lower space velocities or higher pressures. At higher temperatures, the nitric oxide removal decreased and, in fact, nitric oxide was generated at temperatures greater than 800°F. This noble metal catalyst is apparently effective at higher temperatures for Reaction 7-25, the manufacture of nitric oxide from ammonia.

Table 7-10. EFFECT OF AMMONIA FUEL WITH MATTHEY BISHOP CATALYST
(Feed Composition: 1.0% O_2, 1000 ppm NO, 3000 ppm NH_3, Balance N_2)

Date	Temp, °F	Sv_o, hr^{-1}	O_2, %	NO, ppm
6/12	200	20K	0.96	990
6/12	300	20K	0.86	490
6/12	390	20K	0.77	410
6/12	470	20K	0.70	850
6/12	640	20K	0.76	620
6/12	820	20K	0.52	620
7/13	350	20K	0.90	570
7/13	710	20K	0.90	950
7/13	800	20K	0.66	>1000
7/13	900	20K	0.63	>1000
7/13	990	20K	0.88	>1000

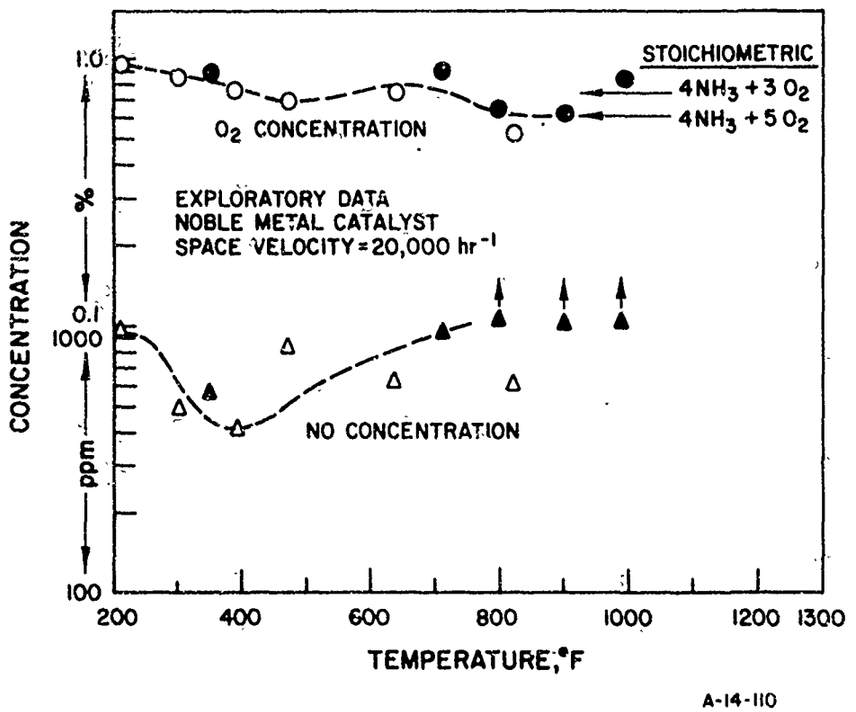

Figure 7-25. EFFECT OF AMMONIA FUEL

7.11.3. Catalytic Effects – Other Reactions

Exploratory tests were made to determine if the Matthey Bishop noble metal catalyst has significant activity for other reactions that might occur in the carbon-hydrogen-oxygen system. A feed gas of the following composition was fed to the reactor at temperatures of 800° to 1100°F and space velocities of 5000 to 20,000 hr^{-1}.

	%
Hydrogen	2.05
Carbon Dioxide	0.60
Carbon Monoxide	0.0085
Nitrogen	(Balance)

No change in this gas composition was noted during the testing, indicating that the catalyst was relatively inactive for the methanation and water-gas shift reactions:

$$CO + 3H_2 \rightleftharpoons CH_4 + H_2O \qquad (7\text{-}17)$$

$$CO_2 + H_2 \rightarrow CO + H_2O \qquad (7\text{-}16)$$

In this test work, we paid particular attention to the concentration of carbon monoxide to determine if it was being manufactured or consumed.

The other reaction which was checked over the catalyst was the reforming of methane:

$$CH_4 + H_2O \rightarrow CO + 3H_2 \qquad (7\text{-}15)$$

This is the reverse of the methanation reaction. The dry gas fed to the reactor contained 0.57% methane in nitrogen, and the nitrogen had been humidified at 150°F. The moist gas should therefore contain about 25% water vapor, greatly in excess of the quantity required for the reforming reaction. No carbon monoxide was detected in the effluent gas stream at a space velocity of 20,000 hr^{-1} and temperatures of 630° to 1090°F. We therefore assume that this noble metal catalyst is not highly active in promoting the reforming reaction. Certain noble metals, such as ruthenium, are active for the reforming reaction in this temperature range, but our tests did not indicate activity for the Type THT-2 catalyst.

These tests appeared to contradict the results of other investigators, who claim that the system equilibrates for the water-gas shift reaction after partial combustion. Perhaps the other investigators used a different catalyst or the reaction was catalyzed by the test equipment.

If the water-gas shift reaction does not equilibrate over this catalyst, a system can be designed to minimize the effluent carbon monoxide concentration. In this case, the natural gas fuel would be reformed and shifted at a high water/gas ratio to minimize the carbon monoxide concentration. After reaction with the oxygen and NO_x at 10% excess fuel ratio, the resulting effluent should be less than 300 ppm carbon monoxide.

7.11.4. Catalyst Degradation Tests

The subject of catalyst degradation in NO_x abatement deserves an exhaustive study. The results of our initial program, as reported in Section 7.7.4, could not offer causes for degradation. In the additional study reported here, we intentionally subjected the catalyst to extreme operating conditions to determine possible modes of degradation. These extremes were as follows:

- Catalyst aging
- Fuel deprivation
- Oxidant starvation
- Loss of preheat temperature
- Temperature excursions

These conditions were only examined on a qualitative basis; time did not permit a thorough analysis of these variables.

Tables 7-11A to 7-11D present the data which were collected in these catalyst degradation studies. Long-term examination of catalyst degradation could not be examined within the scope of the program. Rather, the critical 48 hours after catalyst start-up was investigated for catalyst aging. The results of 2-day tests are presented in Figure 7-26, in addition to Tables 7-11A to 7-11 D.

The first life test was made at 1200°F with a space velocity of 20,000 hr^{-1}. These conditions should result in stable operating characteristics. As indicated in the graph, the test started with relatively low oxygen removal but stabilized with about 90% reduction of the oxygen in the tail gas. No apparent degradation was noted for the catalyst on this 44-hour test. At the conclusion of the life test, the methane fuel was discontinued for 1 hour. After reintroduction of the fuel, the oxygen concentration in the output gas climbed, indicating that the catalyst had degraded. However, in examining later data, this degradation was apparently temporary. Next, the oxygen concentration in the tail gas was temporarily discontinued. After reintroduction of the oxygen, the catalyst activity for the oxygen removal was not apparently impaired, but the nitric oxide concentration in the exhaust was increased. Next, the temperature of the feed gases was dropped to 510°F for 1 hour. After the

Table 7-11A. LIFE STUDY OF MATTHEY BISHOP CATALYST (New), RUN NO. 1, AT 1200°F AND A SPACE VELOCITY OF 20,000 hr^{-1}
(Feed Composition: 1.0% O_2, 0.56% CH_4, 1000 ppm NO, Balance N_2)

hr	Outlet Concn O_2, %	Outlet Concn NO, ppm	$k(O_2)$	Remarks	hr	Outlet Concn O_2, %	Outlet Concn NO, ppm	$k(O_2)$
1	0.30	260	--	O_2 cell was bad; Ignore	32	0.10	200	128.3
2	0.30	190	--		33	0.11	200	123.0
3	0.30	210	--		34	0.12	210	118.1
4	0.29	160	--		35	0.12	210	118.1
5	0.19	170	92.5		36	0.08	140	140.7
6	0.17	180	98.7		37	0.11	160	123.0
7	0.15	200	105.7		38	0.18	170	113.7
8	0.14	180	109.5		39	0.14	210	109.5
9	0.14	180	109.5		40	0.16	230	102.1
10	0.14	180	109.5		41	0.14	210	109.5
11	0.14	180	109.5		42	0.13	210	113.7
12	0.14	180	109.5		43	0.16	240	102.1
13	0.21	220	86.9		44	0.16	210	102.1
14	0.12	190	118.1		45	CH_4 off		
15	0.08	150	140.7		46	0.20	340	90
16	0.13	130	113.7		47	O_2 off		
17	0.16	160	102.1		48	0.22	600	84.6
18	0.10	110	128.3		49	Temp. to 310°F		
19	0.10	60	128.3		50	0.21	690	86.9
20	0.08	100	140.7		51	Temp to 300°F		
21	--	--	--	Check feed flow rate; OK	52	0.10	250	128.3
22	--	--	--					
23	--	--	--					
24	0.11	160	123.0					
25	0.12	130	118.1					
26	0.22	190	84.3					
27	0.22	580	84.3	Cell bad				
28	0.11	120	123.0					
29	0.09	100	134.1					
30	0.12	200	118.1					
31	0.11	210	123.0					

B-24-331

Table 7-11B. LIFE STUDY OF MATTHEY BISHOP CATALYST (New), RUN NO. 2, AT 1500°F AND A SPACE VELOCITY OF 20,000 hr^{-1} (Feed Composition: 1.0% O_2, 0.59% CH_4, 1000 ppm NO)

	Outlet Concn							
hr	O_2, %	NO, ppm	$k(O_2)$	Remarks	hr	O_2, %	NO, ppm	$k(O_2)$
1	--	--	--	Difficult start-up	26	0.28	710	70.9
2	--	--	--		27	0.26	700	75.0
3	--	--	--		28	0.26	720	75.0
4	--	--	--		29	0.27	710	72.9
5	--	--	--		30	0.27	700	72.9
6	0.26	670	75.0		31	0.24	800	79.5
7	0.27	620	72.9		32	0.23	740	81.9
8	0.24	680	79.5		33	0.26	700	75.0
9	0.21	680	86.9		34	0.27	680	72.9
10	0.24	670	79.5		35	0.24	670	79.5
11	0.27	670	72.9		36	0.25	680	77.2
12	0.25	750	77.2		37	0.26	710	75.0
13	0.25	670	77.2		38	0.27	710	72.9
14	0.21	670	86.9		39	0.25	620	77.2
15	0.25	710	77.2		40	0.25	650	77.2
16	0.25	680	77.2		41	0.26	650	75.0
17	0.23	640	81.9		42	0.26	650	75.0
18	0.21	670	86.9		43	0.25	680	77.2
19	0.23	630	81.9		44	0.29	750	69.0
20	0.25	740	77.2		45	0.28	770	70.9
21	0.25	680	77.2		46	0.28	780	70.9
22	0.25	650	77.2		47	0.26	700	75.0
23	0.26	610	75.0		48	0.25	710	77.2
24	0.25	670	77.2		49	--	--	--
25	0.27	820	72.9					

B-24-330

Table 7-11C. TEMPERATURE CYCLING OF MATTHEY BISHOP CATALYST (New), RUN NO. 1, USING CH_4 FUEL AND A SPACE VELOCITY OF 20,000 hr^{-1}
(Feed Composition: 1.0% O_2, 0.58% CH_4, 1000 ppm NO, Balance N_2)

hr	Temp, °F	O_2, % Out	NO, ppm Out	$k(O_2)$	Remarks
1	1200	0.06	0.0	156.7	
2	1400	0.06	0.0	156.7	
3	510	1.0	960	0.0	
4	1200	0.13	640	113.7	
5	1500	0.11	190	123.0	After reading, CH_4 seemed low — increase 10%
6	1500	0.07	0.0	148.1	
7	500	1.0	960	0.0	CH_4 pegged increase was not right — recalibrate
8	500	1.0	1000	0.0	
9	1200	0.08	60	140.7	
10	1500	0.06	0.0	156.7	
11	500	0.98	950	0.0	
12	1600	0.07	0.0	148.1	
13	1600	0.09	10	134.1	

Table 7-11D. TEMPERATURE CYCLING OF MATTHEY BISHOP CATALYST (New), RUN NO. 2, USING CH_4 FUEL AND A SPACE VELOCITY OF 20,000 hr^{-1}
(Feed Composition: 1.0% O_2, 0.58% CH_4, 1000 ppm NO, Balance N_2)

hr	Temp, °F	O_2, % Out	NO, ppm Out	$k(O_2)$	Remarks
1	1200	0.09	210	134.1	
2	1400	0.07	170	148.1	
3	1200	0.13	160	113.7	
4	400	1.0	990	0.0	
5	1500	0.16	430	102.1	
6	1200	0.38	900	53.9	
7	500	1.0	980	0.0	
8	1200	0.44	950	45.7	Degradation
9	1500	0.35	900	58.5	
10	1600	0.20	450	89.7	
11	1200	0.44	790	45.7	No degradation since 8-hr point
12	1500	0.29	750	69.0	
13	500	1.0	980	0.0	No degradation since 11 and 8-hr points
14	1200	0.47	810	42.1	

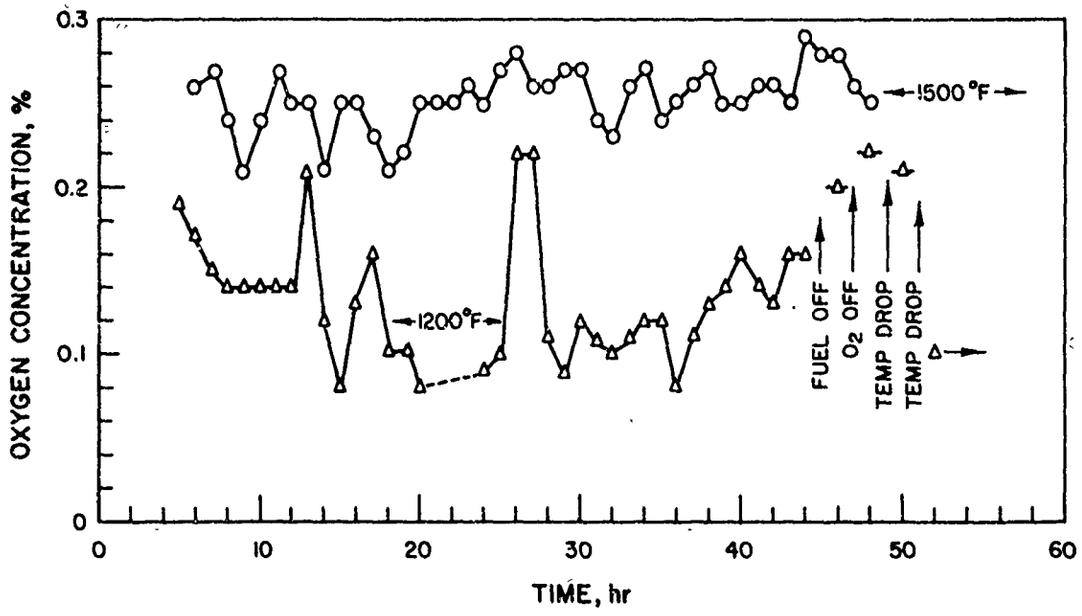

Figure 7-26. OXYGEN REMOVALS; LIFE TESTS

preheat temperature was increased, the oxygen and nitric oxide removals were similar to the preceding test. The preheat temperature was again decreased to 300°F for an hour. But after this test, the oxygen and nitric oxide removals improved, indicating that fuel deprivation, oxygen starvation, or loss of preheat temperature cause only a temporary loss of catalytic activity for the oxygen and nitric oxide removals in this system.

The next test was conducted at an elevated temperature of 1500°F. In this test, we encountered difficulties in start-up, including a power failure, and the catalyst may have been subjected to extreme conditions which were not noted. However, as indicated in Table 7-11 and Figure 7-26, the general performance during this 48-hour test at 1500°F and 20,000 hr^{-1} space velocity was constant but relatively poor. Much greater oxygen removals would have been expected at this temperature of operation; perhaps the catalyst was degraded during the first 6 hours of testing.

In the next two tests, the catalyst was subjected to temperature swings, always returning to the base temperature of 1200°F. In the first of these tests, the catalyst showed no degradation when subjected to temperature swings of 1400°, 500°, and 1500°F. The final temperature of 1600°F showed lower performance, although the difference may not have been significant. *

In the second test with temperature swings, the performance of the catalyst apparently degraded after the first swing to 1500°F. Good oxygen removals were not obtained after the fifth hour of testing.

The results of the catalyst degradation tests were not conclusive. Apparently, catalyst age, in the critical short term, is not important. Also, the deprivation of fuel, oxygen, or preheat temperature is not significant. In the second of two tests, locally high temperatures caused catalyst degradation; however, these effects were not noted in the first of these tests. Apparently, locally high temperatures can cause permanent catalyst degradation, even if these temperatures are experienced only for a short time. However, this effect is not consistent, and the primary variable may be in the precise technique in which the catalyst was prepared.

---

* The performance of the oxygen analyzer was often erratic at low oxygen concentrations. The preferred data for high rate constants were taken in at high space velocities and lower oxygen removal.

8. CYCLICAL REACTOR OPERATION

8.1. Summary

A pair of fixed-bed reactors was operated cyclically with thermal regeneration. This operation simulated the expected performance of the rotary regenerative wheel reactor. The operation of the cyclical fixed-bed reactors was satisfactory, demonstrating the feasibility of the rotary regenerative reactor concept.

During the reaction cycle of this system, 0.3% NO was chemically reduced with methane to 16 ppm. Simultaneously, 99.5% removal of the oxygen in the simulated tail gas was achieved, agreeing with the predictions of the kinetic study. Even with a degraded catalyst on one test, the EPA specifications of 209 ppm NO were achieved.

The cyclical reactor was operated with equal reaction and preheat times, simulating a rotary reactor with a 50:50 proportioning between the reaction and preheat zones. The temperature on the front face of the reactor, while operated in the cocurrent mode, was less than the temperatures deeper in the reactor. This effect was more pronounced with the degraded catalyst. This temperature decrease confirms the temperature profile predicted by the modeling study. Similarly, the greater temperature decrease with the degraded catalyst confirms the predictions at a lower reaction rate and hence a lower Lewis Number.

The only subprogram goal which was not achieved was the determination of the cyclical bed temperature variation using real cycle times. Measurements indicated a temperature range of about $\pm 10^{0}$F, but calculations indicate larger spreads. Perhaps the thermal inertia of the temperature measurement was too great to record larger variation at the relatively short cycle times.

8.2. Objective

The purpose of this phase of the program was to operate a fixed-bed reactor in a thermally regenerative cycling mode, simulating the performance of the proposed rotary regenerative reactor in cocurrent operation.

8.3. Introduction

The feasibility of the rotary regenerative reactor is best tested with fixed-bed reactors operating in a cyclical mode with regenerative heat recovery. The fixed-bed reactors can be more readily instrumented than the rotary reactor – thermocouples can be inserted into the reacting bed – and variations in the cyclic parameters can be readily accomplished by altering the settings of a timer mechanism.

The cyclic reactor is a fixed-bed reactor incorporating heat recovery by alternately passing the reacting and cold gases over the bed. In this case, the bed is fixed and the gases are changed by valves. In the rotary regenerative reactor, on the other hand, the gas flow ducts are stationary and the bed is moved between the ducts. This difference is explained in more detail in Section 3.

The fixed-bed reactor, operated cyclically, was used for the experimental program. However, in industrial practice, the fixed-bed regenerators are operated at longer cycle times. The resulting temperature extremes would be unsatisfactory for this process. Also, fixed-bed regenerators in this process would require valves to operate at 1200°-1400°F, beyond the range of conventional equipment. This concept was useful, however, in this program for simulating the expected performance of the rotary regenerative reactor.

Outputs from both the modeling subprogram (Section 6) and the reaction kinetics subprogram (Section 7) were used in designing the cyclical tests. The reactor modeling subprogram indicated that the preheat (or cooling) cycle of the fixed-bed reactor should be about 40-45 seconds if the reaction cycle were 1 minute because the Lewis Number of the system should be about 0.7. The kinetic study indicated that the design space velocity should be about 11,800 hr^{-1} for achieving satisfactory oxygen and nitric oxide removals at 1200°F operating temperature. Operation at higher pressures would more closely duplicate the present operating systems and permit higher space velocities, but atmospheric-pressure operation was selected because of ease of operation and the availability of pressure scale-up techniques.

8.4. Experimental Apparatus and Procedure

Figures 8-1 and 8-2 present the process flow and the P&I drawings for the cyclical reaction system. This system is similar to the experimental apparatus used for the kinetic studies except that a pair of parallel reactors is used. These reactors are interconnected with four 3-way valves; either reactor could be fed a cold nitrogen stream or the preheated tail gas ready for reaction. Similarly, the exhaust from either reactor could be directed to the gas analyzing system or to the vent. Figure 8-3 is a photograph of the reactors and valving.

The poppet valves (Figure 8-4) were custom designed and constructed for operation on hot gases, and they had operated satisfactorily in an earlier application. The poppet valves were constructed from automotive exhaust valves, ground into boron nitride seats. The valve stems passed through close-fitting tubing fittings for guides and were sealed on the reverse side with flexible bellows welded between the valve stem and the valve guide. The diameter of the bellows was equal to the diameter of the valve, so the gas pressure on the back of the valve was counterbalanced. The valve was spring-loaded in a normally open position and was closed by a heavy-duty solenoid actuator.

Figure 8-5 is a schematic diagram of the electrical circuitry used to actuate the valves for cycling the reactors. The primary timer circuit sets the cycle time for the reaction portion of the paired reactors. Each activation of this circuit reverses the operation of the 3-way valves in the system. Thus one reactor is reacting the preheated simulated tail gas with methane while the other is being cocled by nitrogen. With the next activation of the timer, the functions of these two reactors are reversed. The second timer circuit was used to determine the length of time, during the cooling cycle, that the cold nitrogen was flowing. Additional solenoid valves were used on the cold nitrogen feed and vent lines; these valves were controlled by this timer. Therefore, although the reacting gases might flow for 1 minute, the cooling gases might flow for 45 seconds, with the cooling reactor dead for the remaining 15 seconds of the cycle. The third timer circuit was used to reinitiate the other two timers and had a time delay of less than 1 second.

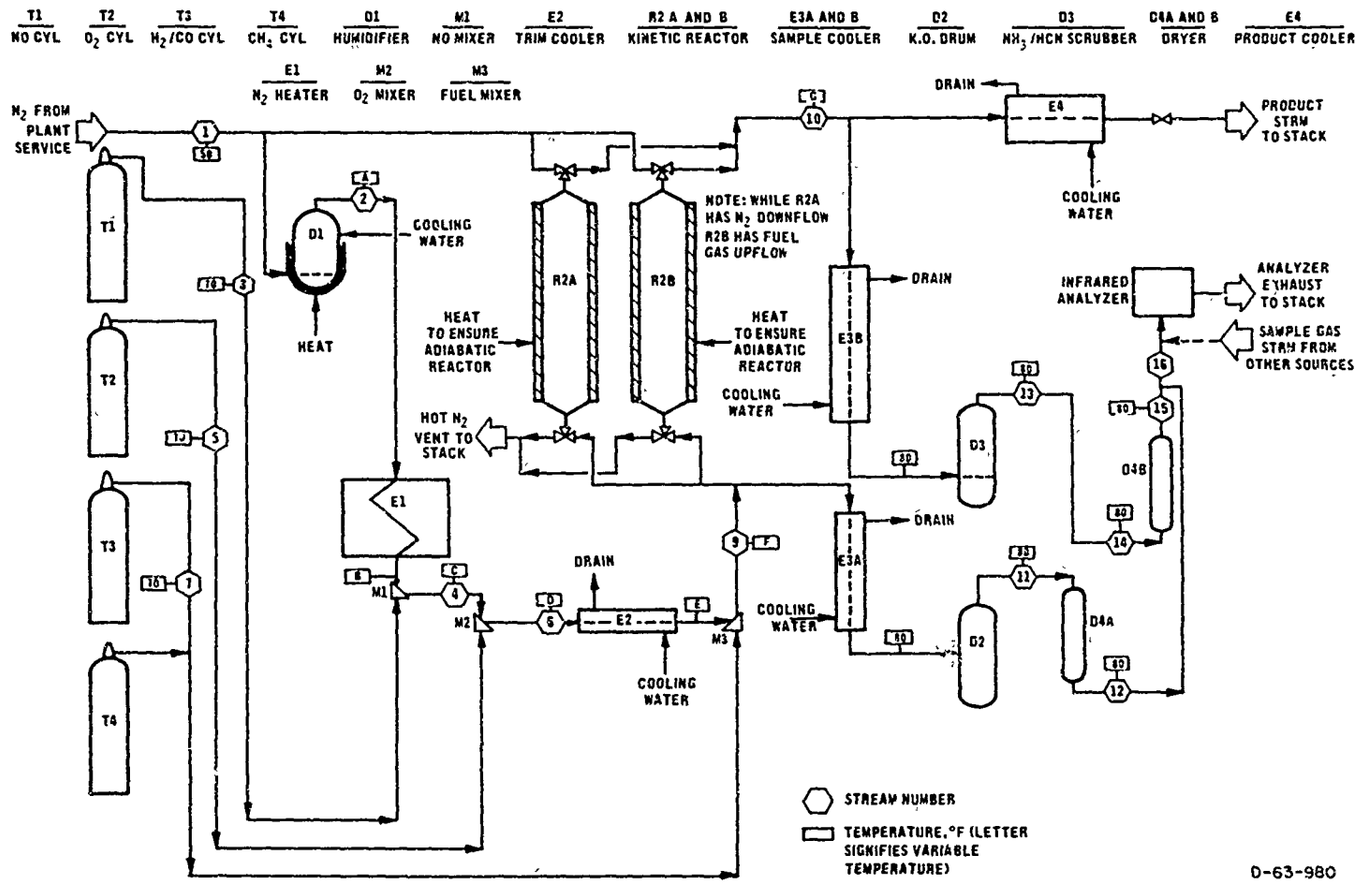

Figure 8-1. PROCESS FLOW – CYCLICAL STUDY

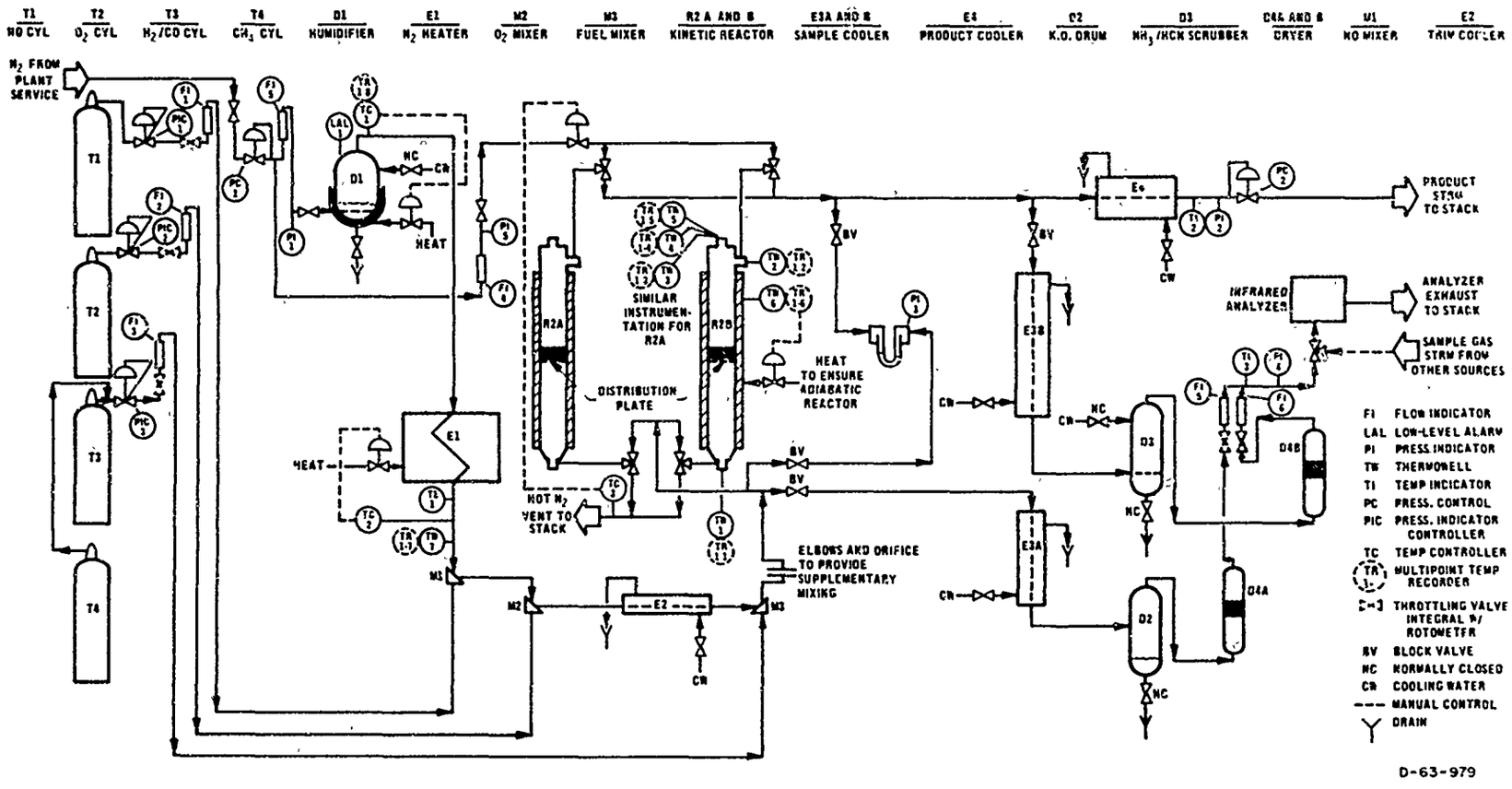

Figure 8-2. PIPING AND INSTRUMENTATION — CYCLICAL STUDY

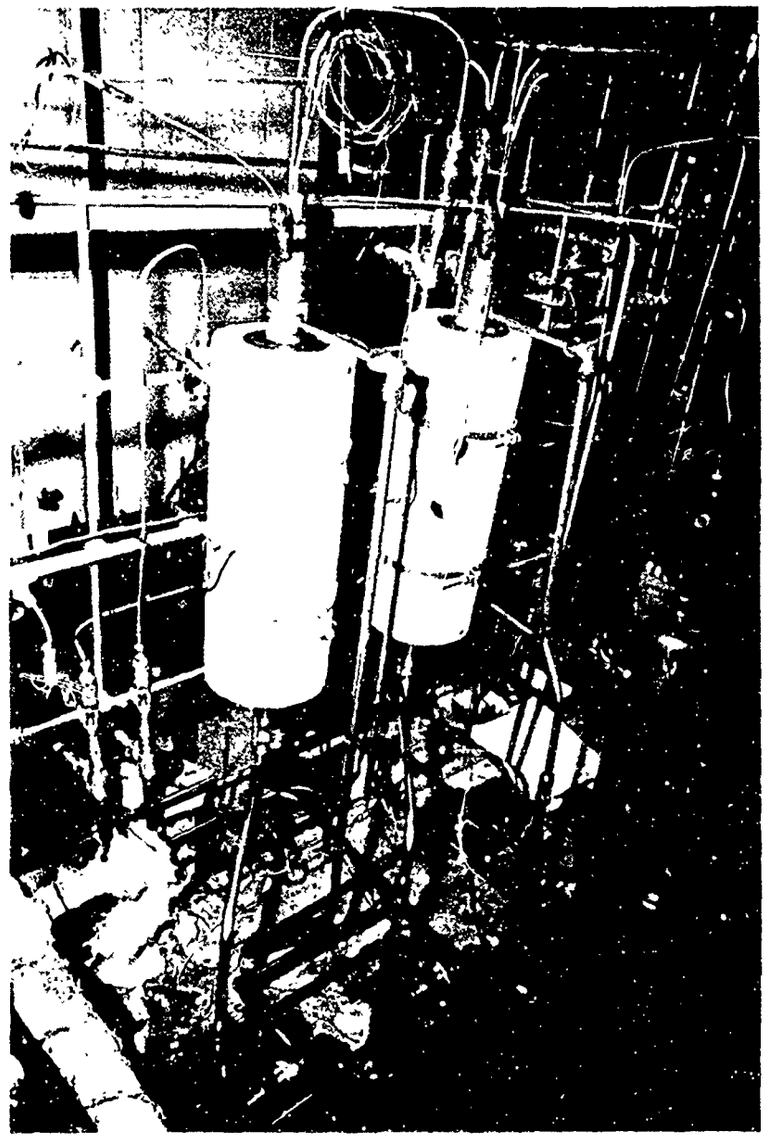

Figure 8-3. PHOTOGRAPH OF PAIRED CYCLICAL REACTORS DURING CONSTRUCTION. NOTE SOLENOID-ACTIVATED 3-WAY VALVE AT BOTTOM OF PHOTOGRAPH

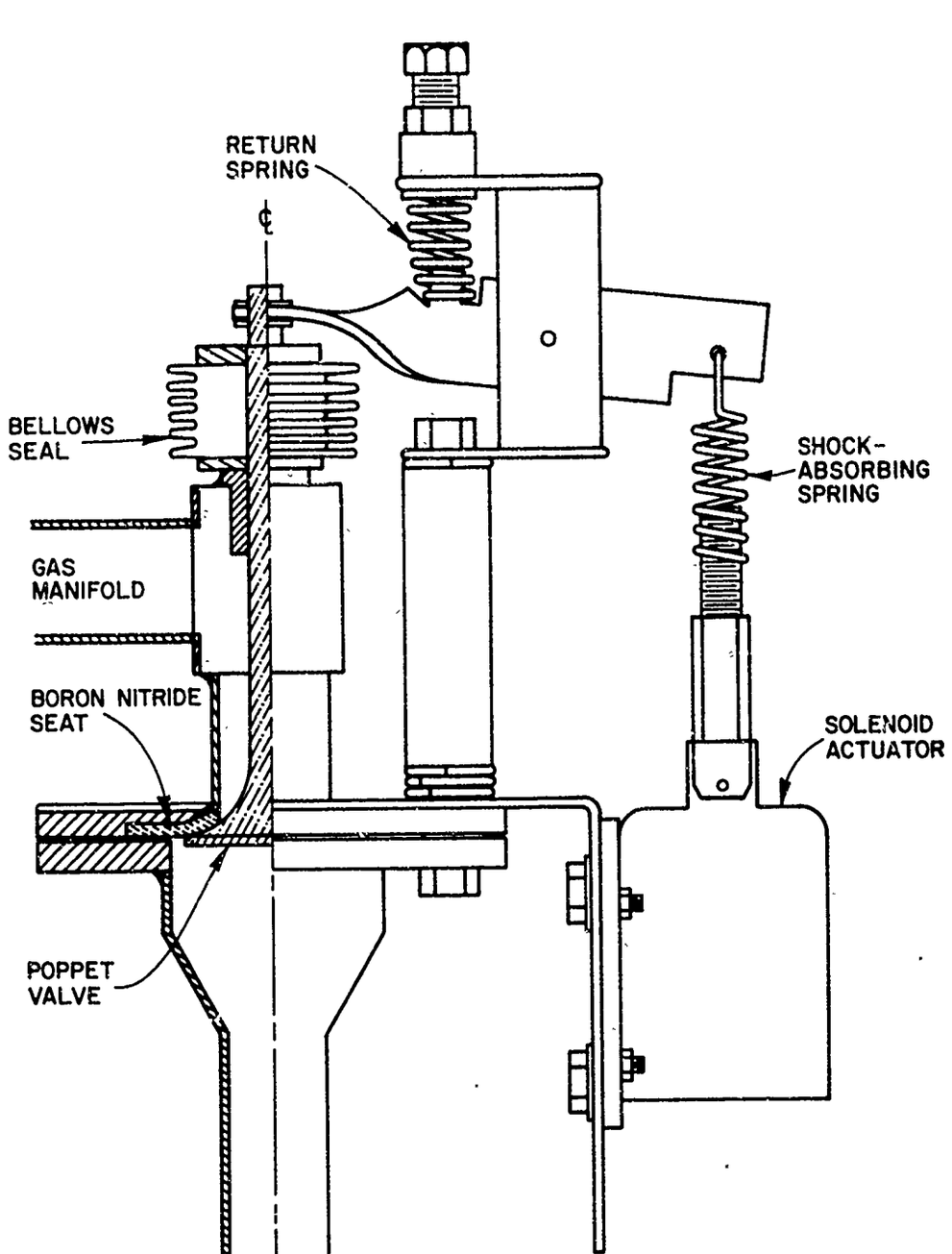

Figure 8-4. SOLENOID POPPET VALVE PAIR

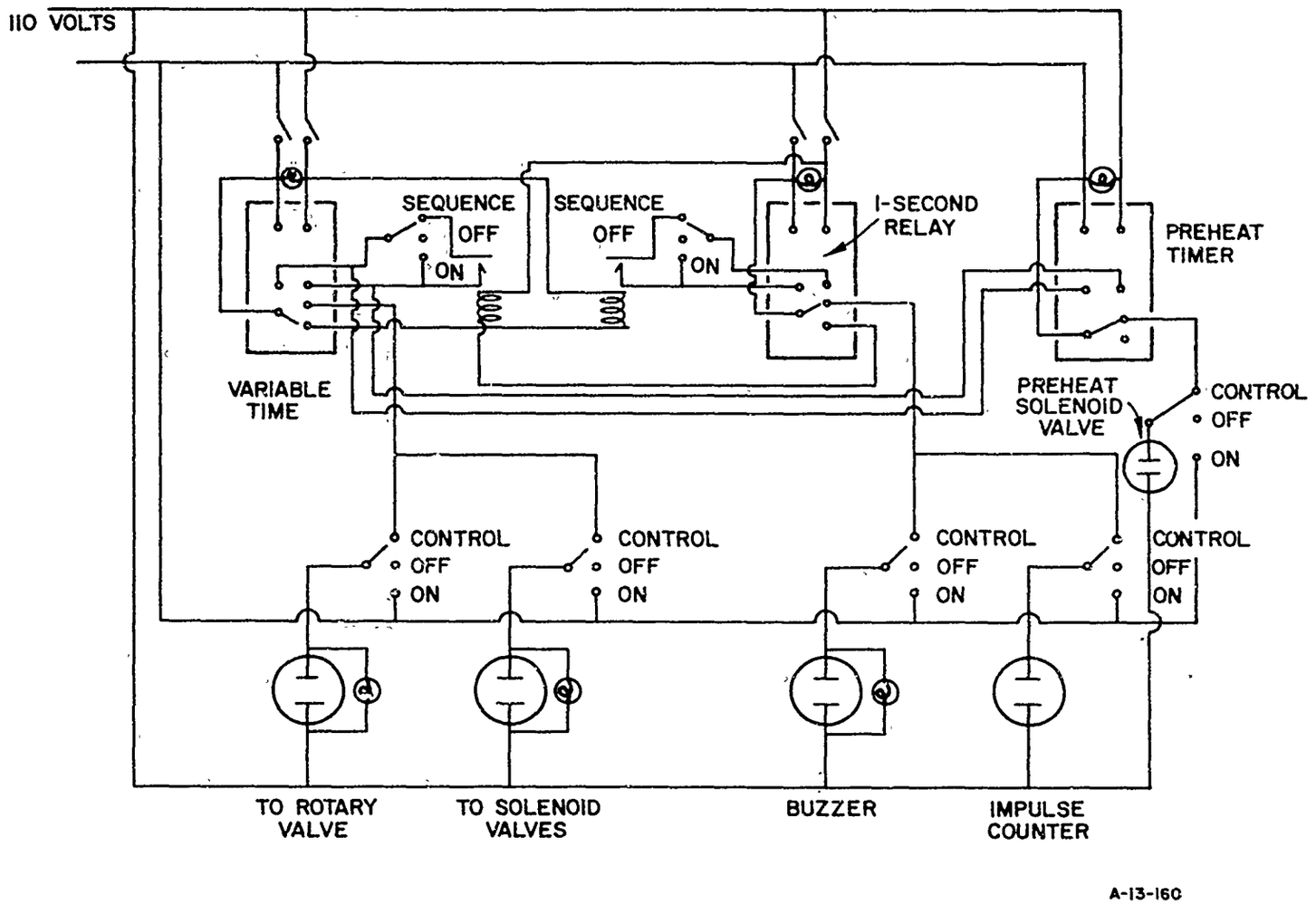

Figure 8-5. SCHEMATIC DIAGRAM OF SEQUENCE TIMER

The system was operated to balance the heat flow in the output of the cooling reactor with the heat flow in the input to the reaction section. In other words, the product of the flow rate, time, and average temperature was adjusted so that the quantity of heat in the product gas from the preheat reactor equalled the quantity of heat in the input gas to the reaction section. This balance would duplicate the operation of the rotary regenerative device. The external heat rate to the reactors was controlled to approach adiabatic operation. The voltage controllers were set to minimize temperature variation from the front to the back of the bed while preheated nitrogen was flowing.

In general, the experimental procedure was similar to that used in the kinetic subprogram. The simulated tail gas, however, contained 5.2% oxygen (by volume) and 3000 ppm nitric oxide. The methane fuel was again added at 10% excess (over stoichiometric requirements for combustion to CO_2 and H_2O), or 2.95%. This gas stream was humidified, preheated, and blended similar to the system used in the kinetic study before it was fed to the cyclical reactors. A secondary gas stream of nitrogen was used in another metered and controlled circuit for the alternate reactor in the cycle.

The catalyst used in this subprogram was the Matthey Bishop TMT-2 noble metal mixture deposited on 1/8-in. ceramic honeycomb. The overall program was based on conventional, noble metal catalysts, and this formulation had provided satisfactory data in the kinetic subprogram. The catalyst samples were 2 in. in diameter by 1 in. deep. Based on the preliminary output of the kinetic studies, the reactors were operated at a standard space velocity of 10,000 hr^{-1}.

8.5. Results

The paired, fixed-bed reactors were operated in a cyclical mode, with regenerative heat recovery, to simulate the operation of the proposed rotary regenerative reactor. The feasibility of this concept would be evaluated in these tests:

a. Determine the operating temperature of the reactor with high oxygen removals and resultant high adiabatic reaction temperature.

b. Demonstrate satisfactory nitric oxide concentrations in the product gas with 3000 ppm NO in the feed, thus checking the output of the kinetic subprogram.

c. Determine the magnitude of the cyclic temperature swings in the bed corresponding to real periods of reaction and cooling.

d. Evaluate the axial temperature profile in the bed in cocurrent operation, checking the output of the reactor modeling subprogram.

The cyclical reactor operation could therefore evaluate the viability of the basic work and demonstrate the feasibility of the continuous, rotary regenerative reactor.

Three of the above subprogram goals were achieved. Detailed evaluation, however, was not possible because shakedown problems limited the number and range of tests that could be conducted.

The cyclic reactors were operated with 5.2% (by volume) oxygen in the simulated tail gas. This concentration corresponds to 5.9% by weight, for a calculated adiabatic temperature rise of approximately 1400°F. The reactor was operated with this simulated tail gas preheated to 1200°F in the reaction mode and ambient nitrogen in the cooling or preheat mode; average bed temperatures ranged from 1200° to 1450°F, proving the basic regenerative heat exchange concept.

The data for the four tests in the cyclical reactor subprogram are presented in Table 8-1. The first three tests were conducted with catalysts which had been used in the system during the shakedown tests; these catalysts had apparently degraded. The last test was conducted with a fresh catalyst sample. All of these tests exhibited relatively high removals of oxygen, yet the operating temperatures were not excessive. On the contrary, the average bed temperature in the first test was relatively low at about 1200°F, indicating insufficient external heat to maintain the adiabatic reaction temperature.

The kinetic data for these tests are shown in Figure 8-6 as an Arrhenius plot. Also included on this graph is the line representing the average performance of this catalyst at 1 atm pressure as determined from Section 7. The rate data for the first three tests fall significantly below the expected behavior. However, when the catalyst sample was replaced for test 4, the expected kinetic behavior was essentially achieved.

Table 8-1. SUMMARY OF DATA FROM CYCLICAL TEST SUBPROGRAM

Test No.	1	2	3	4
Cycle Time, min				
Reaction	2	2	2	1
Preheat	2	2	2	1
Feed Gas				
Standard Space Velocity, hr^{-1}	10,000	10,000	10,000	10,000
Composition, vol %				
O_2	5.2	5.2	5.2	5.2
NO	0.3	0.3	0.3	0.3
CH_4	2.9	2.9	2.9	2.9
Product Gas Composition				
O_2, ppm	1600	1500	1000	300
NO, ppm	310	300	210	16
CH_4, ppm	2500	1000	1500	1000
CO, ppm	300	290	500	800
CO_2, %	2.65	2.7	2.65	2.65
Temperature Range, °F				
Bed Entrance	±10	±10	±5	±10
Bed Center	±10	±10	±5	±10
Bed Exit	±10	±5	±5	±5
Mean Temperature, °F				
Bed Entrance	1190	1350	1495	1310
Bed Center	1210	1380	1540	1330
Bed Exit	1230	1410	1560	1340
Apparent Catalyst Condition	Degraded			Active

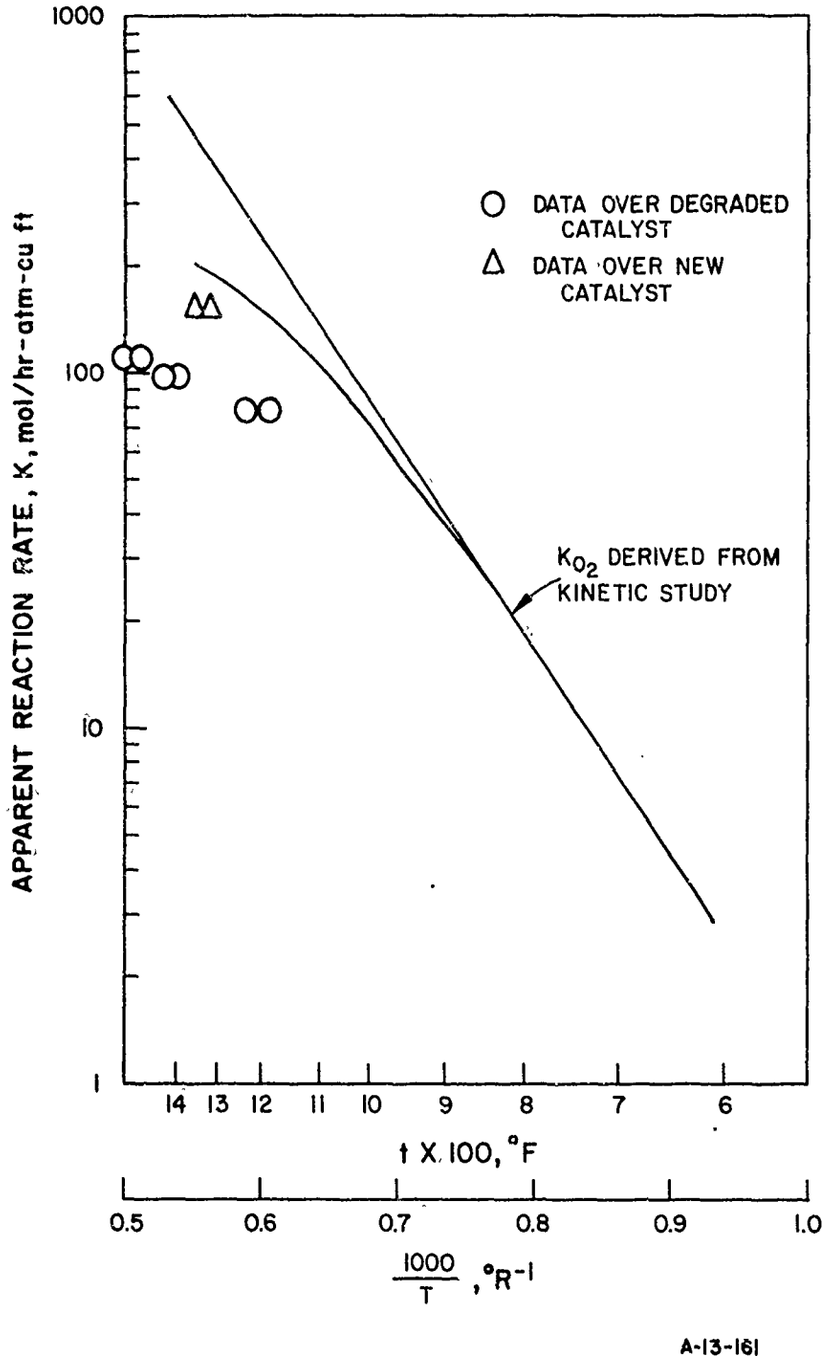

Figure 8-6. APPARENT REACTION RATE FOR CH_4-O_2 REACTION OVER MATTHEY BISHOP CATALYST (Cyclical Study)

The two samples of catalyst which were removed from the paired reactors after test 3 appeared to have suffered the type of degradation discussed earlier in Subsection 7.7.4. The cell walls were thicker, with the catalyzed surface apparently covered by a ceramic scale.

The nitrogen oxide removals are graphed in Figure 8-7.

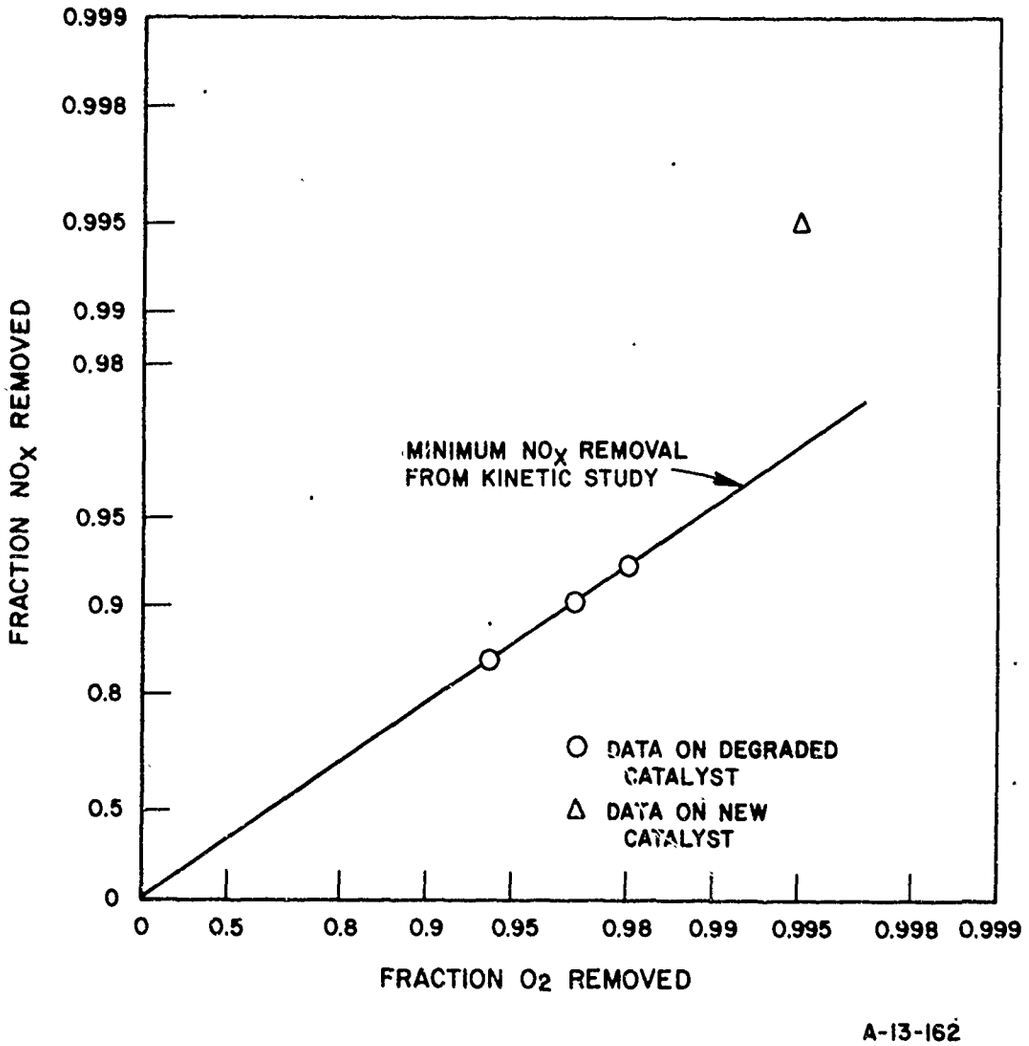

Figure 8-7. FRACTION NITRIC OXIDE REMOVED VERSUS FRACTION OXYGEN REMOVED (Cyclical Study With Matthey Bishop Catalysts)

The three data points for the degraded catalyst lie precisely on the line for minimum performance predicted from Subsection 7.7.2. The EPA standards of 209 ppm were met in one of these tests, even with degraded catalyst. The data point for the fresh catalyst showed much better performance, with 99.5% removal of the nitric oxide content at a similar oxygen conversion. These data prove that satisfactory nitric oxide conversions may be achieved using methane fuel in the regenerative reactor.

The carbon monoxide concentrations in the effluent product gas were satisfactorily low. The highest measured CO concentration was 800 ppm, only 40% of the currently permissible CO concentration in large industrial furnaces. This carbon monoxide concentration was achieved by using minimal excess fuel in the reaction.

The temperature of the bed must vary during the operational cycle. This effect was expected, but could not be predicted in our simplified model, which assumed infinitely fast rotational speed. Unfortunately, our data might not define the magnitude of the temperature cycles. The measured fluctuation (Table 8-1) is about $\pm 10^{0}$F; however, approximate calculations predict much greater variation. The measured cycling may be in error because high time constants (or thermal inertia) could mask the true temperature with short cycle time.

Mechanical problems in the hot valves forced us to operate the paired reactors with equal cycles of preheat and reaction. This cycle schedule corresponds to a rotary regenerative reactor with equal areas in the preheat and reaction zones. Our reactor modeling subprogram (Section 6) had predicted that the temperature at the bed inlet should be lower than the remainder of the bed in this chemical system with a Lewis Number less than 1.0. This effect was observed experimentally. The effect was more pronounced with the degraded catalyst than with the fresh catalyst. This observation is consistent with theory; a greater temperature difference from the front to the rest of the bed in this system is caused by a lower Lewis Number. The lower Lewis Number is caused by a lower reaction rate which, in turn, is consistent with a degraded catalyst. This effect would be counteracted on a rotary reactor by changing the fraction of the reactor which was in the preheat zone.

These reactors were operated with 5.2 volume percent O_2 in the tail gas for an adiabatic reaction temperature rise of 1400°F. The design reaction temperature of 1200°F would be reached at 4.1 volume percent O_2. Even lower oxygen concentrations could be used at the design reaction temperature by preheating the tail gas either in the ammonia burner or by exchange with the treated tail gas.

9. DESIGN OF A PILOT-UNIT ROTARY REGENERATIVE REACTOR

9.1. Summary

This phase of the program was charged with the conceptual design of a prototype rotary regenerative reactor capable of processing 1000 SCF/hr of simulated tail gas. We designed a versatile reactor sized for operation between 300 and 1200 SCF/hr, depending upon the configuration used. The reactor design incorporates a movable partition between the preheating and reacting zones. Adjustment of the ratio of these two sections can compensate for variation in the chemical characteristics of the system. The reactor wheel is 7 in. in diameter with incremental depths of 1, 2, or 3 in. The deepest wheel would process 1000-1200 SCF/hr, based upon the output from the reactor modeling and kinetic subprograms. If proposed bed modifications are included, the pilot unit reactor might treat 2800 SCF/hr of tail gas to 150 ppm NO_x.

Concepts are presented for both cocurrent and countercurrent flow of reacting gases with the preheating gas. In the cocurrent mode of operation, the wheel should operate at nearly constant temperature as predicted by the mathematical model. The countercurrent configuration was developed to demonstrate the concept of mixed metal catalysts and uncatalyzed heat exchange area, as presented in Subsection 6.6. At this time, the operation of the countercurrent system is more conjectural than the cocurrent system, but offers promise for the longer term.

9.2. Objective

The purpose of this phase of the development program was to prepare a conceptual engineering design of a prototype rotary regenerative reactor. This reactor should be capable of processing 1000 SCF/hr of simulated nitric acid tail gas.

9.3. Inputs

9.3.1. Concept

The idea for the rotary regenerative reactor was the heart of this program. It was first introduced in Subsection 3.5 as a countercurrent device. The ideal behavior of the cocurrent reactor, with its constant temperature profile under certain conditions, was discovered during the course of the program. This concept was introduced in Subsection 6.7.

9.3.2. Reactor Modeling

The reactor modeling subprogram was presented in Section 6. The output of that program specifies the physical configuration of the rotary device.

When the reaction is operated cocurrently on the wheel, with the preheating and reacting gases passing through the wheel in the same direction, the axial temperature profile can be nearly constant. This will occur if the ratio of the area in the preheat zone to the area in the reacting zone is equal to the Lewis Number (or pseudo-Lewis Number) of the system. The experimental reaction rate, as determined in the kinetic subprogram (Section 7), indicates that the process is controlled by both the chemistry of the system and the rate of diffusion of the reactants. The pseudo-Lewis Number will be in the range of 0.5-0.8. Therefore, for operating cocurrently, the reactor should be constructed with a movable partition between the preheat and reaction zones permitting the area fraction of the preheat zone to be varied between 33 and 45% of the total cross-sectional area of the reactor wheel.

When operating in the countercurrent mode, the axial temperature gradient in the bed is minimized when the area fraction of the preheat zone is the smallest. However, practical considerations limit the minimum size of the preheat zone to about 15-20% of the total wheel area. Even with this small preheat fraction, the temperature on the hotter face of the countercurrent wheel reactor is too high for operation with noble metal catalysts. Also, with low oxygen concentrations in the tail gas, the temperature of the cooler face of the wheel may be too low for a sufficient reaction rate. Therefore, the front face of the wheel contains uncatalyzed heat exchange area for elevating the temperatures on the catalyzed surfaces. For use with a tail gas containing 4% oxygen, the wheel would be 4 in. deep with 1 in. of uncatalyzed honeycomb, 1 in. of noble metal catalyst, and 2 in. of non-noble catalyst, which will operate at higher temperatures.

9.3.3. Reaction Rate

The experimental program, discussed in Section 7, produced data that proved that the noble metal catalyst can operate satisfactorily. Oxygen removals of 98-99% should be realized at 1200°F and 90 psig at standard space velocities of 27,500-32,000 hr^{-1}. The expected NO_x concentration in the effluent under these conditions is 150-200 ppm.

These results can be used directly when the reactor wheel operates in the cocurrent mode. This temperature would be reached in the reactor if the tail gas contained 5 weight percent oxygen (or with lower oxygen concentrations and external preheat).

The operation in the countercurrent mode is more difficult to estimate because the temperature is continuously varying through the bed. Also, the higher temperature sections of the bed use less active catalysts which have not yet been fully characterized. At present, we estimate that a space velocity of 20,000 hr^{-1} would be adequate to process the tail gas.

9.4. Wheel Sizing

The pilot unit rotary wheel reactor was sized at 7 in. in diameter by 3 in. deep. The inside diameter of the wheel was chosen at 2 in., to allow for the drive shaft and the seal against the wheel. This reactor size, coupled with 60% average area in the reaction zone and a design space velocity of 27,500 hr^{-1}, gives a flow capacity in the cocurrent mode of 1000 SCF/hr. This space velocity should result in 99% removal of the oxygen in the tail gas and an effluent NO concentration of about 150 ppm, with an operating temperature of 1200°F. Higher flow rates are obtainable with reduced efficiency; flow rates of 1200 SCF/hr will be possible without exceeding the EPA NO_x standards.

If the bed modifications proposed in Subsection 7.7.3 are included in this design, the space velocity increases to 66,000 hr^{-1} at 1200°F. Also, the area in the reaction zone increases to about 70% because of the reduced pseudo-Lewis Number. These factors increase the capacity of the pilot unit to an estimated 2800 SCF/hr at 150 ppm NO in the exhaust.

In the countercurrent mode of operation, an additional inch of wheel depth is required for uncatalyzed heat exchange volume. A greater

fraction of the wheel area, about 85%, is available for reaction. The 7-in.-diameter by 4-in.-deep wheel can process 1000 SCF/hr at a design space velocity of 20,000 hr^{-1}, based on catalyst in the reaction zone.

9.5. Conceptual Reactor Mechanical Design

The drawings presented with this section of the report are conceptual; they are not finalized. Although they are drawn to scale with a 7-in.-diameter reactor wheel, they are not dimensioned because mechanical engineering considerations may dictate changes in the construction of the pilot-unit reactor.

The figures illustrate the construction of a countercurrent reactor. The construction of a cocurrent reactor is similar, and the differences will be detailed later in this subsection.

Figure 9-1 is an exploded isometric view of the rotary wheel reactor illustrating the seven primary pieces.

- The primary component of the reactor is the catalyzed rotary regenerative reactor wheel, labeled "E" in Figure 9-1. The catalyst honeycomb is mounted in segments in a carrier to compensate for thermal expansion. Wheels of different depths would be constructed to test the effects of gas flow rates over a wider range.

- The wheel is rotated by a concentric shaft, labeled "A." The wheel is keyed to this shaft, and the shaft is externally driven by chain and sprocket, reducers, and a variable-system drive (not shown in the drawing).

- Two headpieces, labeled "B," fit against the catalyst wheel. Seal material on the headpiece flange rubs against the rotating flange of the catalyst wheel, minimizing gas bypassing. The headpieces contain a fixed partition, part of the mechanism for separating the reactants from the preheating gases within the reactor.

- Two movable partitions, labeled "C," are mounted within the headpieces. The movable partitions are welded to heavy-walled tubing which fits concentrically on the drive shaft, but does not normally rotate. The movable partition has seal material around its outside edge to ride against the inside of the headpiece, forming part of the gas seal between the preheat and reaction gases. A similar seal on the fixed partition rides against the tube of the movable partition, and both partitions have seal material facing the catalyst wheel.

- The last major part of the reactor is a spool piece, labeled "D," mounted between the two headpieces and around the catalyst wheel. Spool pieces of various depths (1, 2, 3, and 4 in.) would be constructed to correspond to different catalyst bed depths.

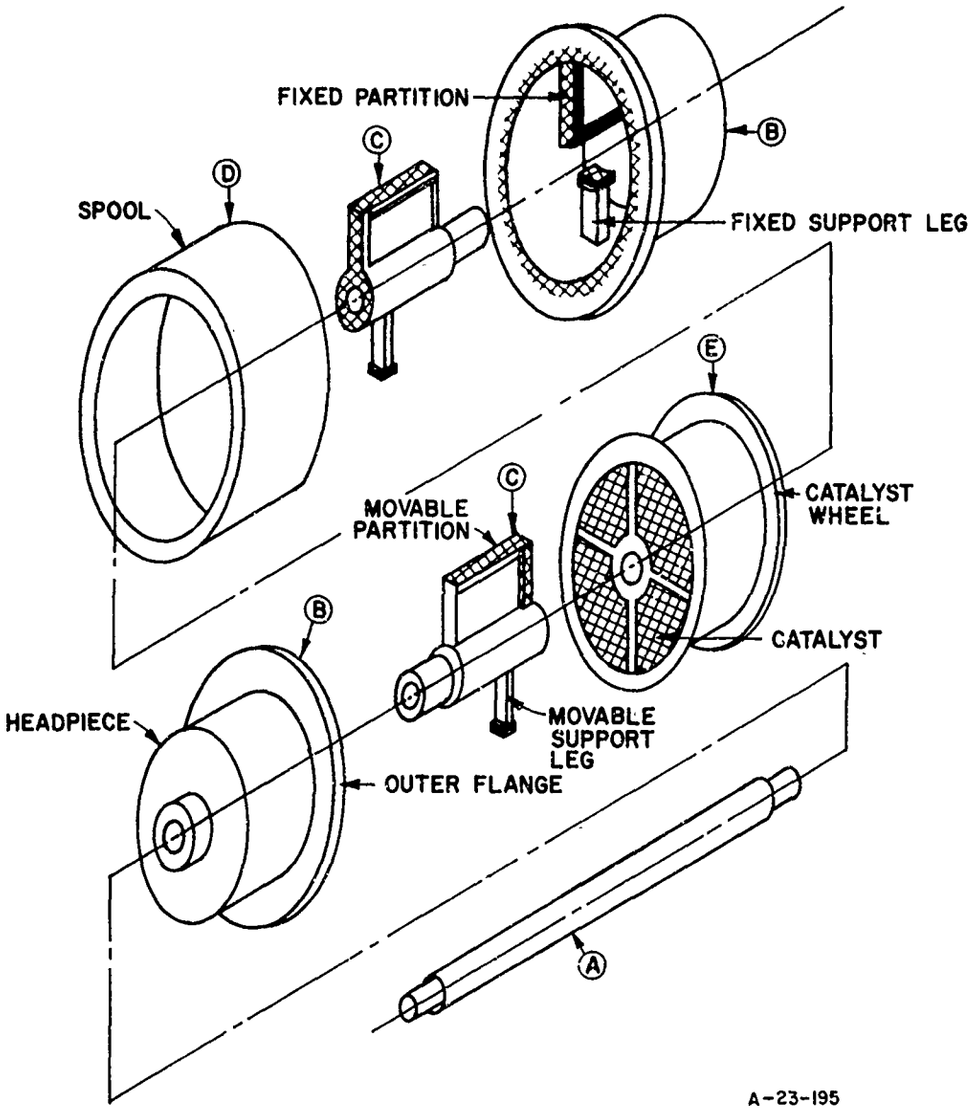

Figure 9-1. EXPLODED ISOMETRIC VIEW OF ROTARY WHEEL REACTOR

The reactor, as sketched in Figure 9-1, includes support legs for centering the movable partition (and hence the drive shaft and catalyst wheel). The support legs use seal material at the moving points for bearing surfaces. The primary difference between the countercurrent reactor, as shown, and a cocurrent reactor is the positioning of these support legs. In the configuration shown, the movable partition may be varied to allow preheat fractions of 12-37% before interference of the partitions with the support legs. For the cocurrent reactor, a pair of fixed support legs would be used, attached to the headpiece perpendicular to the fixed partition. These support legs would ride against the tube of the movable partition, permitting movement of the partition which would allow from 33 to 67% of the reactor area in the preheat zone. This configuration would provide adequate support for the movable partition and drive shaft, yet permit more than sufficient movement for the movable partition.

The tubes of the movable partition would extend through the centering bearings in the headpiece. They would be keyed to interconnected lever arms for locating the movable partitions. Set screws in the bearings would be used to fix the position when adjusted.

The drive shaft, keyed to the catalyst wheel, would extend through the tubes of the movable partitions. It would be positioned by self-centering outboard bearings, external to the headpieces of the reactor. The shaft would be driven, through gear reduction, by a variable-speed motor. The satisfactory operation of the cyclical reaction indicates a design speed of 0.4-4 min/rev.

The metallic components of the rotary regenerative reactor would be manufactured of Inconel for maximum strength at the temperatures which might be encountered with non-noble catalysts in the countercurrent mode. The seal material is a sintered, high-nickel alloy. This material will compress and abrade to conform to the catalyst wheel surface, yet has minimum pore volume for high resistance to gas flow across the seal.

Figure 9-2 is a sectional view through one of the reactor headpieces, illustrating the relative location of the partitions and support legs in the countercurrent reactor.

Figures 9-3 and 9-4 are axial cross-sectional views through a headpiece illustrating the fixed partition and the movable partition, in assembly. These views show the location of the seals riding against the catalyst wheel, the movable partition, and the inner surface of the headpiece. This simple seal arrangement should be adequate for the small pilot-unit reactor using a catalyst wheel with low pressure drop characteristics. A more refined sealing technique would be required for a larger, semiworks rotary regenerative reactor.

The remaining drawings in this section illustrate the method for locating the catalyst segments within the rotary wheel (Figures 9-5 and 9-6), the connection nozzles on the head of the reactor (Figure 9-7), and a support base welded to the spool piece (Figure 9-8). Details of the outboard bearings and center shaft drive mechanism have not been prepared.

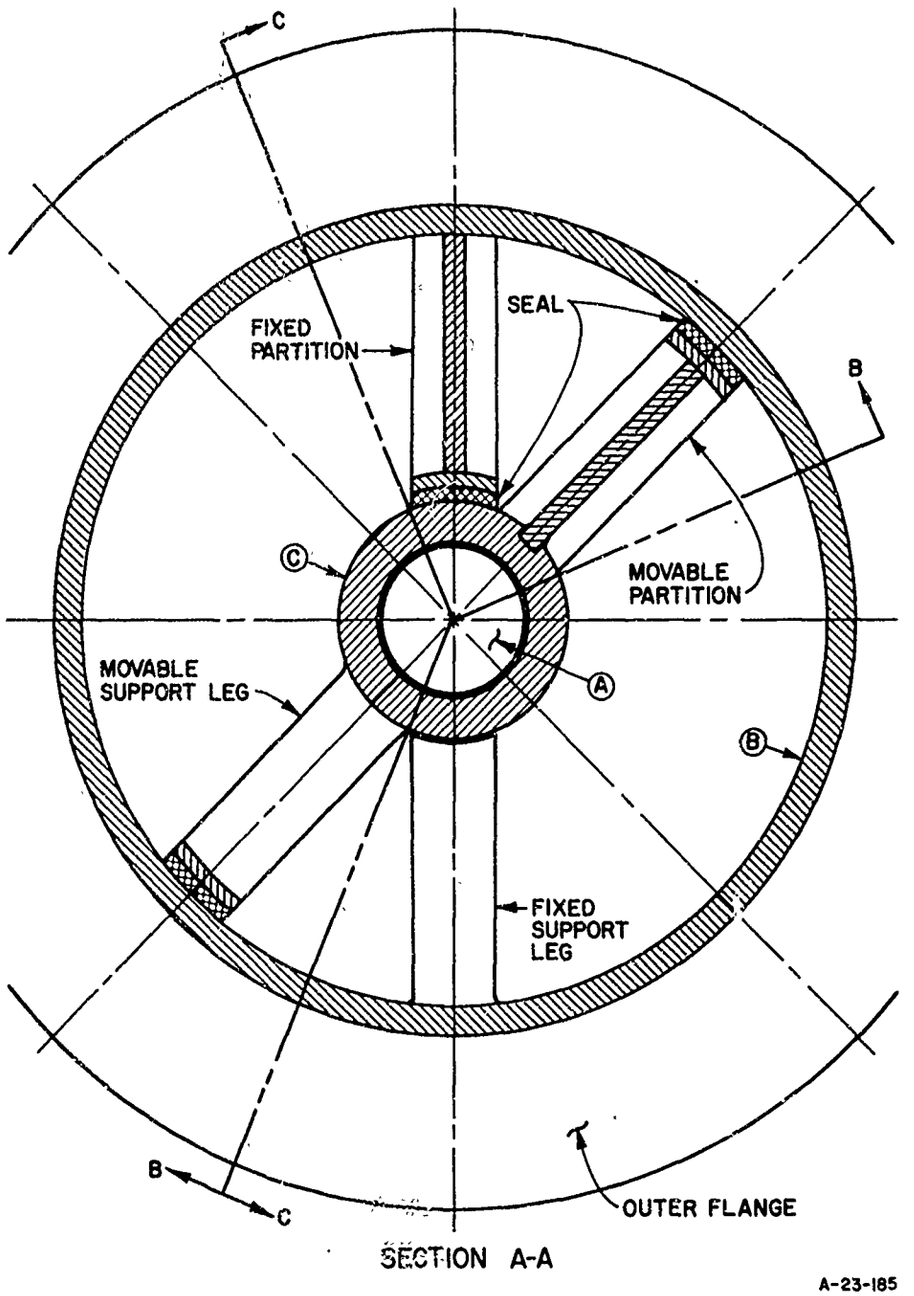

Figure 9-2. SECTIONAL VIEW OF REACTOR HEADPIECE

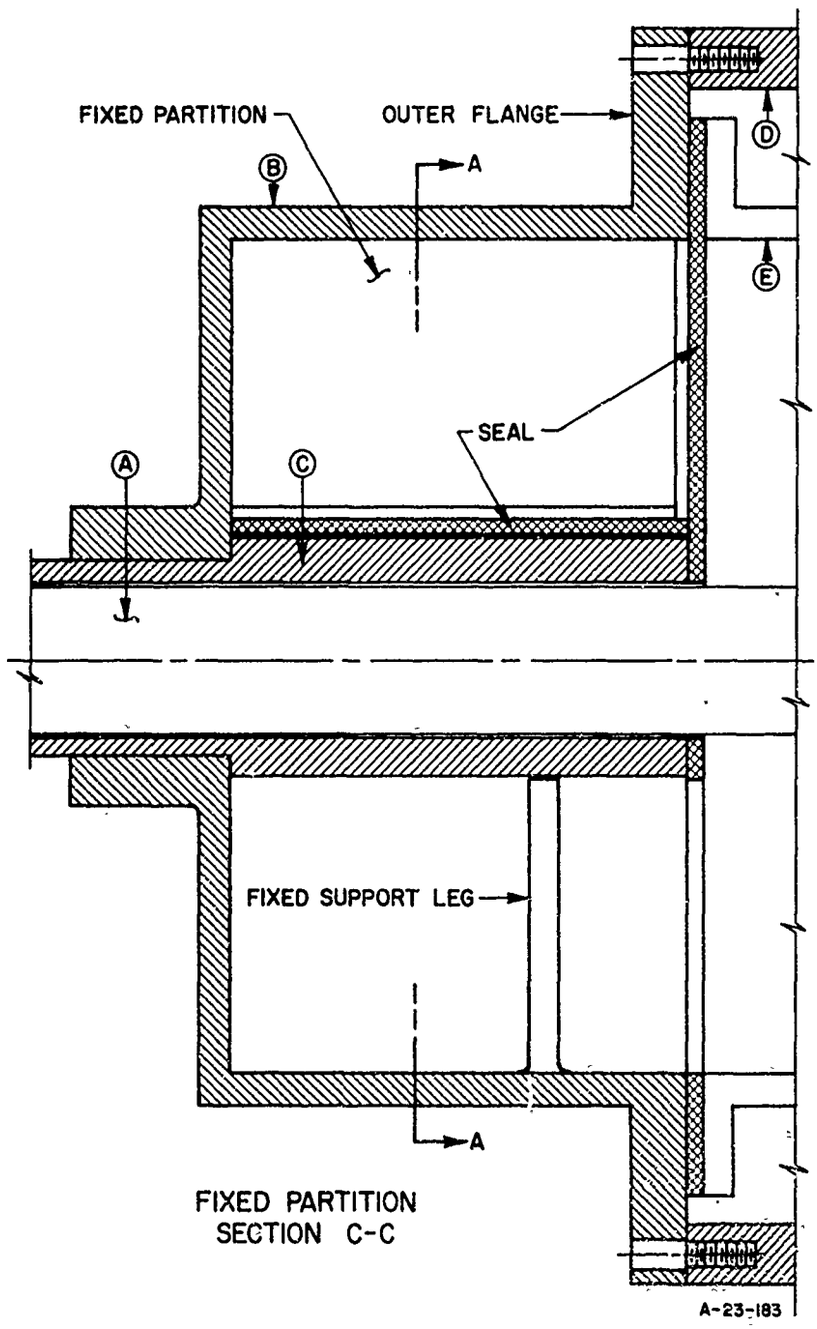

Figure 9-3. AXIAL CROSS-SECTIONAL VIEW THROUGH HEADPIECE (Fixed Partition)

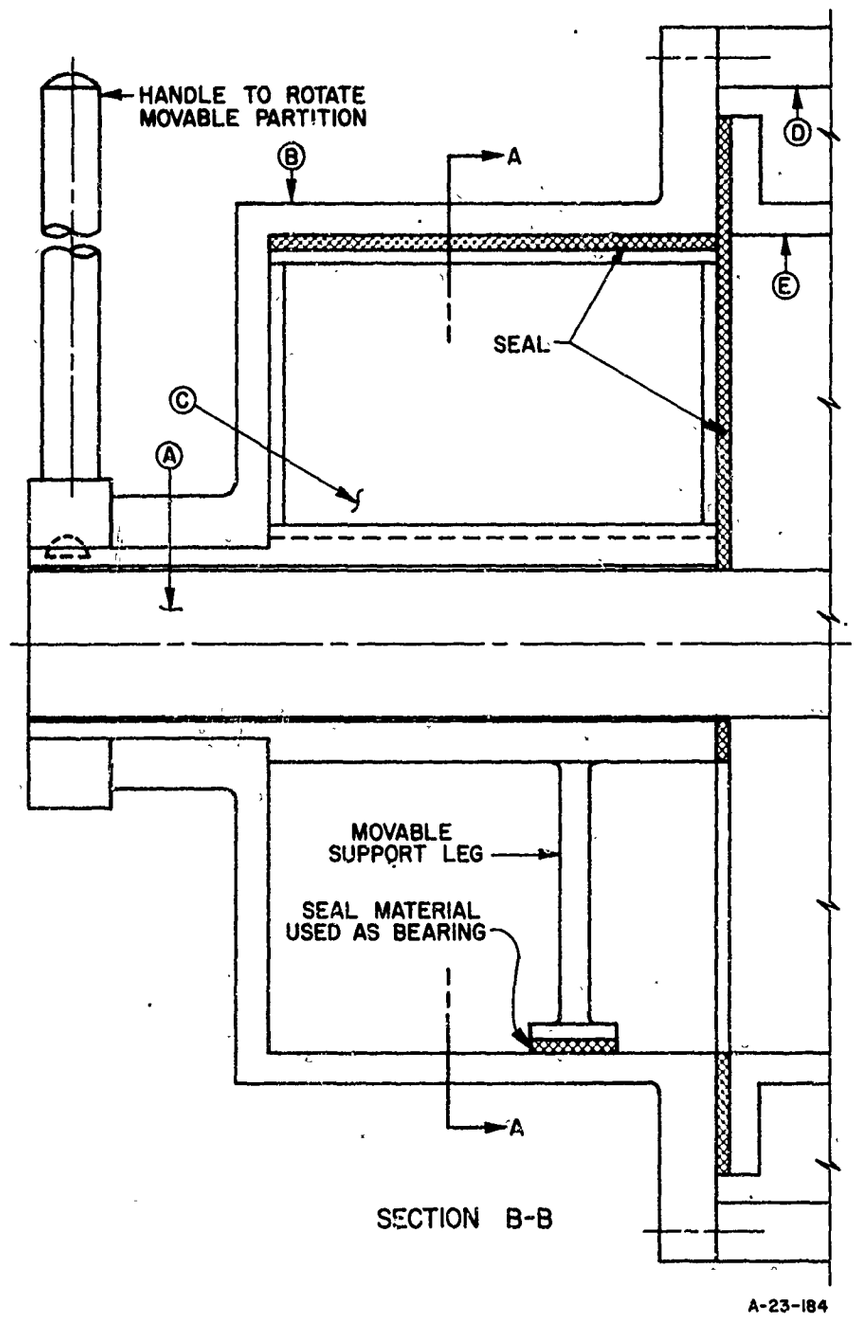

Figure 9-4. AXIAL CROSS-SECTIONAL VIEW THROUGH HEADPIECE (Movable Partition)

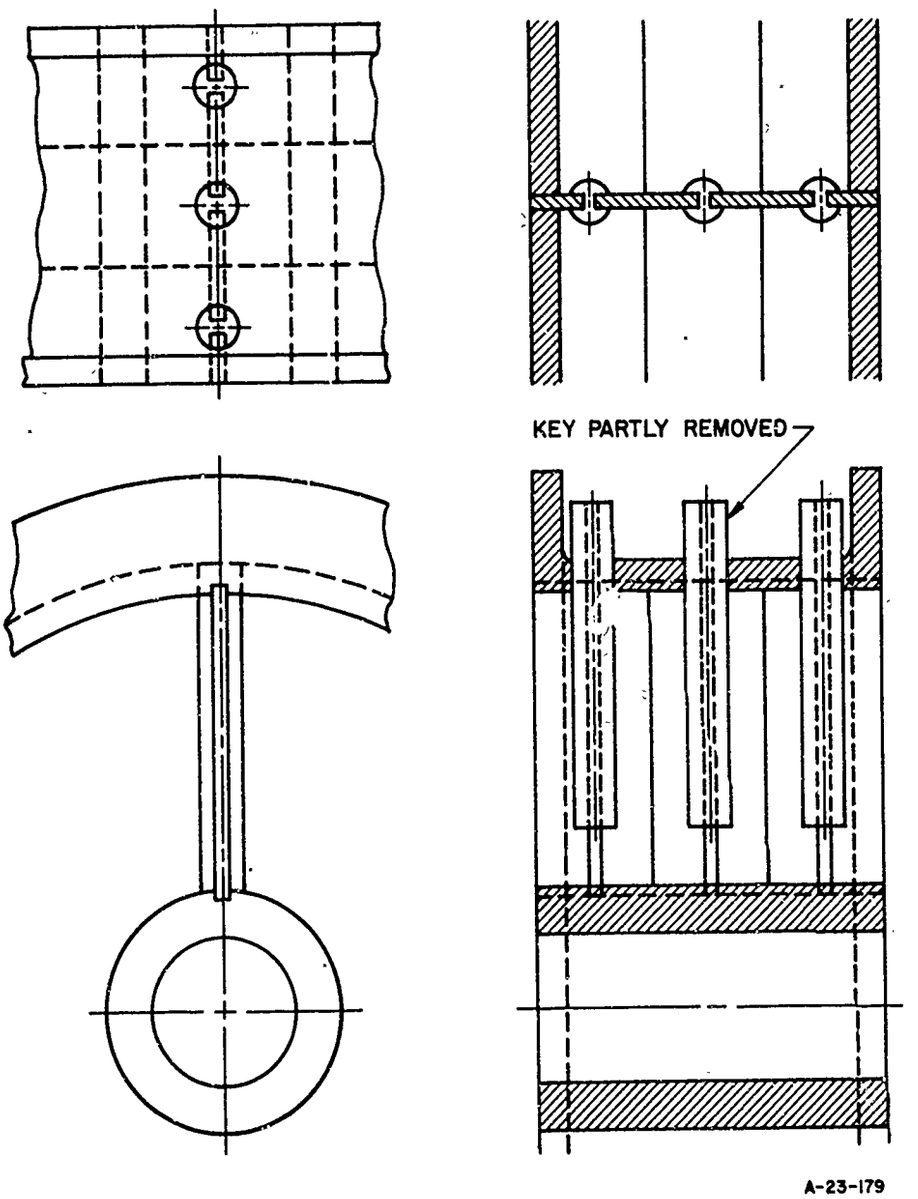

Figure 9-5. DETAIL OF CATALYST LOCKS

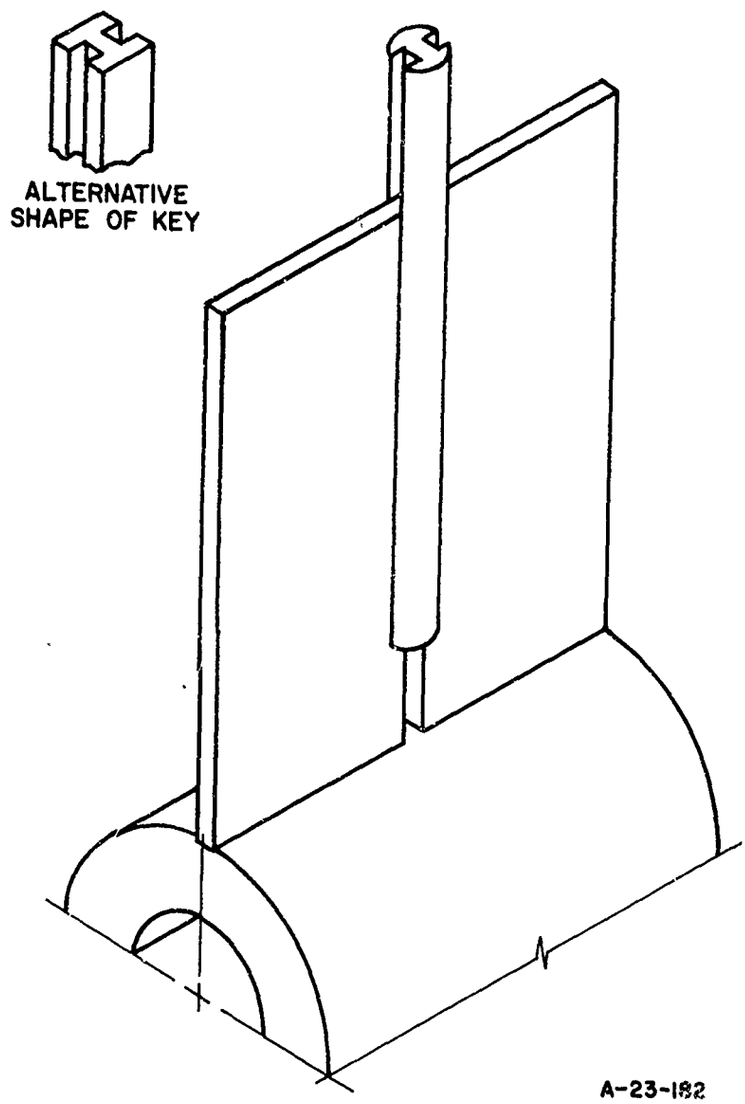

Figure 9-6. DETAIL OF SEGMENT LOCK KEY

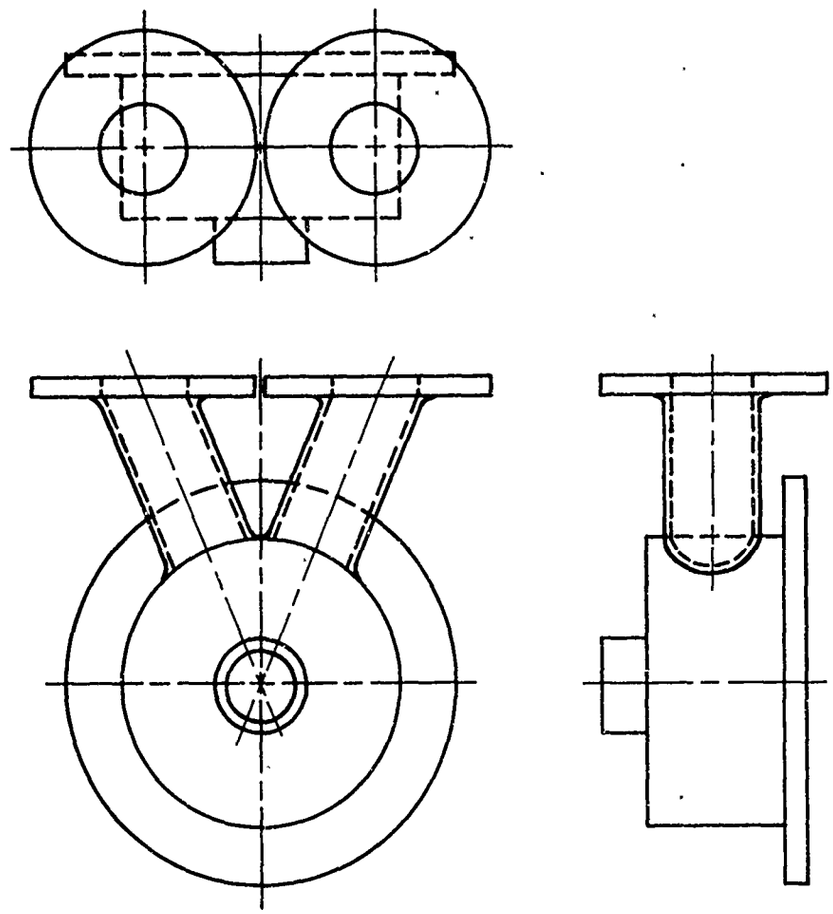

Figure 9-7. DETAIL OF CONNECTION NOZZLES

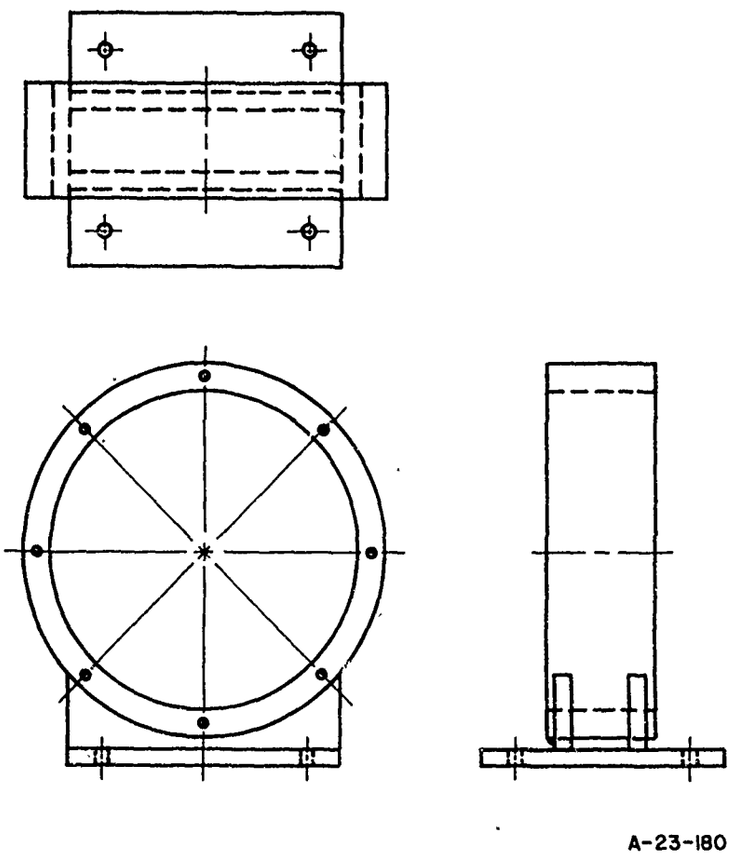

Figure 9-8. DETAIL OF SUPPORT BASE

10. ACKNOWLEDGMENT

The work described in this report was sponsored by the Facilities and Protective Technology Division, Manufacturing Technology Directorate, at Picatinny Arsenal, Dover, New Jersey, under contract DAAA 21-72-C-0455.

11. REFERENCES CITED*

1. Accomazzo, M. A. and Nobe, K., "Catalytic Combustion of C_1 to C_3 Hydrocarbons," I&EC Process Des. Develop. 4, 425-30 (1965) October.

2. Adlhart, O. J., Hindin, S. G. and Kenson, R. E., "Nitrogen Oxide Pollution: Processing Nitric Acid Tail Gas," Chem. Eng. Progr. 67, 73-78 (1971) February.

3. Andersen, R. B. et al., "Catalytic Oxidation of Methane," Ind. Eng. Chem. 53, 809-12 (1961) October.

4. Andersen, H. C., Green, W. J. and Steele, D. R., "Catalytic Treatment of Nitric Acid Plant Tail Gas," Ind. Eng. Chem. 53, 199-204 (1961) March.

5. Ault, J. W. and Ayen, R. J., "Catalytic Reduction of Nitric Oxide With Various Hydrocarbons." Paper No. 13c presented at the 62nd Annual A.I.Ch.E. Meeting, Washington, D.C., November 16-20, 1969.

6. Ayen, R. J. and Amirnazmi, A., "Catalytic Reduction of Nitrogen Dioxide With Hydrogen," I&EC Process Des. Develop. 9, 247-54 (1970).

7. Ayen, R. J. and Ng, Y.-S., "Catalytic Reduction of Nitric Oxide by Carbon Monoxide," Air Water Pollut. Int. J. 10, 1-13 (1966) January.

8. Ayen, R. J. and Peters, M. S., "Catalytic Reduction of Nitric Oxide," I&EC Process Des. Develop. 1, 204-07 (1962) July.

9. Ayen, R. J. and Yonebayashi, T., "Catalytic Reduction of Nitric Oxide by Carbon Monoxide," Atmos. Environ. 1, 307-18 (1967) May.

10. Baker, R. A. and Doerr, R. C., "Catalytic Reduction of Nitrogen Oxides in Automobile Exhaust," J. Air Pollut. Contr. Assoc. 14, 409-14 (1964) October.

11. Bartok, W, et al., "Systems Study of Nitrogen Oxide Control Methods for Stationary Sources," Final Report, Vol. 2, Contract PH-22-68-55 for the National Air Pollution Control Administration by Esso Research and Engineering Company. Washington, D.C., November 1969.

---

* In addition to the selected references listed below, additional information is available in this field. In particular, the excellent literature review in Reference 29 is valuable.

12. Cohn, J. G. E., Haley, A. J., Jr., and Andersen, H. C. (assigned to Engelhard Industries, Inc.), "Method of Effecting the Catalytic Contact of Gases Contining Oxygen and Methane," U.S. Patent 3,056,646 (1962) October 2.

13. "Control Techniques for Nitrogen Oxide Emissions From Stationary Sources," NAPCA Publication No. AP-67. Washington, D.C., 1970.

14. Fed. Regist. 36, No. 247, Part III (1971) December 23.

15. Fornoff, L. L. and Matthews, W. G., "The Purasiv-N Process — A New Molecular Sieve Process for NO_x Removal and Recovery From Nitric Acid Plant Tail Gas." Paper No. 27e presented at the 64th Annual A.I.Ch.E. Meeting, San Francisco, November 28-December 2, 1971.

16. Gillespie, G. R., Boyum, A. A. and Collins, M. F., "Nitric Acid: Catalytic Purification of Tail Gas," Chem. Eng. Progr. 68, 72-77 (1972) April.

17. Hawthorn, R. D., "Afterburner Catalysts — Effects of Heat and Mass Transfer Between Gas and Catalyst Surface." Paper No. 29c presented at the 71st Natural Meeting of the A.I.Ch.E., Dallas, February 20-23, 1972.

18. Jakob, M., Heat Transfer, Vol. 2. New York: John Wiley, 1957.

19. Kays, W. M. and London, A. L., Compact Heat Exchangers, 2nd Ed. New York: McGraw-Hill, 1964.

20. Malinsky, J., "Catalytic Combustion of Methane," Erdol Kohle 24, 82-85 (1971) February (German text).

21. Mezaki, R. and Watson, C. C., "Catalytic Oxidation of Methane," I&EC Process Des. Develop. 5, 62-65 (1966) January.

22. "A New Non-Noble Metal Catalyst for Nitric Acid...," Chem. Week 105, 68 (1969) September 13.

23. Newman, D. J., "Nitrogen Oxide Pollution: Nitric Acid Plant Pollutants," Chem. Eng. Progr. 67, 79-84 (1971) February.

24. Newman, D. J. and Klein, L. A., "Nitric Acid: Recent Developments in Nitric Acid Manufacture," Chem. Eng. Progr. 68, 62-66 (1972) April.

25. "Process Survey — Nitric Acid," Supplement to Eur. Chem. News, London, January 30, 1970.

26. Romeo, P. L. (assigned to Engelhard Industries, Inc.), "Nitric Acid Tail Gas Purification," U.S. Patent 3,425,803 (1969) February 4.

27. Rossini, F. D. et al., Selected Values of Physical and Thermodynamic Properties of Hydrocarbon and Related Compounds. Pittsburgh: Carnegie Press (published for the American Petroleum Institute), 1953.

28. Sauchelli, V., Ed., Fertilizer Nitrogen, 99-127. New York: Reinhold, 1964.

29. Shelef, M. and Kummer, J. T., "The Behavior of Nitric Oxide in Heterogeneous Catalytic Reactions. Paper No. 13f presented at the 62nd Annual A.I.Ch.E. Meeting, Washington, D.C., November 16-20, 1969.

30. Shelef, M. and Otto, K., "Appearance of N_2O in the Catalytic Reduction of NO by CO," J. Catal. 10, 408-12 (1968).

31. Shelef, M. and Otto, K., "Simultaneous Catalytic Reaction of Oxygen and Nitric Oxide With Carbon Monoxide and Solid Carbon," J. Colloid Interface Sci. 31, 73-78 (1969).

32. Stein, K. C. et al., "Catalytic Oxidation of Hydrocarbons," Bureau of Mines Bull. No. 608. Washington, D.C.: U.S. Department of Interior, 1963.

33. Stein, K. C. et al., "Catalytic Oxidation of Hydrocarbons," Ind. Eng. Chem. 52, 671-74 (1960) August.

34. Stull, D. R. and Prophet, H., Eds., JANAF Thermochemical Tables, 2nd Ed. Washington, D.C.: U.S. Department of Commerce, National Bureau of Standards, June 1971.

35. Sundaresan, B. B. and Harding, C. I. (assigned to Nitram Chemicals, Inc.; Wilson-Toomer Division of the Emhart Corp.; and the University of Florida), "Methods of Recovering Gases and Vapors," U.S. Patent 3,389,961 (1968) June 25.

36. Voorhoeve, R.J.H. et al., "Rare-Earth Oxides of Manganese and Cobalt Rival Platinum for the Treatment of Carbon Monoxide in Auto Exhaust," Science 177, 353-54 (1972) July 28.

APPENDIX A. Derivation of Thermodynamic Equilibrium Equations

Determination of Equilibrium Composition of N-O System

Assume: NO, NO_2, etc. = moles of named species

NO_i, NO_{2_i}, etc. = initial moles

K_f = equilibrium constant of formation of subscripted species as determined by nonlinear least mean squares regression analysis of primary data

Material Balance Equations:

Nitrogen

$$N_2 + N_2O + 1/2\,NO + 1/2\,NO_2 = N_{2_i} + N_2O_i + 1/2\,NO_i + 1/2\,NO_{2_i}$$

Oxygen

$$O_2 + NO_2 + 1/2\,N_2O + 1/2\,NO = O_{2_i} + NO_{2i} + 1/2\,N_2O_i + 1/2\,NO_i$$

Total

$$\text{Total} = N_2 + N_2O + NO + NO_2 + O_2$$

Equilibrium Equations:

$$NO_2 = (K_{f\ NO_2})\ (O_2)\ (N_2)^{1/2}\ (\text{Total})^{-1/2}$$

$$NO = (K_{f\ NO})\ (O_2)^{1/2}\ (N_2)^{1/2}$$

$$N_2O = (K_{f\ N_2O})\ (O_2)^{1/2}\ (N_2)\ (\text{Total})^{-1/2}$$

Initial Values:

N_{2_i} = 0.962

O_{2_i} = 0.035

NO_{2_i} = 0.0015

NO_i = 0.0015

N_2O_i = 0.0

Read: $\frac{NO_2}{\text{Total}}$, $\frac{NO}{\text{Total}}$, $\frac{N_2O}{\text{Total}}$

Determination of Equilibrium Composition of C-H-N-O System, Assuming Combustion of NO_x with CH_4

Assume: NO, CH_4, H_2O, etc. = moles of named species

NO_i, CH_{4_i}, H_2O_i, etc. = initial moles

K_f = equilibrium constant of formation of subscripted species.

Ignore higher hydrocarbons, amines, etc.

Material Balances:

Carbon

$$CO_2 + CO + CH_4 + HCN = CO_{2_i} + CO_i + CH_{4_i} + HCN_i$$

Hydrogen

$$4CH_4 + 3NH_3 + 2H_2O + 2H_2 + HCN = 4CH_{4_i} + 3NH_{3_i} + 2H_2O_i + 2H_{2_i} + HCN_i$$

Nitrogen

$$HCN + NH_3 + NO_2 + NO + 2N_2O + 2N_2 = HCN_i + NH_{3_i} + NO_{2_i} + NO_i + 2N_2O_i + 2N_{2_i}$$

Oxygen

$$2NO_2 + NO + N_2O + 2CO_2 + CO + H_2O + 2O_2 =$$
$$2NO_{2_i} + NO_i + N_2O_i + 2CO_{2_i} + CO_i + H_2O_i + 2O_{2_i}$$

Total

$$\text{Total} = N_2 + N_2O + NO + NO_2 + O_2 + H_2O + H_2 + CO_2 + CO + CH_4 + HCN + NH_3$$

Equilibrium Equations:

Basis: N_2, CO, CO_2, H_2O

Reaction: $NO_2 = 1/2\ N_2 + 2\ CO_2 - 2CO$

$$NO_2 = K_1\ (CO_2)^2\ (CO)^{-2}\ (N_2)^{1/2}\ (\text{Total})^{1/2}$$

$$K_i = (K_{f\,NO_2})\ (K_{f\,CO})^2\ (K_{f\,CO_2})^{-2}$$

Reaction: $NO = 1/2\ N_2 + CO_2 - CO$

$$NO = K_2\ (CO_2)\ (CO)^{-1}\ (N_2)^{1/2}\ (\text{Total})^{1/2}$$

$$K_2 = (K_{f\,NO})\ (K_{f\,CO})\ (K_{f\,CO_2})^{-1}$$

Reaction: $N_2O = N_2 + CO_2 - CO$

$$N_2O = K_3\ (N_2)\ (CO_2)\ (CO)^{-1}$$

$$K_3 = (K_{fN_2O})\ (K_{fCO})\ (K_{fCO_2})^{-1}$$

Reaction: $H_2 = H_2O + CO - CO_2$

$$H_2 = K_4\ (H_2O)\ (CO)\ (CO_2)^{-1}$$

$$K_4 = (K_{fCO_2})\ (K_{fH_2O})^{-1}\ (K_{fCO})^{-1}$$

Reaction: $CH_4 = 2H_2O + 4CO - 3CO_2$

$$CH_4 = K_5\ (H_2O)^2\ (CO)^4\ (CO_2)^{-3}\ (\text{Total})^{-2}$$

$$K_5 = (K_{fCH_4})\ (K_{fCO_2})^3\ (K_{fH_2O})^{-2}\ (K_{fCO})^{-4}$$

Reaction: $O_2 = 2CO_2 - 2CO$

$O_2 = K_6 (CO_2)^2 (CO)^{-2} (Total)$

$K_6 = (K_{fCO})^2 (K_{fCO_2})^{-2}$

Reaction: $NH_3 = 1/2N_2 + 3/2H_2O + 3/2CO - 3/2CO_2$

$NH_3 = K_7 (N_2)^{1/2} (H_2O)^{3/2} (CO)^{3/2} (CO_2)^{3/2} (Total)^{-1}$

$K_7 = (K_{fNH_3}) (K_{fCO_2})^{3/2} (K_{fCO})^{-3/2} (K_{fH_2O})^{-3/2}$

Reaction: $HCN = 1/2N_2 + 1/2H_2O + 5/2CO - 3/2CO_2$

$HCN = K_8 (N_2)^{1/2} (H_2O)^{1/2} (CO)^{5/2} (CO_2)^{-3/2} (Total)^{-1}$

$K_8 = (K_{fHCN}) (K_{fCO_2})^{3/2} (K_{fCO})^{-5/2} (K_{fH_2O})^{-1/2}$

Input:

N_{2_i}	= 0.962	H_{2_i}	= 0
O_{2_i}	= 0.035	CO_i	= 0
NO_{2_i}	= 0.0015	CO_{2_i}	= 0
NO_i	= 0.0015	N_2O_i	= 0
H_2O_i	= 0.070	NH_{3_i}	= 0
		HCN_i	= 0

$$CH_{4_i} = (1 + xs) (1/2O_{2_i} + 1/2NO_{2_i} + 1/4NO_i)$$

Let xs = 0.2, 0.1, 0.05, 0.02, 0.0
−0.2, −0.1, −0.05, −0.02

Read all 12 components as $\frac{NO_2}{Total - H_2O}$, etc.

If unstable at xs = negative, derive similar equilibria equations based on N_2, CO_2, H_2O, O_2.

APPENDIX B. Derivation of Heat Exchange Equations

Consider a system of adiabatic, countercurrent heat exchange with an external chemical reaction as illustrated below. The cold feed gas enters the system at temperature T_o. It is heated in the adiabatic exchanger (no heat loss to the surroundings). At point x in the exchanger, the gas in the preheat section (Section 1) has been heated to temperature T_1. At the end of the exchanger, the preheated gas temperature is T_p. The gas then reacts exothermally and adiabatically to a reaction temperature T_R. The gases pass back through the exchanger in Section 2, countercurrent to the flow in Section 1. At point x, the gas temperature is T_2 and the solids separating the Sections 1 and 2 are at temperature T_s. The gas finally leaves the system at a temperature T_f.

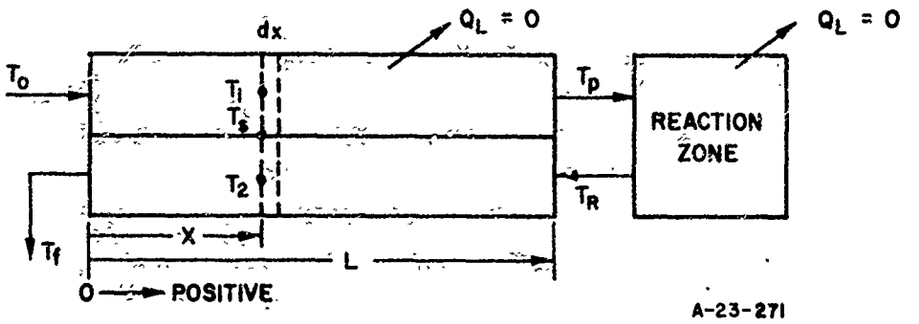

Let

A_{ci} = cross-sectional area of section i, sq ft

A_{si} = heat transfer surface area of section i, sq ft

T_i = temperature of gas in section i, ^0F

G_i = flow rate in section i, lb/hr-sq ft

F_i = mass flow in section i = $G_i A_{ci}$, lb/hr

C_{pi} = heat capacity of gas in section i, Btu/lb-^0F

C_i = heat capacity flow in section i = $F_i C_{pi}$, Btu/hr-^0F

h_i = heat transfer coefficient in section i, Btu/hr-sq ft-^0F

Preceding page blank

The heat transfer surface in each section is proportional to the cross-sectional area in that section:

$$\frac{A_{si}}{\Sigma A_{si}} = \frac{A_{ci}}{\Sigma A_{ci}} \tag{B-1}$$

In this problem, the heat is transferred between the individual gas streams and the solid surface. At steady state —

$$\Sigma h_i A_{si}(T_i - T_s) = 0 \tag{B-2}$$

The temperature gradients in Sections 1 and 2 are —

$$\frac{d T_1}{dx} = \frac{h_1 A_{s1}}{C_1 L} (T_s - T_1) \tag{B-3}$$

and

$$\frac{d T_2}{dx} = \frac{h_2 A_{s2}}{C_2 L} (T_s - T_2) \tag{B-4}$$

The temperature difference gradient can be derived from the above equations:

$$\frac{\partial (T_2 - T_1)}{\partial x} = - (T_2 - T_1)(\frac{1}{C_1} + \frac{1}{C_2}) \frac{A_{c1}}{\Sigma A_{ci}} \frac{A_{c2}}{\Sigma A_{ci}} \frac{h \Sigma A_{si}}{L} \tag{B-5}$$

where $h = h_1 = h_2$ by the mechanical configuration of the heat exchanger. However, in this countercurrent flow, $C_2 = -C_1$.

Therefore, $T_2 - T_1$ is constant.

$$\begin{aligned} T_2 - T_1 &= T_f - T_o \\ &= T_R - T_p \end{aligned} \tag{B-6}$$

From Equations B-2 and B-6 —

$$T_s - T_1 = (T_f - T_o) A_{c2} / \Sigma A_{ci} \tag{B-7}$$

And from Equation B-3 —

$$T_1 = \frac{h}{C_1} \frac{A_{s_1} A_{c_2}}{\Sigma A_{c_i}} \frac{x}{L} (T_f - T_o) + T_o \qquad \text{(B-8)}$$

Temperatures T_p and T_R can be determined at $x = L$.

In this system, the heat exchange surface is generated by a honeycomb. With reasonable flow rates, fully developed laminar flow exists and the Nusselt Number is constant and equal to 4.0.

$$Nu = \frac{hd_H}{k} = 4.0 \qquad \text{(B-9)}$$

where k is the thermal conductivity of the gas and d_H is the hydraulic diameter of the channel. By definition of hydraulic diameter —

$$A_{si} = 4L\, A_{ci}/d_H \qquad \text{(B-10)}$$

With these factors, Equation B-8 may be written in terms of the physical constants of the system, at $x = L$:

$$T_p = T_o + \frac{4\, Nu\, k}{C_p\, d_H^2\, F/L\Sigma A_{ci}} \frac{A_{c1}}{\Sigma A_{ci}} \frac{A_{c2}}{\Sigma A_{ci}} (T_f - T_o) \qquad \text{(B-11)}$$

By substitution, the heat exchange efficiency, η —

$$\eta = \frac{T_p - T_o}{T_R - T_o} \qquad \text{(B-12)}$$

$$\eta = 1/\left(1 + \frac{4\, Nu\, k}{C_p\, d_H^2\, F/L\Sigma A_{ci}} \frac{A_{c_1}}{\Sigma A_{ci}} \frac{A_{c_2}}{\Sigma A_{ci}}\right) \qquad \text{(B-13)}$$

where —

$F/L\,\Sigma A_{ci}$ = flow rate/unit volume of exchanger, lb/hr-cu ft

$A_{ci}/\Sigma A_{ci}$ = fraction of exchanger in preheat

$A_{c2}/\Sigma A_{ci}$ = fraction of exchanger in cooling

Nu = Nusselt Number = 4.0 for fully developed laminar flow in circular channels

k = gas thermal conductivity

C_p = gas heat capacity

APPENDIX C-1. Derivation of Equations – Diffusion-Controlled Reaction With Heat Transfer

Preceding page blank

Consider a simple reactor with the reaction rate controlled by the rate of diffusion of the reactants to the catalytic wall. The reaction occurs on the catalyst, and the heat of reaction is released into the solids and convectively transferred to the gas under laminar flow conditions in the reactor channels.

In the system below, the cold gas enters the reactor at temperature, T_0; flow rate, G, lb/sq ft; and reactant concentration ξ_0, weight fraction.

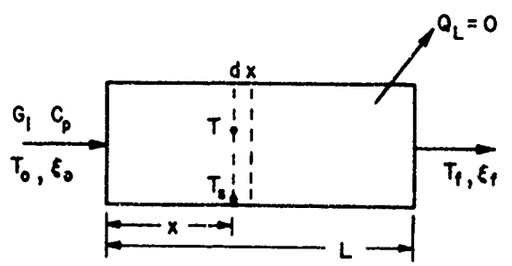

A-23-270

Let:

A_c = cross-sectional area, sq ft

A_s = surface area, sq ft

C = heat capacity flow, Btu/hr-^{0}F

= $GA_c C_p$

C_p = heat capacity, Btu/lb-^{0}F

G = mass flow rate, lb/hr-sq ft

h = heat transfer coefficient, Btu/hr-^{0}F

H_r = heat of reaction, Btu/lb reactant

K_g = mass transfer coefficient, cu ft/hr-sq ft

Q_s = heat release at surface, Btu/hr

T = gas temperature

T_0 = initial gas temperature

T_s = solids temperature

ρ = gas density

ξ = reactant concentration, wt fraction

λ = Lewis Number = $K_g \rho_g C_p / h$

The temperature gradient in the gas stream is determined by the heat balance:

$$C \frac{dT}{d\,x/L} = h A_s (T_s - T)$$

At steady state, the heat release to the solids is equal to the heat transferred:

$$Q_s = h A_s (T_s - T)$$

and the heat release is a function of the concentration:

$$Q_s = H_r K_g A_s \rho_g \xi$$

The reactant concentration gradient is —

$$G A_c \frac{d\xi}{d\,x/L} = -K_g A_s \rho_g (\xi - \xi_s);\ \xi_s = 0$$

$$\xi = \xi_0 e^{-K_g A_s \rho_g x/G A_c L}$$

$$= \xi_0 e^{-\alpha x/L}$$

Let: $\alpha = K_g A_s \rho_g / G A_c$ $\qquad \alpha = \dfrac{K_g A_s \rho_g}{C/C_p}$

$\beta = H_r K_g A_s \rho_g \xi_0$ $\qquad \dfrac{\alpha C}{h A_s} = \dfrac{K_g A_s \rho C_p}{h A_s}$

$Q_s = \beta e^{-\alpha x/L}$ $\qquad = \lambda$

$$\frac{dT}{d\,x/L} = \frac{1}{C} \cdot \beta e^{-\alpha x/L}$$

$$T - T_0 = \frac{\beta}{C\alpha} (1 - e^{-\alpha x/L})$$

$$T_s - T_0 = \frac{\beta}{h A_s} e^{-\alpha x/L} + T$$

$$= \frac{\lambda}{C\alpha} \beta e^{-\alpha x/L} + \frac{\beta}{CL} (1 - e^{-\alpha x/L})$$

$$T_s - T_0 = \frac{\beta}{C\alpha} [1 - (1-\lambda) e^{-\alpha x/L}]$$

APPENDIX C-2. Derivation of Equations — Diffusion-Controlled Reaction With Regenerative Heat Exchange (Countercurrent Flow)

Consider a system similar to the simple heat exchange problem presented earlier, except that the exothermic chemical reaction takes place in Section 2, rather than externally. The reaction occurs on the surface of Section 2, perhaps catalytically, and the rate is controlled by diffusion of the reactants to the surface.* Note that the heat exchange surface in Section 2 is also the diffusion surface. The heat is generated on that surface by the chemical reaction and is transferred to the gases by the laws of heat exchange under laminar flow conditions.

In the system illustrated below, the cold feed gas enters the system at temperature T_1^0. It is heated in Section 1 of the reactor with no heat loss to the surroundings. At point x, the inlet gas has been heated to T_1, and at the end of the reactor, the temperature is T_1^f. The gas immediately returns back through Section 2. By the convention of the figure, the gas temperature at this point is T_2^0 and the reactant concentration (weight fraction) is ξ_o. At point x, these parameters are T_2 and ξ_i and at the end of the reactor, T_2^f and ξ_f.

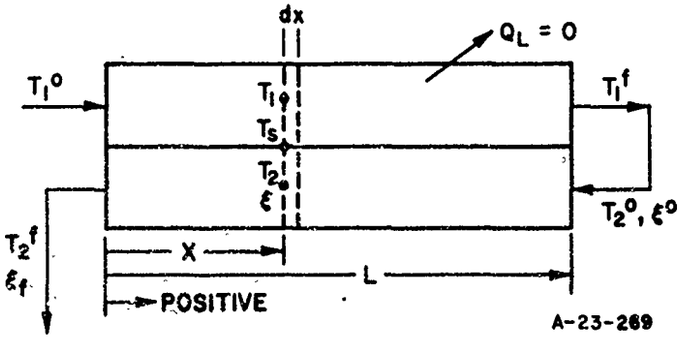

* The equations for diffusion-control are identical to first-order reaction rate control, so the derivation is also applicable in that situation.

Let

A_{ci} = cross-sectional area of section i

A_{si} = surface area of section i

T_i = gas temperature in section i

T_s = surface temperature

ξ = reactant concentration, weight fraction

G_i = flow rate in section i

C_{pi} = heat capacity in section i

C_i = heat capacity flow in section i

$= G_i A_{ci} C_{pi}$

h_i = heat transfer coefficient

K_g = mass transfer coefficient

ρ_g = gas density

Q_s = heat release at surface

H_r = heat of reaction

d_H = hydraulic diameter of channel

Nu = Nusselt Number = $h\, d_H/k$

λ = Lewis Number = $k_g\, \rho_g\, C_p/h$

K = thermal conductivity of gas

$d_H = 4\, A_{ci}\, L/A_{si}$; d_H assigned

$h = Nu\, k/d_H$; Nu $\cong$ 4 in laminar flow

$K_g = \lambda h/\rho_g\, C_p$; λ assigned

Using the positive direction toward the right, the temperature gradients in the two sections are —

$$C_1 \frac{\partial T_1}{\partial x/L} = h_1 A_{s_1}(T_s - T_1) \qquad \text{(C-2-1)}$$

and

$$C_2 \frac{\partial T_2}{\partial x/L} = -h_2 A_{s_2}(T_s - T_2) \qquad \text{(C-2-2)}$$

At steady state, the heat release is equal to the total heat transfer:

$$\Sigma h_i A_{si}(T_s - T_i) = Q_s \qquad \text{(C-2-3)}$$

The heat release is —

$$Q_s = H_r \text{ (reaction rate)} \qquad \text{(C-2-4)}$$

The reaction rate is the diffusion rate:

$$\text{rate} = K_g A_{s_2} \rho g(\xi - \xi_s) \qquad \text{(C-2-5)}$$

$$= G_2 A_{c_2} \frac{\partial \xi}{\partial x/L}$$

At $\xi_s = 0$

$$\xi = \xi_f e^{K_g \rho_g A_{s_2} x/G_2 A_{c_2} L} \qquad \text{(C-2-6)}$$

Let

$$\alpha = K_g \rho_g A_{s_2}/G_2 A_{c_2} \qquad \text{(C-2-7)}$$

$$\beta = H_r K_g A_{s_2} \rho_g \xi_f \qquad \text{(C-2-8)}$$

$$\therefore T_s = \frac{\beta e^{\alpha x/L} + \Sigma h_i A_{s_i} T_i}{\Sigma h_i A_{si}} \qquad \text{(C-2-9)}$$

From Equations C-2-1 and C-2-2 —

$$\frac{\partial(T_2 - T_1)}{\partial x/L} = -\frac{h_2 A_{s_2}}{C_2}(T_s - T_2) - \frac{h_1 A_{s_1}}{C_1}(T_s - T_1) \qquad \text{(C-2-10)}$$

Let

$$\eta_i = h_i A_{si} / \sum_{j=1}^{2} h_j A_{s_j} \qquad \text{(C-2-11)}$$

$$N_{tu} = \frac{1}{C_1}[1/(1/h_1 A_{s_1} + 1/h_2 A_{s_2})] \qquad \text{(C-2-12)}$$

From C-2-9 —

$$T_s - T_i = \frac{\beta e^{\alpha x/L} + h_j A_{s_j}(T_j - T_i)}{\Sigma h_i A_{s_i}} \qquad \text{(C-2-13)}$$

$$\therefore \frac{\partial(T_2 - T_1)}{\partial\, x/L} = -\beta\left(\frac{\eta_1}{C_1} + \frac{\eta_2}{C_2}\right) e^{+\alpha\, x/L} - N_{tu}(T_2 - T_1)\left(1 - \frac{C_1}{C_2}\right) \qquad \text{(C-2-14)}$$

$$\text{Let} \quad \gamma_a = -\beta\left(\frac{\eta_1}{C_1} + \frac{\eta_2}{C_2}\right); \quad \gamma_b = N_{tu}(1 - C_1/C_2) \qquad \text{(C-2-15,16)}$$

$$T_2 - T_1 = \frac{\gamma_a}{\gamma_b + \alpha} e^{\alpha\, x/L} - \frac{\gamma_a}{\gamma_b + \alpha}\left(e^{\alpha + \gamma_b}\, e^{-\gamma_b\, x/L}\right) \qquad \text{(C-2-17)}$$

because

$$T_2^{\,0} = T_1^{\,f} \text{ at } x = L$$

From Equations C-2-1 and C-2-13 –

$$C_1 \frac{\partial\, T_1}{\partial\, x/L} = \frac{h_1 A_{s_1}}{\Sigma h_i A_{si}}\left[\beta e^{\alpha x/L} + h_2 A_{s_2}(T_2 - T_1)\right] \qquad \text{(C-2-18)}$$

$$T_1 = T_1^{\,0} + \left(\frac{\eta_1 \beta}{C_1} + \frac{N_{tu}\, \gamma_a}{\gamma_b + \alpha}\right)\left(\frac{e^{\alpha x/L} - 1}{\alpha}\right) + \frac{\gamma_a}{\gamma_b + \alpha} e^{\gamma_b + \alpha} N_{tu}\left(\frac{e^{-\gamma_b\, x/L} - 1}{\gamma_b}\right) \qquad \text{(C-2-19)}$$

$$T_s = \frac{\beta\, e^{\alpha\, x/L}}{h_1 A_{s_1} + h_2 A_{s_2}} + \eta_1 T_1 + \eta_2 T_2 \qquad \text{(C-2-20)}$$

$$= \frac{\beta\, e^{\alpha x/L}}{h_1 A_{s_1} + h_2 A_{s_2}} + (\eta_1 + \eta_2) T_1 + \eta_2(T_2 - T_1) \qquad \text{(C-2-21)}$$

Equations C-2-17, 19, and 21 define the temperatures in the system. At $|C_1| = |C_2|$ and $h = h_1 = h_2$ –

$$\gamma'_a = \frac{-\beta}{C}(\eta_1 + \eta_2) = \frac{-\beta}{C}$$

$$\gamma_b' = 0$$

$$(T_2 - T_1)_{x=0} = \frac{\beta}{C\alpha}(e^{\alpha} - 1) = \text{adiabatic temperature rise}$$

APPENDIX C-3. Derivation of Equations — Diffusion-Controlled Reaction With Regenerative Heat Exchange (Cocurrent Flow)

Consider a system of regenerative heat and reaction in cocurrent flow, as illustrated by the schematic diagram below. This system is very similar to the countercurrent system, so only the differences in the derivations will be presented.

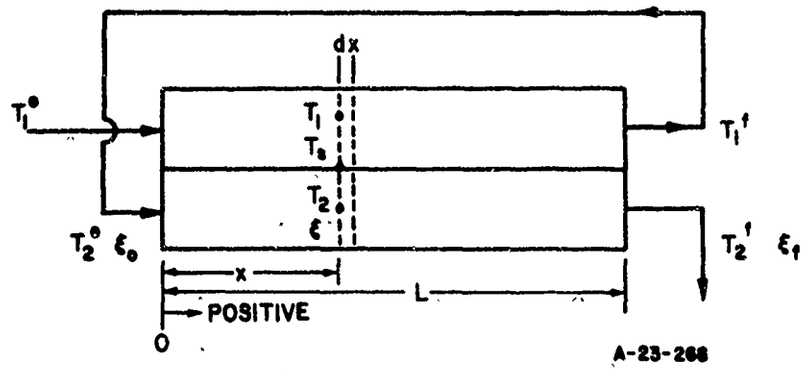

$$C_2 \frac{\partial T_2}{\partial x/L} = + h_2 A_{s_2} (T_s - T_2)$$

$$\text{Rate} = G_2 A_{c_2} \frac{\partial \xi}{\partial x/L} = -K_g \rho_g A_{s_2} \xi$$

$$\xi = \xi_0 \, e^{-\alpha}$$

$$\beta = H_r K_g A_{s_2} \rho_g \xi_0$$

$$T_s = (\beta e^{-\alpha x/L} + \Sigma h_i A_{si} T_i)/\Sigma h_i A_{si}$$

$$\frac{\partial (T_2 - T_1)}{\partial x/} = + \frac{h_2 A_{s_2}}{C_2} (T_s - T_1) - \frac{h_1 A_{s_1}}{C_1} (T_s - T_1)$$

$$\gamma_a = \beta \left(\frac{\eta_2}{C_2} - \frac{\eta_1}{C_1}\right)$$

Preceding page blank

$$\gamma_b = N_{tu}\,(1 + C_1/C_2)$$

$$T_2 - T_1 = \frac{\gamma_a}{\gamma_b - \alpha}\, e^{-\alpha x/L} + b\, e^{-\gamma_b x/L}$$

$$b = \frac{+\dfrac{\eta_1 \beta}{C_1 \alpha}\,(1 - e^{-\alpha}) + \dfrac{\gamma_a}{\gamma_b - \alpha}\left[\dfrac{N_{tu}}{\alpha}\,(1 - e^{-\alpha}) - 1\right]}{1 - \dfrac{N_{tu}}{\gamma_b}\,(1 - e^{-\gamma_b})}$$

$$T_1 = T_1^0 + \left(\frac{\eta_1 \beta}{C_1 \alpha} + \frac{\gamma_a}{\gamma_b - \alpha}\,\frac{N_{tu}}{\alpha}\right)(1 - e^{-\alpha x/L})$$

$$+ b\, N_{tu}\,\left(\frac{1 - e^{-\gamma_b x/L}}{\gamma_b}\right)$$

$$T_s = \frac{\beta e^{-\alpha x/L}}{h_1 A_{s_1} + h_2 A_{s_2}} + (\eta_1 + \eta_2)\, T_1 + \eta_2\,(T_2 - T_1)$$

$$\gamma_a = \frac{\beta}{C}\,(\eta_2 - \eta_1); \quad \gamma_b = 2\, N_{tu}$$

T_s is constant at $\eta_2 = \eta_1 = 1/2$, $\lambda = 1.0$, and equal to the adiabatic reaction temperature.

T_s is nearly constant at $\lambda = \eta_1/\eta_2$

APPENDIX C-4. Derivation of Equations — Three-Pass Operation

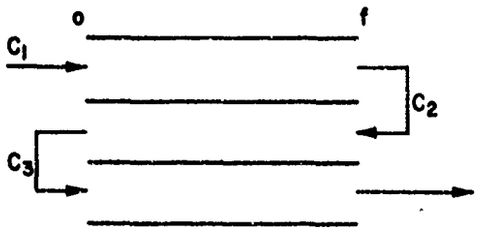

A-23-267

$$|C_1| = |C_2| = |C_3| = C$$

$$C_i = Cd_i$$

$$d_i = 1 \text{ if } C_i > 0$$

$$d_i = -1 \text{ if } C_1 < 0$$

$$C_i = G_i A_{ci} C_{pi}$$

$$C_i \frac{d T_i}{d x/L} = h_i A_{si}(T_s - T_i)$$

$$x/L = y;\ h_i = h;\quad \Sigma A_{ci} = 1;\ A_{si}/\Sigma A_{si} = \eta_i;\ \frac{h A_{si}}{C} = \sigma_i$$

$$d_i \frac{d T_i}{dy} = \sigma_i (T_s - T_i)$$

$$G_i A_{ci} \frac{d \xi_i}{dy} = -K_g \rho_g A_{si} \delta_i \xi_i$$

$$= \frac{d_i C}{C_p} \frac{d \xi_i}{dy}$$

$$d_i \frac{d \xi_i}{dy} = -\alpha_i \delta_i \xi_i$$

$\delta_i = 1$ if reaction
$= 0$ if no reaction

$$\alpha_i = K_g \rho_g A_{si} C_p / C$$

$$\lambda = K_g \rho_g C_p / h$$

$$\therefore \alpha_i = \lambda \sigma_i$$

Preceding page blank

$$Q_s = \sum_i h A_{si}(T_s - T_i) = \sum_i K_g \rho_g A_{si} \delta_i H_r \xi_i$$

$$\Sigma \sigma_i (T_s - T_i) = \sum_i \lambda H_r \sigma_i \delta_i \xi_i / C_p$$

$$\beta_i = \lambda H_r \sigma / C_p = \alpha_i H_r / C_p$$

$$\sum_i \sigma_i (T_s - T_i) = \sum_i \beta_i \delta_i \xi_i$$

$$\xi_i = \xi_i^0 e^{-\alpha_i \delta_i y/d_i}$$

3- boundary conditions:

$\delta_1 = 0$

$\delta_2 = 1 \qquad d_2 = -1$

$\delta_3 = 1 \qquad d_3 = +1$

$\xi_1^0 = \xi^0 \rightarrow \xi_1^f = \xi^0$

$\xi_2^0 = \xi_0^0 e^{-\alpha_2} \leftarrow \xi_2^f = \xi^0$

$\xi_3^0 = \xi_2^0 \rightarrow \xi_3^f = \xi_3^0 e^{-\alpha_3}$

Assign ξ^0, ξ_2^0, ξ_3^f

$$\sum_i \sigma_i (T_s - T_i) = \delta_2 \beta_2 \xi_2^0 e^{\alpha g} + \delta_3 \beta_3 \xi_3^0 e^{-\alpha_3 y}$$

$$= \Sigma \delta_i \beta_i \xi_i^0 e^{-\alpha_i \delta_i y/di}$$

To eliminate T_s:

$$\sum_i d_i \, dT_i/dy = \sum_i \delta_i \beta_i \xi_i^0 e^{-\alpha_i \delta_i y/d_i}$$

$$\frac{d_i}{\sigma_i} \frac{dT_i}{dy} - \frac{d_i \, dT_1}{\sigma_1 \, dy} = T_1 - T_i$$

$$\sum_i di \frac{d(T_i - T_1)}{dy} + \sum_i d_i \frac{d T_r}{dy} = \sum_i \delta_i \beta_i \xi_i^0 e^{-\alpha_i \delta_i y/d_i}$$

$$\frac{d\,T_1}{dy} = \frac{\Sigma \delta_i\, \beta_i\, \xi_i^{\,0}\, e^{-\alpha_i\, \delta_i\, y/d_i}}{\Sigma d_i} - \frac{\Sigma d_i\,(T_i - T_1)'}{\Sigma d_i}$$

$$\therefore \frac{d_i}{\sigma_i}(T_i - T_1)' + (T_i - T_1) - \left(\frac{d_i}{\sigma_i} - \frac{d_1}{\sigma_1}\right)\frac{\Sigma d_j (T_j - T_1)'}{\Sigma d_j}$$

$$= -\left(\frac{d_i}{\sigma_1} - \frac{d_1}{\sigma_1}\right) \sum_j \frac{\delta_j \beta_j \xi_j^{\,0}\, e^{-\alpha_j \delta_j\, y/d_j}}{\Sigma d_j}$$

$$a_{22} = \frac{d_2}{\sigma_2} - \left(\frac{d_2}{\sigma_2} - \frac{d_1}{\sigma_1}\right)\frac{d_2}{\Sigma d_i} \qquad b_2 = -\left(\frac{d_2}{\sigma_2} - \frac{d_1}{\sigma_1}\right)/\Sigma d_i$$

$$a_{23} = -\left(\frac{d_2}{\sigma_2} - \frac{d_1}{\sigma_1}\right)\frac{d_3}{\Sigma d_i} \qquad b_3 = -\left(\frac{d_3}{\sigma_3} - \frac{d_1}{\sigma_1}\right)/\Sigma d_i$$

$$a_{32} = -\left(\frac{d_3}{\sigma_3} - \frac{d_1}{\sigma_1}\right)\frac{d_2}{\Sigma d_i}$$

$$a_{33} = \frac{d_3}{\sigma_3} - \left(\frac{d_3}{\sigma_3} - \frac{d_1}{\sigma_1}\right)\frac{d_3}{\Sigma d_i}$$

$$a_{22}(T_2 - T_1)' + (T_2 - T_1) + a_{23}(T_3 - T_1)' = b_2 S$$

$$a_{32}(T_2 - T_1)' + (T_3 - T_1) + a_{33}(T_3 - T_1)' = b_3 S$$

$$(T_3 - T_1) = \left(\frac{a_{33}a_{22}}{a_{23}} - a_{32}\right)(T_2 - T_1)' + \frac{a_{33}}{a_{23}}(T_2 - T_1) + \left(b_3 - \frac{b_2 a_{33}}{a_{23}}\right) S$$

Let

$$e_2 = [a_{33} + a_{22} - a_{32} + a_{23}]$$

$$e_1 = [a_{22} + a_{33}]$$

$$D = \frac{-e_1 \pm [e_1^{\,2} - 4e^2]^{1/2}}{2e_2}$$

$$f_j = b_2\, \delta_j\, \beta_j\, \xi_j + (a_{23}\, b_3 - a_{32}\, b_2)\, \delta_j \beta_j\, \xi_j^{\,0}\, \alpha_j/d_j$$

$$r_i = f_i/(e_2\, \alpha_i^{\,2}\, \delta_i^{\,2}/d_1^{\,2} \quad - e_1\, \alpha_i\, \delta_i/d_i + 1)$$

General Solution

$$T_2 - T_1 = A\, e^{D_1 y} + B\, e^{D_2 y} + \sum_i r_i\, e^{-\alpha_i \delta_i y/d_i}$$

$$T_3 - T_1 = (T_2 - T_1)^1 \left(\frac{a_{33}a_{22}}{a_{23}} - a_{32}\right) + \frac{a_{33}}{a_{23}} (T_2 - T_1)$$

$$+ \left(b_3 - b_2 \frac{a_{33}}{a_{23}}\right) \sum_j \delta_i \rho_j \xi_j^0\, e^{-\alpha_j \delta_i y/d_j}$$

Boundary

$$T_2 - T_1 = 0 \text{ at } y = 1$$

$$T_3 - T_2 = 0 \text{ at } y = 0$$

$$(T_3 - T_1) - (T_2 - T_1) = 0 \text{ at } y = 0$$

$$\left(\frac{d_2}{\sigma_2} - \frac{d_1}{\sigma_1}\right) \frac{d\,T_1}{dy} = -(T_2 - T_1) - \frac{d_2}{\sigma_2} \frac{d(T_2 - T_1)}{dy}$$

$$\left(\frac{d_2}{\sigma_2} - \frac{d_1}{\sigma_1}\right)(T_1 - T_1^0) = -\frac{A}{D_1} e^{D_1 y} - \frac{B}{D_2} e^{D_2 y} + \sum_i r_i\, e^{-\alpha_i \delta_i y/d_i}$$

$$+ \frac{A}{D_1} + \frac{B}{D_2} - \Sigma r_i$$

$$- \frac{d_2}{\sigma_2} \left[(T_2 - T_1) - (T_2 - T_1)_0\right]$$

$$T_s = T_1 + \frac{d_1}{\sigma_1} \frac{d\,T_1}{dy}$$